Role of actomyosin-mediated tension in a tissue on spindle positioning during mitosis

Maxine Lam

A thesis submitted to University College London

for the degree of Doctor of Philosophy

2016

Supervised by Professor Buzz Baum

MRC Laboratory for Molecular Cell Biology

University College London

DECLARATION

I, Maxine Lam, confirm that the work presented in this thesis is my own. Where information has been obtained from other sources, I confirm that this has been indicated in the thesis.

Signed:

Abstract

Almost all animal cells construct a mechanically rigid and contractile actomyosin cortex as they enter mitosis. The process is best understood in isolated cells, where this cortex helps drive mitotic cell rounding - generating space for spindle morphogenesis. The actomyosin cortex has also been suggested to play a role in spindle orientation, by regulating cell shape and by polarizing canonical spindle-orienting proteins. Furthermore, extrinsic force via actin-based retraction fibers in isolated cells has been proposed to reposition the spindle – implying that the process is mechanosensitive. However, cells in a tissue sit in much more complex biochemical and mechanical landscapes, where the role of the actomyosin cortex is unclear.

To shed light on this, I investigate the role of the mitotic actomyosin cortex and mechanical tension in spindle positioning within an epithelium – the *Drosophila* notum. I find that i) mitotic rounding occurs in a crowded tissue even when levels of actin and myosin activity are compromised; ii) actin and myosin have cell-autonomous roles in centrosome movement and spindle centering; and iii) mechanical tension appears to play a non-autonomous role in orienting the spindle. Although spindle alignment has been shown to be along the cell long axis in many systems, I find that this is not always the case. Cells under isotropic tension actively orient their spindles along the long axis, while this is less efficient in cells under lower tension due to crowding of the tissue or reduced myosin activity, despite having a well-defined long axis.

Finally, I suggest a model of dynamic spindle positioning in an epithelium, where the mitotic actomyosin cortex provides mechanical rigidity to facilitate efficient and balanced pulling forces on the centrosomes by astral microtubules, and where extracellular tension through actomyosin activity and cell-cell adhesion provides external cues for spindle orientation to cell long axis.

Acknowledgements

This thesis and the findings within would not be possible without the help and support of many people. I cannot thank everyone enough, but I will try anyway.

I would like to thank Buzz, for being a great supervisor and giving me the freedom to wander through the apparently impenetrable woods of science, all the while reminding me that there is a path to be forged if I simply looked hard enough. The devil is indeed in the details.

To the lab, for being great fun to work with but also the worst critics I have encountered – you have pushed me to be a better scientist with cake, beer and 'constructive' criticism. Special thanks to Helen, who patiently read this thesis. To everyone in the MRC LMCB for being wonderful, helpful friends and inspiring scientists. To my year group at the Wellcome Trust PhD programme for Developmental and Stem Cell Biology – a rare breed of people. We made it to the other side and Sara still owes everyone dinner.

To the Agency for Science, Technology and Research (ASTAR) in Singapore for funding and support. 9 years ago, they took a bet on a drama kid with good marks in Biology and opened up the world of scientific inquiry to me. To Pernille, who taught me that anyone can learn something new, but to discover the unknown requires incredible hard work. To Adam and David for Advice to a Young Scientist (we finally found out which book was for me). To Claire and Mike for showing me how fun it is to work in a lab, and never holding it against me when I first showed up in stilettos. To Ray for the years of advice and support.

Finally, to my amazing family and friends, who constantly think of new and exciting reasons to lure me out of the lab, motivating me to work even harder so I can always come out and play. Especially to Carlo, who always made sure I was well-fed and loved.

Table of contents

Chapter 1 Introduction

1.1 Mitosis and the spindle

> "The body is composed entirely of cells and their products, the cell being the unit of structure and function and the primary agent of organization."
> – Cell Theory, by Matthias Schleiden and Theodor Schwann, 1828 (Sharp 1921)

Shortly after the establishment of Cell Theory, the growth and division of cells was established as the main mode of growth in multicellular organisms (Sharp 1921; Wilson 1925). As early as the end of the 19th century, the mitotic spindle was observed as the apparatus that organised and segregated chromosomes during cell division (Flemming 1882). However, it would be many decades later before its role in also determining the site of furrow ingression was discovered (Rappaport 1997; Green et al. 2012). In this section, I outline how microtubules (MTs) are reorganised into a bipolar spindle during mitosis, and how the spindle is positioned to ensure appropriate cell division.

1.1.1 The microtubule cytoskeleton

1.1.1.1 Structure and formation

MT filaments are polymers of the basic monomeric unit, consisting of a α- and β-tubulin heterodimer, bound in a head to tail configuration. Typically, each MT consists of 13 such heterodimers oriented laterally in a cylindrical pattern to form a hollow filament ~24 nm in width. This ordered arrangement of heterodimers means that MT filaments have an intrinsic polarity, with β-tubulin exposed at the fast-growing end termed the plus-end and α-tubulin exposed at the slow-growing end termed the minus-end (Desai & Mitchison 1997; Nogales & Wang 2006).

β-tubulin hydrolyses GTP during MT polymerization, while α-tubulin remains bound to GTP. GTP-bound tubulin is stable, and promotes MT polymerization, while hydrolysis of GTP into GDP is thought to destabilize the MT lattice. This has lead to the development of the theory known as the GTP Cap Model, to explain the phenomena known as dynamic instability, where the growing MT

filament stochastically switches between periods of growth and shrinkage. In this model, a minimal amount of GTP-bound tubulin is at the end of the MT during the growth phase, when this minimal amount of GTP-bound tubulin at the end is hydrolysed, microtubules depolymerize rapidly, a process known as catastrophe (Desai & Mitchison 1997). Upon reaching a GTP-bound remnant in the MT filament, MTs can spontaneously beginning polymerizing again ('rescue') (Dimitrov et al. 2008). Most recently, new subunits have been seen being incorporated into the bulk of the filament at sites of mechanical damage, suggesting that MT nucleation may not be limited to the plus-end (Schaedel et al. 2015).

a

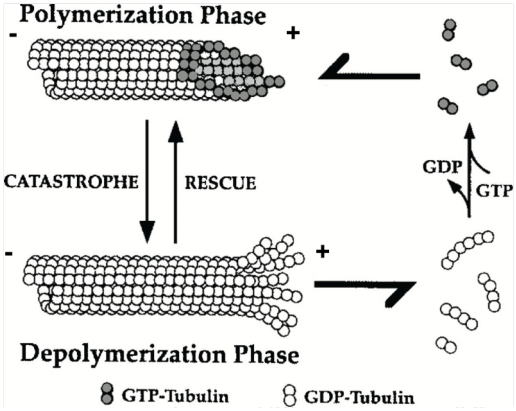

(Adapted from Desai & Mitchison 1997)

Figure 1.1: MT growth and shrinkage phases.

a. GTP-bound tubulin is added to the plus end of the MT during polymerization. Hydrolysis of GTP at the plus end leads to catastrophe, where MTs rapidly depolymerize and lose GDP-bound tubulin. Rescue of MT polymerization occurs when GTP-bound tubulin is again exposed at the plus ends.

1.1.1.2 Regulation of dynamics

In order to carry out its various functions in the cell, from providing structure to organelles to tracks for intracellular trafficking, the inherent dynamic instability of MTs has to be regulated by MAPs (Microtubule Associated Proteins). MAPs can either promote the polymerization or rescue of MTs, or the depolymerisation or catastrophe (Andersen 2000; Howard & Hyman 2007; Vicente & Wordeman 2015).

A unique class of MAPs are those which specifically bind to the growing plus-ends of MTs, collectively known as +TIPs (Akhmanova et al. 2010). Because of their unique location they serve important roles in allowing MTs to interact with their environment. Some examples of their function include regulation of MT dynamics, interactions with MTs and the actin cortex, regulation of MT attachment and dynamics at kinetochores, cargo loading for microtubule transport, and formation of MT arrays such as the mitotic spindle (Howard & Hyman 2007; Akhmanova et al. 2010; Jiang & Akhmanova 2011; de Forges et al. 2012).

Other mechanisms of regulation include MT nucleation, most recognisably by the centrosome. The centrosome itself is made up of a pair of tubulin-based centrioles surrounded by a matrix of proteins collectively known as the PCM (Pericentriolar material). The PCM and the centriole pair recruit an assortment of proteins to anchor (e.g. Ninein, Centrosomin, GCP proteins) (Mogensen et al. 2000; Delgehyr et al. 2005; Terada et al. 2003; Lüders et al. 2006; Kollman et al. 2011) and nucleate MT growth (γ-tubulin and associated proteins) (Bornens 2002; Lüders & Stearns 2007).

1.1.1.3 MT motors: Kinesins and dyneins

The intrinsic polarity of the MT filament allows MT motor proteins such as most kinesins and dynein to move in a directed manner towards the plus-ends and minus-ends respectively. This directionality of MT motor proteins is important for intracellular trafficking, spindle assembly, as well as positioning. Both motors hydrolyse ATP to generate movement along MTs, with a head domain that binds to MTs and a tail domain that binds to cellular structures or cargo. However they differ significantly in structure and processivity (Schliwa & Woehlke 2003; Mallik et al. 2013).

The best studied kinesin is conventional kinesin (Kinesin-1). Kinesin 1 exists as a homodimer that binds to MTs through the head domains. ATP hydrolysis in the one kinesin head domain leads to a conformational change that translates into a step as the flexible neck linker domain repositions the ADP-bound kinesin along the MT while the ATP-bound kinesin remains attached. The structure of Kinesin-1 is such

that it is only able to move forward (towards the plus-ends), which makes it a highly processive motor (Schliwa & Woehlke 2003; Yildiz et al. 2004; Mallik et al. 2013). Besides the transportation of cargo along MTs, some kinesins also regulate MT dynamics at the plus ends through interaction with +TIP proteins (Jiang & Akhmanova 2011; Vicente & Wordeman 2015). For example, members of the Kinesin-13 family such as KLP10A in *Drosophila* and MCAK in vertebrates are able to track growing plus-ends and induce depolymerisation (Wu et al. 2006). And some kinesins are able to track to plus-ends even during MT catastrophe (Lombillo et al. 1995; Grissom et al. 2009).

In contrast, dynein homodimers are much less processive. Instead of a stepwise movement along the MTs, the motor domains of dynein homodimers are often seen to move independent of one another (Schliwa & Woehlke 2003; Bhabha et al. 2016). The movement of the leading dimer versus the lagging dimer appears to be stochastic, such that the leading dimer may move multiple steps before the lagging dimer moves. However, dyneins are thought to function in groups, which significantly increases its MT-binding ability and allows it to bear larger loads (Mallik et al. 2013). Furthermore, dyneins are able to interact with a multitude of adaptor proteins, which improve processivity (Kardon & Vale 2009; McKenney et al. 2014).

1.1.1.4 MT organization in epithelia

MTs are organised in an apical and basal mesh beneath the cell surface in epithelia, as well as in longitudinal arrays along the cell height with their minus-ends at the apical surface and their plus-ends at the basal surface (Clark et al. 1997). Plus- or minus-end directed motors are thus able to facilitate the establishment and maintenance of the apical-basal polarity of epithelia (Rodriguez-Boulan & Macara 2014; Müsch 2004). In interphase, most MTs are non-centrosomal and the centrosome is located beneath the apical surface. The non-centrosomal nucleation of MTs is not well-understood, but multiple lines of evidence suggest that the establishment of mature epithelia-specific cell-cell contacts such as adherens junctions and the polarity protein PAR1 are required (Borisy et al. 2000; Cohen et al.

2004; Meng et al. 2008; Jiang et al. 2015). Ninein functions to anchor MTs to adherens junctions (Moss et al. 2007).

1.1.2 Spindle formation

In S phase, centrioles duplicate and mature into mother and daughter centrioles. In prophase, the mother and daughter centriole pair separates and form two centrosomes that rapidly nucleate MTs (Zhai & Borisy 1994) due to γ-Tubulin recruitment (Khodjakov & Rieder 1999). This generates radial arrays of MTs centred on two centrosomes. MT dynamics also change dramatically, as MTs become shorter and more dynamic once cells enter mitosis (Piehl & Cassimeris 2003; Niethammer et al. 2007). Centrosomes separate through a combination of pushing forces generated by short polymerizing MTs, MT-motor activity and interactions with the overlaying actin cortex (discussed in further detail in Chapter 1.3). In *Drosophila*, dynein localized to the cortex facilitates the separation of centrosomes, while the minus-end directed kinesin Ncd counteracts separation by crosslinking the MTs between the centrosomes (Sharp et al. 2000). The plus-end directed kinesin-5 motors (Eg5 in vertebrates, KLP61F in *Drosophila*) promote the anti-parallel sliding of astral MTs, and therefore spindle pole separation. While this is true in vertebrates, in *Drosophila*, KLP61F is localised to the nucleus until NEB (Sharp, McDonald, et al. 1999), and live-imaging after depletion revealed that it did not have an effect on prophase centrosome separation (Sharp, Yu, et al. 1999; Sharp et al. 2000; Goshima & Vale 2003). Importantly, double depletion of dynein and Ncd resulted in a rescue of wildtype centrosome separation rates, indicating the presence of an alternate pathway (Sharp et al. 2000).

After NEB however, KLP61F (*Drososphila* kinesin-5) is required to promote bipolar spindle formation through the anti-parallel sliding of interpolar MTs (Sharp et al. 2000; Goshima & Vale 2003). The kinetochores of chromosomes also capture free plus-ends of MTs, bundling MTs along these attachments, forming kinetochore-fibres which power chromosome movements and align them along a metaphase plate (Goshima et al. 2007).

Additionally, chromosomes themselves act to nucleate MTs during mitosis. The nucleotide exchange factor for Ran, RCC1, decorates chromatin and creates a local region of RanGTP that releases important MAPs from importin to promote local MT nucleation and stabilization (Goshima & Kimura 2010; Clarke & Zhang 2008; Heald & Khodjakov 2015). Furthermore, the CPC (chromosome passenger complex) can promotes MT assembly, independent of a Ran gradient (Maresca et al. 2009). This is clearly seen in spindles lacking key centrosomal proteins and functional centrosomes, but are still able to organise chromosomes and form bipolar spindles (Giansanti et al. 2001; Basto et al. 2006; Mahoney et al. 2006; Goshima & Kimura 2010). However, spindles forming without centrosomes lack astral MTs, although interpolar and kinetochore MTs are still present.

Once all chromosomes have been captured by kinetochore MTs the spindle assembly checkpoint is triggered, and cells enter anaphase (Foley & Kapoor 2013; Chang & Barford 2014; Logarinho et al. 2004).

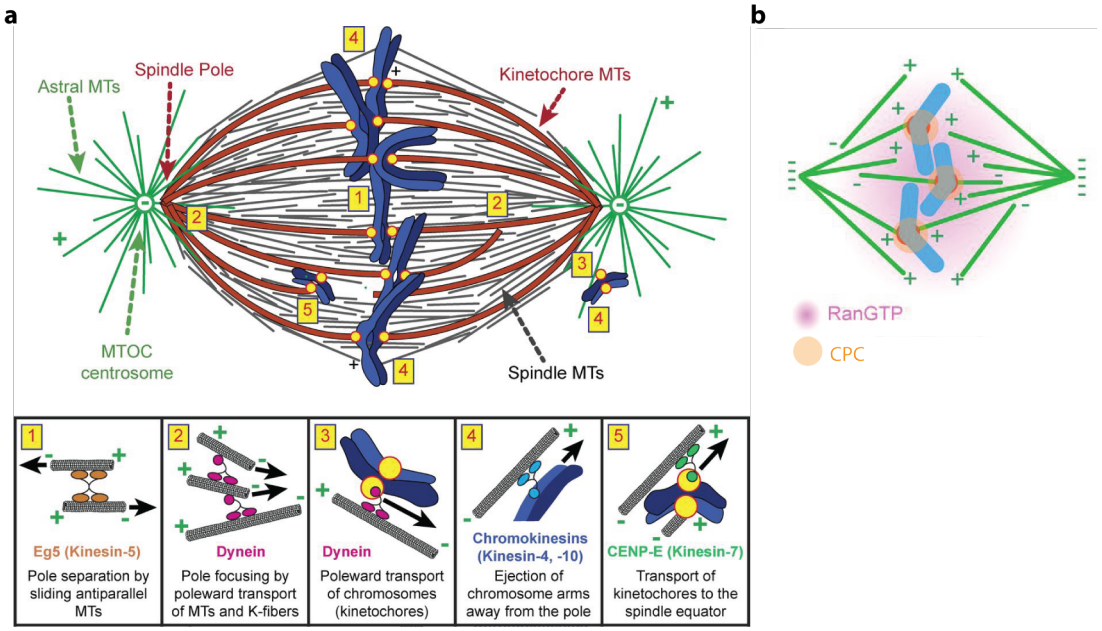

(Adapted from Heald & Khodjakov 2015)

Figure 1.2: Spindle formation is aided by MT molecular motors and MT nucleation factors.

a. The respective MT motors and their known roles in spindle formation and organisation.

b. MT nucleation around the chromosomes is mediated by a local RanGTP gradient and the CPC.

1.1.3 Forces that position the spindle

1.1.3.1 Astral MTs as force-bearing structures

Besides interpolar MTs and kinetochore MTs, spindles also contain astral MTs. These MTs are able to contact the cortex and are thought to position the spindle relative to the cellular environment, through a combination of pushing and pulling forces (Grill & Hyman 2005). In the absence of astral MTs such as in acentrosomal spindles, or when MT dynamics are perturbed, spindles frequently mis-orient. This emphasises the importance of astral MT regulation in spindle positioning (di Pietro et al. 2016).

Pushing forces generated by the polymerization of MTs can be significant at short distances, due to the stiffness of MT filaments at short lengths, but have a tendency to buckle at longer lengths (Dogterom et al. 2005). Because of this, pushing forces are likely be involved in systems where the centrosome is in close proximity to the cortex or cell boundary, as in fission yeast (Tolić-Nørrelykke et al. 2004).

Pulling forces on the other hand are thought to dominate in larger cells. Tension along astral MTs has been visualised in experiments using laser ablation or local depolymerisation, and are abrogated upon dynein depletion (Grill & Hyman 2005; Kotak & Gönczy 2013; Bosveld et al. 2016). Pulling forces can be generated by the depolymerisation of astral MTs that remain tethered at the cortex as they shorten, or by the action of a cortically-bound minus-end directed motor dynein walking towards the spindle pole (Dujardin & Vallee 2002; Dogterom et al. 2005; Grill & Hyman 2005; Laan et al. 2012; Lu & Johnston 2013). In systems where the cell is much larger than the spindle, cytoplasmic dynein localised along astral MTs, anchored by a proposed 'cytoplasmic scaffold' or viscous drag against cellular components has been proposed to exert pulling forces on the spindle (Wühr et al. 2010; Minc et al. 2011). However, for the majority of systems, dynein is found at the cortex. This localisation is facilitated by a range of cortical localisation factors, and loss of cortical-specific dynein can lead to spindle orientation defects (Dujardin & Vallee 2002; Kotak & Gönczy 2013; di Pietro et al. 2016).

1.1.3.1.1 The Mud/ Pins/ Gαi proteins

Current studies into cortical factors localizing dynein in different systems have converged on the functionally homologous set of proteins: Mud (Mushroom body defect, NuMA in vertebrates, LIN-5 in *C. elegans*), Pins (Partner of inscuteable, LGN in vertebrates, GPR1/2 in *C. elegans*), and the heterotrimeric G protein Gαi (GOA-1 in *C. elegans*) (di Pietro et al. 2016). In *Drosophila*, these proteins were initially studied in the context of asymmetrically dividing cells, where they function downstream of apical proteins (Morin & Bellaïche 2011; Lu & Johnston 2013). This led to the discovery that Mud interacts with the dynein-dynactin complex by binding with Ctp (Cut up, dynein light chain) and Ana2 (Anastral spindle 2) (Wang et al. 2011), while also binding directly to Pins via its conserved C-terminal domain (Izumi et al. 2006; Siller et al. 2006; Bowman et al. 2006). Pins can exist in an autoinhibitory conformation, and its activation requires the cooperative binding of Mud via its TPR domain and Gαi along its three consecutive GoLoco domains (Nipper et al. 2007). The entire ternary complex is localized to the cortex in a Ric-8 dependent manner by Gαi through its N-terminal myristylation site (David et al. 2005; Hampoelz et al. 2005; Wang et al. 2005).

Perturbing any of these proteins results in spindle mispositioning (di Pietro et al. 2016). However, using *in vitro* induced polarity assays with *Drosophila* S2 cells, it was found that loss of Mud only partially impaired spindle orientation (Johnston et al. 2009). Complete spindle orientation required the Pins TPR domain bound to Mud, as well as the Linker domains. The Linker domain of Pins is activated by Aurora A and binds to Dlg (Discs large) via its GUK domain (Johnston et al. 2009; Bellaïche et al. 2001; Siegrist & Doe 2005). The activity of the Pins Linker domain appears to require Khc73 (Kinesin heavy chain 73, kinesin 13 family), which binds to Dlg also via its GUK domain (Siegrist & Doe 2005). It was proposed that Khc73 and Dlg form a Pins module that capture astral MTs, while dynein and Mud form a module that allow for force generation (Johnston et al. 2009; Lu & Johnston 2013). Finally, Khc73 was found to link to dynein in the same system through a 14-3-3 heterodimer that binds to the dynein adaptor, NudE, thus coupling the two modules (Lu & Prehoda 2013). Interestingly, human Dlg has been shown to bind to GAKIN (Khc 73

in humans) (Hanada et al. 2000), although a role for the Dlg/ Khc73 pathway has not been shown in vertebrates.

With the same *in vitro* assays, it was further found that Mud/ Pins co-localisation at the cortex requires Cno (Canoe, Afadin in mammals) and RanGTP (Wee et al. 2011). Cno bound to the Pins TPR domain, while its RA domains bound to RanGTP (Wee et al. 2011). This contrasts with what happens in human cells, where RanGTP/ importin-β around the chromosomes are thought to inhibit LGN/ NuMA from localizing to the cortex (Kiyomitsu & Cheeseman 2013). Despite the difference in effect of RanGTP, Afadin has recently been shown to bind concomitantly to F-actin and LGN through neighbouring domains, where it is required to localise LGN and subsequently NuMA and cortical dynactin to the cortex (Carminati et al. 2016). Cno similarly possesses an actin-binding domain just next to its Pins-binding domain (Wee et al. 2011), suggesting that the interaction might be conserved.

1.1.3.1.2 Alternative methods of localizing Mud and dynein

In *Drosophila* sensory organ precursor (SOP) cells and during zebrafish gastrulation, the planar cell polarity (PCP) protein Dsh (Dishevelled) binds Mud and restricts its localization to the posterior side of the cell (Ségalen et al. 2010). Using *in vitro* induced polarity assays with *Drosophila* S2 cells, a small fragment of Fz was found to recruit the Dsh DEP domain, which binds to the C-terminus of Mud. Genetic interactions were confirmed *in vivo* in the *Drosophila* SOP cells, where Mud recruitment to the posterior cortex required Dsh. Intriguingly, Mud also binds to Pins at the anterior cortex via the same C-terminal domain (Izumi et al. 2006; Siller et al. 2006; Bowman et al. 2006; Ségalen et al. 2010).

In symmetrically-dividing epithelial cells, Mud has also recently been observed to be cortically-enriched at tricellular junctions (TCJs, where 3 or more cells meet within an epithelium) (Bosveld et al. 2016; Bergstralh et al. 2016). This localization is evident even before NEB, in contrasts to vertebrate cells where NuMA is nuclear until NEB. Mud localisation to the TCJs is Pins-independent and appears

to be dependent on TCJ integrity, which is dependent on Dlg- and Gli (Gliotactin) (Bosveld et al. 2016).

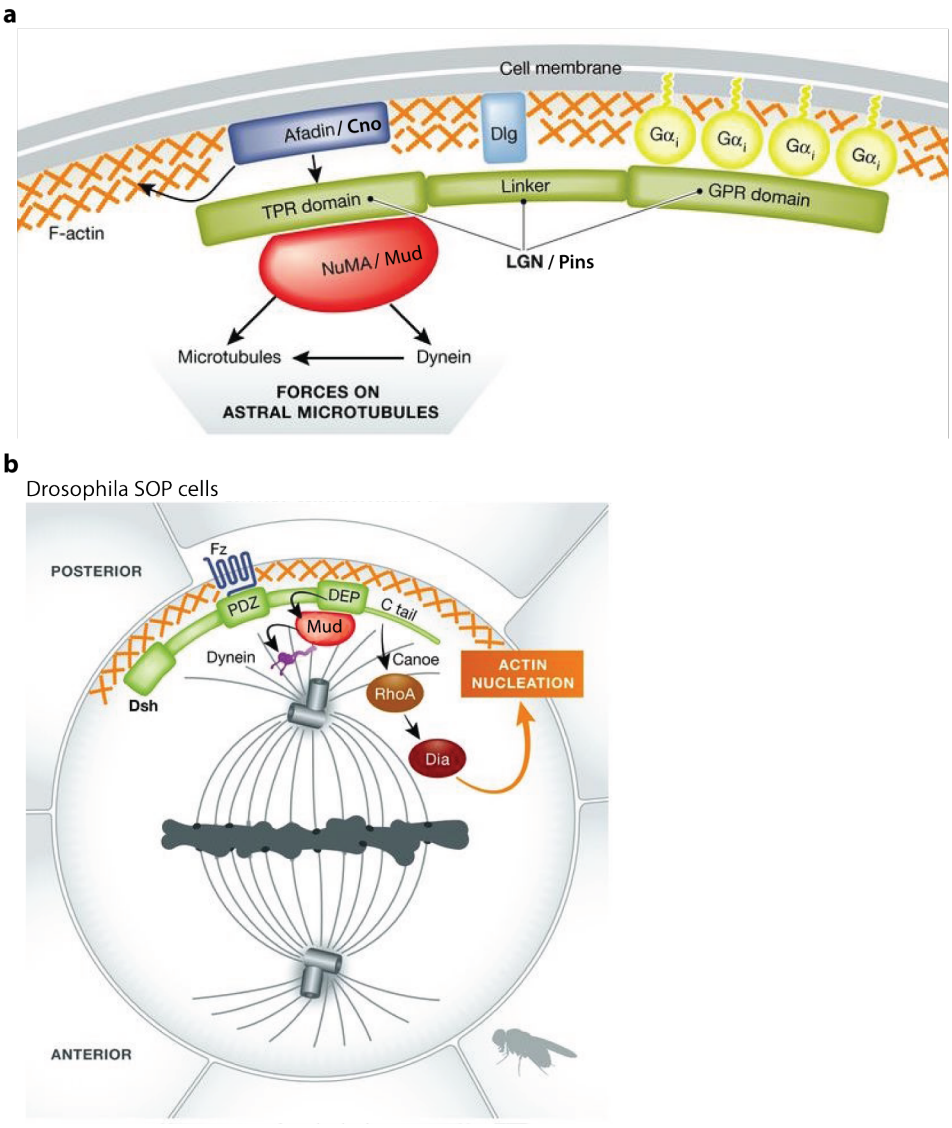

(Adapted from di Pietro et al. 2016)

Figure 1.3: Cortical proteins involved in spindle orientation.

a. The evolutionarily-conserved proteins Gαi, Pins and Mud are involved in localising dynein to the cortex, thereby generating pulling forces on astral MTs and orienting the spindle during mitosis.

b. Localisation of Mud to the cortex can also occur via Dsh and Fz in *Drosophila* SOP cells.

1.1.4 Spindle positioning within an epithelium

The protein interactions involved in spindle orientation appear to be largely conserved across animals, from single cells to multicellular contexts (di Pietro et al. 2016). However, cell division in various tissues occurs differently. I now consider the unique challenges of dividing within an epithelium and discuss some of the cell autonomous and non-autonomous factors that affect spindle positioning.

1.1.4.1 Epithelial polarity and spindle orientation

Epithelial cells have a clearly defined apical and basal region, defined by unique polarity proteins which negatively regulate each other to ensure proper separation of these domains (Bilder et al. 2000; Laprise & Tepass 2011; Rodriguez-Boulan & Macara 2014). Disruption of the intrinsic polarity of these cell by perturbing any of the polarity proteins therefore results in spindle mispositioning relative to the apicobasal axis (di Pietro et al. 2016).

Symmetric division within this tissue therefore has to be well-controlled, such that daughter cells inherit both the apical and basal domains (Morin & Bellaïche 2011; di Pietro et al. 2016). Deviation from this plane results in changes in tissue architecture (Williams & Fuchs 2013; Luxenburg et al. 2011), as well as increased levels of apoptosis (Nakajima et al. 2013; Padash-Barmchi et al. 2013; Poulton et al. 2014). Recently one coping mechanism has been identified to mitigate the effects of spindle orientation outside of the plane of the epithelium. *Drosophila* epithelial cells forced to orient their spindles perpendicular to the plane of the tissue result in daughter cells extruding from the tissue (Bergstralh et al. 2015). However, the lateral adhesion molecules Fas 2 and Nrg allow these cells to re-integrate into the tissue (Bergstralh et al. 2015).

On the other hand, asymmetrically dividing stem cells within epithelia often divide orthogonal to the plane of the tissue, and must therefore override the spindle positioning cues in their symmetrically dividing neighbours (Williams et al. 2011; Williams & Fuchs 2013; di Pietro et al. 2016). Polarity proteins are often incorporated into these pathways, and are relocalised into apical or basal domains that relocalises cortical force generators accordingly. One good example is the

localisation of Dlg, in asymmetric versus symmetric divisions. Dlg was first identified as a basolateral protein, and therefore is localised beneath the apical plane occupied by adherens junctions in interphase. However, in asymmetrically dividing neuroblasts it is apically enriched (Morin & Bellaïche 2011; Lu & Johnston 2013). In addition, it is directly involved in cortical force generation by binding to Pins and Khc73 (Johnston et al. 2009). In symmetrically dividing cells within the *Drosophila* follicular epithelium or chick neuroepithelium however, it is localised in a lateral belt that is thought to limit the spindle within the plane of the epithelium (Bergstralh et al. 2013; Saadaoui et al. 2014). Meanwhile in the *Drosophila* wing disc, it is dispensable for planar divisions (Bergstralh et al. 2016), and previous studies implicating it in planar orientation actually arose due to pleiotropic effects of Dlg on tissue polarity and organisation (Nakajima et al. 2013).

1.1.4.2 Cell height: a physical constraint on spindle z-positioning

In the squamous basal cells of the developing mouse neuroectoderm, as well as in cultured MDCK monolayers, it has been observed that when cortical force generators are perturbed spindles can still orient within the plane of the epithelium (Williams et al. 2011; Lazaro-Dieguez et al. 2015). This is thought to be due to the limit of the cell height within these cells, such that the maximum tilt of the mispositioned spindle is constrained within the plane of the epithelium (Williams et al. 2011; Lazaro-Dieguez et al. 2015). On the other hand, in psueudostratified epithelia where cells are extremely tall and narrow, the perturbation of the actomyosin cortex prevents cells from remodelling their cell shape. In this case, spindles orientation is defined by the cell width leading to division along the apicobasal axis (Nakajima et al. 2013). At the same time, the spindle might have an intrinsic ability to position along the long axis of the cell, as discussed below.

1.1.4.3 Spindle positioning within the x-y geometry of the cell – finding the centre and the long axis

Ever since cell divisions have been observed, it was noted that the mitotic spindle in symmetrically dividing cells tends to be in the centre and aligned along the long axis of the cell. The positioning of the spindle at the cell centre allows for the equal distribution of cellular material to daughter cells, which has implications for

daughter cell fate (Cadart et al. 2014; Kiyomitsu 2015); while positioning the division plane across the long axis impacts cell packing and mechanical strain within an epithelium (Gibson & Gibson 2009; Mao et al. 2011; Campinho et al. 2013).

Cells dividing in this way are said to follow the 'long axis rule' or 'Hertwig's rule', after Oscar Hertwig who formalised a series of rules for oriented cell divisions in 1884 by observing the first divisions of frog embryos. He noticed that the spindles were predictably aligned to the intrinsic long axis or the imposed one, after deformation between glass plates (Wilson 1925). In much similar fashion, later work using micromanipulation of mammalian and sea urchin cell shape in culture showed that spindles constantly survey cell geometry, and are able to dynamically re-position to the long axis (O'Connell & Wang 2000; Minc et al. 2011). Importantly, these studies showed that dynein and microtubules are required for this behaviour. Minc et al. further develop a theoretical model where the pulling forces on astral MTs scale with MT length and are balanced on both spindle poles. This faithfully replicates their experimental data to within 15°. Spindle orientation along the long axis *in vivo* has also been observed in cells with no or incomplete mitotic rounding, leading to the hypothesis that this might be a common mechanism for spindle orientation in symmetrically dividing cells (di Pietro et al. 2016).

Spindle orientation to the long axis and spindle centring during mitosis is proposed to go about by forces along the lengths of the astral MTs (Grill & Hyman 2005; Wühr et al. 2010; Kimura & Kimura 2011; Minc et al. 2011; Kotak & Gönczy 2013). This process of spindle positioning to the cell centre and long axis is most well-studied and understood in single cells. There are two main models for this: the first involves dynein in the cytoplasm, and the other involves dynein at the cortex.

In the first model, which appears to explain the behaviour in large embryos of sea urchins and frogs, cytoplasmic dynein attaches to astral MTs and generates pulling forces which scale with their length (Kimura & Kimura 2011; Wühr et al. 2010; Minc et al. 2011). Forces are therefore highest along the cell length and the spindle is pulled towards the cell length, while centring is maintained by balancing forces on both spindle poles (Kimura & Kimura 2011; Minc et al. 2011; Wühr et al.

2010). This however, requires that astral MTs are long enough to probe the entire cell space.

In the second model, for cells where dynein is observed to be cortical and astral MTs do not fill the cell space, the forces on the spindle are instead determined by the distribution of cortical factors for dynein such as the Mud/ Pins/ Gαi complex (Grill & Hyman 2005; Kotak & Gönczy 2013). Hela cells are a case in point – Here, the spindle oscillates about the cell centre due to a 2-part dynamic feedback system. After NEB, RanGTP near the chromosomes locally inhibits LGN and NuMA at the cortex, restricting cortical force generators to the cell poles (Kiyomitsu & Cheeseman 2012; Dimitracopoulos 2016). Cortical force generators acting on astral MTs then cause the spindle pole to move towards the cortex. But due to an asymmetry perhaps in the initial position, one pole moves closer and pulls the spindle off-centre. The authors propose that Plk1 at the spindle poles then inhibits the cortical localization of dynein as it approaches the cortex, while RanGTP inhibition at chromosomes has also shifted towards this half of the cell. This results in a net increase in cortical pulling force from the other half of the cell, and the spindle is restored in the opposite direction (Kiyomitsu & Cheeseman 2012).

In the absence of cortical force generators, these spindle oscillations disappear, and the spindle remains in its initial position, determined by the position of the nucleus at the centre at NEB (Pecreaux et al. 2006; Grill & Hyman 2005). This idea was recently tested by mechanically moving spindles during mitosis in the absence of cortical force generators in *C. elegans*. Surprisingly, it was found that the maintenance of the spindle at the centre during mitosis was independent of cortical force generators, and instead dependent on MT polymerisation and nucleation (Garzon-Coral et al. 2016). The authors conclude that pushing forces by dynamic astral MTs are sufficient to centre the spindle during mitosis. It is worth noting that in this study, the role of cytoplasmic dynein was not tested, therefore it is not possible to rule out cytoplasmic pulling forces.

1.1.4.4 Spindle positioning to the interphase cell shape after mitotic rounding

The models for spindle orientation to the long axis described so far appear to apply if the cell has a long axis during mitosis. However, many animal cells round up during mitosis, including those of *Drosophila* epithelial cells. This raises a further question of if and how cells 'remember' their interphase long axis during division. This question was first explored in mammalian cells in culture growing on substrates of varying patterns. Cells were found to have an apparent 'memory' of interphase adhesion geometry, through the retraction fibres they leave behind when they round up in mitosis (Théry et al. 2005; Théry et al. 2007). These retraction fibres polarize the actin cortex through phosphorylated ERMs (pERMS) (Théry & Bornens 2006), and pERM localization subsequently polarizes LGN and NuMA (Machicoane et al. 2014). LGN and NuMA thus are proposed to be part of the 'memory' system.

A similar phenomena of interphase long axis memory has been observed *in vivo* and a tissue-specific model has evolved to explain this – the tricellular junction model (Bosveld et al. 2016). The TCJ model derives from the observation that Mud is localized preferentially to TCJs in the *Drosophila* notum and TCJs tend to be closer along cell poles for cells which are elongated at interphase (Bosveld et al. 2016). This anisotropy in TCJ distribution persists despite efficient mitotic rounding, and therefore orients the spindle towards the interphase cell long axis through the biasing of cortical force generators (Bosveld et al. 2016). While this nicely resolves the conundrum, such a localization for Mud has not been observed outside of *Drosophila* wing discs and notum (which forms from the wing disc) (Radulescu & Cleveland 2010), which prevents this model from being generalizable. Furthermore, the theoretical model developed for the TCJ model (adapted from Minc et al. 2011), based on Mud at TCJs biasing the forces on astral MTs, is only able to predict experimental data to within 30° (Bosveld et al. 2016). This suggests that other mechanisms might be involved (Dimitracopoulos et al. 2016).

1.1.4.5 The impact of extracellular forces on spindle positioning

It has also been suggested that mechanical tension on the mitotic cell can re-orient the spindle. When cells in culture were grown on patterned substrates such that they had a long axis, spindles oriented along the long axis, However if at

prometaphase cells were stretched perpendicular to the long axis, creating a round cell with a tension axis, the spindle re-orients to this tension axis (Fink et al. 2011). The authors propose this goes through a polarization of subcortical actin, which I will discuss in Chapter 1.3.

Within a tissue, tension has also been proposed to play a role in spindle orientation. In these tissues, cells are subject to anisotropic tension (i.e. a stretch in one direction), which results in majority of cells being elongated in the direction of stretch. It has been proposed that spindles then orient according to the long axis rule (Mao et al. 2013; LeGoff et al. 2013; Campinho et al. 2013; Wyatt et al. 2015). Notably, Wyatt et al. found that the minority of cells not elongated along the tension axis divided with the cell long axis rather than the tension axis. The authors therefore concluded that tension in tissues orient divisions indirectly by polarizing cell shape.

The coordination of the orientation of cell divisions within a tissue leads to local elongation and spreading of the tissue (Lecuit & Lenne 2007; Baena-López et al. 2005; da Silva & Vincent 2007; Mao et al. 2011). Cell divisions according to the cell long axis induced under stretch conditions therefore results in a redistribution of cell mass in the tissue that appear to reduce the local tissue tension (Campinho et al. 2013), and are proposed to equilibrate tension across the whole tissue (Mao et al. 2013; Wyatt et al. 2015).

1.2 The actomyosin cortex

I have just discussed the importance of cell shape and tissue tension on spindle orientation. Both cell shape and tension are largely determined by the actomyosin cortex (Pollard et al. 2009; Heisenberg & Bellaïche 2013; Ramkumar & Baum 2016). Here I detail the components of the actomyosin cortex, how it generates tension and how it is remodelled during mitosis.

1.2.1 Actin dynamics and regulation

1.2.1.1 Basic structure and formation

Actin can exist as a monomer (G-actin) or a linear polymer (F-actin). G-actin binds head-to-tail with each new actin monomer rotating 166°, resulting in the helical structure of F-actin with an intrinsic polarity. Microfilaments of F-actin in the cytoskeleton consist of two parallel F-actins forming a double helix (Pollard et al. 2009). The critical nucleus for F-actin polymerization is a trimer of G-actin. However, the formation of a trimer is unfavourable under physiological conditions and F-actin formation *in vivo* requires nucleators (Sept & Mccammon 2001; Pollard 2007). When formed in steady-state conditions, F-actin can be seen 'treadmilling' due to ATP hydrolysis of new ATP-bound monomers joining at the plus- (barbed) end and ADP-bound monomers leaving the minus- (pointed) end (Wegner 1976). However, F-actin can in fact polymerise bidirectionaly, but the rate of monomer association is much higher at the barbed end, leading to filament growth being predominantly at the barbed end in physiological conditions (Pollard & Mooseker 1981).

The main actin nucleators involved in assembly of the cortex of human cells in culture have recently been identified as the formin mDia1 and the Arp2/3 complex (Bovellan et al. 2014). Formins promote the growth of elongated actin filaments, while the Arp2/3 complex mediates nucleation from the minus end and branching of pre-existing filaments (Pollard 2007). In *Drosophila*, a single formin Dia (Diaphanous) represents the mammalian Diaphanous class of formins (Liu et al. 2010) and the homologues of Arp2 and Arp3 have been identified (Fyrberg & Fyrberg 1993; Hudson & Cooley 2002).

1.2.1.2 Regulation of dynamics and organization

Actin dynamics is regulated by a host of actin binding proteins. Profilin promotes filament elongation through the exchange of ADP- to ATP-G-actin. Profilin-bound ATP-G-actin monomers are then recruited by FH1 domain of formins where they are incorporated into the growing barbed ends of filaments (Paul & Pollard 2008). Meanwhile, ADF/cofilin leads to the severing and disassembly of ADP-actin filaments (Andrianantoandro & Pollard 2006). Upon dissociation, Cofilin-bound G-actin monomers are sequestered in an ADP-bound form preventing them from rebinding, before being recycled by profilin. In addition, capping proteins terminates polymerisation at free barbed ends of filaments, which is counteracted by formins (Pollard 2007).

Bundling and crosslinking of F-actin is achieved by proteins such as fascin or filamin and α-actinin, respectively (Schmidt & Hall 1998; Bartles 2000; Jayo & Parsons 2010; Fletcher & Mullins 2010). These change the organization of the actin network, but also its mechanical properties (Fletcher & Mullins 2010; Fritzsche et al. 2016).

For many processes, local actin remodelling is directed by Rho family GTPases. Rho proteins act as molecular switches, through their conversion between inactive GDP-bound and active GTP-bound conformational states. Rho proteins have an intrinsic ability to hydrolyse GTP, and are therefore also known as Rho GTPases, and normally exist in the 'off' state. This can be locally counteracted by GEFs (guanine-nucleotide-exchange factors) or facilitated by GAPs (GTPase-activating proteins) (Schmidt & Hall 1998; Spiering & Hodgson 2011; Sit & Manser 2011). Rho GTPases and their role in F-actin reorganisation is highly conserved, especially in the distinct effects of Rho, Rac and Cdc42 (Hall 1998). In many eukrayotes, Rho1 organises F-actin into contractile bundles like those in stress fibres and the mitotic cortex; Rac is required for the formation of a short branched actin network in lamellipodia; and Cdc42 is required for the formation of many of structures, including filopodia in some systems, which consist of short bundles of parallel actin filaments (Hall 2012; Maddox & Burridge 2003; Rosa et al. 2015), and lamellipodia (Block et al. 2012). Interestingly, Rosa et al 2015 also found that Rho and Cdc42

cooperated in the formation of the mitotic actin cortex, adding to the observation that Rho family proteins engage in crosstalk (Hall 2012; Sit & Manser 2011; Spiering & Hodgson 2011).

1.2.2 Formation and contractility of the actomyosin cortex

Actin filaments alone can generate pushing forces by polymerisation (Mogilner & Oster 2003; Footer et al. 2007; Kovar & Pollard 2004). However, the actin cytoskeleton can also generate pulling forces when acted upon by the plus-end directed Myosin motors. Together with non-muscle Myosin II, actin filaments form a contractile network that in animal cells localises just beneath the plasma membrane (Salbreux et al., 2012).

1.2.2.1 Myosin II and the generation of tension in the actin network

Non-muscle Myosin II (Myo II) is a myosin motor protein that both crosslinks and generates mechanical tension within an actin gel (Vicente-Manzanares et al. 2009). Myo II consists of two heavy chains (MHCs) encoded by *zipper* in *Drosophila*, two regulatory light chains (MRLCs) encoded by *spaghetti-squash* and two essential light chains (Sellers 2000). Myo II homodimerises and assembles to form bipolar antiparallel "microfilaments" with the head domains facing out. When Myo II microfilaments crosslink with parallel actin filaments, ATP hydrolysis by Myo II results in a rotation in the head domains that causes attached actin filaments to slide in opposite direction, generating tension in the network (Vicente-Manzanares et al. 2009).

The activity of Myo II is regulated by phosphorylation by kinases, such as ROCK (Rho-associated kinase), citron kinase and MLCK (Myosin light chain kinase), as well as by phosphatases such as PP1/PP2A together with the regulatory subunits, such as Sds22 and MYPT (Matsumura 2005). The assembly of Myo II minifilaments requires phosphorylation at serines 21 and threonine 20 (serine 19 and threonine 18 in mammalian cells). Phospho-mimetic or non-phosphorylatable mutations at these sites therefore positively or negatively affect processes that require the generation of tension in the actomyosin network, such as cytokinesis and

tissue morphogenesis (Jordan & Karess 1997; Matsumura 2005; Winter et al. 2001; Bertet et al. 2004; Moon & Matsuzaki 2013; Kim et al. 2015).

1.2.3 Coupling actomyosin forces to the cell surface

As in any structural system, forces at a surface are transmitted at points of anchorage to their underlying support. In cells, the forces generated at the cell surface by the actomyosin cortex are transmitted through its connections to neighbouring cells, the plasma membrane, and the substratum (Bray & White 1988; Ingber 1997; Lecuit et al. 2011; Lecuit & Yap 2015).

1.2.3.1 Adherens junctions

Within an epithelia, cells are physically linked by adherens junctions. In Drosophila the adherens junction localises to a discrete portion of the apical domain (Harris 2012). Here, the extracellular domains of Shotgun molecules (E-cadherin in vertebrates) of neighbouring cells form homodimers that attach cells to one another (Tepass et al. 1996; Zhang et al. 2009; Brasch et al. 2012). The actin cytoskeleton is then linked to the adherens junctions indirectly, through direct binding with α-catenin, which binds to ß-catenin bound to cadherin (Yonemura 2011; Baum & Georgiou 2011; Desai et al. 2013).

1.2.3.2 Attachment to the plasma membrane

The actin mesh must also be attached to the plasma membrane to change cell shape. This is the role of ERM (Ezrin, Radixin and Moesin) proteins, which connect actin filaments in the animal cell cortex to PIP2 (Phosphatidylinositol 4,5-biphosphate) membrane domains as well as other membrane proteins at the plasma membrane (Fehon et al. 2010). In *Drosophila,* Moesin is the sole ERM protein (McCartney & Fehon 1996).

1.2.3.3 Focal adhesions

The actomyosin cortex also couples cells to the extracellular matrix (ECM) via focal adhesions through integrin-based focal adhesions. These consist of α/ β integrin heterodimers that bind to the ECM on the outside of the cell and a variety of

additional adaptor proteins on the inside of the cell via their long cytoplasmic tails. These adaptors include talin and filamin, which then recruit actin to focal adhesions (Wegener & Campbell 2008; Schwartz 2010).

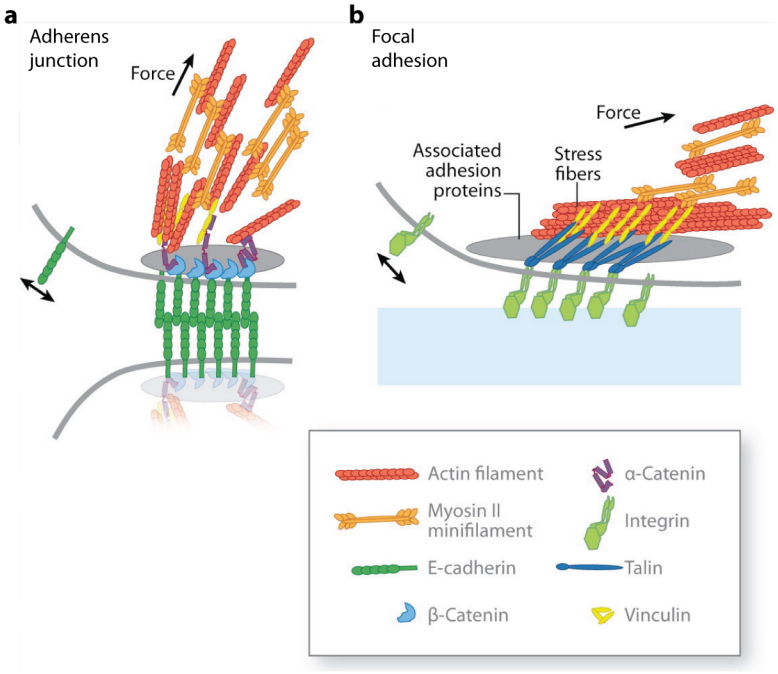

(Adapted from Lecuit & Yap 2011)

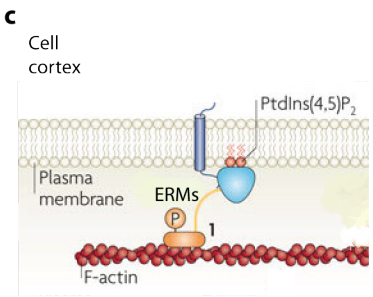

(Adapted from Fehon et al. 2010)

Figure 1.4: The actomyosin network is coupled to the cell surface through adherens junctions, focal adhesions and ERM proteins.

a. Actomyosin is linked to the adherens junctions (E-cadherin) indirectly through α-catenin and β-cadherin. This leads to force-coupling between cells through their adherens junctions.

b. Actomyosin is localised to focal adhesions indirectly through talin and vinculin, allowing force to be exerted on the extracellular surface.

c. Actomyosin is linked to the plasma membrane via association with ERM proteins, resulting on tension along the cell surface.

1.2.4 Changes in cell shape during mitosis

As a result of the coupling of the forces of the actomyosin cortex to the overlaying plasma membrane and to neighbouring cells and the ECM, changes in the reorganization and contractility of the actomyosin cortex are able to drive corresponding changes in the shape of the cell. This is clearly visible during passage through mitosis, when the cell undergoes a series of dramatic changes in cell shape that function to accurately partition the cell at division (Ramkumar & Baum 2016).

1.2.4.1 Entering mitosis: Mitotic rounding

This process begins with mitotic rounding. Almost all animal cells adopt a round morphology during mitosis, with a few exceptions (Stout et al. 2006; Woolner & Papalopulu 2012; Campinho et al. 2013), leading to the suggestion that it plays a important and conserved role in mitosis. The mechanisms that drive mitotic rounding have begun to be discerned, which has paved the way to an understanding of the function of mitotic rounding. Currently, three main drivers of mitotic rounding have been reported – loss of integrin-mediated adhesion (Dao et al. 2009), the building of a contractile and rigid actomyosin cortex (Maddox & Burridge 2003; Kunda et al. 2008; Carreno et al. 2008; Matthews et al. 2012; Stewart et al. 2011a; Ramanathan et al. 2015), and increase in cell volume (Son et al. 2015; Zlotek-Zlotkiewicz et al. 2015).

1.2.4.1.1 Loss of integrin-mediated adhesion

The role of adhesion loss has been most thoroughly studied in single cells in culture, where mitotic rounding is preceded by disassembly of focal adhesions and the retraction of the cell margin that leaves behind actin-rich retraction fibres, which result in cells becoming round (Cramer & Mitchison 1997). Although many of the adhesion complex components are directly phosphorylated during mitosis (Yamakita et al. 1999; Curtis et al. 2002; Suzuki & Takahashi 2003), the small GTPase Rap1 seems to be the main regulator in integrin-mediated adhesion (Dao et al. 2009). Rap1 activates almost all the integrins linked to the actin cytoskeleton, and is downregulated just before nuclear envelope breakdown (NEB) (Dao et al. 2009). Constitutively active Rap1 prevents basal de-adhesion and cells remain flat and

spread during mitosis, indicating definitively the requirement for basal de-adhesion for normal mitotic rounding (Dao et al. 2009; Lancaster et al. 2013). Cells forced to remain spread during mitosis through the expression of constitutively active Rap1 are delayed in their progression through mitosis as the result of spindle aberrations, impaired chromosome capture and cytokinesis defects (Dao et al. 2009; Lancaster et al. 2013). This led to the proposal that mitotic rounding creates an isotropic shape that simultaneously creates an optimal space for spindle morphogenesis and limits the space for chromosome capture for the timely organisation and separation of chromosomes. Indeed, when cells were mechanically confined to mimic the height and spread of cells with constitutively active Rap1, the same spindle aberrations were observed (Lancaster et al. 2013; Cattin et al. 2015).

A loss of integrin-mediated adhesion and mitotic rounding is also seen *in vivo* in neuroepithelia and radial glia cells, and other pseudo-stratified epithelia such as the *Drosophila* larval wing disc. In these cells, cells round to the apical side of the tissue upon entry into mitosis, leaving thin actin-rich basal processes that remains in contact with the basal lamina (Kosodo & Huttner 2009; Fietz et al. 2010; Meyer et al. 2011). Although Rap1 and its role in integrin signalling is highly conserved (Rebstein et al. 1993; Bos et al. 2001; Ohba et al. 2001), the role of Rap1 in mediating basal remodelling and mitotic rounding *in vivo* is unknown. Studies of Rap1 in epithelia have instead focused on its role in promoting and maintaining the formation of adherens junctions (Bos et al. 2001; Retta et al. 2006; Wang et al. 2013; O'Keefe et al. 2012), while a recent study has found a role for Rap1 in setting up apical polarity in asymmetrically dividing *Drosophila* neuroblasts (Carmena et al. 2011).

In one instance, mitotic rounding in an epithelium has been shown to facilitate invaginations during morphogenesis (Kondo & Hayashi 2013), most likely due to a local shortening of the tissue, which has been linked more generally to tissue buckling (Mao & Baum 2015; Kondo & Hayashi 2015). Shortening the cell along the apico-basal axis has also been proposed to allow the spindle to align along the plane of the epithelium by removing the long axis in the orthogonal direction (Meyer et al. 2011; Nakajima et al. 2013). However, not all epithelia are densely packed, and the formation of perfectly isotropic cell in mitosis is not always favourable. In epithelia

such as MDCK monolayers or the developing mouse epidermis, cells are wider and shorter in interphase, and mitotic rounding is not always complete. In the absence of spindle positioning factors, the spindle remarkably remains within the plane of the epithelium (Williams et al. 2011; Lazaro-Dieguez et al. 2015). It is proposed that the incomplete rounding during mitosis actually facilitates this, either because the spindle cannot position along the height of the cell due to steric hindrance (Lazaro-Dieguez et al. 2015) or because the spindle has an intrinsic ability to find the longest axis of the cell (Williams et al. 2011).

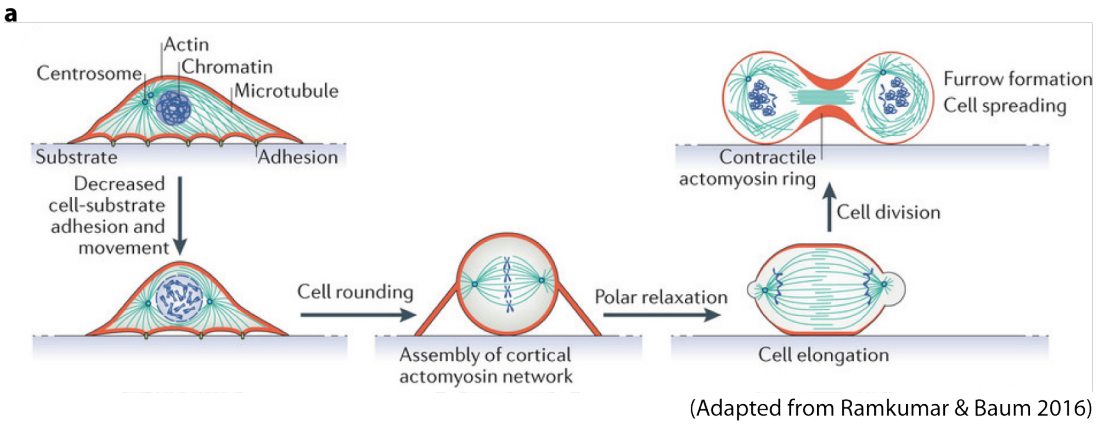

Figure 1.5: Changes in cell shape and actomyosin organisation during mitosis.
a. Cells round up significantly during mitosis, as a consequence of a decrease in substrate adhesion and the formation of a contractile actomyosin cortex. At anaphase, actin is relocalised to the presumptive cytokinetic furrow, while the cell elongates in the direction of the separating spindle poles. During cytokinesis and furrow ingression, a contractile actin ring forms that pinches the mother cell in half.

1.2.4.1.2 Building of a contractile and rigid actomyosin mitotic cortex

Following rounding, mitotic cells assemble a relatively stiff mitotic cortex. This is organised into a thin, contractile and rigid cortical meshwork around the cell (Maddox & Burridge 2003; Matthews et al. 2012). This is facilitated by the release of Ect2 from the nucleus to the cytoplasm, which is regulated by the mitotic kinase Cdk1 (Matthews et al. 2012). Ect2 is a Rho GEF that activates RhoA, which leads to MyoII activation by ROK (Maddox & Burridge 2003; Matthews et al. 2012; Cramer & Mitchison 1997; Meyer et al. 2011). Most recently, it has been found that Pbl (*Drosophila* Ect2) behaves similarly in *Drosophila*, where it regulates the

relocalization and activation of the actin nucleator Dia (via the GTPases Rho and Cdc42) to promote the formation of an isotropic mitotic actin cortex (Rosa et al. 2015). The requirement for formins like Dia but not nucleators of branched actin such as Arp2/3 for actin recruitment to the cortex was independently confirmed in cultured cells (Ramanathan et al. 2015). Dia promotes the formation of parallel F-actin, which is thought to be the preferred substrate for myosin to bind to and generate contractile forces (Reymann et al. 2012). Linking the actin cortex to the plasma membrane through activated ERM proteins is also important for mitotic rounding, presumably because this stabilizes the system by coupling the cortex to the cell surface (Kunda et al. 2008; Carreno et al. 2008).

The changes in the contractile actomyosin cortex and its linkage to the plasma membrane at mitosis results in an increase in apparent cell stiffness at mitosis, which can be measured directly in single cells (Maddox & Burridge 2003; Kunda et al. 2008; Stewart et al. 2011a; Matthews & Baum 2012; Salbreux et al. 2012). The actomyosin cortex counteracts the increase in hydrostatic pressure (discussed below) and the combined efforts of both the increase in cortical tension and hydrostatic pressure generate a so-called rounding pressure (Stewart et al. 2011a). Rounding pressure helps the cell resist mild compression of 15kPa, to allow cell division to occur relatively unperturbed in these conditions (Lancaster et al. 2013). Cells seeded between deformable micropillars also use this rounding pressure to escape lateral confinement during mitosis. This reduced likelihood of apoptosis and allowed spindle alignment along the horizontal plane (Sorce et al. 2015), analogous to cell division within the plane of the tissue.

Rounding pressure is likely to be important in crowded tissues, to allow cells to overcome these crowding by neighbouring cells and generate sufficient space for the spindle to align along its preferred axis (Williams et al. 2011; Nakajima et al. 2013; Lazaro-Dieguez et al. 2015). However, it has been anecdotally observed that mitotic rounding is often incomplete in tissues, likely reflecting the inability of the mitotic cell to overcome these tissue-level mechanical stresses (Williams et al. 2011; Mao et al. 2011; Lazaro-Dieguez et al. 2015; Wyatt et al. 2015). Interestingly, Lazaro-Dieguez et al. observed that cells in MDCK monolayers with impaired mitotic rounding had deformed metaphase plates, suggesting rounding-mediated cell

height plays a role in spindle morphogenesis, as in single cells (Kunda et al. 2008; Lancaster et al. 2013).

1.2.4.1.3 Increase in cell volume and hydrostatic pressure

Additionally, an increase in intracellular hydrostatic pressure was found to contribute to mitotic rounding (Stewart et al. 2011a; Fischer-Friedrich et al. 2014). Consistent with this, it has been shown that mammalian cells also increase their volume during mitosis (Son et al. 2015; Zlotek-Zlotkiewicz et al. 2015). Increase in cell volume and hydrostatic pressure seems to be primarily driven by the influx of water, through electro-neutral ion exchange by the Na-H exchanger (Stewart et al. 2011a; Son et al. 2015) and is calculated to be on the order of ~100kPa, which would be sufficient to deform almost any tissue (Zlotek-Zlotkiewicz et al. 2015). Meanwhile, surface tension due to the actomyosin cortex acts inwards against this increase in cell volume, albeit on a much smaller scale ($\sim$0.1 – 1 kPa) (Salbreux et al. 2012). Therefore changes in the actomyosin cortex cannot induce a significant change in cell volume (Stewart et al. 2011a; Salbreux et al. 2012; Zlotek-Zlotkiewicz et al. 2015).

All three mechanisms appear to run parallel to each other to drive mitotic rounding. As is observed, for example, by the building of an actomyosin cortex despite constitutive integrin signalling (Dao et al. 2009; Lancaster et al. 2013; Dimitracopoulos 2016); by the ectopic rounding in interphase by overexpression of Ect2 in single cells (Matthews et al. 2012) or Cdc42 or Dia in the *Drosophila* notum (Rosa et al. 2015); and by the increase in cell volume in cells lacking an actomyosin cortex or substrate adhesion (Son et al. 2015; Zlotek-Zlotkiewicz et al. 2015).

1.2.4.2 Exiting mitosis: Cell division

As cells exit mitosis, they undergo the second series of dramatic cell shape changes where the cell elongates to allow for spindle elongation at anaphase, and forms a cytokinetic ring to divide the mother cell into two.

1.2.4.2.1 Relocalization of actomyosin to the presumptive furrow

The positioning of the division plane in animal cells is defined by the position of the overlapping microtubules in the spindle midzone during anaphase (Rappaport 1996; Rappaport 1997). Here, the spindle midzone recruits a set of proteins collectively known as the centralspindlin complex which recruit Ect2 to the spindle midzone (Green et al. 2012; Cheffings et al. 2016). Just as before, where Ect2 localization to the cortex resulted in the formation of the actomyosin cortex, Ect2 now directs the assembly of an actomyosin network at the site of furrow ingression (Ramkumar & Baum 2016).

While the spindle midzone is able to organize the cortical actomyosin network, asymmetries in the cortical localization of myosin are able to influence the positioning of the site of furrow ingression as well. Asymmetric myosin is able to affect anaphase elongation and therefore the position of the spindle midzone (Ou et al. 2010) or directly induce ectopic sites of furrow ingression independent of the spindle midzone (Cabernard et al. 2010; Pacquelet et al. 2015).

The redistribution of actomyosin to the furrowing region of the cell results in a gradient of contractility across the cell, with contractility concentrated at the site of furrow ingression. Although a gradient of contractility in itself may not be sufficient to specify the division plane (Rappaport 1999), theoretical papers suggest it may be important in some cases (Turlier et al. 2014; Sehring et al. 2015). A local reduction of polar cortical contractility once furrow ingression initiates is important for the progression of cytokinesis as it releases the transient increase in hydrostatic pressure as the furrow ingresses (Sedzinski et al. 2011). In cells, this is aided by the inactivation of phosphorylated ERM at the cell poles, which previously bound actin to the plasma membrane (Rodrigues et al. 2015). The overall result being the formation of the typical peanut shape during cytokinesis, as the cell constricts in the middle and balloons at the poles.

1.2.4.3 Mechanical constraints on furrow ingression

In polarized tissues such as epithelia, furrow ingression occurs from the basal to the apical plane (Bourdages & Maddox 2013; Le Bras & Le Borgne 2014), while

in adherent cells in culture, furrow ingression is much more likely to occur from the non-adherent plane towards the substrate (Taneja et al. 2016). In both cases, the anchoring of the cytokinetic ring to either adherens junctions or mitotic focal adhesions, results in the asymmetric closing of the cytokinetic ring. In a similar way, furrow ingression in mitotic cells in an epithelia is also mechanically restricted by neighbouring cells. This resistance against furrow ingression maintains the cell boundaries apart for the formation of a straight junction between the two daughter cells (Herszterg et al. 2013).

1.3 Coordinating the actin and microtubule cytoskeleton during mitosis

1.3.1 The actomyosin cortex and centrosome separation

The cortical flow of actomyosin has been shown to facilitate centrosome separation and position at NEB (Rosenblatt et al. 2004; De Simone et al. 2016). De Simone et al. propose a mechanism where dynein is crosslinked to the actomyosin cortex, coupling cortical flows to the centrosomes and facilitating their separation. Similarly, the expanding actin cap in *Drosophila* embryos has been shown to promote centrosome separation through the physical linkage of the cortex and astral MTs of the centrosome (Robinson et al. 1999; Sharp et al. 2000; Buttrick et al. 2008; Cao et al. 2010).

Most recently, the actin and MT cytoskeleton have been shown to emanate from the same structure – the centrosome. WASH and Arp2/3 localise to isolated centrosomes where they nucleate the formation of F-actin (Farina et al., 2016). This opens up the possibility that actin at the centrosome might directly interact with actin at the cortex through actin-binding proteins. Intriguingly, ROK (the major activator of Myo II) has also been identified at the centrosome in mammalian cells, where it was shown to be required for centrosome positioning in interphase, but not mitosis (Chevrier et al. 2002).

1.3.2 The actomyosin cortex and spindle formation

Actomyosin cortical flows were also shown to be important after NEB, to promote the further separation of centrosomes into bipolar structures, as 'lopsided' spindles were often seen upon inhibition of cortical flows (Rosenblatt et al. 2004). Actin has also been suggested to directly interact with the spindle, through Myosin X (Myo X). Myo X is a unique myosin motor as it can bind simultaneously to MTs as well as actin (Homma et al. 2001; Weber et al. 2004; Homma & Ikebe 2005). It is found at mitotic spindle poles in *X. laevis* embryos and is required to prevent spindle pole fragmentation, but also to link subcortical actin to the spindle. Here, subcortical actin appears to result in spindle lengthening, possibly by pulling on spindle poles (Woolner et al. 2008). Myo X has also been proposed to play a role in spindle

formation, through its interaction with the actin-binding protein, Adducin (Kwon et al. 2015; Chan et al. 2014).

1.3.3 The actomyosin cortex and spindle positioning

It has been observed that a loss of actin at the cortex leads to a corresponding loss of the proteins involved in cortical force generation at the cortex in some cell types (Luxenburg et al. 2011; Zheng et al. 2013; Johnston et al. 2013; Machicoane et al. 2014). The actomyosin cortex might affect localization of spindle-orienting proteins indirectly through its role in cell polarity maintenance, or it might directly bind cortical force generators. The recent discovery that Afadin (Canoe in *Dros*) can bind LGN (Pins in *Dros*) and F-actin concomitantly provided the first evidence that the actin cortex might be directly linked to the cortical force generation machinery (Carminati et al. 2016). In *Drosophila*, Canoe binds to Pins and promotes its cortical localization (Wee et al. 2011). However, a direct link to F-actin was not demonstrated in the study. In another system, Canoe has been shown bind to Dsh in the context of the Dsh/ Mud/ dynein complex, where it has been proposed to recruit Rho to locally activate Dia and F-actin (Johnston et al. 2013).

F-actin and MT stabilization also directly communicate in many systems. Some appear to be in a positive feedback, for example, Dia has been shown to stabilise MTs (Pawson et al. 2008; Vitiello et al. 2014), while the +TIP protein CLIP-170 binds to Dia and promotes actin plus-end polymerization (Henty-Ridilla et al. 2016). Another actin-binding protein, Moe was also shown to bind to and stabilise MTs at the cell cortex in *Drosophila* S2 cells (Solinet et al. 2013). Interestingly, activated ERMs in human cells have been correlated to the localization of NuMA and LGN at the cortex (Machicoane et al. 2014), demonstrating further the potential role for ERMs in spindle positioning. Others are in a negative feedback, such as the activation of Rho GEF-H1 after the loss of MT-binding (Krendel et al. 2002).

The attachment of astral MT plus-ends at the cortex might also couple actomyosin flows to spindle movement, as has been observed for interphase centrosomes and during centrosome separation, and proposed to be involved in planar positioning of spindles in *X. laevis* embryos (Woolner & Papalopulu 2012). In

line with this, Myo II or ROK inhibitors result in spindles mis-aligning with the cell shape and simultaneous defects in spindle rotation (Campinho et al. 2013; Wyatt personal communication).

Astral MT-cortex interactions might also promote the delivery of cortical force generators to the cortex by MT plus ends, as the loss of actin results in an increase in cortical force generators localised to MT minus ends at the spindle poles (Zheng et al. 2013). Once cortical force generators are localised to the cortex, the rigidity provided by the activity of actomyosin might resist the tension along astral MTs, allowing the spindle pole to be pulled towards the cortex effectively. This theory was proposed after observations that at low cortical tension, membrane invaginations can be seen towards the spindle poles (Redemann et al. 2010).

Most recently, actin extending out from the cortex into the cytoplasm has been suggested to directly interact with the spindle and orient it towards so-called subcortical actin. This is well-established in meiotic divisions in many systems, where chromosomes must be gathered together in a huge egg to form a spindles in the absence of centrosomes (Field & Lénárt 2011). In mice, spindle positioning is effected instead by an actin cage that extends from the cortex and forms around the spindle, moving the spindle off-centre and towards the cortex (Schuh & Ellenberg 2008; Chaigne et al. 2013).

Subcortical actin has also been observed in human cells (Fink et al. 2011; Kwon et al. 2015) and *X. laevis* embryos (Woolner et al. 2008). In human cells, this actin cloud is generated by the Arp2/3 complex (Mitsushima et al. 2010) spindles appear to move towards subcortical actin clouds in the x-y plane (Fink et al. 2011), in a Myo X-dependent manner (Kwon et al. 2015). Myo X in these cells is localised to the cortex, and promotes end-on attachment of astral MTs, while dynein promotes lateral movement of the astral MTs along the cortex, and the two mechanisms act in complementary fashion (Kwon et al. 2015). It is not clear how subcortical actin and MTs interact in this system, if Myo X is localised to the cortex. In *X. laevis* embryos, a basal to apical flow of actin is present along the cell cortex during mitosis (Woolner & Papalopulu 2012). In this system, Myo X is instead localised to the spindle poles, where it is presumed to bridge the spindle and subcortical actin

(Woolner et al. 2008), and is required to counteract the cortical actomyosin flow by promoting the lengthening of astral MTs between the spindle and the apical surface (Woolner & Papalopulu 2012).

1.4 The *Drosophila* notum as a model system

The model system I use is the *Drosophila* pupal notum, which gives rise to the adult dorsal thorax (Simpson 2007). The tissue is formed by the fusion of part of the larval wing discs that have moved from the lateral sides to the middle of the animal along the anterior-posterior axis, in a way that is similar to embryonic dorsal closure (Zeitlinger & Bohmann 1999).

The notum is a cuboidal epithelial monolayer, and is polarized along the apical to basal planes by canonical polarity proteins (Rosa 2013). During the course of pupal development, the tissue also develops a thin underlying basement membrane (Curran 2015). During development, the notum undergoes a series of simple cellular events that alter cell packing, including adherens junction remodelling, cell division, cell delamination and apoptosis (Marinari et al. 2012; Curran 2015). These events serve to refine the tissue such that it achieves hexagonal packing towards the end of development (Curran 2015), which is indicative of mechanical equilibrium (Gibson & Gibson 2009).

1.4.1 Tissue mechanics of the notum

In the early stages of development, from 12-14h after pupariation (AP), the middle of the tissue along the anterior-posterior axis termed the midline (ML) appears crowded by the regions lateral to it, termed outside the midline (OML). Apical areas and nuclei of ML cells appear deformed laterally, such that they are elongated along the anterior-posterior axis, and their nuclei are displaced further basally within the tissue (Marinari et al. 2012). As adherens junctions are under constitutive actomyosin-generated tension that is increased along cell-cell contacts upon externally applied stretch (Borghi et al. 2012), they are a good indicator of tissue tension. Laser cuts of adherens junctions in the notum revealed that ML cells are under little to no tension, while adherens junctions of OML cells are under significantly higher tension (Marinari et al. 2012). This suggested that the elongated shape of ML cells is due to crowding rather than tension in the region.

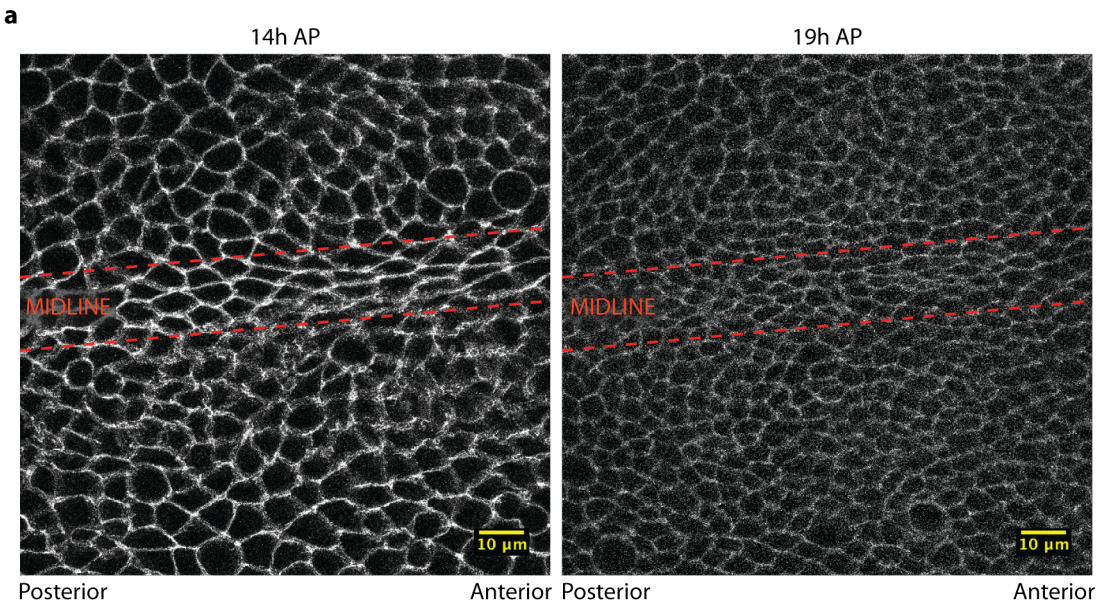

Figure 1.6: Topology of the *Drosophila* notum during development.

a. Cells are outlined with Dlg::YFP (white), which labels septate junctions and lateral membrane. The midline (ML) is marked out with red dashed lines. Cells appear much more elongated in the ML than OML at 14h AP before divisions occur in this tissue. By 19h AP, cell shapes are similar between the ML and OML region of the tissue.

1.5 Aims of the thesis

As is evident from the discussion above, much is known about spindle positioning in animal cells, and there are many suggestions of crosstalk between the cell cortex and the spindle. However, many questions remain regarding the role of actomyosin in spindle positioning, especially in the context of the epithelium. In this thesis I aim to investigate this further using the *Drosophila* notum as a model system, where genetic tools are readily available and live-imaging is possible. Furthermore, by comparing elongated cells under different mechanical environments (inside and outside the midline), I can explore the role of cell shape and mechanics in spindle orientation in symmetrically dividing cells.

To do this, my first goal was to understand cell shape changes during mitosis in the epithelium, and the role of actomyosin and tissue mechanics in regulating these changes. After identifying the degree of cell shape change in a tissue during mitosis, I then moved on to investigating the role of cell shape in spindle positioning. I began by studying the dynamic nature of spindle positioning independent of cell shape, and the role of forces along astral MTs in regulating this. I next placed this dynamic movement in the context of spindle positioning relative to the cell shape, and study the role of tissue mechanics and myosin activity with regard to dynamic spindle positioning relative to cell shape.

In the next chapters, I present the methods used to address these questions and to analyse the findings of these experiments.

Chapter 2 Materials and methods

2.1 Live-imaging

Drosophila pupae were selected at the white pre-pupal stage, 0h after pupariation (AP), and imaged at 14.5h AP for 2-3h at room temperature. Developmental time was halved when incubated at 29°C; and doubled when incubated at 18°C. Pupae for live imaging were attached to a glass slide ventral side down with double-sided tape between spacers made with small glass coverslips. The pupal case was removed from the dorsal side of the animal and a glass coverslip coated with mineral oil on one side was placed over the spacers, just touching the dorsal tissue of the pupa. The entire set-up was placed under the microscope for live-imaging (Zitserman and Roegiers, 2011; Georgiou and Baum, 2010).

Imaging was done on Leica SPE and SP5 confocal microscopes with a 63X lens (1.4 N.A.) or 60X lens (1.3 N.A.) respectively.

2.2 Immunohistochemistry

Drosophila pupae for immunostaining were dissected at 15h AP. Pupae were pinned with sharpened wires dorsal side down onto a PDMS dish filled with PBS. The pupal head was removed with small surgical scissors and the ventral length of the pupa was cut out. The dorsal tissue around the notum was isolated and transferred into glass wells with micropippettes for fixing and staining. Dissected nota were stained with the following antibodies and probes:

Antibody/ probe	Concentration	Source
Mouse anti-Discs large	1: 100	DSHB
Rabbit anti-Mushroom body defect (Mud)	1: 500	Basto, R.
Guinea pig anti-Centrosomin (Cnn)	1: 1000	Dobbelaere, J.
DAPI	1 μg/ ml	Molecular Probes

Mouse anti-GFP	1: 500	Abcam
Phosphorylated myosin II light chain (S19, T18)	1: 50	Cell Signalling

Alexa conjugated fluorophores were used in secondary stains. Immunostained nota were imaged on Leica SPE confocal microscopes with a 63X lens (1.3 N.A.)

2.3 Fly stocks used

2.3.1 Background and visualising of cell outline and mitotic structures

Stock	Source
w^{1118};;;	BL 3605
w^{1118};; pnr-GAL4;	BL 3039
w^{1118};; UAS-Lifeact-GFP;	Schnorrer, F.
;; Spider-GFP;	Flytrap Insertion (BL 59025)
; DE-Cadherin-GFP;;	Cambridge Protein Trap Insertion (DGRC 115375)
Discs large (Dlg)-YFP;;;	Cambridge Protein Trap Insertion (DGRC 115375)
; Basigin-GFP;;	Cambridge Protein Trap Insertion (DGRC 115366)
w*;; sqh-Sqh-mCherry;	Wieschaus, E.
w^{1118}; ubi-RFP-Cnn;;	Raff, J.
; actin-GAL4, UAS-mCherry-α-Tubulin;;	Recombined from BL4414 and

	BL25774 by Rodrigues N.
w*; UAS-mCherry-α-Tubulin;;	BL 25774

2.3.2 RNAi-mediated silencing

Interfering RNA transcripts targeting expression of proteins were expressed using the GAL4/ UAS system (Brand and Perrimon, 1993; Busson and Pret, 2007). GAL4 expression was under the control of the *pannier* gene (Pnr-GAL4) (Calleja et al., 2002), restricting GAL4 binding of UAS response elements and subsequent expression of constructs to the central region of the notum. Pupae in RNAi experiments were incubated at 25°C or 29°C from 9-14.5h AP or 0-14.5h AP to ensure efficient expression of GAL4. Where lethality was seen under these conditions, pupae were incubated at 18°C from 0-14.5h AP to reduce the activity of GAL4.

The following fly stocks were used in RNAi-mediated silencing:

Stock	Source
Diaphanous (Dia)	VDRC 103914 (Rosa et al. 2015)
Discs large (Dlg)	NIG 17525R-1 (Wang et al. 2015)
Mushroom body defective (Mud)	BL 35044 (Nakajima et al. 2011)

2.3.3 Protein coding constructs

Constructs were expressed using the GAL4/ UAS system (Brand and Perrimon, 1993; Busson and Pret, 2007). GAL4 expression was under the control of the *pannier* gene (Pnr-GAL4) (Calleja et al., 2002), restricting GAL4 binding of UAS response elements and subsequent expression of constructs to the central region

of the notum. All pupae were incubated at 25°C or 29°C from 9-14.5h AP or 0-14.5h AP to ensure efficient expression of GAL4.

Stock	Source
;; UAS-Sqh^{AA}/ TM6B, Tb;;	Winter et al., 2001
;; UAS-Sqh^{EE}/ TM6B, Tb;;	Winter et al., 2001
; UAS-Rap1^{V12};;;	Boettner et al., 2003

2.3.4 Asterless^{mecD} experiments

;; Asl^{mecD}/ TM6B, Tb;; flies were a gift from Raff, J. Experiments were done by crossing Dlg-YFP;; Asl^{mecD}/ TM6B, Tb;; flies with ; actin-GAL4-UAS-mCherry-α-Tubulin; Asl^{mecD}/ TM6B, Tb;; flies. Pupae homozygous for the Asl^{mecD} allele were identified by selecting against TM6, Tb (tubby phenotype).

2.4 Image analysis

2.4.1 Quantification of cell shape

The medial plane was identified as the plane where majority of the spindle was located, which was usually the plane with both spindle poles visible. The cell outline in the medial plane was manually marked out in FIJI (http://fiji.sc/Fiji). The centroid of the outline was taken as the cell centre, while the major length and minor length of the fit ellipse to the outline were taken as length and width of the cell. The angle of the major length of the fit ellipse was taken as the orientation of the long axis of the cell.

2.4.2 Quantification of spindle movements

Spindle movement was tracked by drawing a line between the visible spindle poles from NEB through to anaphase. Spindle angle, centroid and length were recorded, and spindle pole coordinates were calculated from these values. Spindle pole coordinates for a spindle with centroid coordinates (x, y), length l and angle θ,

were calculated as $(x + \frac{l}{2} \cdot \cos\theta\,, y + \frac{l}{2} \cdot \sin\theta)$ and $(x - \frac{l}{2} \cdot \cos\theta\,, y - \frac{l}{2} \cdot \sin\theta)$. Spindles were not considered for analysis if apparent spindle poles were more than 1.5 μm height apart. Spindle measurements were taken with Tubulin-mCherry marking the spindle or Centrosomin-RFP marking the spindle poles. Calculations of spindle angles were similar for measurements done with Tubulin or Centrosomin as a marker, and so the results were pooled. Calculations of spindle length and centroid (including spindle pole coordinates) were significantly different when comparing between measurements taken with Tubulin or Centrosomin as a marker. This was likely due to tubulin being less precise for identifying the spindle poles and therefore spindle length and centre. These measurements were separated based on markers across perturbations, and the markers used in each analysis are identified in the text. Spindle movement was tracked every 1 min or 30sec. When comparing between datasets imaged at different time intervals, data obtained at 30 sec intervals was artificially reduced to 1 min intervals.

2.4.3 Identification of mitotic events

Mitotic time was taken as the time from nuclear envelope breakdown (NEB) till anaphase onset. NEB was identified as the first timeframe when nuclear exclusion of background fluorescent signal disappeared. Anaphase onset was identified in cells expressing Tubulin-mCherry as the first timeframe when tubulin accumulation towards the spindle poles was observed, ~ 3min before furrow ingression begins. In movies using only Centrosomin-RFP as a marker, anaphase onset was taken as the timeframe 3min before furrow ingression begins. Late metaphase was defined as 1min before anaphase onset.

2.5 Statistical analysis and data visualisation

Two sample Wilcoxon ranked sum test was performed to compare medians between data, using the wilcox.test() function in R. Two sample Kolmogorov-Smirnov test was performed to compare distributions of datasets, using the ks.test() function in R. Random uniform distributions were generated with the runif() function in R.

Graphpad Prism and R (ggplot2 library) were used to generate graphs representing the data. Line plots representing median over time, with error bars representing interquartile range were generated in Prism. Individual line plots representing spindle orientation over time were generated in R. Boxplots were generated with the geom_boxplot() function in R, with the boxes representing the upper quartile, median and lower quartile of the data, and whiskers representing the data within 1.5 times the interquartile range flanking the upper and lower quartiles. All remaining data (outliers) are represented as points. All data was plotted, unless stated otherwise in the text. Density plots were generated with the geom_density() function in R, with the default binwidth of 1. Dotplots were generated with the geom_dotplot() function in R, with binwidths stated in the text. Linear regressions were performed with the lm() and geom_smooth(method=lm) function in R, and best-fit linear mean lines with standard error of the mean were plotted. All stated R^2 values are adjusted R^2 values.

Chapter 3 Changes in cell morphology during mitosis

3.1 Introduction

Experiments confining cells in culture suggest that mitotic rounding is important for cells to push against confinement by neighbouring cells in epithelium (Lancaster et al. 2013; Sorce et al. 2015; Fischer-Friedrich et al. 2016). In line with this, perturbations of ROK in the pseudostratified epithelium of the *Drosophila* wing disc observe that mitotic rounding is defective, and the authors propose that this led to spindle orientation defects (Nakajima et al. 2013). However, this was done in fixed tissues, and to link mitotic rounding to spindle orientation requires tracking of the changes in cell geometry relative to the spindle morphogenesis and orientation. I therefore begin by observing and tracking the changes in cell shape as the cell enters mitosis in a *Drosophila* notum epithelium. I then investigate the impact of tissue packing on mitotic rounding, before testing the role of actomyosin and integrin signalling in mitotic rounding in an epithelium.

3.2 Cells round up during mitosis in a crowded epithelium similar to isolated cells in culture

3.2.1 Cell rounding in the epithelium during mitosis

To observe if a similar process of basal de-adhesion occurs in columnar epithelia like the *Drosophila* notum, I expressed LifeAct-GFP to visualise the mitotic cell (Fig 3.1a). As cells enter mitosis, it leaves behind a space devoid of actin signal in the basal plane of the epithelium. These gaps in the expression of LifeAct-GFP persist until cytokinesis (Fig 3.1a). Blebs, which are commonly seen during cytokinesis, can be seen occasionally extending into this region absent of actin (Fig 3.1a). By the end of cytokinesis, and before midbody dissolution, the daughter cells have re-established basal adhesion (Fig 3.1b), apparently in the same adhesion space as the mother cell.

To better visualise changes in cell shape before, during and after mitosis, I imaged cells where Shotgun (*Drosophila* ECadherin) was endogenously tagged with

GFP and where the basolateral protein Dlg was endogenously tagged with YFP. Although NEB could not be visualised with these markers, mitotic rounding could be observed. This was first seen as an increase in area and circularity in the mediolateral plane of the cell. Subsequently, cell area increased in the lateral and apical planes, and most of the cell mass moved apically (Fig 3.2). Cells were at the roundest by late metaphase (Fig 3.2, 21 min). The cell pictured is close to a hemisphere, with cell height (~4 μm) close to half of cell length and width at the apical plane (~11 μm and ~9 μm, respectively).

It is important to note that the observed cell morphology was not consistent from apical to basal planes. That is, the shape and orientation of cell shapes at the apical surface, marked by cadherin was significantly different to that seen at the mediolateral and basal planes of cells. This was true during interphase, and upon entry into mitosis, where mitotic rounding is significantly more complete in medial planes (the widest plane of the mother cell). The apical plane of the cell did not change much from interphase to mitosis. This might be explained by the presence of cadherins and actomyosin at adherens junctions, which resist deformation at the apical surface.

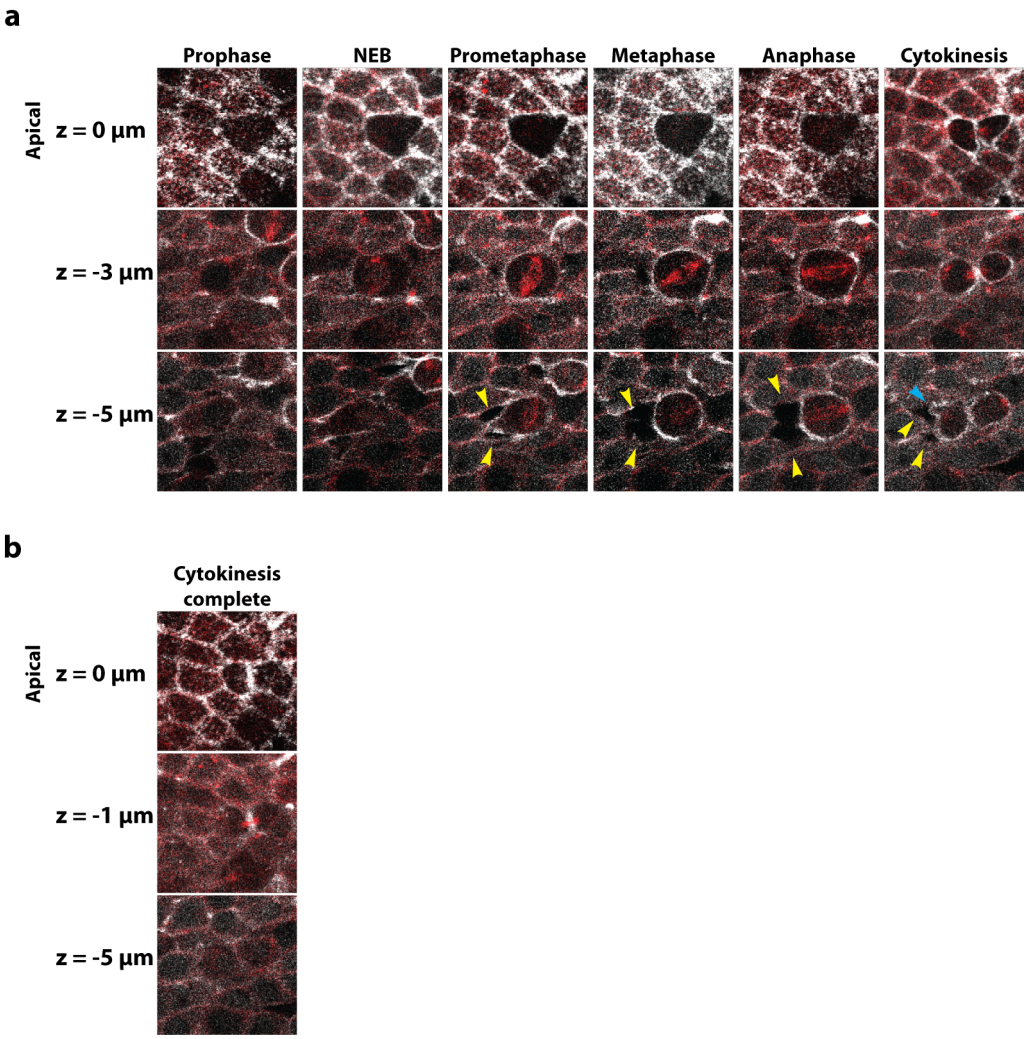

Figure 3.1: Cells undergo basal remodelling and mitotic rounding in an epithelium.
a. Representative cell dividing in the *Drosophila* notum. Mitotic cell outline is labelled with LifeAct-GFP (white) and tubulin is labelled with Tubulin-mCherry (red). NEB was defined as the first timepoint when nuclear exclusion of Tubulin-mCherry disappeared (compare z = -3µm for Prophase and NEB). Actin recruitment to the basolateral planes of the mitotic cell are visible at NEB. As mitosis proceeds, cells get rounder and spaces in the actin signal between neighbouring cells in the basal plane can be seen (yellow arrowheads). By late metaphase (timeframe before anaphase onset), a clear absence in actin signal is visible in the basal plane (yellow arrowheads). Basal actin is absent through anaphase and cytokinesis. Blebs can be seen during cytokinesis (blue arrowhead) into the space without actin.
b. Daughter cells lose round morphology and basal actin is restored at the end of cytokinesis, before abscission.

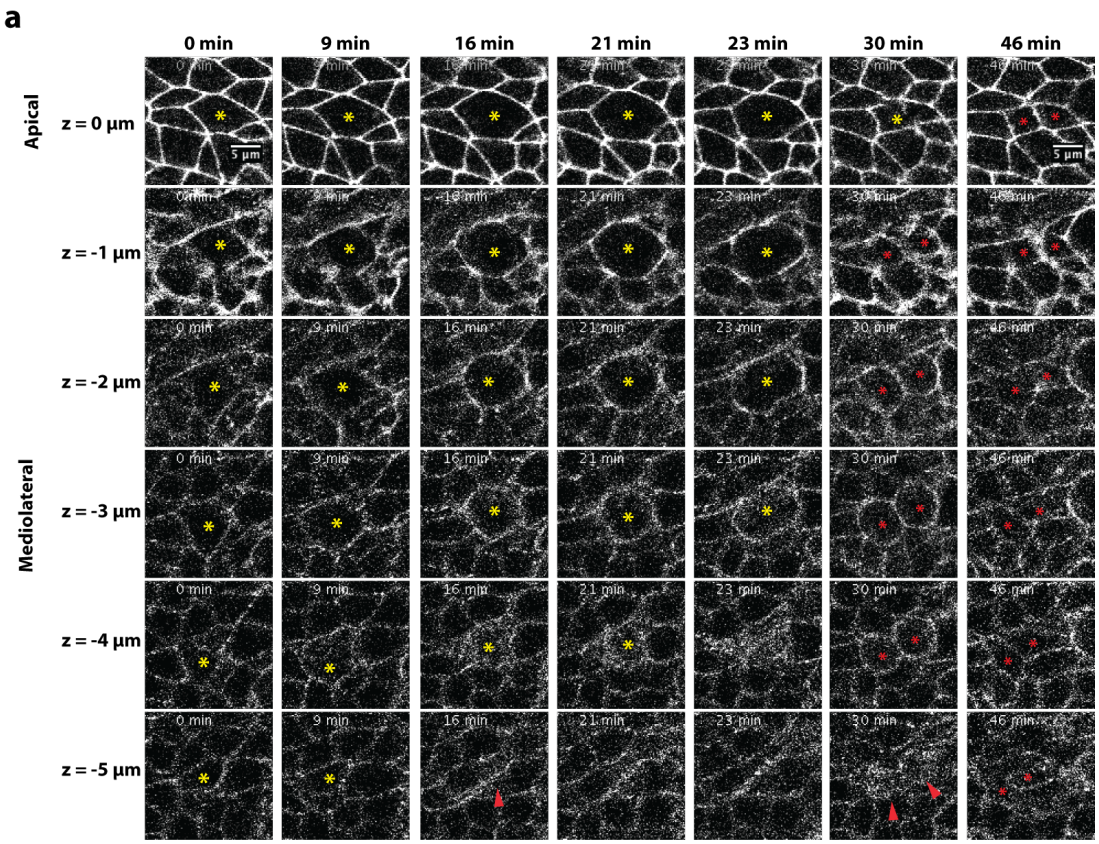

Figure 3.2: Cell shape changes vary significantly between apical and basolateral planes of the epithelium.

a. Representative cell dividing in the *Drosophila* notum (yellow asterisk) with daughter cells marked with red asterisks. Cell outlines are marked with DECadherin (DCad)-GFP and Discs large (Dlg)-YFP (white). NEB is not visible in this background. Before mitotic rounding (0 min), cell shape varies significantly from apical to the basal plane. Mitotic cell rounding begins at the mediolateral plane (compare z = -3 µm to z = 0 µm and z = -5 µm at 9 min). Basal remodelling occurs as mitotic rounding proceeds (red arrowheads), and the mitotic cell is no longer clearly visible (compare z = -5 µm at 9 min and 16 min). Furrow ingression during cytokinesis proceeds from the basolateral to the apical plane (compare 23 min and 30 min). Daughter cells occupy a similar adhesion area as the mother cell (compare 46 min and 0 min).

3.2.1.1 Changes in cell shape are concomitant with myosin recruitment

Actomyosin at the cortex has been suggested to be the main driver of cell shape changes in mitosis (Cramer & Mitchison 1997; Maddox & Burridge 2003; Matthews et al. 2012; Ramkumar & Baum 2016). I therefore tracked the changes in localisation of myosin in the cell to see if cell shape changes correlated with myosin at the cortex (Fig 3.3).

Consistent with this, I observed in the *Drosophila* notum that mitotic rounding and the recruitment of myosin to the basolateral plane of the mitotic cell was visible before NEB (Fig 3.3), likely due to the slow export of Pbl from the nucleus in prophase (Rosa et al. 2015). After NEB and as mitosis proceeds, myosin recruitment around the cell periphery in the mediolateral planes continues and the cell becomes increasingly round (Fig 3.3).

In cells in a tissue, during anaphase (indicated by cell elongation in the medial plane), myosin was seen to relocalise to the equator of the cell in the more basal plane (Fig 3.3). This was the site of later furrow ingression, which propagates from the more basal planes towards the apical plane as previously described in other epithelia (Morais-de-Sá & Sunkel 2013; Herszterg et al. 2013; Guillot & Lecuit 2013a; Le Bras & Le Borgne 2014).

The observation that myosin localization is concomitant with changes in cell shape during mitosis is consistent with proposed models where the dynamic relocalization of Ect2/ Pbl and consequently the actomyosin network, are major drivers of changes in cell shape during mitosis (Matthews et al. 2012; Ramkumar & Baum 2016).

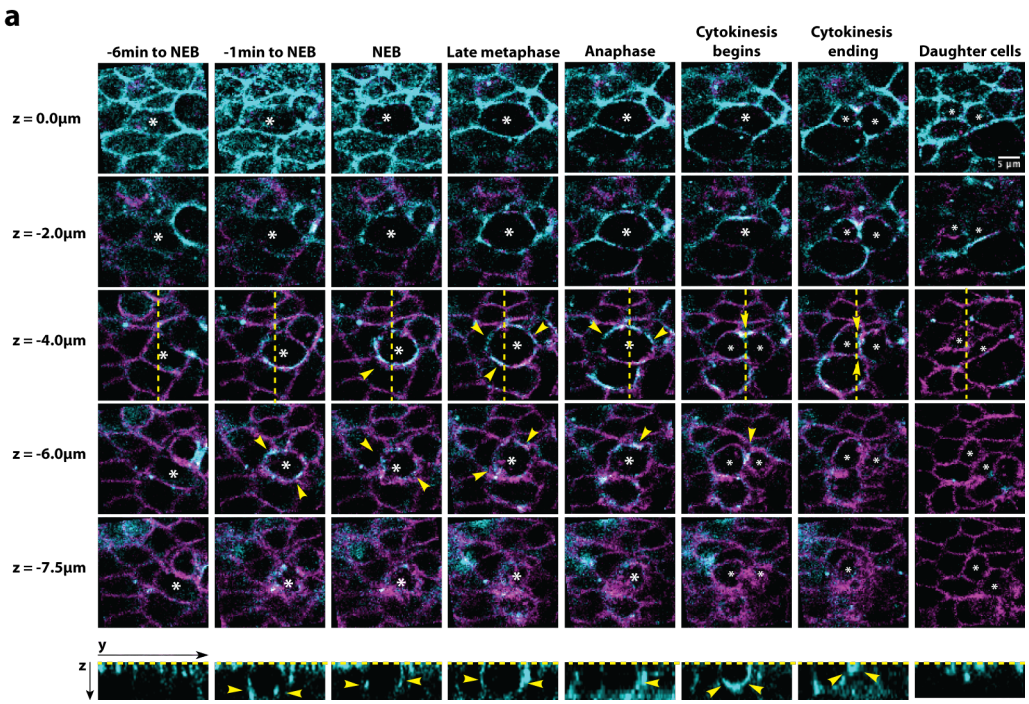

Figure 3.3: Myosin relocalisation during mitotic rounding.

a. Representative cell dividing (white asterisk). Myosin is labelled with Squash-mCherry (Sqh-mCh, cyan) and the basolateral membrane of the cell is labelled with Basigin-GFP (Bsg-GFP, magenta). Apical plane is z=0.0 µm and yellow dashed line indicates orthogonal section shown in the YZ panel. NEB was identified as the first time point where nuclear exclusion of background Sqh-mCh signal disappeared. Basal remodelling (note the membrane blebbing) and myosin recruitment (yellow arrowheads) can be seen before NEB (-1min to NEB). Further myosin recruitment (yellow arrowheads) can be seen from NEB up till late metaphase (timeframe before anaphase onset). By late metaphase, mitotic rounding is significant in the basolateral planes (z = -4 to -7.5 µm, marked by Bas-GFP), while the apical planes (z = 0 to -2 µm, marked by Sqh-mCh only) retain a clear long axis and strongly resemble the pre-mitotic shape. Myosin relocalises to the presumptive cleavage furrow at anaphase onset (Anaphase, yellow arrowhead at z = -6.0µm). Furrow ingression occurs from the basal plane to the apical plane (compare apical to basal planes in Cytokinesis begins). Daughter cells assume a similar shape to the interphase shape of mother cell after division (compare Daughter cells to -6 min to NEB).

3.2.1.2 Mitotic rounding is affected by tissue mechanics

Having established the sequence of mitotic rounding I wanted to see how it was affected in different regions of tissue. This is likely to be affected by neighbourhood local constraints that can manifest as local stretch when cells are sparsely packed (in some regions outside the midline [OML]) or local compression where cells are densely packed (such as within the midline [ML])(Lecuit & Lenne 2007; Guillot & Lecuit 2013b; Heisenberg & Bellaïche 2013; LeGoff & Lecuit 2015; Mao & Baum 2015). Indeed, it was often observed that a significant proportion of OML and ML did not round up perfectly by metaphase (Fig 3.4, 3.5).

To better understand the cause of incomplete mitotic rounding, I used the membrane marker Spider-GFP, to follow changes in cell shape throughout the height of the cell. I focused on the degree of mitotic rounding in the medial plane of the mitotic cell, as this was where changes in cell shape were most dramatic. I further restricted the analysis to cells with some elongation in the medial plane (aspect ratio > 1.1) during late metaphase (before the onset of anaphase) as I reasoned that these cells were likely to be under mechanical constraints. As it was difficult to identify the cell outline at interphase with Spider-GFP due to its nuclear signal, my analysis was limited to early in the onset of mitotic rounding (at NEB), up to late metaphase (before the onset of anaphase) (Fig 3.4a, 3.5a).

This revealed that cells that were the most anisotropic at metaphase were also the most anisotropic at NEB ($R^2 = 0.2121$). This was however, not due to a restricted ability to round up, as cells that were the most anisotropic at NEB, reduced their ellipticity the most ($R^2 = 0.6578$). This suggests that cells are attempting to achieve a minimal energy state (i.e. a round morphology) and the cells furthest from the isotropic state reduce their anisotropy the most. However, while mitotic rounding is significant for cells that are initially very anisotropic, it is not sufficient to overcome the constraints due to cell-cell adhesion and cell crowding.

I then analysed the degree of change in mitotic rounding in ML cells (Fig 3.5), where I expect forces due to cell crowding to be much larger than in OML cells, and the consequent effects on mitotic rounding to be greater.

ML cells reduce their anisotropy significantly from NEB to metaphase, and cells that were the most anisotropic at metaphase were also the most anisotropic at NEB (Fig 3.5b). However, the percentage decrease in ellipticity is lower in ML cells compared to OML cells (Fig 3.5c), especially for cells that are more anisotropic at NEB. This is consistent with the idea that external forces in the form of cell crowding in a tissue imposes limits on mitotic rounding.

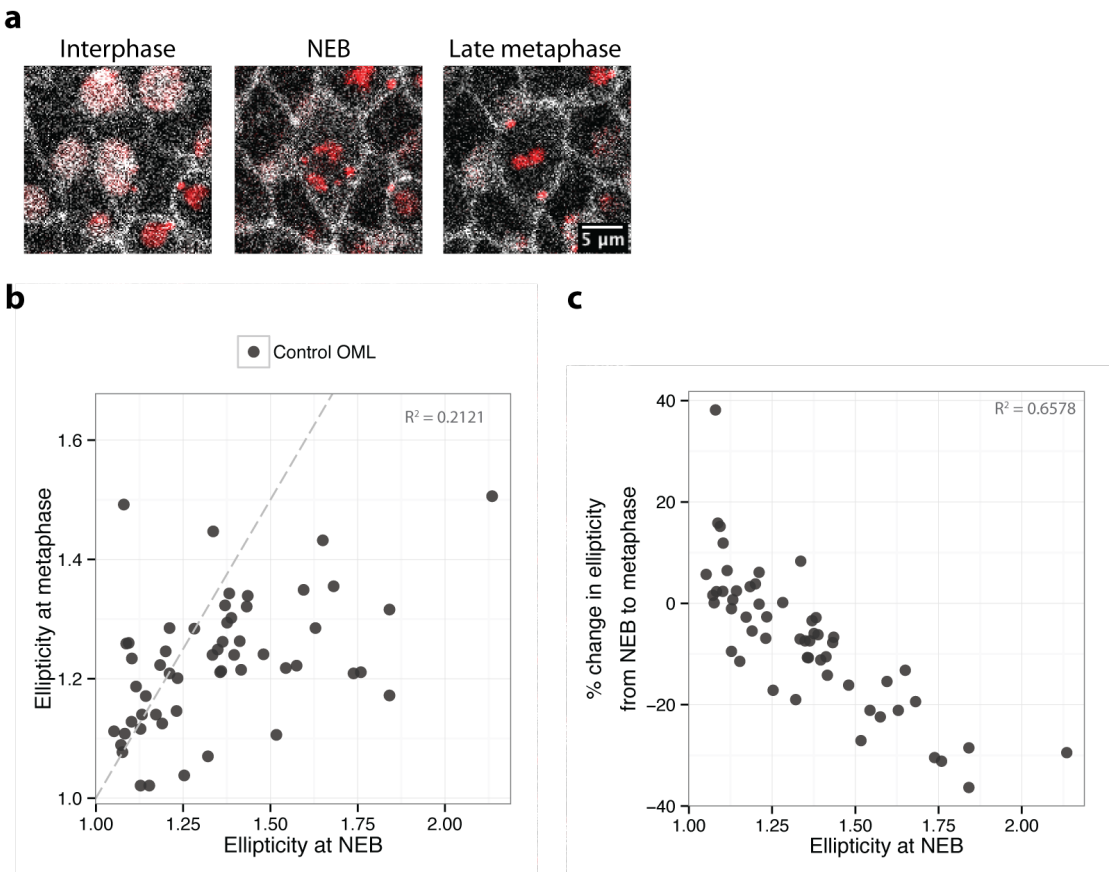

Figure 3.4: Incomplete mitotic rounding at metaphase reflects previous cell shape deformation.

a. An elongated cell outside the midline entering and exiting mitosis. Cell outlines are marked with Spider-GFP. Cells with a clear long axis in interphase retain this long axis in mitosis and have an elliptical shape during mitosis.

b. Cell ellipticity (ratio of major length to minor length of fit ellipse) of the medial plane at metaphase against cell ellipticity of the medial plane at NEB for WT OML cells with slight elongation at metaphase (Ellipticity > 1.1 at metaphase). Grey dotted line represents region where ellipticity at metaphase equals that at NEB. Most values lie below this line, indicating ellipticity has decreased from NEB to metaphase. Ellipticity at metaphase has a weak correlation to ellipticity at NEB (R^2 value = 0.2121, n = 54 cells).

c. Percentage change in ellipticity of the medial plane from NEB to metaphase against ellipticity of the medial plane at NEB for cells in **b**. Percentage change in ellipticity of the medial plane from NEB to metaphase has a strong negative correlation with ellipticity of the medial plane at NEB (R^2 value = 0.6578, n = 54 cells). This means that the more elongated cells were at NEB, the more they round up by metaphase.

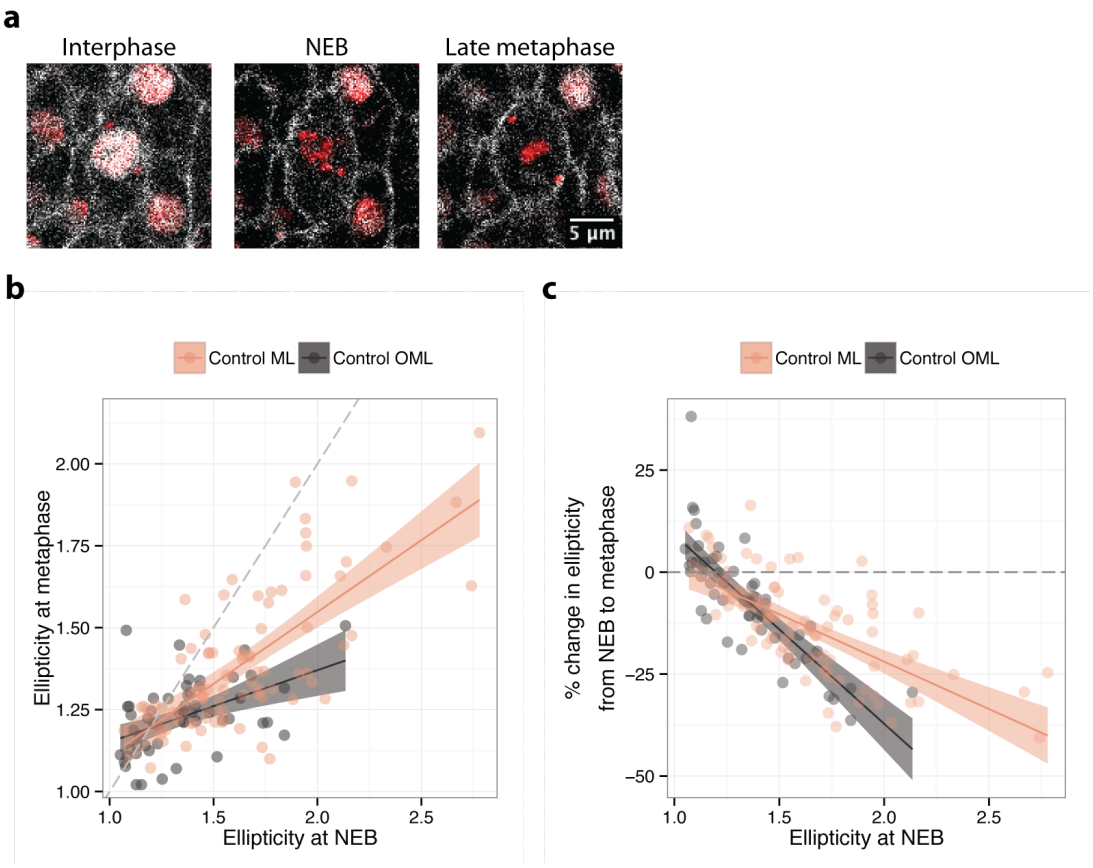

Figure 3.5: Mitotic rounding is impaired in the midline.

a. An anisotropic cell in the midline entering and exiting mitosis. Cell outlines are marked with Spider-GFP. Cells with a clear long axis in interphase retain this long axis in mitosis and have an elliptical shape during mitosis.

b. Cell ellipticity (ratio of major length to minor length of fit ellipse) of the medial plane at metaphase against cell ellipticity of the medial plane at NEB for WT OML and ML cells with slight elongation at metaphase (Ellipticity > 1.1 at metaphase). Lines represent the best-fit mean and shaded areas represent the standard error of the mean. Grey dotted line represents region where ellipticity at metaphase and NEB are equal. Most values lie below this line, indicating ellipticity has decreased from NEB to metaphase. Ellipticity at metaphase has a weak correlation to ellipticity at NEB (R^2 value = 0.4972, n = 85 cells [ML]). Ellipticity at metaphase is higher for WT ML cells compared to OML cells for equivalent ellipticities at NEB.

c. Percentage change in ellipticity of the medial plane from NEB to metaphase against ellipticity of the medial plane at NEB for WT OML and ML cells. Lines represent the best-fit mean and shaded areas represent the standard error of the mean. Percentage change in ellipticity from NEB to metaphase is decreased for ML cells with higher ellipticity at NEB compared to OML cells (R^2 value = 0.4272, n = 85 cells [ML]).

3.3 The actomyosin cortex plays a minor role in mitotic rounding within the *Drosophila* notum epithelium

3.3.1 Cells still expand significantly against neighbouring cells during mitosis when myosin activity is compromised

Contractility of the mitotic actomyosin cortex is proposed to oppose the hydrostatic pressure in order to generate osmotic pressure to push against confinement (Stewart et al. 2011a). In crowded epithelia, it has been suggested to facilitate the shape changes required to push out against neighbouring cells, and allow spindles to align orthogonal to the epithelial plane. To test if cortical contractility was required for mitotic rounding in the *Drosophila* notum, I expressed a phospho-dead mutant of myosin (SqhAA) which acts like a dominant-negative, dimerising with endogenous myosin and perturbing myosin activity.

Surprisingly, cells still expand and appear rounded at mitosis both at the apical and mediolateral plane in cells expressing SqhAA (Fig 3.6a). SqhAA cells still exhibited basal remodelling, as seen from the smaller area in the basal portion of the cell. Both poles of the spindle could be seen within a single plane of the epithelium, indicating spindle morphogenesis and spindle positioning relative to the plane of the epithelium were not compromised (Fig 3.6a).

When the changes in the medial plane from NEB to metaphase were quantified, I found that cell rounding in SqhAA cells was reduced slightly compared WT cells from NEB to late metaphase (Fig 3.6b). However, the increase in cross-sectional area was significantly more in SqhAA cells compared to WT cells (Fig 3.6c).

3.3.2 Cells expand significantly against neighbouring cells during mitosis with almost no actin cortex

As an additional method to test the requirement for actomyosin, I sought to significantly impair the formation of an actin cortex during mitosis. Diaphanous (Dia) was recently shown to be the main formin required to build an actin cortex during mitosis in the *Drosophila* notum (Rosa et al. 2015). I thus targeted the expression of Dia with RNAi-mediated silencing (DiaIR).

Cells still expand and appear more round at mitosis in cells absent of Dia, and spindle morphogenesis was not affected. However, cross-sectional areas expanded significantly in the medial plane in DiaIR cells, similar to SqhAA cells (Fig 3.7c). Also similar to SqhAA cells, DiaIR cells rounded slightly less from NEB to metaphase compared to WT cells (Fig 3.7b).

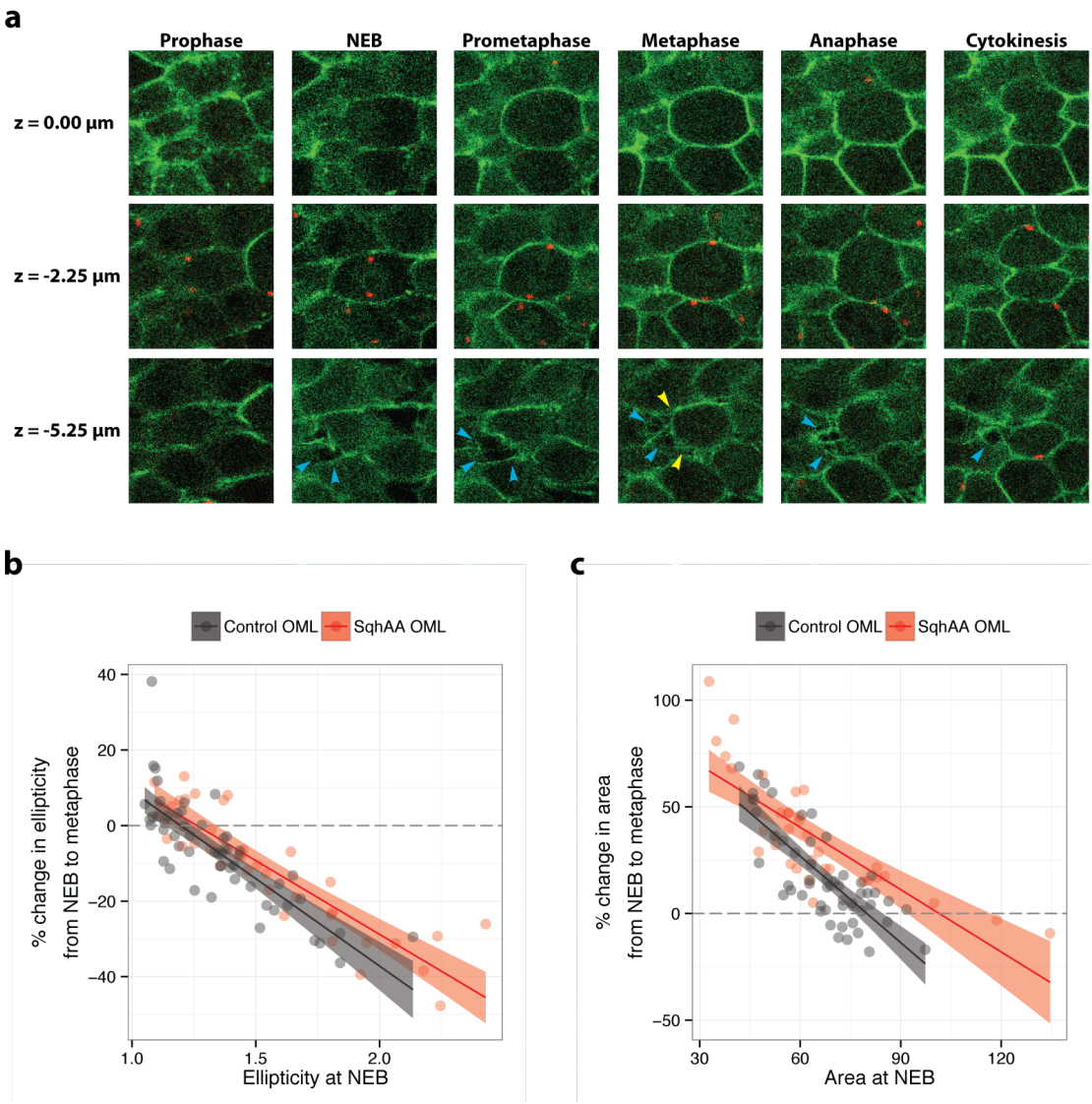

Figure 3.6: Myosin activity affects change in anisotropy and cross-sectional area during mitotic rounding.

a. Representative OML cell expressing SqhAA dividing. See Fig 3.1 for comparable WT cell. Mitotic cell outline is labelled with LifeAct-GFP (green) and spindle poles are labelled with Centrosomin-RFP (red). NEB was defined as the timepoint when nuclear exclusion of background Centrosomin-RFP disappeared. Actin recruitment to the basolateral planes of the mitotic cell are visible at NEB. As mitosis proceeds, cells expand and appear less elliptical. Gaps in the LifeAct-GFP signal in the basal plane are seen from NEB (blue arrowheads) indicating basal remodelling. Note that basal remodelling does not appear to be impaired, as the basal plane (z = -5.25 µm) is significantly smaller and rounder (yellow arrowheads) than the medial plane (z = -2.25 µm) at metaphase, indicating low mechanical constraints in the basal plane.

b. Percentage change in ellipticity of the medial plane from NEB to metaphase against

ellipticity of the medial plane at NEB for WT OML and SqhAA OML. Lines represent the best-fit mean and shaded areas represent the standard error of the mean. Percentage change in ellipticity is slightly lower in SqhAA cells compared to WT (R^2 value = 0.7744, n = 35 cells [SqhAA]).

c. Percentage change in area of the medial plane from NEB to metaphase against area of the medial plane at NEB for WT OML and SqhAA OML. Lines represent the best-fit mean and shaded areas represent the standard error of the mean. The percentage change in area for SqhAA OML cells is higher than WT OML cells for equivalent areas at NEB, indicating that cells are expanding more in the medial plane (R^2 value = 0.6257, n = 35 cells [SqhAA]).

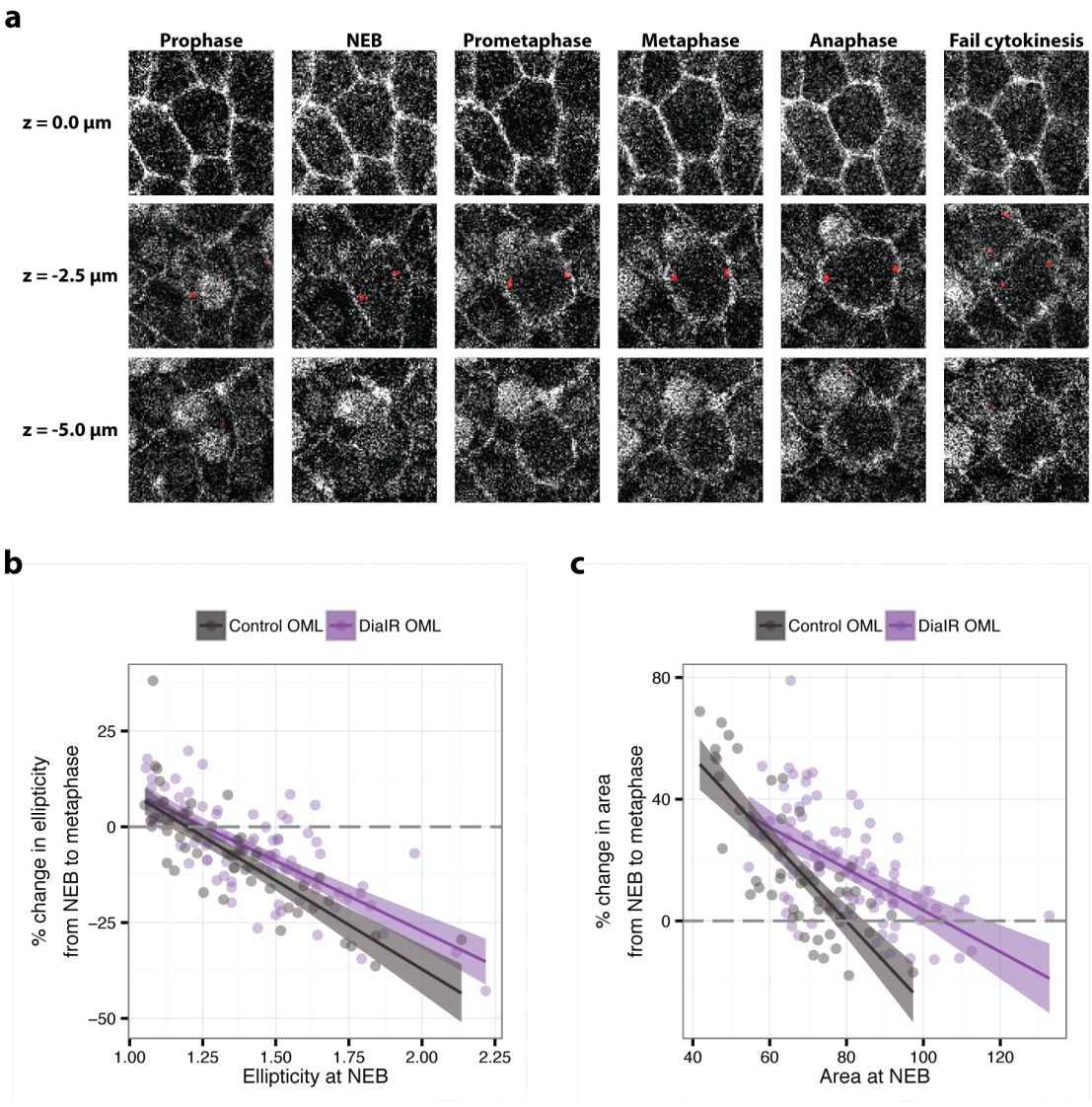

Figure 3.7: The mitotic actin cortex is involved in changes in cross-sectional area and anisotropy during mitotic rounding.

a. Representative OML cell expressing DiaIR dividing. Mitotic cell outline is labelled with Spider-GFP (green) and spindle poles are labelled with Centrosomin-RFP (red). NEB was defined as the timepoint when Spider-GFP nuclear signal disappeared. As mitosis proceeds, cells expand and appear less anisotropic. Note that basal remodelling does not appear to be impaired, as the basal plane (z = -5.0 µm) is significantly smaller and rounder than the medial plane (z = -2.5 µm).

b. Percentage change in ellipticity of the medial plane from NEB to metaphase against ellipticity of the medial plane at NEB for WT OML and DiaIR OML. Lines represent the best-fit mean and shaded areas represent the standard error of the mean. Percentage change in ellipticity is slightly lower in DiaIR cells compared to WT for cells which are more anisotropic at NEB (R^2 value = 0.3051, n = 90 cells [DiaIR]).

c. Percentage change in area of the medial plane from NEB to metaphase against area of the medial plane at NEB for WT OML and DiaIR OML. Lines represent the best-fit mean and shaded areas represent the standard error of the mean. The percentage change in area for DiaIR OML cells is significantly higher than WT OML cells for equivalent areas at NEB, indicating that cells are expanding even more in the medial plane (R^2 value = 0.5331, n = 90 cells [DiaIR]).

3.4 Basal remodelling of the cell during mitosis contributes significantly to mitotic rounding in the mediolateral plane.

Because actomyosin seemed to have a minor contribution to mitotic rounding, I looked to the other driver of mitotic rounding – integrin signalling and basal de-adhesion. In cell cultures, focal adhesion disassembly during mitosis is regulated by Rap1. Overexpression of Rap1 in mitosis prevents cells from de-adhering, and cell remain spread (Dao et al. 2009; Lancaster et al. 2013; Dimitracopoulos 2016). However, its role in basal de-adhesion in mitotic cells in an epithelia has never been shown.

Interestingly, despite a minimal ECM in the *Drosophilia* notum (Curran 2015), expression of constitutively active Rap1 ($Rap1^{V12}$) with a pan-notum driver (Pannier-Gal4) did indeed prevent basal de-adhesion during mitosis in the tissue (Fig 3.8a). $Rap1^{V12}$ cells retained significant area of the mitotic cell in the basal plane and no or few spaces in actin signal between the mitotic cell and neighbouring cells. Despite remaining adhered basally, cells overall still appeared to expand and round up slightly during mitosis. Both spindle poles could be seen in a single plane as well, indicating that spindle morphogenesis and planar positioning was not perturbed (Fig 3.8a).

When quantifying the effects on cell shape, I found that the change in rounding from NEB to metaphase was similar between $Rap1^{V12}$ OML and WT OML cells (Fig 3.8b), but the increase in cross-sectional area is reduced in $Rap1^{V12}$ OML cells (Fig 3.8c). This indicates that basal remodelling contributes to mitotic rounding in a tissue by allowing the bulk redistribution of the cell towards the middle of the tissue, rather than regulating the elongation of the cell.

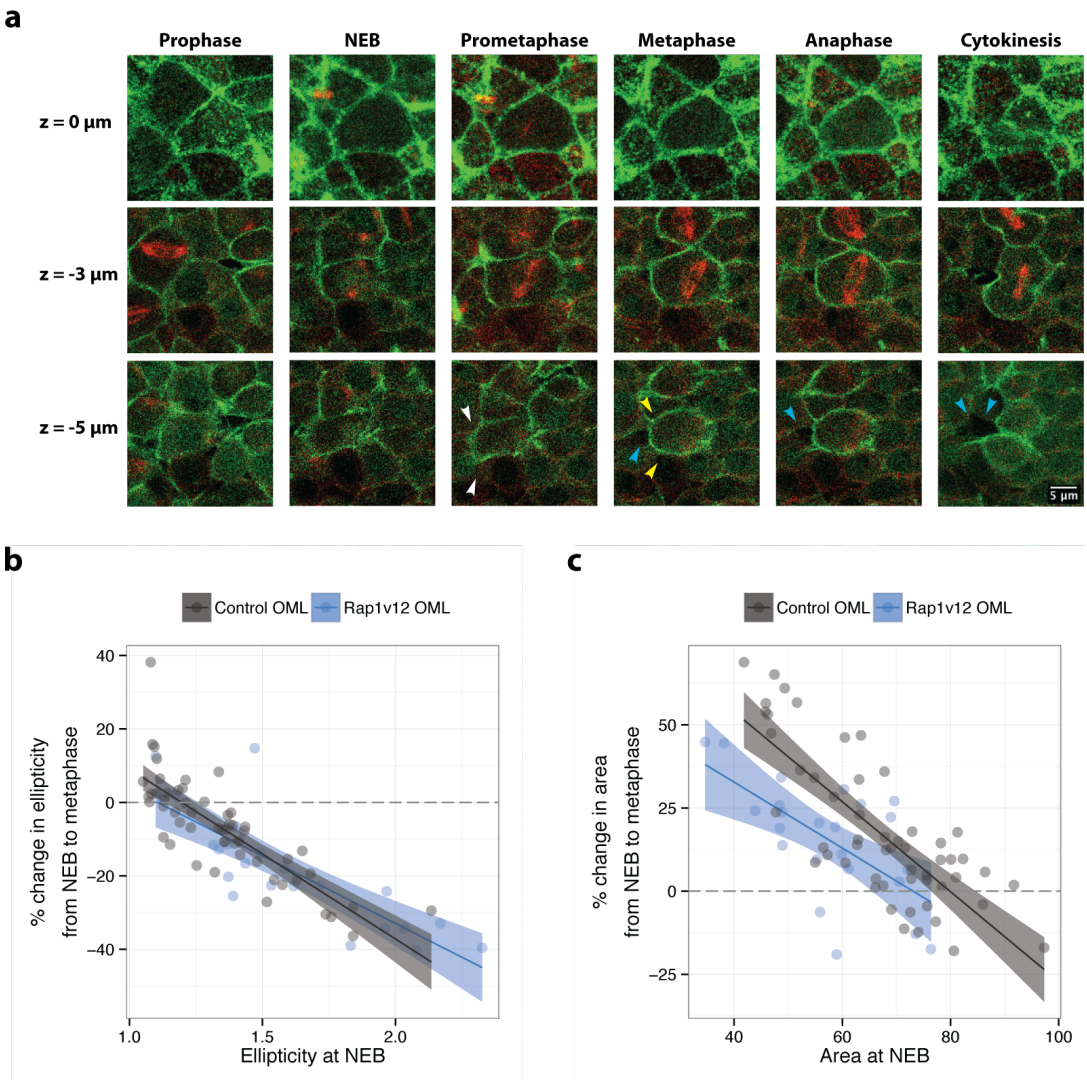

Figure 3.8: Rap1 is involved in basal remodelling and bulk redistribution during mitosis.

a. Representative OML cell expressing Rap1^{V12} dividing. See Fig 3.1 for comparable control cell. Mitotic cell outline is labelled with LifeAct-GFP (green) and tubulin is labelled with Tubulin-mCherry (red). NEB was defined as the timepoint when nuclear exclusion of Tubulin-mCherry disappeared. Actin recruitment to the basolateral planes of the mitotic cell are visible at NEB. As mitosis proceeds, cells expand and appear more elliptical. In contrast to control cells, no gaps in the LifeAct-GFP signal in the basal plane are seen during prometaphase (white arrowheads). Small gaps in the actin signal can be seen sometimes from metaphase (blue arrowheads). The cell remains mostly attached at the basal surface despite mitotic rounding visible from the elliptical shape of the cell at metaphase (yellow arrowheads). Gap in the actin signal becomes more striking when furrowing occurs from this point (blue arrowheads).

b. Percentage change in ellipticity of the medial plane from NEB to metaphase against

ellipticity of the medial plane at NEB for control OML and Rap^{V12} OML. Lines represent the best-fit mean and shaded areas represent the standard error of the mean. The relationship between the percentage change in ellipticity and ellipticity at NEB is unchanged for $Rap1^{V12}$ cells (R^2 value = 0.6584, n = 23 cells [$Rap1^{V12}$]).

c. Percentage change in area of the medial plane from NEB to metaphase against area of the medial plane at NEB for control OML and Rap^{V12} OML. Lines represent the best-fit mean and shaded areas represent the standard error of the mean. The percentage change in area for $Rap1^{V12}$ OML cells is lower than control OML cells for equivalent areas at NEB, indicating that cells are expanding less in the medial plane (R^2 value = 0.3788, n = 23 cells [$Rap1^{V12}$]).

3.5 Conclusions

In conclusion, I show in this chapter that cells undergo mitotic rounding in the *Drosophila* notum epithelium, beginning from the mediolateral planes towards the apical plane. This correlates to the recruitment of myosin, and suggests that actomyosin is regulating the shape changes in mitosis. I also find that cell shape differs significantly from the apical to basal planes of the epithelium, and this difference persists in mitosis, where cells are significantly rounder in the mediolateral planes compared to the apical plane. This leads to cell shape being largely similar from NEB to metaphase at the apical planes, while mitotic rounding is most significantly in the mediolateral planes. Meanwhile, cells also appear to de-adhere from the basal plane of the tissue, and have a small, round area at the basal section of the mitotic cell.

While there was obvious mitotic rounding, many cells remained elongated at mitosis. Cells that were very elongated at NEB, remained so at late metaphase, suggesting that mitotic rounding cannot overcome the constraints of tissue packing on cell shape. I further find that the degree of mitotic rounding is impaired in ML cells, consistent with mitotic rounding being sensitive to the amount of local cell crowding in the tissue. Inducing overgrowth of the tissue through the manipulation of the Hippo pathway to increase the effects of cell crowding might allow for direct testing of the hypothesis that cell crowding within the tissue restricts mitotic rounding.

When testing the contribution of actomyosin on changes in cell shape, I find that a contractile actomyosin cortex is not required for the expansion of the cell in the medial plane, but instead might be required to resist the increase in cross-sectional area of the cell. I also find that Rap1 is involved in basal remodelling of the mitotic cell in an epithelium, similar to what has been shown in single cells in culture (Lancaster et al. 2013; Plak et al. 2014; Dimitracopoulos 2016). $Rap1^{V12}$ expression reduced the increase in cross-sectional area in the middle of the cell from NEB to late metaphase, likely by preventing the bulk redistribution of cell mass towards the middle of the tissue. However, $Rap1^{V12}$ expression did not affect the change in rounding of the cell in terms of its ellipticity. It is worth noting that these

experiments were done with a pan-notum driver, and that the mechanical properties of the neighbouring cells might have changed due to these perturbations. Single-cell experiments using clonal analysis might be help to control for these effects.

In all perturbation conditions, spindle morphogenesis and planar positioning did not seem to be affected, as both spindle poles were consistently observed in a single plane of the epithelium. This is probably because the cross-sectional area of the cell still increased in all conditions, while lateral adhesions retained during mitosis support cell height, and overall there is sufficient space for the spindle to position in a single plane along the epithelium.

Furthermore, in all cells, I found a negative correlation between increase in area and area at NEB (i.e. cells that are small at NEB expand the most), and between decrease in ellipticity and ellipticity at NEB (i.e. cells that are very elongated at NEB reduce their elongation the most). In all perturbations, these general relationships persist. Multiple possible mechanisms exist to explain these observations – cells could either be reaching the same volume, and therefore a similar shape in 3-dimensions (i.e. same height and cross-sectional area); or that relative intracellular pressure is highest at cell widths in elongated and narrow cells, resulting in a decrease in elongation that scales with initial elongation; or that cortical contractility is highest at cell poles of very elongated cells, which could result in a decrease in cell length and therefore elongation that scales with initial elongation.

Chapter 4 Dynamics of spindle positioning during mitosis

4.1 Introduction

In the previous chapter, I described the changes in cell shape that occur during mitosis within the notum. There, I showed that incomplete mitotic rounding is visible as cells are appear to be unable to overcome tissue-level forces such as cell packing and cell crowding. However, spindle morphogenesis appeared relatively unperturbed in these conditions.

In this chapter, I take advantage of the fact that spindles appear unperturbed to analyse the dynamics of spindle movement of cells in the notum. I then investigate the effects of pulling forces along astral MTs in regulating the dynamics of spindle movement and spindle centring. This will form the foundation upon which I later explore how cortical pulling forces act on the spindle to coordinate spindle rotation and cell geometry in the next chapter.

4.2 Mitotic spindle positioning is continuous and dynamic through mitosis

To begin understanding the role of cortical pulling factors, I first characterised spindle positioning over time in mitosis. The spindle behaves much like a rigid rod, whose position in the cell is determined by dynein-dependent pulling forces localized at the cell cortex, acting on astral MTs emanating from the poles. As such, there are two degrees of freedom when considering spindle movement. The spindle can rotate, if the net forces on the spindle poles do not act in the same direction (Fig 4.1a); the spindle can translate, if forces are aligned (Fig 4.1b); and spindles can undergo a combination of translation and rotation, if the forces are in the same direction, but differ in magnitude (Fig 4.1c). To account for this and obtain a comprehensive understanding of spindle movement during mitosis, I analysed spindle movement in terms of the amount of rotation, translation (of the centre of the spindle) and distance moved by individual spindle poles.

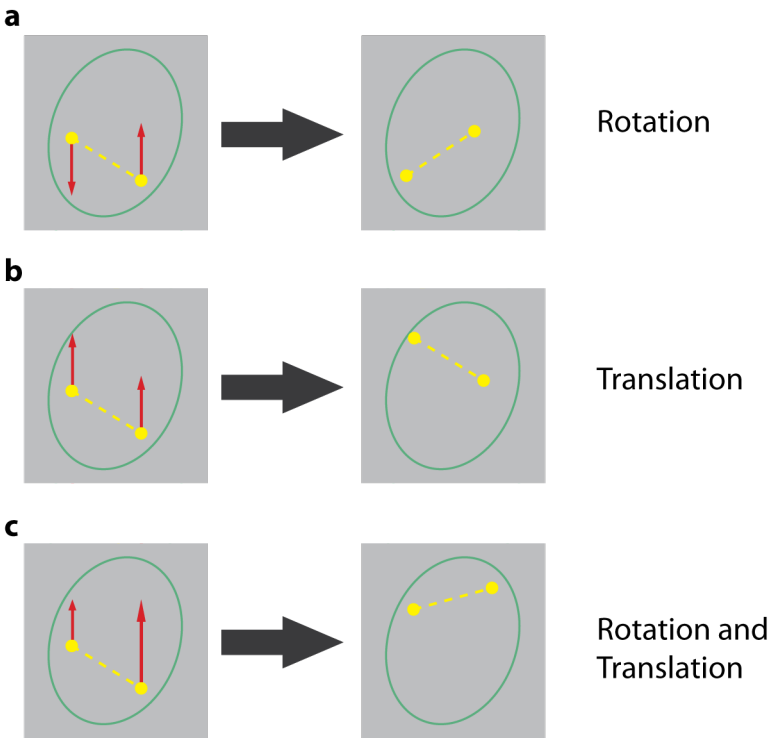

Figure 4.1: Diagram of spindle movement in a cell.

a. Spindle rotation due to equal and opposite net forces on spindle poles.

b. Spindle translation due to equal net forces in the same direction on spindle poles.

c. Spindle rotation and translation due to unequal net forces in the same direction on spindle poles

4.2.1 Spindle length increases significantly in the first half of mitosis

To begin with, I analysed the dynamics of spindle formation to determine when cortical pulling forces first position the spindle. Spindle length was defined as the distance between spindle poles from NEB till anaphase (Fig 4.2a, b). Mitotic time was normalized in order to compare spindles with slightly varying mitotic times – a value of 1.0 was equivalent to the time at NEB, 0.0 was equivalent to anaphase onset and the values at 0.2 intervals were plotted.

I found that on average, spindles elongate significantly from normalised mitotic time (T) = 1.0 to 0.6 (i.e. the first 40% of mitosis) and remains relatively stable after that (Fig 4.2c, d). This corresponds to the period when a clear bipolar spindle has formed (Fig 4.2a).

The average spindle length was 8.342 ± 0.090 μm, and at this value the error in spindle length measured in the *xy*-axis due to the spindle tilting a maximum of 1.5 μm in the *z*-axis is 0.133 μm.

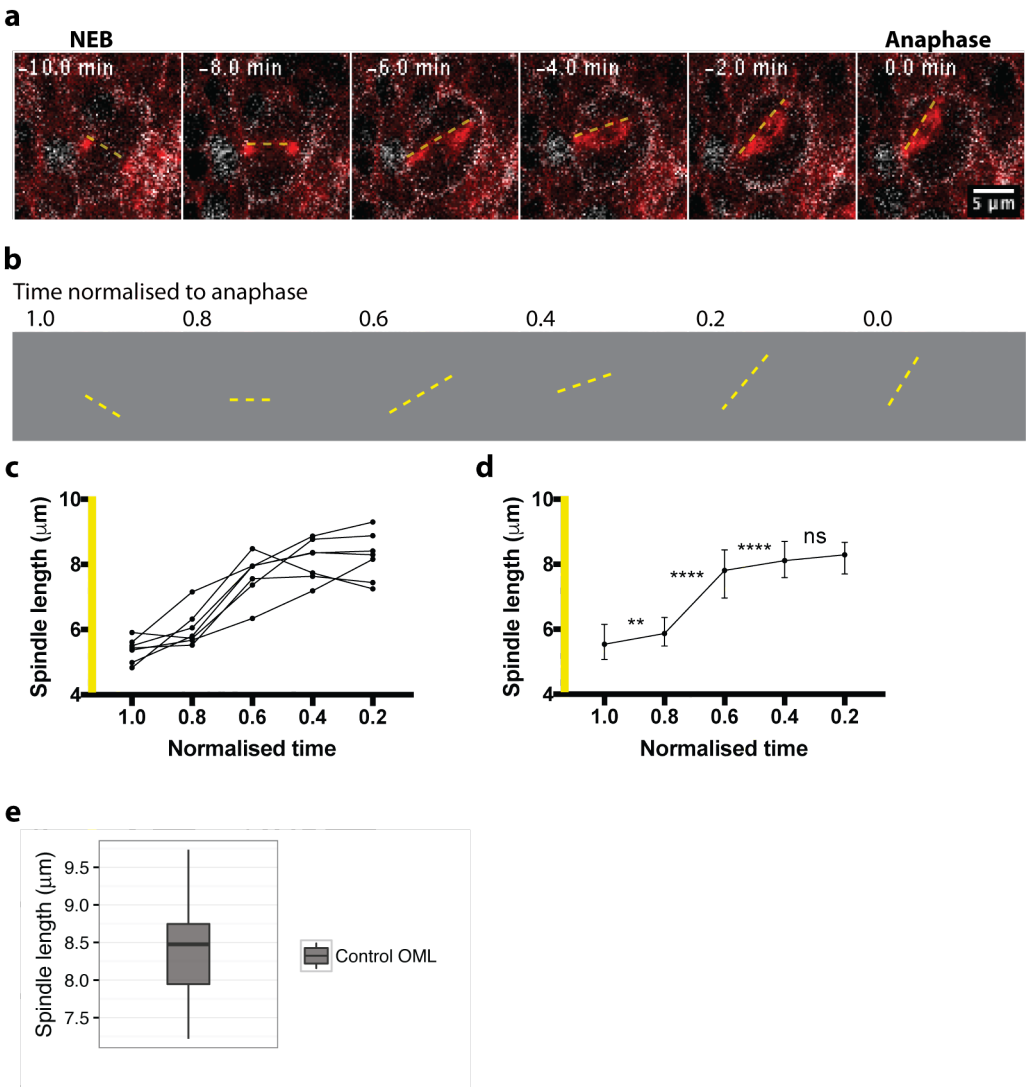

Figure 4.2: Spindles elongate significantly during the first half of mitosis.

a. Representative WT cell outside the midline during mitosis. Spindle is marked with tubulin-mCherry (red) and Cnn-RFP (red), while cell membrane with Spider-GFP (white).

b. Schematic of analysis for spindle length. Spindle length was defined as the distance between the two visible spindle poles. Time was normalised such that 1 is at NEB and 0 is at anaphase.

c. Spindle length over time for 8 representative WT cells (Centrosomin marker).

d. Median spindle length over time for WT cells (Centrosomin marker, N = 41 cells, 3 experiments). Error bars indicate interquartile range. Median spindle length increases most significantly from T = 0.8 to 0.6, and appears to plateau from T = 0.6. Differences between timepoints were calculated with the Wilcoxon matched-pairs signed rank test, ** represents $p < 0.01$; **** represents $p < 0.0001$.

e. Spindle length at late metaphase (before anaphase onset) for WT cells (Centrosomin

marker, Mean = 8.342 ± 0.090 μm, N = 41 cells, 3 experiments). For average spindle length of 8.342 μm, the error due to *z*-tilt of 1.5 μm is 0.133 μm.

4.2.2 Spindle rotation is a continuous and dynamic process

By measuring the change in spindle orientation over time (Fig 4.3a, b), I found that spindles appear to begin rotating from T = 0.8, which is before spindle length stabilises. By the time spindle length appears to stabilise at T = 0.6, the spindle has rotated ~ 13°. The mean rotation from NEB to anaphase was 43.140 ± 9.354° (Fig 4.3c). Although the average rotation appears continuous (Fig 4.3c), individual spindles change directions fairly frequently (Fig 4.3b, 4.4a). This led me to quantify the total amount of rotation in any direction during mitosis (θ_{total}) (Fig 4.4d). This proved much higher than the net rotation from NEB to anaphase ($\theta_{displacement}$) (Fig 4.4c), suggesting that spindle rotation is a noisy process in which spindles often rotate away from their final anaphase position. By taking the ratio of $\theta_{displacement}$ to θ_{total}, I calculated the persistence of directional spindle rotation towards the anaphase position, which is analogous to the measure of directedness in chemotaxis defined by the ratio of the direct path between the start and end points as a fraction of the total accumulated distance travelled. I find that the directional persistence of spindle rotation ($\mathcal{D}_{\text{rotation}} = \frac{\theta_{\text{displacement}}}{\theta_{\text{total}}}$) is only 0.487 ± 0.0346 (Fig 4.4e), where a value of 1 would indicate perfectly directed movement. This suggests that spindles rotate towards the anaphase position about half the time, indicative of a noisy or dynamic process.

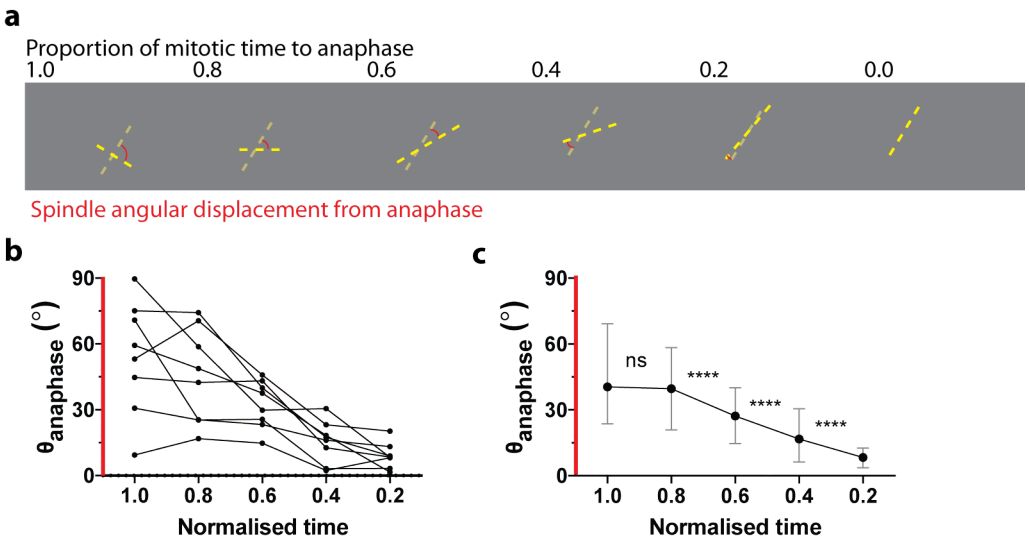

Figure 4.3: Spindles rotate continuously to reach their anaphase positions.

a. Schematic of analysis for angular displacement of spindle ($\theta_{anaphase}$). Time was normalised between NEB to anaphase where 1 is NEB and 0 is anaphase. Angular displacement over time was defined as the angular distance between the spindle at each timepoint and the spindle at anaphase onset.

b. Representative line plots for 8 WT cells showing that spindle rotation from NEB to anaphase is processive.

c. Median angular distance from anaphase position ($\theta_{anaphase}$) over time for WT cells (N = 70 cells, 5 experiments). Error bars indicate interquartile range. Median $\theta_{anaphase}$ decreases over time, indicating that spindles move progressively towards their final position. Differences between timepoints were calculated with the Wilcoxon matched-pairs signed rank test, **** represents $p < 0.0001$.

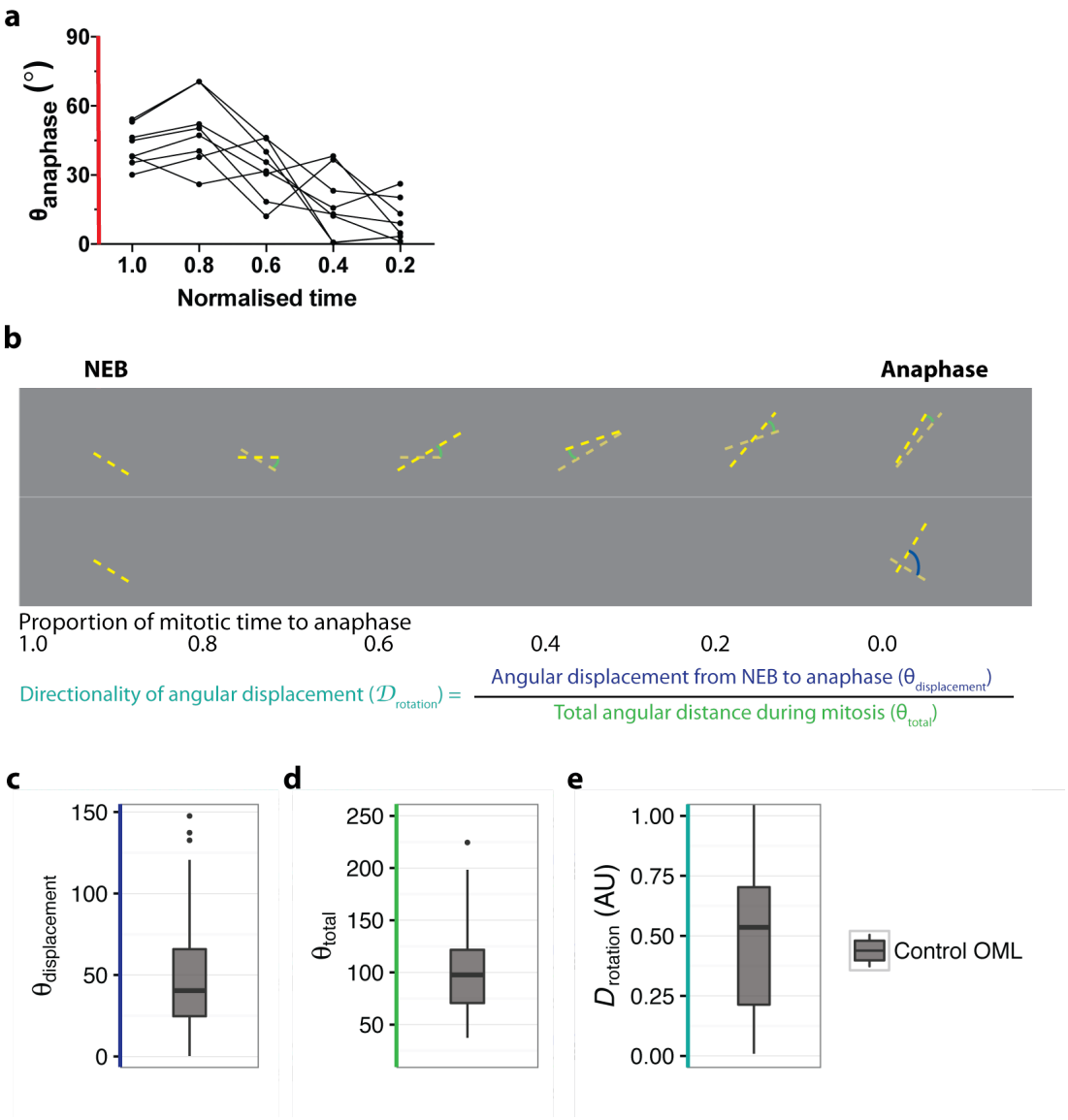

Figure 4.4: Spindle rotation is a dynamic and noisy process.

a. Representative line plots for 8 WT cells showing that spindle rotation is not consistently towards anaphase position. Time was represented as a proportion of the time from NEB to anaphase where 1 is NEB and 0 is anaphase.

b. Schematic of method to determine the directionality of angular displacement ($\mathcal{D}_{rotation}$), which is the ratio of net spindle rotation from NEB to anaphase ($\theta_{displacement}$) to the sum of the rotational movements over time during mitosis (θ_{total}).

c. Net spindle rotation from NEB to anaphase ($\theta_{displacement}$) of WT cells (mean = 43.140 ± 9.354°; N = 70 cells, 5 experiments).

d. Sum of the rotational movements over time during mitosis (θ_{total}) of WT cells (mean = 101.20 ± 4.870°; N = 70 cells, 5 experiments). θ_{total} is much larger than $\theta_{displacement}$ suggesting that spindle rotation is not an efficient process.

e. Directionality of angular displacement for WT cells ($\mathcal{D}_{\text{rotation}} = \frac{\theta_{\text{displacement}}}{\theta_{\text{total}}}$). $\mathcal{D}_{\text{rotation}}$ of WT cells (mean = 0.487 ± 0.0346; N = 70 cells, 5 experiments) indicates that only about half of spindle rotational movement is actually towards the final position.

4.2.3 Spindle translational movements are also continuous and dynamic

To determine the extent of translational spindle movements, I tracked the centre of the spindle, defined as the midpoint between the two spindle poles, from NEB to anaphase (Fig 4.5a). This revealed that spindle centres move continually during the period from NEB to anaphase (Fig 4.5b, c) in order to reach their final anaphase position. Like rotation, spindle translation was a noisy process, in which the total distance moved by the centre ($\mathcal{C}_{\text{total}}$ = 7.650 ± 0.484 μm) (Fig 4.5f) was much larger than the net distance moved from NEB to anaphase ($\mathcal{C}_{\text{displacement}}$ = 2.391 ± 0.199 μm) (Fig 4.5e). Indeed, the directionality of the spindle centre ($D_{\text{spindle centre}} = \frac{\text{C}_{\text{displacement}}}{\text{C}_{\text{total}}}$) was much lower than 1 (Mean: 0.3158 ± 0.020 μm) (Fig 4.5g). This is consistent with the idea that spindle positioning is a dynamic or noisy process.

4.2.4 Spindles are not directed towards the cell centre

It is commonly assumed that the spindle is at the cell centre in symmetrically dividing cells, thus allowing for the division into two equal daughter cells. Since the spindle centre moves continuously, I next sought to test if this movement is directed towards the cell centre by measuring the distance between the spindle centre and that of the cell centre ($\mathcal{C}_{\text{metaphase cell}}$) over time (Fig 4.6a). The cell centre at the end of metaphase (last timepoint before anaphase onset) was used to avoid the change in cell shape that accompanies anaphase elongation. If spindles are moving continuously towards the cell centre, using this measure we would see a progressive decrease in the distance between spindle centre and cell centre.

At NEB, spindles are born with their centre far removed from the cell centre (2.068 ± 0.176 μm) (Fig 4.6c). This corresponds to 18.17 ± 1.559 % of cell length. Subsequently, the spindle centre moves towards the centre from T = 1.o to 0.6, after which the distance between the spindle centre and the cell centre reaches a minimum (Fig 4.6c). The period when spindles move towards the cell centre coincides with the time when spindles are elongating the most, suggesting that centring is driven by MTs of the elongating spindle. In fact, some spindles pass through the cell centre, but then are a distance away by late metaphase (Fig 4.6b,

c). By late anaphase, spindle centres remain 1.008 ± 0.0709 μm from the cell centre (Fig 4.6d). This corresponds to 9.320 ± 0.6519 % of cell length. This is surprising, because current models for symmetrical cell division usually rest on the assumption that the spindle is positioned through rotation about a fixed point - the cell centre. However, these data show that in these symmetrically dividing cells, spindles are not always positioned about the geometric cell centre.

Where it has been studied, spindle positioning at the cell centre has been proposed to be affected by cell size (Dumont and Mitchison, 2009; Goshima and Scholey, 2010; Levy and Heald, 2012). To see if spindles were more likely to be off-centre in larger cells, I plotted $\mathcal{C}_{\text{metaphase cell}}$ against cell area, and cell length (Figure 4.7a, b). I found no correlation between $\mathcal{C}_{\text{metaphase cell}}$ and cell area or cell length, suggesting that in this case spindle centering is not dependent on cell size. Due to the natural variation in spindle lengths and cell lengths, there might be instances where spindles are much shorter than the cell length, which might lead to spindles being off-centre in a relatively large cell. To correct for this, I calculated the spindle scaling factor (spindle length as a ratio of cell length) and plotted $\mathcal{C}_{\text{metaphase cell}}$ against this (Fig 4.7c). Again, I found no correlation between $\mathcal{C}_{\text{metaphase cell}}$ and the spindle scaling factor. This indicates that spindles were not off-centre in cells due to a larger cell area or cell length, or due to a failure in spindle length scaling to cell length.

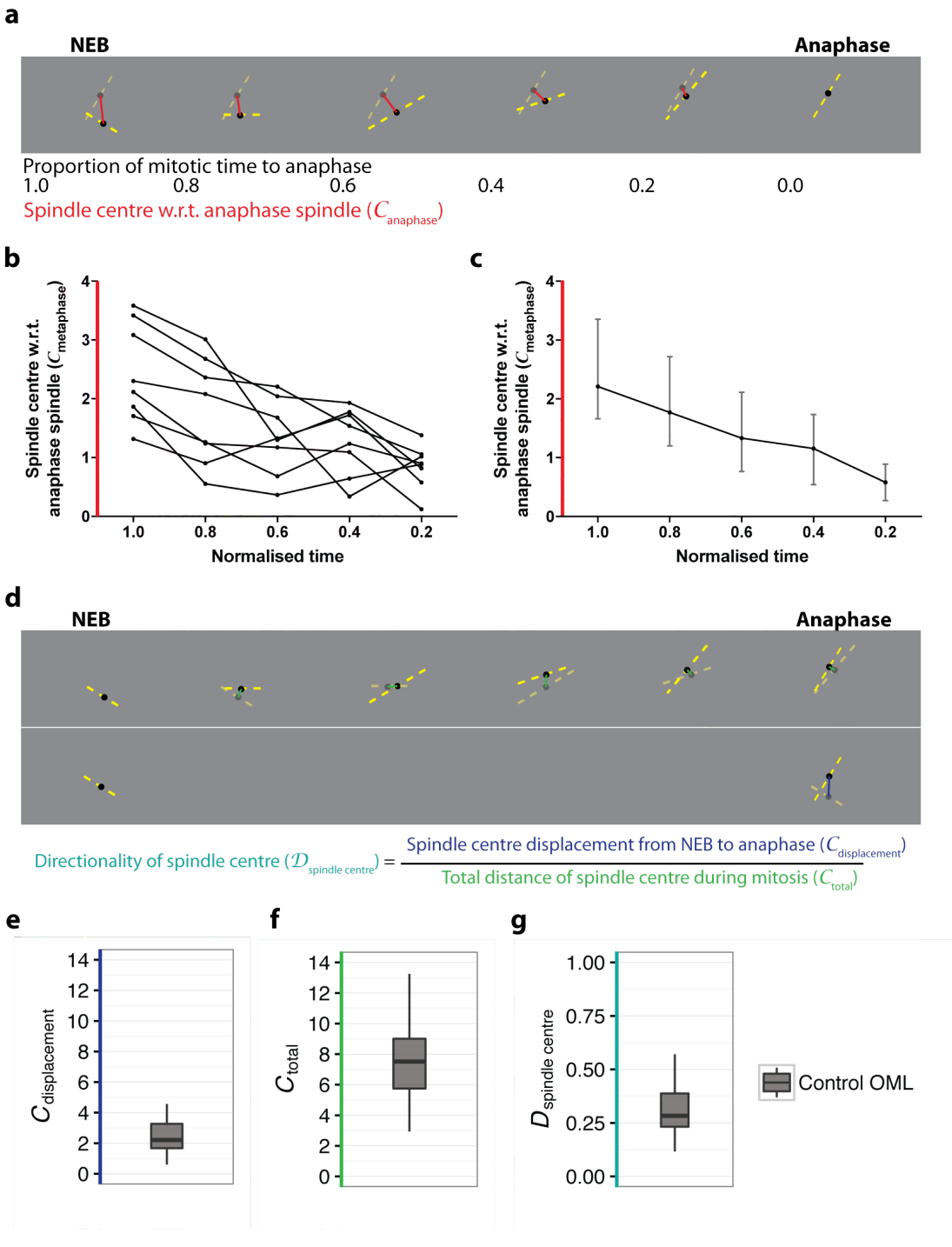

Figure 4.5: Spindle translation is a continuous and noisy process.

a. Schematic of analysis of spindle translation during mitotic progression - depicting the distance over time of the spindle centre from its final position ($\mathcal{C}_{anaphase\ spindle}$). Time was represented as a proportion of the time from NEB to anaphase where 1 is NEB and 0 is anaphase.

b. Representative line plots for 8 WT cells (Tubulin marker) showing that spindle centres move towards their anaphase position, but movement is not always persistent.

c. Median $\mathcal{C}_{\text{anaphase spindle}}$ for WT cells (Tubulin marker). Error bars indicate interquartile range (N: 30 cells, 2 experiments). Like spindle rotation, spindle positioning is a continuous process.

d. Schematic of analysis of total distance moved by spindle centres from NEB to anaphase ($\mathcal{C}_{\text{displacement}}$) and during mitosis ($\mathcal{C}_{\text{total}}$). Directionality of movement of the spindle centre ($D_{\text{spindle centre}}$) is the ratio between $\mathcal{C}_{\text{displacement}}$ and $\mathcal{C}_{\text{total}}$.

e. Distance moved by spindle centre from NEB to anaphase ($\mathcal{C}_{\text{displacement}}$) for WT cells. (Mean: 2.391 ± 0.199 μm; N: 30 cells, 2 experiments).

f. Total accumulated distance moved by spindle centre during mitosis ($\mathcal{C}_{\text{total}}$) for WT cells (Mean: 7.650 ± 0.484 μm; N: 30 cells, 2 experiments). $\mathcal{C}_{\text{total}}$ is much larger than $\mathcal{C}_{\text{displacement}}$, indicating non-linear movement of the spindle centre.

g. Directionality of movement of the spindle centre ($D_{\text{spindle centre}} = \frac{\text{C}_{\text{displacement}}}{\text{C}_{\text{total}}}$) for WT cells (Mean: 0.3158 ± 0.020 μm; N: 30 cells, 2 experiments). $D_{\text{spindle centre}}$ is far from 1, implying that spindle translation, like spindle rotation, is a noisy process.

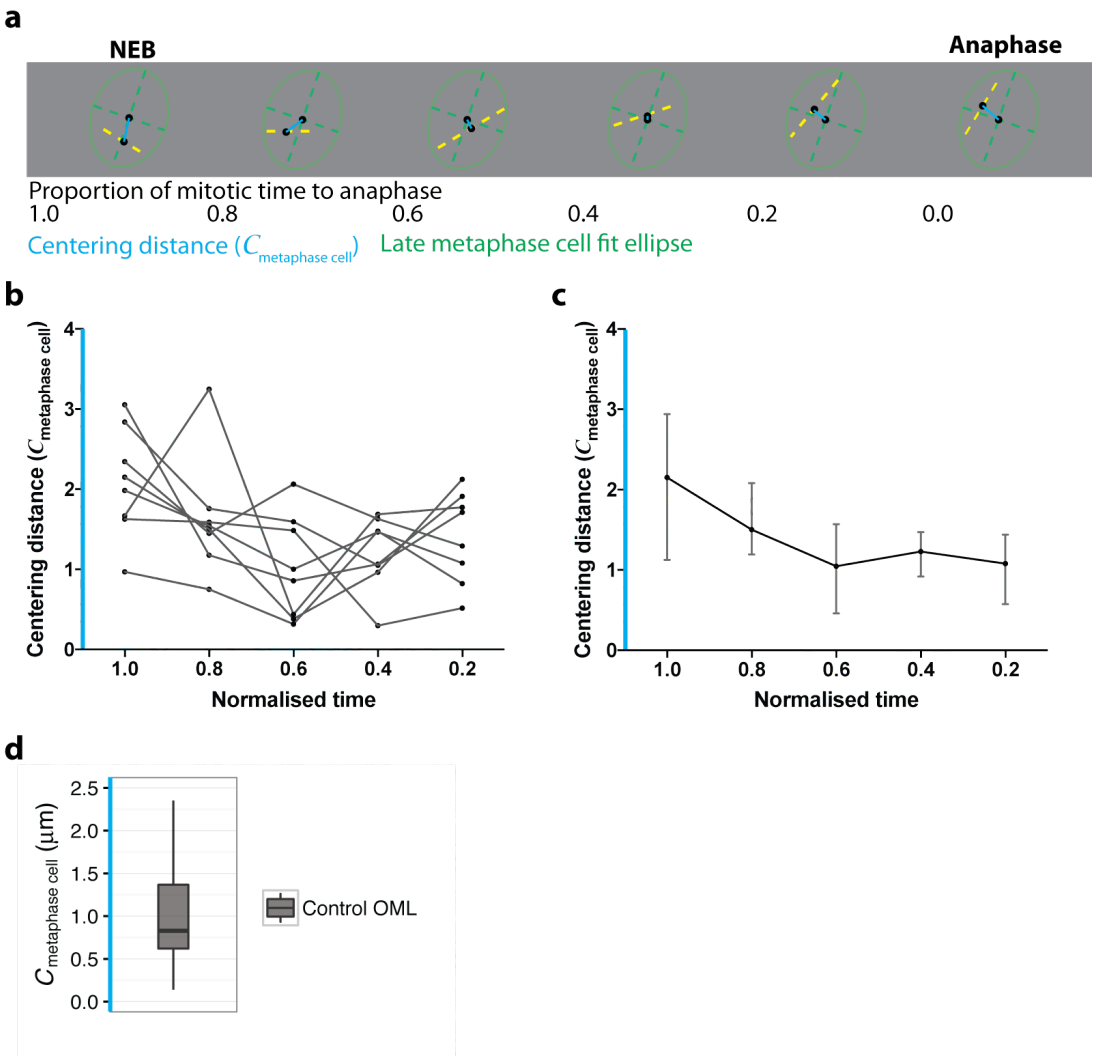

Figure 4.6: Spindles do not reach cell centre by late metaphase.

a. Schematic of analysis of the distance between the spindle centre and the cell centre ($\mathcal{C}_{\text{metaphase cell}}$). Time was represented as a proportion of the time from NEB to anaphase where 1 is NEB and 0 is anaphase. The distance of the spindle from the cell centre was defined as the distance between the centre of spindle over time and the centre of the cell in the plane of the spindle measured just before anaphase onset.

b. $\mathcal{C}_{\text{metaphase cell}}$ for 8 representative WT cells (Tubulin marker) as a function of proportion of mitotic time. Spindles centre as they form, but often pass through the centre and end up off-centre, as indicated by the decrease in $\mathcal{C}_{\text{metaphase cell}}$ followed by an increase.

c. Median $\mathcal{C}_{\text{metaphase cell}}$ for WT cells (Tubulin marker) as a function of proportion of mitotic time. Error bars indicate interquartile range. Median $\mathcal{C}_{\text{metaphase cell}}$ decreases initially from T = 1.0 to 0.6, but spindles remain a distance from the cell centre from T = 0.6 even though spindle centres are continually move until T = 0.2 (Fig 4.4c).

d. $\mathcal{C}_{\text{metaphase cell}}$ in WT cells (Tubulin marker) at late metaphase, just before anaphase onset. Spindles are 1.008 ± 0.0709 μm from cell centre at late metaphase. (N: 30 cells, 2 experiments)

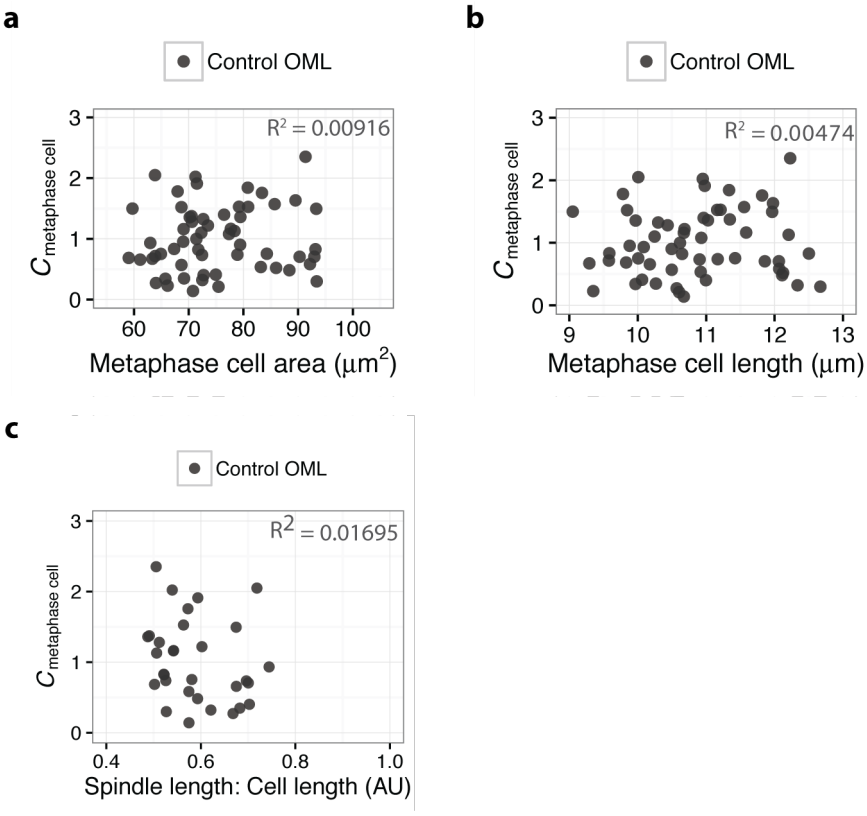

Figure 4.7: Spindle centering is not correlated with cell size or length.

a. Distance between the spindle centre and the cell centre at late metaphase ($\mathcal{C}_{\text{metaphase cell}}$) against cell area at late metaphase. Spindles do not appear to be significantly more off-centre in larger cells ($R^2 = 0.00916$, p-value = 0.475).

b. Distance between the spindle centre and the cell centre at late metaphase ($\mathcal{C}_{\text{metaphase cell}}$) against cell length at late metaphase. Spindles do not appear to be significantly more off-centre in longer cells ($R^2 = 0.00474$, p-value = 0.6078).

c. Distance between the spindle centre and the cell centre at late metaphase ($\mathcal{C}_{\text{metaphase cell}}$) against spindle length as a ratio of cell length. Spindles do not appear to be significantly off-centre when spindle lengths do not scale with cell length ($R^2 = 0.01695$, p-value = 0.2279).

4.2.5 Spindle poles movement is also a continuous and dynamic process

Finally, since the forces applied at spindle poles result in spindle rotation and translation, it was important to also analyse the movements of individual spindle poles. This analysis is therefore a good measure for overall movement of the spindle. As the initial part of this analysis, I combined the movement of both spindle poles in each cell. The total accumulated distance moved by both spindle poles during mitosis ($\mathcal{P}_{\text{total}}$) was quantified, and compared against the shortest path linking the positions at NEB and anaphase ($\mathcal{P}_{\text{displacement}}$) (Fig 4.8a). Again, $\mathcal{P}_{\text{total}}$ (17.96 ± 0.593 μm) was much larger than $\mathcal{P}_{\text{displacement}}$ (6.850 ± 0.334 μm) (Fig 4.8b, c). Using $\mathcal{P}_{\text{displacement}}/\mathcal{P}_{\text{total}}$ as a measure of the persistence of spindle pole movements ($\mathcal{D}_{\text{spindle poles}}$), I found that 36.1 ± 0.0220 % of spindle pole movements guide the pole towards its final position (Fig 4.8d). This is similar to the result for $\mathcal{D}_{\text{rotation}}$, and indicative of spindle pole movements that are noisy rather than directed.

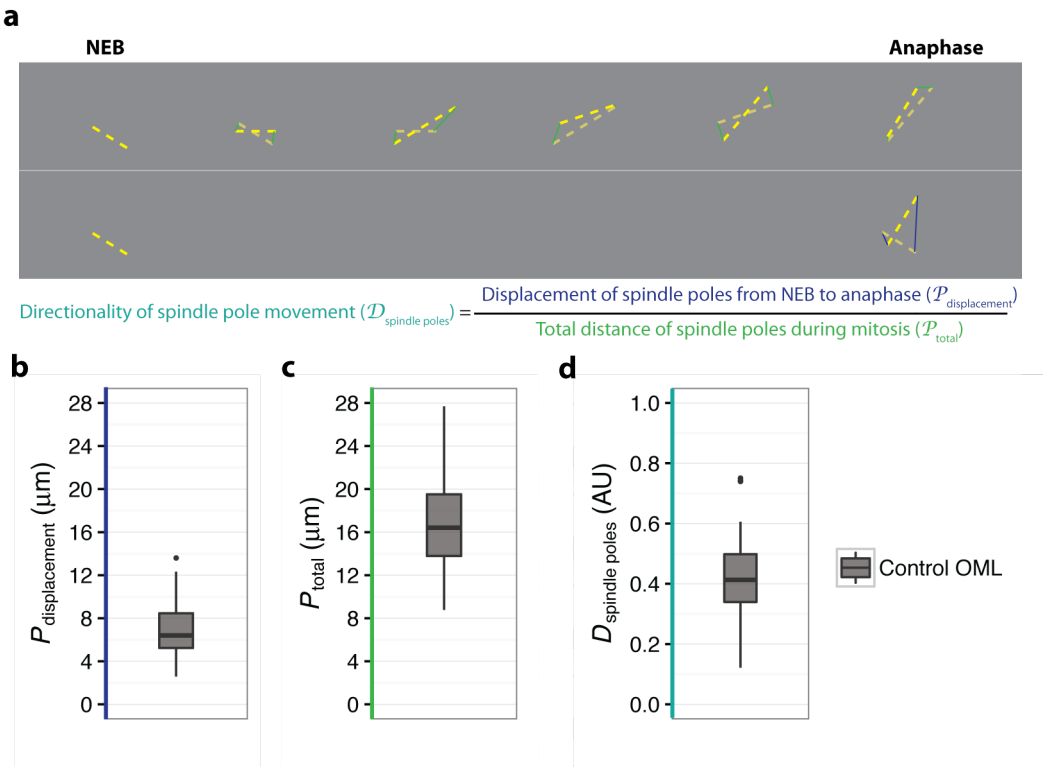

Figure 4.8: The movement of individual spindle poles is also dynamic and noisy.

a. Schematic of spindle pole analysis – Total spindle pole movement was calculated as the sum of distances moved by both spindle poles per minute ($\mathcal{P}_{\text{total}}$), and the net displacement from NEB was calculated as the distance moved by both spindle poles from NEB to anaphase ($\mathcal{P}_{\text{displacement}}$). Directionality of spindle pole movement was calculated as the ratio between displacement and total distance moved by spindle poles ($\mathcal{D}_{\text{spindle poles}}$).

b. $\mathcal{P}_{\text{displacement}}$ for spindle poles of WT cells. Spindle poles move 6.850 ± 0.334 µm from NEB to anaphase.

c. $\mathcal{P}_{\text{total}}$ for spindle poles of WT cells. Spindle poles move a total of 17.96 ± 0.593 µm during mitosis. $\mathcal{P}_{\text{total}}$ is larger than $\mathcal{P}_{\text{displacement}}$, suggesting that spindle pole movement, just like spindle rotation, is not an efficient process.

d. $\mathcal{D}_{\text{spindle poles}}$ for WT cells. $\mathcal{D}_{\text{spindle poles}}$ is significantly below 1 (0.361 ± 0.0220), indicating that spindle pole movement is noisy, and that only $\sim 1/3$ of spindle pole movements from NEB to anaphase contribute to their reaching their final position.

4.3 The canonical spindle orienting protein Mud is required for dynamic spindle positioning

Mud (NuMA in mammalian cells) is part of an evolutionarily conserved pathway that is involved in spindle orientation. Its main function in spindle orientation is thought to be to bind to dynein and promote dynein-mediated pulling forces on the spindle pole, directing spindle poles toward Mud-enriched sites around the cell cortex (Lu & Johnston 2013). It has mostly been studied in the context of asymmetric cell division where the localization of Mud is polarized (Morin & Bellaïche 2011). More recently it has been shown to play a role in symmetric cell division in orienting the spindle to the interphase cell shape within the *Drosophila* notum (Bosveld et al. 2016). Interestingly, the data presented in this paper show that the majority (88%) of cells with Mud mutations are still able to maintain the spindle within the plane of the epithelium, i.e. only a minority (12%) of cells exhibit defects in Z-positioning. Moreover, the study did not address whether Mud is involved in maintaining the spindle position or in dynamically orienting the spindle during mitosis.

To test the role of the canonical spindle orientation pathway in spindle positioning within the XY plane of the tissue, I used dsRNAs to target the Mud for RNAi-mediated silencing (MudIR). In keeping with Bosveld et al, I found that the majority of MudIR cells exhibited minimal Z-positioning defects (data not shown). By restricting my analysis to this group of cells (Fig 4.9a), I was able to determine the role of Mud in spindle rotation, translation, and spindle pole movement.

4.3.1 Mud is required for dynamic spindle rotation

Consistent with previous studies, this analysis revealed that Mud is required for spindle rotation in the XY plane. Thus, the extent of spindle rotation from NEB to anaphase angle ($\theta_{anaphase}$) was severely (>2 fold) reduced in MudIR cells relative to the WT (Tubulin-cherry or Centrosomin-RFP) (Fig 4.9b, c) – the mean angular difference between the spindle orientation at NEB and anaphase ($\theta_{displacement}$) was 18.170 ± 1.862° in MudIR flies and 48.620 ± 4.266° in the WT (Kolmogorov-Smirnov test p-value = 4.048^{e-10}). The total accumulated rotation during mitosis (θ_{total}) was also lower in MudIR cells relative to the WT (Fig 4.9d) (Mean: 101.20 ±

4.97° [WT] and 59.84 ± 2.758° [MudIR], Mann-Whitney U test p-value = 1.121^{e-11}). It is likely that part of the residual rotation measured in the MudIR flies is due to the effects of the increase in spindle length that accompanies spindle morphogenesis, which occurs in the first 40% of mitotic time (i.e. from T = 1.0 to 0.6).

Interestingly, on knock-down of Mud, I rarely observed changes in spindle direction (Fig 4.10a). As a qualitative measure of this, I calculated the persistence of spindle rotation ($\mathcal{D}_{rotation} = \frac{\theta_{displacement}}{\theta_{total}}$) in MudIR cells. The average $\mathcal{D}_{rotation}$ was smaller in MudIR cells compared to WT (Fig 4.10b) (Mean: 0.487 ± 0.0346 [WT] and 0.308 ± 0.0262 [MudIR], Kolmogorov-Smirnov test p-value = 5.373^{e-05}). However, since $\mathcal{D}_{rotation}$ is directly proportional to $\theta_{displacement}$, and since $\theta_{displacement}$ is on average much lower in MudIR flies than in the WT (18.170 ± 1.862° [MudIR] and 48.620 ± 4.266° [WT]), I plotted $\mathcal{D}_{rotation}$ as a function of $\theta_{displacement}$ for MudIR and WT cells (Fig 4.10c). Using this as a measure it is clear that for the same degree of displacement, $\theta_{displacement} > 25°$, $\mathcal{D}_{rotation}$, is higher in MudIR cells than in WT cells. Thus, when undergoing the same angular rotation, MudIR spindles change directions less frequently than spindles in WT cells. This is consistent with a theory where cortically generated forces pull on spindle poles and cause spindles to change directions.

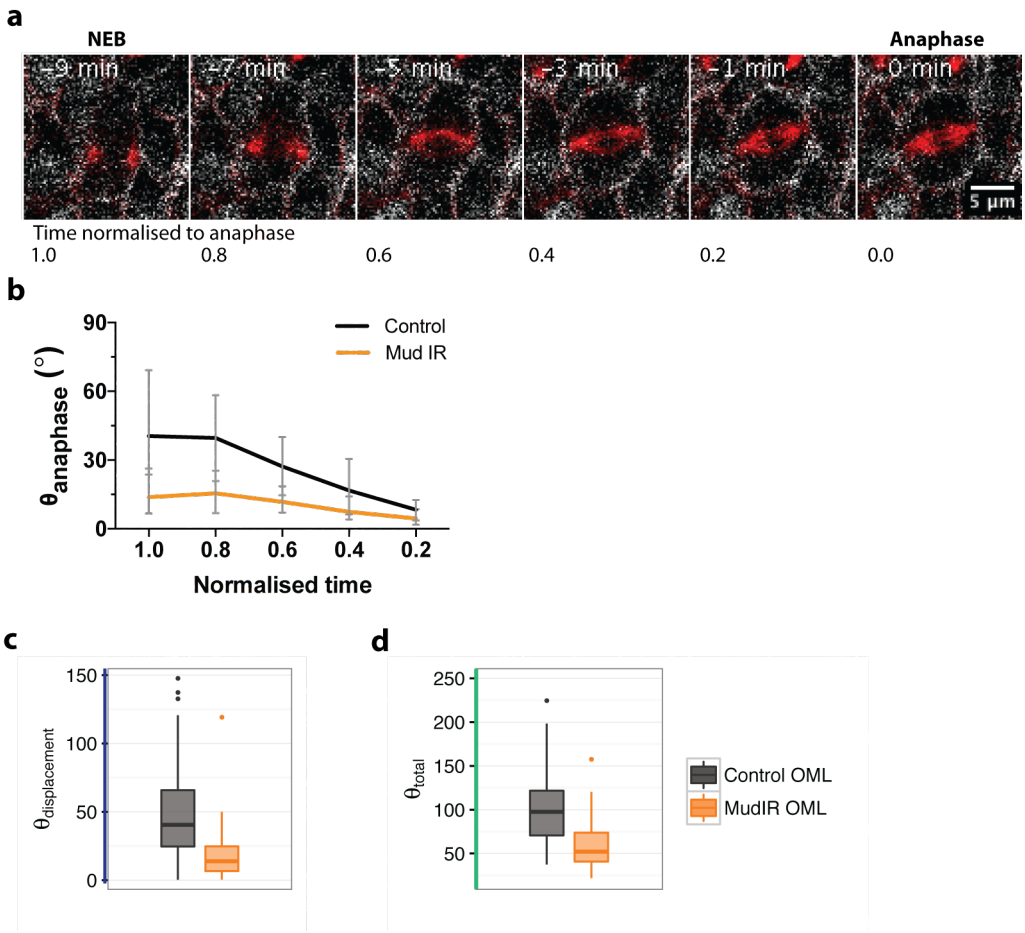

Figure 4.9: Mud is required for spindle rotation.

a. Representative Mud IR cell during mitosis. Spindled labelled with tubulin-Cherry (red) and cell membrane with SpiderGFP (white). NEB and anaphase are indicated above, and corresponding proportion of mitotic time below the montage. Spindle positioning in the apico-basal axis was not perturbed in majority of the cells such as the one shown here. These cells with a planar spindle were used for the analysis below.

b. Median angular distance from anaphase position ($\theta_{anaphase}$) for Mud IR and WT cells. Error bars represent interquartile range. $\theta_{anaphase}$ does not decrease significantly for MudIR cells, indicating that spindle rotation is abolished.

c. Net spindle rotation from NEB to anaphase ($\theta_{displacement}$) of WT and MudIR cells. $\theta_{displacement}$ of MudIR cells is significantly lower than that of WT. (Mean: 48.620 ± 4.266° [WT] and 18.170 ± 1.862° [MudIR], Kolmogorov-Smirnov test p-value = 4.048^{e-10}).

d. Sum of the rotational movements over time during mitosis (θ_{total}) of WT and MudIR. θ_{total} of MudIR cells is significantly lower than that of WT. (Mean: 101.20° ± 4.87° [WT] and 59.84° ± 2.758° [MudIR], Mann-Whitney U test p-value = 1.121^{e-11}).

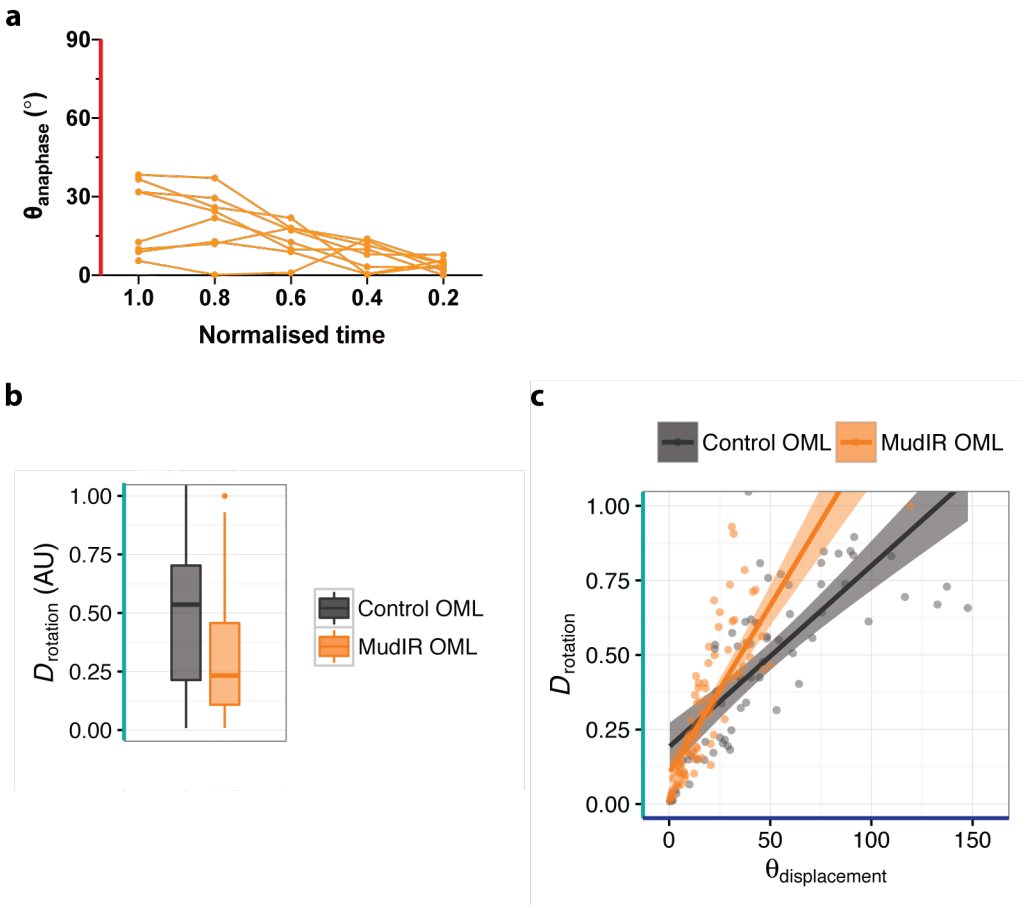

Figure 4.10: MudIR is required for changing directions when spindles displace from NEB position.

a. Representative line plots for MudIR cells showing that spindles that rotate more than 25° consistently move towards anaphase position (8 cells, 4 experiments).

b. Directionality of angular displacement ($\mathcal{D}_{rotation}$) for WT and MudIR cells. $\mathcal{D}_{rotation}$ of MudIR cells is lower than WT cells (Mean: 0.487 ± 0.0346 [WT] and 0.308 ± 0.0262 [MudIR], Kolmogorov-Smirnov test p-value = 5.373^{e-05}). This is expected, since $\mathcal{D}_{rotation}$ is proportional to $\theta_{displacement}$, which is also smaller in MudIR cells compared to WT.

c. $\mathcal{D}_{rotation}$ as a function of $\theta_{displacement}$ for WT and MudIR cells. Lines indicate best-fit mean line and filled areas represent standard error of the mean. In general, $\mathcal{D}_{rotation}$ increases with $\theta_{displacement}$ as expected. However for $\theta_{displacement} > 25°$ in MudIR cells, the mean $\mathcal{D}_{rotation}$ is higher than that of WT. This indicates MudIR spindles that do rotate change directions less than those in WT cells.

4.3.2 Mud is required for dynamic spindle translation and moving the spindle away from the cell centre

Because of the effect of MudIR on spindle rotation, I expected a similar effect on spindle translation, using the movement of the spindle centre to the cell centre as a proxy. Consistent with this, the total distance travelled by the spindle centre ($\mathcal{C}_{\text{total}}$) was significantly lower in MudIR cells than in WT (Fig 4.11e) ($\mathcal{C}_{\text{total}}$ mean: 7.650 ± 0.484μm [WT] and 4.660 ± 0.118 μm [MudIR], Mann-Whitney U test p-value = $1.462^{\text{e-08}}$). Surprisingly however, spindle centres in MudIR cells moved a similar amount from NEB to anaphase ($\mathcal{C}_{\text{displacement}}$) as WT cells (Fig 4.11b, d) ($\mathcal{C}_{\text{displacement}}$ mean: 2.391 ± 0.199 μm [WT] and 1.910 ± 0.095 μm [MudIR], Kolmogorov-Smirnov test p-value = 0.2393). This immediately suggested that spindle translation, as measured as the movement of the spindle centre, was less noisy in MudIR cells than it was in WT cells. Indeed, computing the directionality of the spindle centre ($\mathcal{D}_{\text{spindle centre}} = \frac{\mathcal{C}_{\text{displacement}}}{\mathcal{C}_{\text{total}}}$), I found that this was higher in MudIR cells than in WT cells (Fig 4.11f) (Mean: 0.3158 ± 0.020 μm [WT; N: 30 cells, 2 experiments] and 0.4175 ± 0.020 [MudIR; N: 84 cells, 3 experiments], Mann-Whitney U test p-value = 0.003594).

4.3.3 Spindles are centred in the absence of Mud

Surprisingly, when I measured the distance of the spindle centre to the cell centre ($\mathcal{C}_{\text{metaphase cell}}$), I found that MudIR spindles move toward the cell centre throughout mitosis, while WT cells often move away from the cell centre after initially moving towards it (Fig 4.6b and Fig 4.12b, c). At NEB, the distance of the spindle centre relative to the cell centre ($\mathcal{C}_{\text{metaphase cell}}$) was similar for WT and MudIR (Fig 4.12c). Implying that Mud is not required for nuclear or centrosome positioning in prophase.

The spindle centre then moved towards the cell centre at a rate that was similar to that in WT cells until T = 0.6 of mitotic time. At this stage, MudIR spindles continued to move steadily towards the cell centre and as a result spindle centres were closer to the cell centre in MudIR cells than it in WT cells (Mean: 1.008 ± 0.0709 μm [WT] and 0.603 ± 0.0493 μm [MudIR], Kolmogorov-Smirnov test p-

value = 0.00790). This suggests that in WT cells, Mud-dependent forces do not affect initial spindle positioning, but instead actively pull spindles off-centre during dynamic spindle rotation.

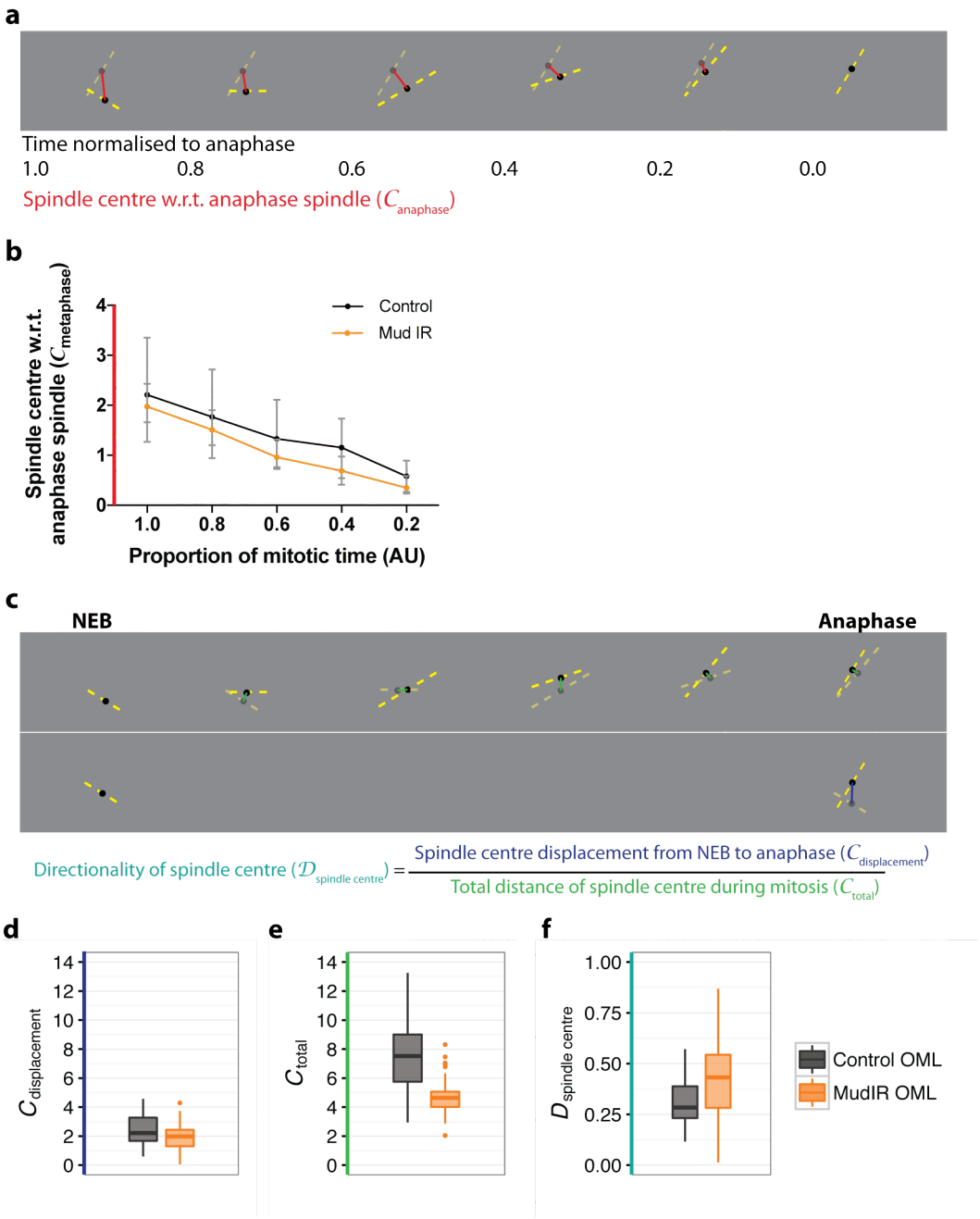

Figure 4.11: Mud is required for dynamic spindle translation.

a. Schematic of analysis of spindle translation during mitotic progression - depicting the distance over time of the spindle centre from its final position ($\mathcal{C}_{\text{anaphase spindle}}$).

b. Median $\mathcal{C}_{\text{anaphase spindle}}$ for MudIR and WT cells (Tubulin marker). Error bars indicate interquartile range. Spindle centres move a similar distance during mitosis for MudIR and WT cells.

c. Schematic of analysis of total distance moved by spindle centres from NEB to anaphase ($\mathcal{C}_{\text{displacement}}$) and during mitosis ($\mathcal{C}_{\text{total}}$). Directionality of movement of the spindle centre ($D_{\text{spindle centre}}$) is the ratio between $\mathcal{C}_{\text{displacement}}$ and $\mathcal{C}_{\text{total}}$.

d. Distance moved by spindle centre from NEB to anaphase ($\mathcal{C}_{\text{displacement}}$) for WT and MudIR cells (Tubulin marker). $\mathcal{C}_{\text{displacement}}$ is similar for WT and MudIR cells (Mean: 2.391 ± 0.199 µm [WT; N: 30 cells, 2 experiments] and 1.910 ± 0.0950 µm [MudIR; N: 84 cells, 3 experiments], Mann-Whitney U test p-value = 0.0652).
e. Total accumulated distance moved by spindle centre during mitosis ($\mathcal{C}_{\text{total}}$) for WT and MudIR cells (Tubulin marker). $\mathcal{C}_{\text{total}}$ in MudIR significantly lower (~ half) of that in WT cells. (Mean: 7.650 ± 0.484 µm [WT; N: 30 cells, 2 experiments] and 4.660 ± 0.118 µm [MudIR; N: 84 cells, 3 experiments], Mann-Whitney U test p-value = $1.462^{\text{e-08}}$).
f. Directionality of movement of the spindle centre ($D_{\text{spindle centre}}$) for WT and MudIR cells (Tubulin marker). $D_{\text{spindle centre}}$ is significantly higher in MudIR cells than in WT cells, indicating fewer changes in direction, which is consistent with the hypothesis that Mud is required for dynamic spindle positioning. (Mean: 0.3158 ± 0.020 µm [WT; N: 30 cells, 2 experiments] and 0.4175 ± 0.020 [MudIR; N: 84 cells, 3 experiments], Mann-Whitney U test p-value = 0.00359).

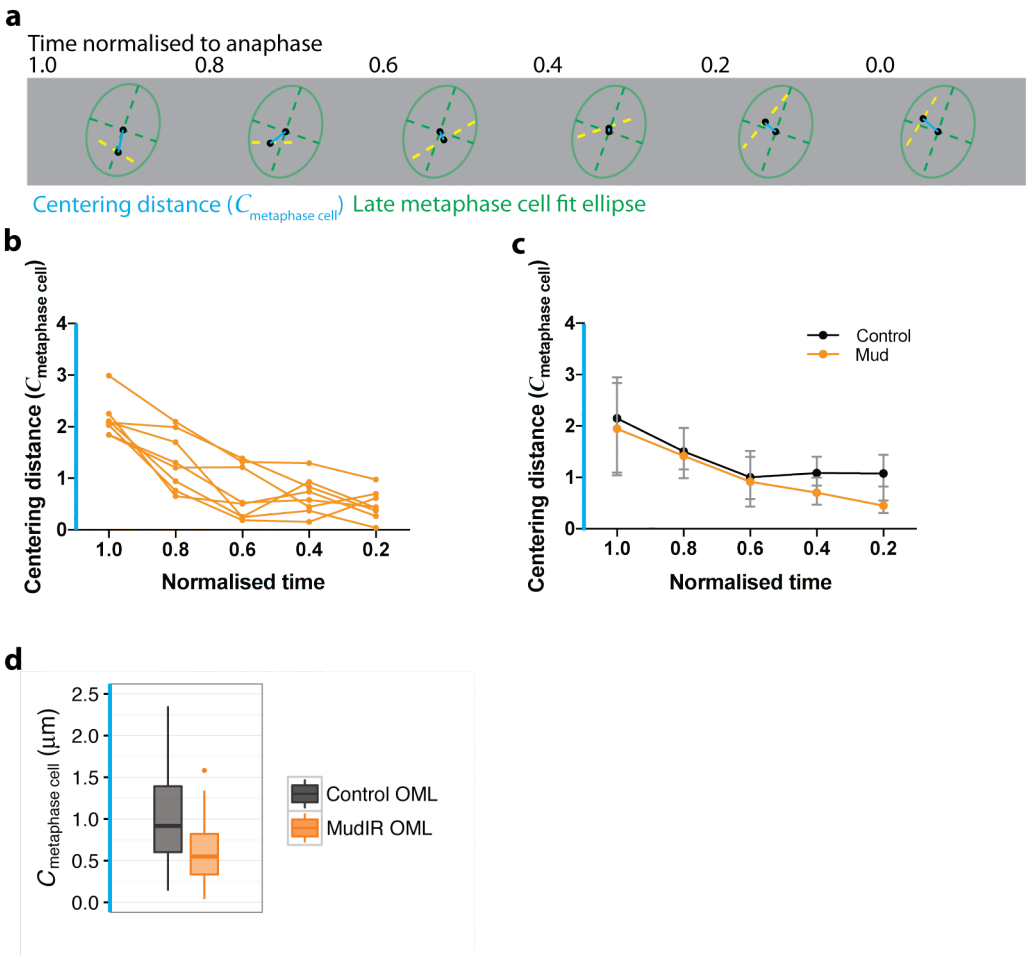

Figure 4.12: Spindles are centred in the absence of Mud.

a. Schematic of analysis of distance of the spindle centre from the cell centre (measured at late metaphase) during mitosis ($\mathcal{C}_{\text{metaphase cell}}$).

b. The distance of the spindle centre from the cell centre ($\mathcal{C}_{\text{metaphase cell}}$) over time for 8 representative MudIR cells. $\mathcal{C}_{\text{metaphase cell}}$ decreases over time and is close to the cell centre by late metaphase.

c. Median $\mathcal{C}_{\text{metaphase cell}}$ over time of MudIR and WT cells (Tubulin marker). Error bars indicate interquartile range. At NEB, $\mathcal{C}_{\text{metaphase cell}}$ of MudIR is similar to that of WT cells (2.391 ± 0.199 µm [WT; N: 30 cells, 2 experiments] and 1.963 ± 0.128 µm [MudIR; N: 84 cells, 3 experiments], Kolmogorov-Smirnov test p-value = 0.1751), suggesting Mud is not involved in the initial setting of spindle positioning at NEB. After NEB, $\mathcal{C}_{\text{metaphase cell}}$ of spindles in MudIR and WT cells decreases initially. However, while $\mathcal{C}_{\text{metaphase cell}}$ of WT cells remains a distance from the cell centre after the initial decrease, $\mathcal{C}_{\text{metaphase cell}}$ of MudIR cells continues to decrease. This indicates that for MudIR cells, spindle centres get progressively closer to the centre of the cell at late metaphase while spindle in WT cells remain a distance from the cell centre.

d. $\mathcal{C}_{\text{metaphase cell}}$ for WT and MudIR cells (Tubulin marker) at late metaphase, just before anaphase onset. Spindle centres are closer to the cell centre at late metaphase in MudIR cells than in WT cells. (Mean: 1.008 ± 0.0709 μm [WT; N: 30 cells, 2 experiments] and 0.603 ± 0.0493 μm [MudIR; N: 84 cells, 3 experiments], Kolmogorov-Smirnov test p-value = 0.00790).

4.3.4 Mud is required for dynamic spindle pole movement

As before, to get an overall view of the effect of Mud on spindle positioning, I then analysed spindle pole dynamics in MudIR cells (Fig 4.13). Spindle pole movements were significantly reduced in MudIR cells relative to the WT, both in terms of the distance moved from NEB to anaphase (Fig4.13b) ($\mathcal{P}_{\text{displacement}}$ mean: 6.892 ± 0.508 μm [WT] and 4.244 ± 0.208 μm [MudIR], Kolmogorov-Smirnov test p-value = 0.000517), as well as the total distance moved during mitosis (Fig 4.13c) ($\mathcal{P}_{\text{total}}$ mean: 19.26 ± 0.957 μm [WT] and 11.600± 0.344 μm [MudIR], Kolmogorov-Smirnov test p-value = 1.399^{e-08}).

Again, $\mathcal{P}_{\text{total}}$ was higher than $\mathcal{P}_{\text{displacement}}$ indicating a certain level of noise in the movement of individual spindle poles. Calculating the directionality of spindle pole movement ($\mathcal{D}_{\text{spindle poles}} = \frac{\mathcal{P}_{\text{displacement}}}{\mathcal{P}_{\text{total}}}$) for MudIR cells, we find that $\mathcal{D}_{\text{spindle poles}}$ was indeed far from 1. Once again, $\mathcal{D}_{\text{spindle poles}}$ for MudIR cells was similar to that of WT (Fig 4.13d). Plotting $\mathcal{D}_{\text{spindle poles}}$ as a function of $\mathcal{P}_{\text{displacement}}$, we see a similar trend as seen for spindle rotation, where for values of $\mathcal{P}_{\text{displacement}}$ that are similar to WT, MudIR cells actually have a higher directionality (Fig 4.13e). Thus, when undergoing a similar movement, spindle poles in MudIR cells experience less noise and undergo fewer changes in position. This is consistent with the hypothesis that Mud-dependent pulling forces drive changes in the direction of spindle pole movement.

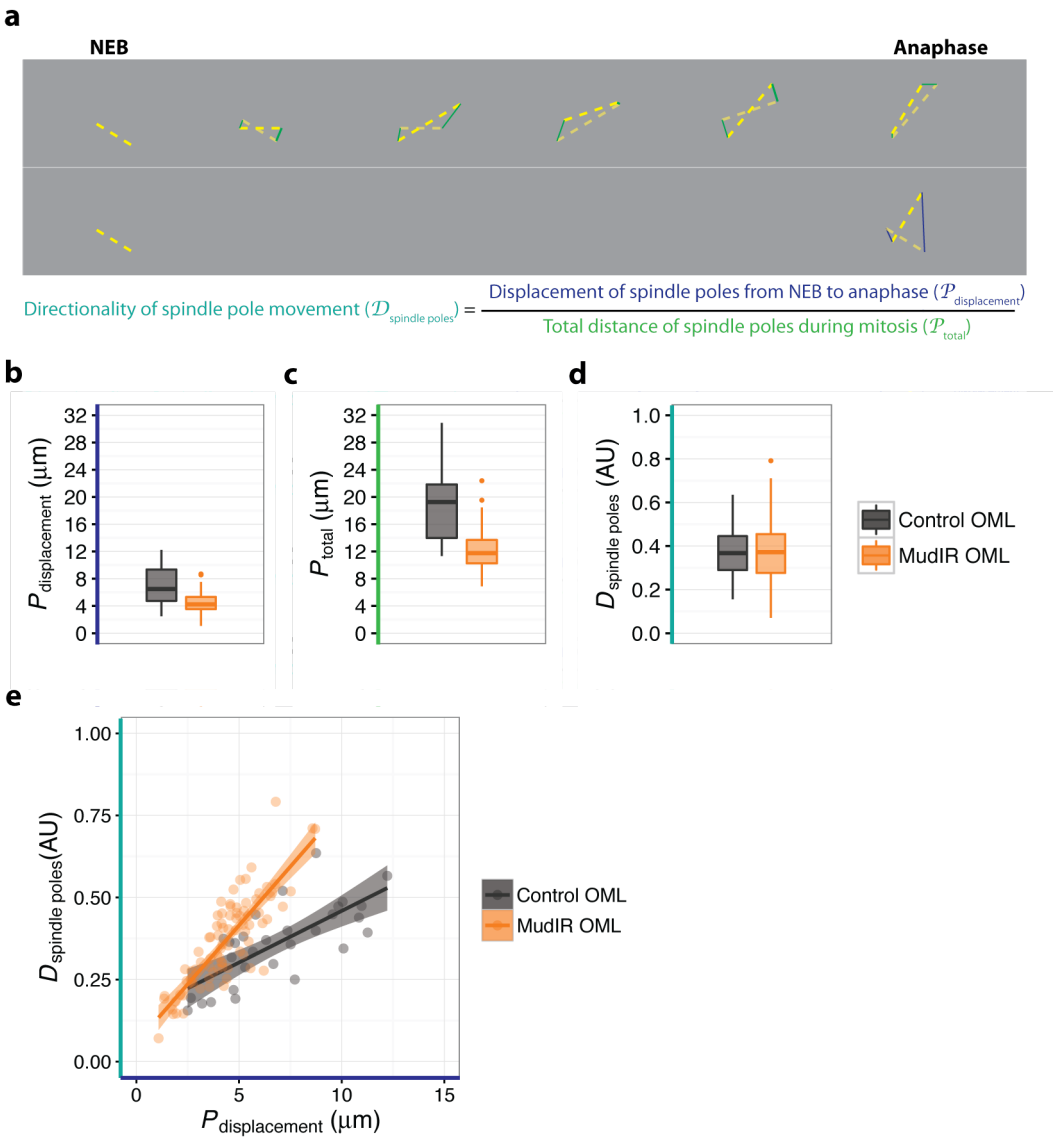

Figure 4.13: Mud is required for the dynamic movement of spindle poles.

a. Schematic of analysis of spindle pole movement.

b. Distance moved by spindle poles from NEB to anaphase ($\mathcal{P}_{displacement}$) for WT and MudIR cells (Tubulin marker). $\mathcal{P}_{displacement}$ is lower in MudIR cells compared to WT (mean: 6.892 ± 0.508 µm [WT; N: 30 cells, 2 experiments] and 4.244 ± 0.208 µm [MudIR; N: 84 cells, 3 experiments], Mann-Whitney U test p-value = 1.342^{e-05}).

c. Total distance moved by spindle poles during mitosis ($\mathcal{P}_{total}$) for WT and MudIR cells (Tubulin marker). $\mathcal{P}_{total}$ is much lower in MudIR cells compared to WT (mean:19.26 ± 0.957 µm [WT; N: 30 cells, 2 experiments] and 11.600 ± 0.344 µm [MudIR; N: 84 cells, 3 experiments], Mann-Whitney U test p-value = 1.065^{e-10}).

d. Directionality of spindle pole movement ($\mathcal{D}_{spindle\ poles}$) for WT and MudIR cells (Tubulin marker). $\mathcal{D}_{spindle\ poles}$ is similar for both WT and MudIR cells. (Mean: 0.3613 ± 0.0219 [WT;

N: 30 cells, 2 experiments] and 0.3706 ± 0.0148 [MudIR; N: 84 cells, 3 experiments], Mann-Whitney U test p-value = 0.7944). This is unexpected, since $\mathcal{D}_{\text{spindle poles}}$ is proportional to $\mathcal{P}_{\text{displacement,}}$ which is larger in WT than in MudIR cells.

e. $\mathcal{D}_{\text{spindle poles}}$ as a function of $\mathcal{P}_{\text{displacement}}$ for WT and MudIR cells (Tubulin marker). Lines indicate best-fit mean line and filled areas represent standard error of the mean. In general, $\mathcal{D}_{\text{spindle poles}}$ increases with $\mathcal{P}_{\text{displacement}}$ as expected, however where $\mathcal{P}_{\text{displacement}}$ is similar in MudIR and WT spindles, the mean $\mathcal{D}_{\text{spindle poles}}$ of MudIR spindles is higher than that of WT. This suggests that MudIR spindles poles change directions less frequently than WT spindles, and are therefore less dynamic.

4.4 Dlg-mediated localization of cortical pulling forces is required for dynamic spindle positioning.

These results suggested a role for Mud-mediated pulling forces in dynamic spindle positioning. However, Mud is localized both to the cortex as well as to spindle poles, where it plays a role in tethering MTs to the centrosome, as well as in focusing microtubule minus ends (Radulescu & Cleveland 2010). Therefore, perturbations of Mud may also affect spindle integrity, not just cortical forces regulating spindle movement. Recently, it was shown that Dlg appears to specifically regulate the localization of Mud at tricellular junctions (Bosveld et al. 2016). This had the effect of reducing apparent pulling forces at astral MTs that have been proposed to orient the spindle (Bosveld et al. 2016). Dlg has also been shown to interact with Pins, another canonical spindle orienting protein localized to the cell cortex, to coordinate spindle orientation in asymmetric cell divisions (Siegrist & Doe 2005; Johnston et al. 2009). Therefore, in order to specifically test the contribution of cortical pulling forces in dynamic spindle positioning, I used RNAi-mediated silencing to reduce levels of Dlg in the tissue (DlgIR).

4.4.1 Dlg is required for dynamic spindle rotation

Dlg has a role in maintaining apicobasal polarity and tissue organisation (Nakajima et al. 2013). By minimising the depletion of Dlg in the tissue, through low level RNAi expression or with small mutant clones, and preventing gross tissue disorder, it was recently found to have no effect on planar positioning in the *Drosophila* imaginal wing disc and notum (Bergstralh et al. 2016; Bosveld et al. 2016). Using the same strategy as Bergstralh et al., I lowered RNAi expression against Dlg in the pupal notum by keeping pupae at 18°C, which reduced Dlg expression significantly (Fig 4.14), but tissue organization was minimally perturbed. To further control for any apparent planar positioning defects, I again restricted my analysis of spindle positioning to cells where both spindle poles were within 1.5 μm.

Consistent with previous studies, spindle rotation in DlgIR cells was reduced compared to WT cells (Tubulin-cherry and Centrosomin-RFP); both in terms of total accumulated rotation during mitosis (θ_{total}) (Fig 4.15d) (Mean: 101.20

± 4.87° [WT] and 76.20 ± 6.052° [DlgIR], Mann-Whitney U test p-value = 5.333^{e-05}) and the net angular displacement from NEB to anaphase ($\theta_{displacement}$) (Fig 4.15b, c) (Mean: 48.620 ± 4.266° [WT] and 32.39 ± 3.447° [DlgIR], Kolmogorov-Smirnov test p-value = 0.03189). The decrease in $\theta_{displacement}$ for DlgIR cells was less dramatic than that observed in MudIR cells (Fig 4.9 and Fig 4.15c). Although the efficiency of RNAi can vary between treatments, this leaves open the possibility that non-cortical populations of Mud contribute towards spindle movement. Nevertheless, similar to MudIR, spindles in DlgIR cells appear to change direction less frequently than the WT, and plotting the directionality of spindle rotation ($\mathcal{D}_{rotation} = \frac{\theta_{displacement}}{\theta_{total}}$) it was apparent that for $\theta_{displacement} > 25°$ in DlgIR cells, the mean $\mathcal{D}_{rotation}$ is higher than that of WT (Fig 4.15e). This indicates that for similar amounts of angular displacement in WT spindles, DlgIR spindles change directions less frequently. This is consistent with the hypothesis that dynamic spindle rotation is directed by cortical pulling forces which depend on both Dlg and Mud.

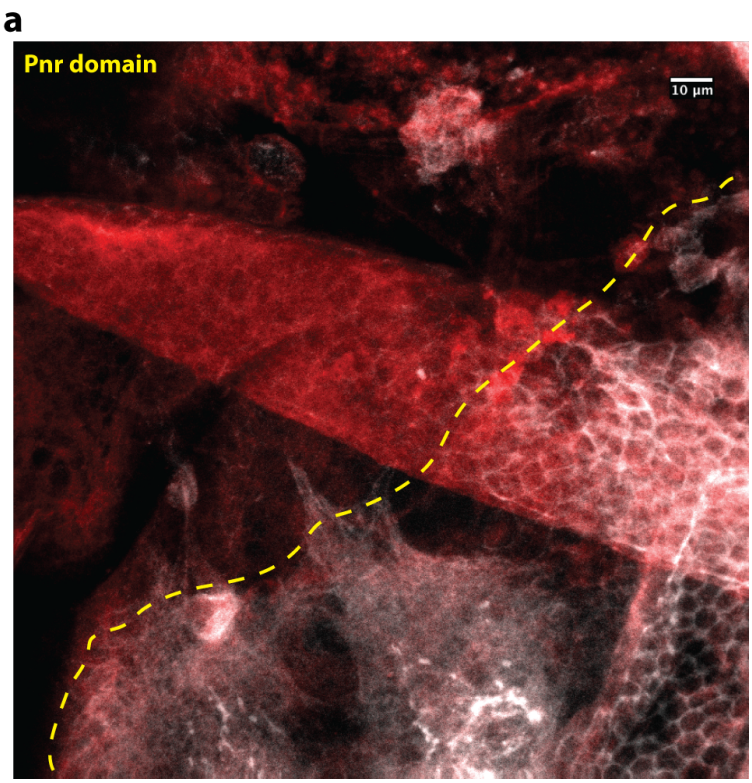

Figure 4.14: Dlg depletion by RNAi expression under the PnrGal4 driver

a. Dissected notum of pupa expressing UAS-DlgIR under the control of the PnrGal4 driver, with SpiderGFP in the background. Notum was stained for GFP (red) and Dlg (white). Image shows the part of the notum with the edge of Pnr domain expression outlined in yellow. Dlg expression is strongly reduced within the Pnr domain of the notum.

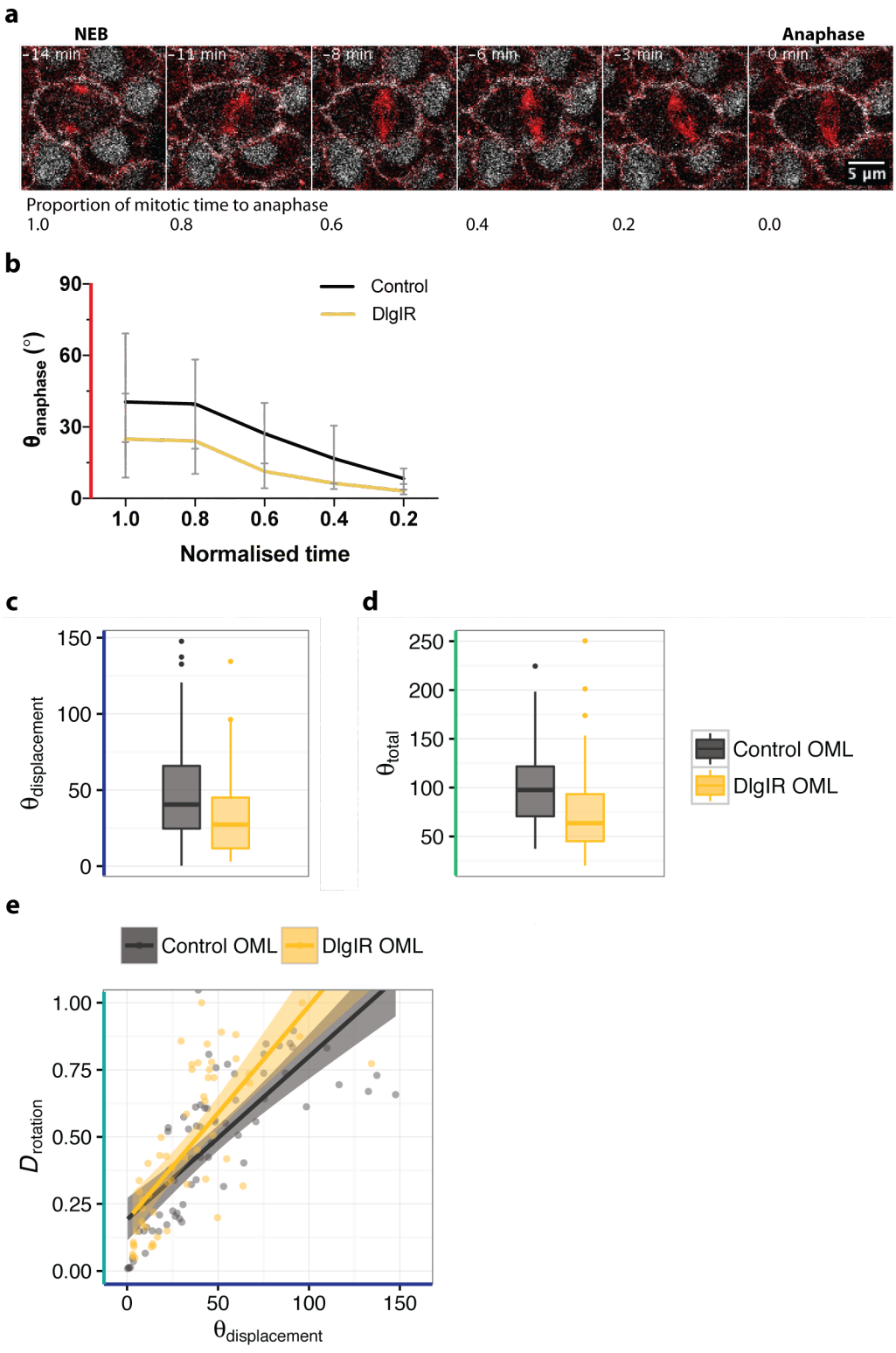

Figure 4.15: Dlg is also required for dynamic spindle rotation.

a. Representative Dlg IR cell during mitosis. Spindle labelled with tubulin-Cherry (red) and cell membrane with SpiderGFP (white). NEB and anaphase are indicated above the montage, and corresponding proportion of mitotic time below the montage.

b. Median angular distance from anaphase position ($\theta_{anaphase}$) for DlgIR and WT cells. Error bars represent interquartile range. $\theta_{anaphase}$ does not decrease as dramatically for DlgIR cells, indicating that spindle rotation is impaired.

c. Net spindle rotation from NEB to anaphase ($\theta_{displacement}$) for WT and DlgIR cells. $\theta_{displacement}$ of DlgIR cells is significantly lower than that of WT. (Mean: 48.620 ± 4.266° [WT; N: 68 cells, 5 experiments] and 32.39 ± 3.447° [DlgIR; N: 58 cells, 3 experiments], Kolmogorov-Smirnov test p-value = 0.03189).

d. Sum of the spindle rotational movements over time during mitosis (θ_{total}) for WT and DlgIR cells. θ_{total} of DlgIR cells is significantly lower than that of WT. (Mean: 101.20 ± 4.87° [WT; N: 68 cells, 5 experiments] and 76.20 ± 6.052° [DlgIR N: 58 cells, 3 experiments], Mann-Whitney U test p-value = 5.333^{e-05}).

e. Directionality of angular displacement ($\mathcal{D}_{rotation}$) as a function of $\theta_{displacement}$ for spindles in WT and DlgIR cells. Lines indicate best-fit mean line and filled areas represent standard error of the mean. In general, $\mathcal{D}_{rotation}$ increases with $\theta_{displacement}$ as expected, however for $\theta_{displacement} > 25°$ in DlgIR cells, the mean $\mathcal{D}_{rotation}$ is higher than that for WT. This indicates that spindles in DlgIR cells that rotate change directions less than those in WT cells.

4.4.2 Dlg is required for dynamic spindle translation

The effect of DlgIR on spindle rotation was similar to that of MudIR. Thus, I expected a similar trend when analysing spindle translation, as indicated by the movement of the spindle centre. Spindle centres moved progressively from NEB towards the anaphase position in a similar way in DlgIR and WT cells (Centrosomin-RFP marker) (Fig 4.16b). And the distance moved by spindle centre from NEB to anaphase ($\mathcal{C}_{\text{displacement}}$) for WT and DlgIR cells (Centrosomin marker) was similar (Fig 4.16d) (Mean: 1.544 ± 0.141 μm [WT] and 1.5580 ± 0.1250 μm [DlgIR], Kolmogorov-Smirnov test p-value = 0.3816). However, the total accumulated distance moved by spindle centre during mitosis ($\mathcal{C}_{\text{total}}$) for DlgIR was less than half of that of WT cells (Fig 4.16e). (Mean: 7.755 ± 0.2884 μm [WT] and 3.309 ± 0.1320 μm [DlgIR], Kolmogorov-Smirnov test p-value = $6.661^{\text{e-16}}$). Consequently, the directionality of spindle translation ($\mathcal{D}_{\text{spindle centre}} = \frac{\mathcal{C}_{\text{displacement}}}{\mathcal{C}_{\text{total}}}$) was higher for DlgIR than WT cells (Fig 4.16f) (Mean: 0.2147 ± 0.0225 μm [WT] and 0.4700 ± 0.0313 μm [DlgIR], Mann-Whitney U test p-value = $3.356^{\text{e-09}}$). Once again, this indicates that DlgIR spindles go through fewer changes in direction, consistent with the hypothesis that cortical pulling forces are required for dynamic spindle positioning.

4.4.3 Spindles are more centred in the absence of Dlg

When analysing the distance between spindle centres and the cell centre at late metaphase ($\mathcal{C}_{\text{metaphase cell}}$), I found that although both DlgIR and WT spindles were at a similar distance from the cell centre at NEB (Fig 4.17b), spindles get progressively closer to the cell centre for DlgIR cells while WT spindles remain a distance from the cell centre (Fig 4.17b). Thus, as was seen in MudIR cells, DlgIR spindles were significantly closer to the cell centre than WT spindles at late metaphase (Fig 4.17c) ($\mathcal{C}_{\text{metaphase cell}}$ mean: 0.7468 ± 0.0669 μm [WT] and 0.4606 ± 0.0411 μm [DlgIR], Mann-Whitney U test p-value = 0.0005131). This supports the idea that cortical pulling forces are involved in the dynamic spindle positioning after NEB, which moves spindles away from the cell centre.

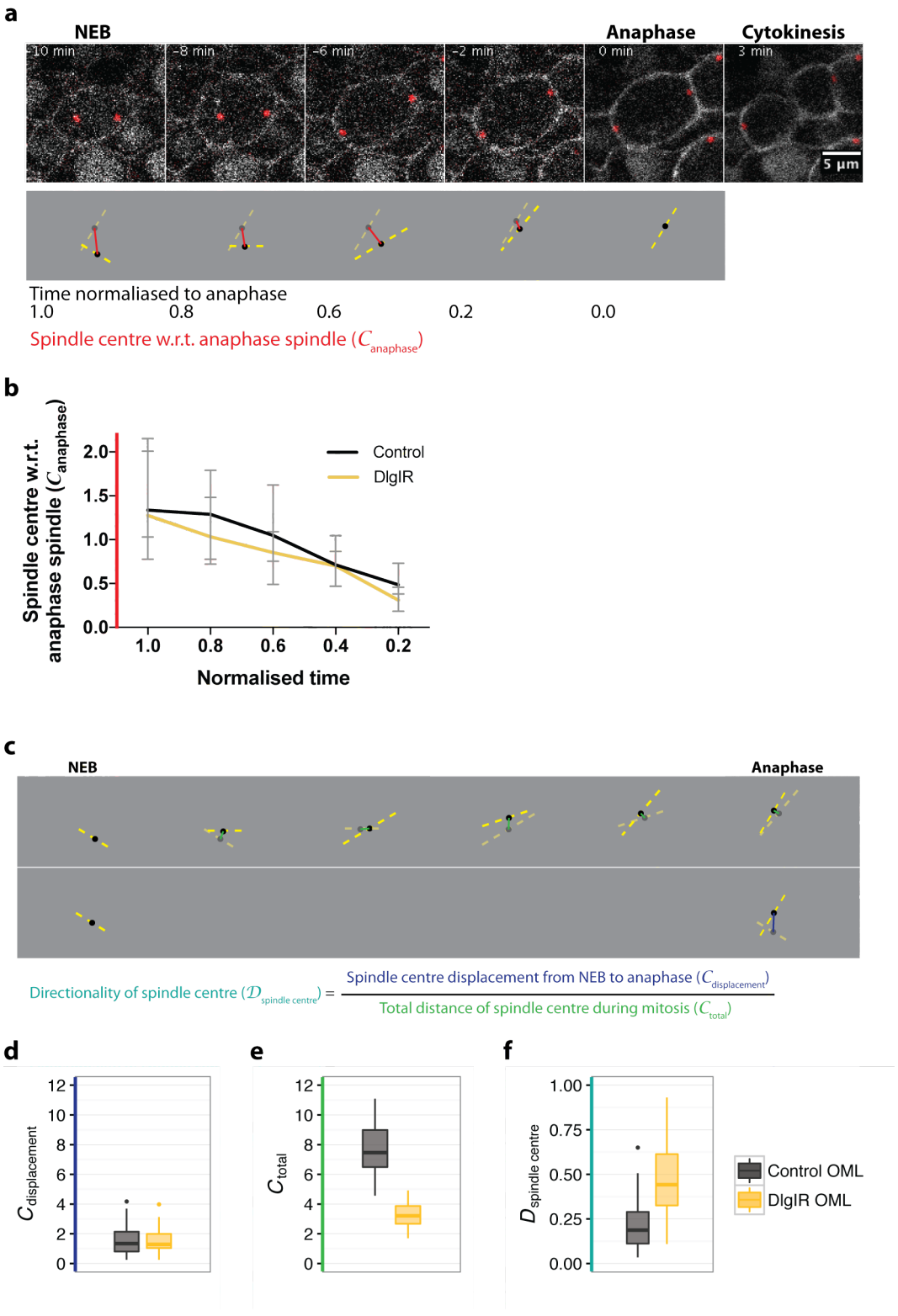

Figure 4.16: Dlg is required for dynamic spindle translation.

a. Schematic of analysis of spindle translation during mitotic progression - depicting the distance over time of the spindle centre from its final position ($\mathcal{C}_{\text{anaphase spindle}}$).

b. Median $\mathcal{C}_{\text{anaphase spindle}}$ for DlgIR and WT cells (Centrosomin marker). Error bars indicate

interquartile range. Spindle centres move a similar distance during mitosis for DlgIR and WT cells (N: 38 cells, 3 experiments [WT] and 41 cells, 3 experiments [DlgIR]).

c. Schematic of analysis of total distance moved by spindle centres from NEB to anaphase ($\mathcal{C}_{\text{displacement}}$) and during mitosis ($\mathcal{C}_{\text{total}}$). Directionality of movement of the spindle centre ($D_{\text{spindle centre}}$) is the ratio between $\mathcal{C}_{\text{displacement}}$ and $\mathcal{C}_{\text{total}}$.

d. Distance moved by spindle centre from NEB to anaphase ($\mathcal{C}_{\text{displacement}}$) for WT and DlgIR cells (Centrosomin marker). $\mathcal{C}_{\text{displacement}}$ is similar for WT and DlgIR cells (Mean: 1.544 ± 0.141 μm [WT; N: 38 cells, 3 experiments] and 1.5580 ± 0.1250 μm [DlgIR; N: 41 cells, 3 experiments], Kolmogorov-Smirnov test p-value = 0.3816).

e. Total accumulated distance moved by spindle centre during mitosis ($\mathcal{C}_{\text{total}}$) for WT and DlgIR cells (Centrosomin marker). $\mathcal{C}_{\text{total}}$ in DlgIR is significantly lower than (~half) in WT cells. (Mean: 7.755 ± 0.2884 μm [WT; N: 38 cells, 3 experiments] and 3.309 ± 0.1320 μm [DlgIR; N: 41 cells, 3 experiments], Kolmogorov-Smirnov test p-value = 6.661^{e-16}).

f. Directionality of movement of the spindle centre ($D_{\text{spindle centre}}$) for WT and DlgIR cells (Centrosomin marker). $D_{\text{spindle centre}}$ is higher in DlgIR cells than in WT cells, indicating fewer changes in direction, which is consistent with the hypothesis that cortical Mud-dependent pulling forces are required for dynamic spindle positioning. (Mean: 0.2147 ± 0.0225 μm [WT; N: 38 cells, 3 experiments] and 0.4700 ± 0.0313 μm [DlgIR; N: 41 cells, 3 experiments], Mann-Whitney U test p-value = 3.356^{e-09}).

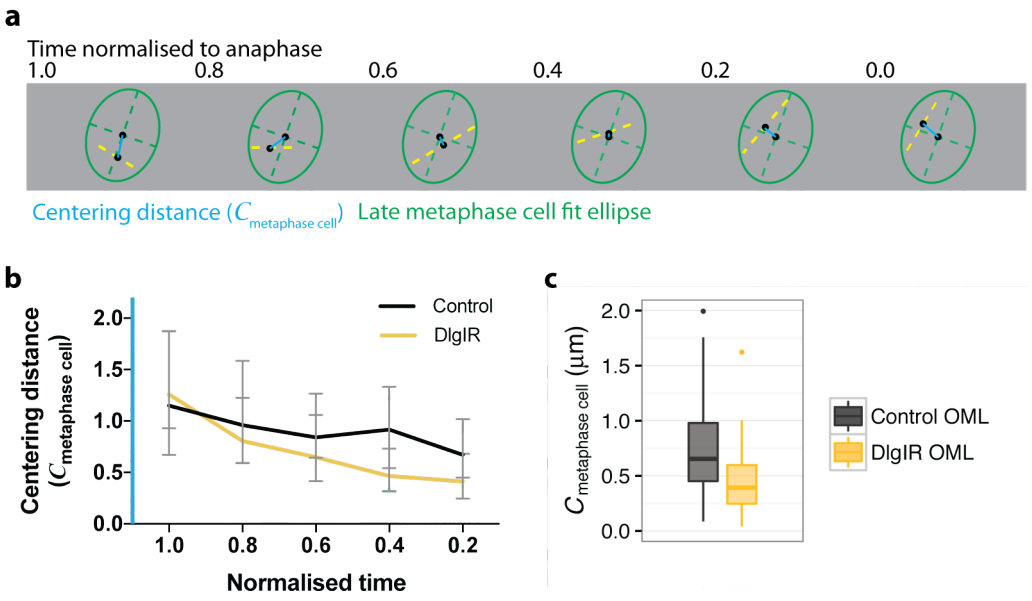

Figure 4.17: Dlg is required to move spindles off-centre

a. Schematic of analysis of distance of the spindle centre from the cell centre at late metaphase ($\mathcal{C}_{\text{metaphase cell}}$) during mitosis.

b. Median $\mathcal{C}_{\text{metaphase cell}}$ over time for DlgIR and WT cells (Centrosomin marker). Error bars indicate interquartile range. At NEB, $\mathcal{C}_{\text{metaphase cell}}$ of DlgIR is similar to that of WT cells (1.3600 ± 0.1468 µm [WT; N: 38 cells, 3 experiments] and 1.442 ± 0.1163 µm [DlgIR; N: 41 cells, 3 experiments], Kolmogorov-Smirnov test p-value = 0.2714), consistent with the hypothesis that Mud-dependent cortical pulling forces are not involved in the initial setting of spindle positioning at NEB. After NEB, $\mathcal{C}_{\text{metaphase cell}}$ of DlgIR and WT cells decreases initially. However, spindles in WT cells remain a distance from the cell centre after the initial decrease, while the value of $\mathcal{C}_{\text{metaphase cell}}$ for DlgIR cells continues to decrease over time. This is similar to the trend in cells lacking Mud.

c. Distance between spindle centre and metaphase cell centre ($\mathcal{C}_{\text{metaphase cell}}$) at late metaphase (just before anaphase onset) for WT and DlgIR cells. At late metaphase, $\mathcal{C}_{\text{metaphase cell}}$ is lower in DlgIR cells compared to WT. (Mean: 0.7468 ± 0.0669 µm [WT; N: 38 cells, 3 experiments] and 0.4606 ± 0.0411 µm [DlgIR; N: 41 cells, 3 experiments], Mann-Whitney U test p-value = 0.0005131). This is similar to MudIR cells, suggesting that cortical Mud-mediated pulling forces move spindles away from the cell centre during dynamic spindle positioning.

4.4.4 Dlg is required for dynamic spindle pole movement

When analysing spindle pole movement, which encompasses spindle translation and rotation, I also find that Dlg is required for dynamic movement. Interestingly, there was no difference between DlgIR and WT cells (Centrosomin marker) when looking at the distance moved from NEB to anaphase ($\mathcal{P}_{\text{displacement}}$) (Fig 4.18b) (Mean: 6.817 ± 0.4481 μm [WT] and 6.710 ± 0.2644 μm [DlgIR], Mann-Whitney U test p-value = 0.8262). However, there was a significant decrease in the total accumulated distance moved by spindle poles during mitosis ($\mathcal{P}_{\text{total}}$) in DlgIR cells compared to WT cells (Fig 4.18c) (Mean: 16.93 ± 0.4481 μm [WT] and 11.970 ± 0.3740μm [DlgIR], Mann-Whitney U test p-value = 3.37^{e-08}). This suggests less dynamic movement of spindle poles in DlgIR, and indeed the directionality of spindle poles ($\mathcal{D}_{\text{spindle poles}} = \frac{\mathcal{P}_{\text{displacement}}}{\mathcal{P}_{\text{total}}}$) for DlgIR is higher than that for WT (Fig 4.18d, e) (Mean: 0.4139 ± 0.0251 [WT] and 0.5647 ± 0.0175 [DlgIR], Mann-Whitney U test p-value = 3.673^{e-06}).

Overall, this supports the hypothesis that Mud and Dlg function together at the cortex as part of the cortical force generators that generate pulling forces on astral MTs responsible for dynamic spindle positioning.

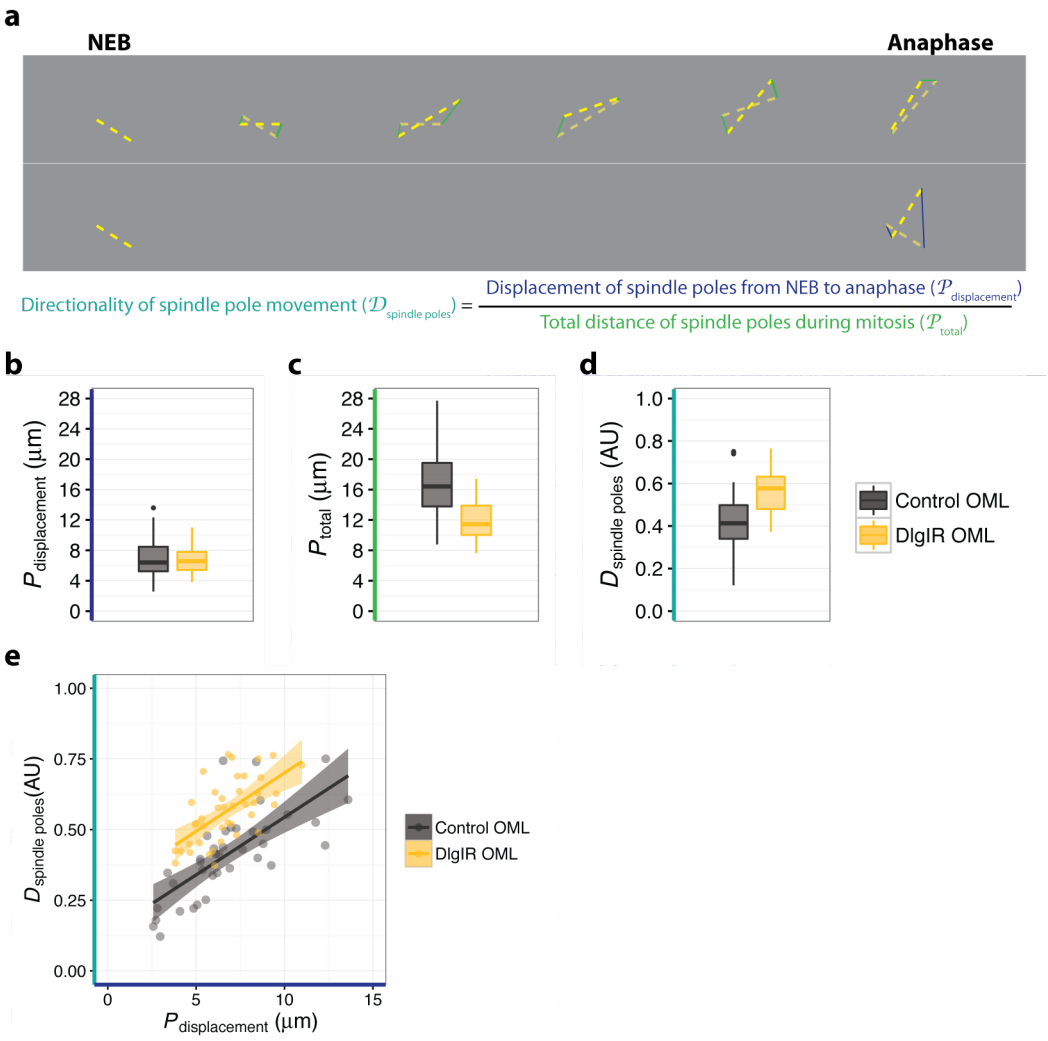

Figure 4.18: Dlg is required for the dynamic movement of spindle poles.

a. Schematic of analysis of spindle pole movement.

b. Distance moved by spindle poles from NEB to anaphase ($\mathcal{P}_{\text{displacement}}$) for WT and DlgIR cells (Centrosomin marker). $\mathcal{P}_{\text{displacement}}$ in DlgIR cells is similar to WT (mean: 6.817 ± 0.4481 µm [WT; N: 38 cells, 3 experiments] and 6.710 ± 0.2644 µm [DlgIR; N: 41 cells, 2 experiments], Mann-Whitney U test p-value = 0.8262).

c. Total distance moved by spindle poles during mitosis ($\mathcal{P}_{\text{total}}$) for WT and DlgIR cells (Centrosomin marker). $\mathcal{P}_{\text{total}}$ is much lower in DlgIR cells than in WT cells (mean: 16.93 ± 0.4481 µm [WT; N: 38 cells, 3 experiments] and 11.970 ± 0.3740µm [DlgIR; N: 41 cells, 2 experiments], Mann-Whitney U test p-value = 3.37^{e-08}).

d. Directionality of spindle pole movement ($\mathcal{D}_{\text{spindle poles}}$) for WT and DlgIR cells (Centrosomin marker). $\mathcal{D}_{\text{spindle poles}}$ is significantly higher for DlgIR cells compared to WT. (Mean: 0.4139 ± 0.0251 [WT; N: 30 cells, 2 experiments] and 0.5647 ± 0.0175 [DlgIR; N: 41 cells, 2 experiments], Mann-Whitney U test p-value = 3.673^{e-06}). This suggests that DlgIR

spindles poles change directions less frequently than WT spindles, which is consistent with the hypothesis that cortical Mud-dependent pulling forces are required for dynamic spindle positioning.

e. $\mathcal{D}_{\text{spindle poles}}$ as a function of $\mathcal{P}_{\text{displacement}}$ for WT and DlgIR cells (Centrosomin marker). Lines indicate best-fit mean line and filled areas represent standard error of the mean. In general, $\mathcal{D}_{\text{spindle poles}}$ increases with $\mathcal{P}_{\text{displacement}}$ as expected, however the mean $\mathcal{D}_{\text{spindle poles}}$ of DlgIR spindles is consistently higher than that of WT.

4.5 Astral MTs are required for moving spindles off-centre

Cortical forces are thought to act on the spindle via the astral MTs, which emanate from spindle poles and make contact with the cell cortex (Lu & Johnston 2013; di Pietro et al. 2016). In order to test the involvement of astral MTs directly, I analysed spindle positioning in flies homozygous for the severe loss-of-function allele for Asterless (Asl^{mecD}) (Blachon et al. 2008). Asl^{mecD} mutants lack functional centrioles and therefore lack centrosomal proteins that would normally nucleate astral MTs.

4.5.1 Spindles are closer to cell centre in Asl^{mecD} mutants

Spindle formation in Asl^{mecD} mutants was highly aberrant, leading to spindles with poles that appear diffuse and poorly focused. Astral MTs appear to be critically important for planar positioning, with many spindles failing to lie in the plane of the epithelium after NEB (Fig 4.19a, t = -12.5 to -4.0min). However, a bipolar spindle that lacks clearly focused cell poles is sometimes able to form in the plane of the epithelium by the end of mitosis (Fig 4.19a, t = -0.5min). This aberrant bipolar spindle is able to enter anaphase and initiate cytokinesis, as previously reported (Giansanti et al. 2001; Bonaccorsi et al. 1998)

Because of the unpredictability in the z-positioning in Asl^{mecD} mutants, it is impossible to track spindle poles consistently. I therefore focused my analysis on the spindles which manage to form a bipolar spindle within the plane of the epithelium at late metaphase (Fig 4.19a, b). The distance between the spindle centre and the cell centre ($\mathcal{C}_{\text{metaphase cell}}$) was significantly lower in Asl^{mecD} mutants than in WT cells (Fig 4.19b) (Mean: 1.008 ± 0.0709 μm [WT] and 0.7634 ± 0.0599 μm [Asl^{mecD}], Mann-Whitney U test p-value = 0.00902). This again supports the hypothesis that spindle centering does not require pulling forces. Instead, cortical pulling forces acting on astral microtubules tend to pull the spindle off-centre. This experiment also shows that astral MT dependent pushing forces are not required for spindle centring.

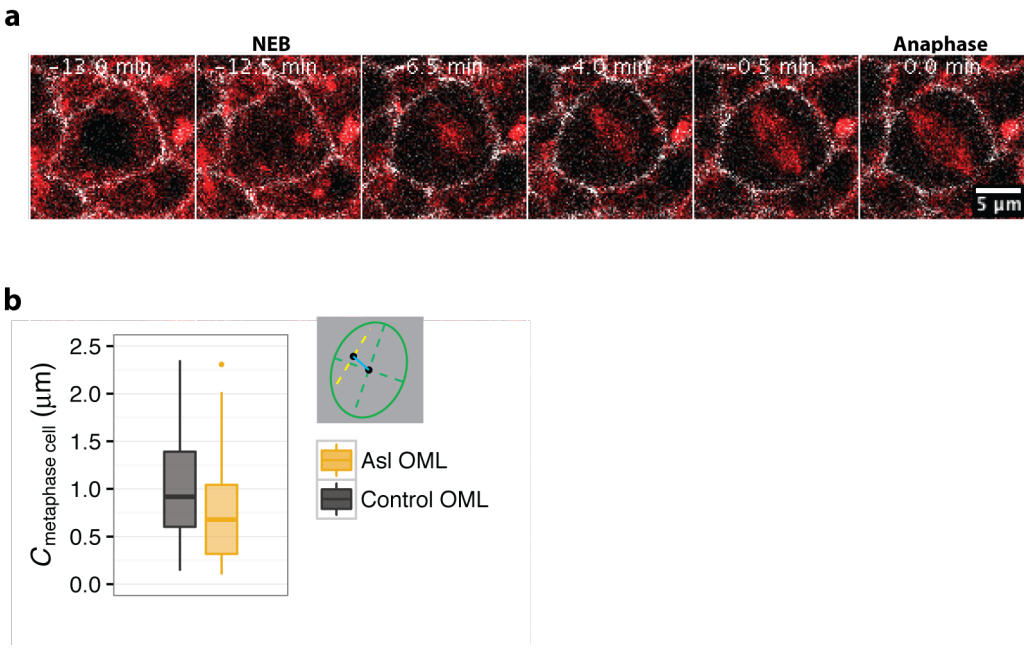

Figure 4.19: Spindles are well centred in Asterless mutants lacking astral MTs.

a. Representative *Asl*^{mecD} mutant cell during mitosis. Spindles are marked with Tubulin-Cherry (red) and cell membranes are marked with Dlg-YFP (white). Note that it is hard to follow the spindle poles from NEB through to anaphase. However, for some cells such as the one shown here, the spindle eventuallys becomes planar. The centre of the spindle can then be identified accurately at late metaphase, just before anaphase onset.

b. $C_{\text{metaphase cell}}$ for WT and *Asl*^{mecD} cells (Tubulin marker) at late metaphase. Spindle centres are significantly closer to the cell centre at late metaphase in *Asl*^{mecD} cells than in WT cells. (Mean: 1.008 ± 0.0709 µm [WT; N: 58 cells, 3 experiments] and 0.7634 ± 0.0599 µm [Asl$^{-/-}$; N: 68 cells, 3 experiments], Mann-Whitney U test p-value = 0.00902). This again supports the hypothesis that spindle centering does not require pulling forces. Instead, cortical pulling forces acting on astral microtubules tend to pull the spindle off-centre.

4.6 Conclusions

In summary, in tracking the spindle trajectories during mitosis, I found that spindle positioning is a continuous and dynamic process. Spindles rotate and translate continually towards their anaphase positions during mitosis, even before spindle length stabilises. However, this movement is not efficient and spindles often change directions. As a result, the total distance moved during rotation and translation is often larger than the net movement from NEB to anaphase. Consequently the directionality index (the ratio of net movement to total movement), which is representative of the efficiency of movement, is low.

Cortical pulling factors such as Mud are proposed to be involved in spindle positioning (di Pietro et al. 2016). Consistent with this, I find that spindle movement is significantly reduced in the absence of Mud. Mud is thought to be localised to the cortex by Dlg in this tissue, and the apparent pulling force on spindles was decreased in cells mutant for Dlg (Bosveld et al. 2016). When I knocked down expression of Dlg in cells, I found that spindle movement was reduced relative to WT, supporting a role for Dlg and Mud in regulating spindle movement.

Interestingly, loss of Mud or Dlg also resulted in a reduction in the noise in spindle movement. Residual spindle movement in MudIR and DlgIR spindles was more directed for the equivalent degree of movement in WT cells. This suggests that the dynamic changes in the orientation of spindle movements are due to cortical pulling forces. It also suggests that the pulling forces due to cortical force generators are not consistent, such that spindle movement is not persistent.

Finally, I found that spindles are often moved away from the cell centre in WT cells. This result was even more surprising, when I found that spindles were more centred in cells depleted of cortical force generators such as Mud and Dlg, or astral MTs. Initial rates of spindle movement towards the cell centre were similar for WT, MudIR and DlgIR, around the time of spindle elongation. After this period, WT spindles remained a distance from the cell centre, while MudIR and DlgIR spindles continued to move towards the cell centre. This suggests that cortical pulling forces acting on astral MTs pull spindles off-centre, and that they might be activated after

spindle elongation. It also indicates that spindles might have an intrinsic ability to find the cell centre in the absence of pulling or pushing forces on astral MTs, as spindles with no astral MTs as in the *Asterless*^{mecD} mutants were more centred at late metaphase compared to WT. One possibility is that the spindle forms around DNA, which is centred in the cell, and that the apparent movement of the spindle centre is really due to the movement of the cell mass towards the apical surface of the tissue during mitotic rounding. Tracking of DNA movement, and under conditions where rounding to the apical surface such as in Rap1^{V12}-expressing cells would be helpful in testing this hypothesis.

Chapter 5 Role of dynamic spindle positioning

5.1 Introduction

From Chapter 4 it is evident that most spindles constantly rotate towards their anaphase position, and this rotation is dynamic, with spindles changing directions occasionally or rotating away then back to their original positions.

If spindles exhibit a wide range of dynamic movements during mitosis, one might ask whether these movements serve a function? Implicit in this question is the issue of when is the appropriate spindle orientation achieved - at NEB or at anaphase? Spindle orientation at anaphase has been studied extensively and appears to be an active process involving the molecular motor dynein, following its recruitment to specific sites around the cell cortex by upstream polarity proteins (di Pietro et al. 2016; Lu & Johnston 2013). However, it remains unclear if these same forces contribute to positioning of the centrosomes before NEB, and as the spindle forms soon after NEB.

In the developing epithelia of the *Drosophila* larval wing disc and pupal dorsal thorax (which derives from the larval wing disc), it has been shown that cells that are clearly elongated at interphase and metaphase divide across the long axis of the cell (Gibson et al. 2011; Bosveld et al. 2016). This too this has been shown to be a dynein- and Mud-dependent process (Bosveld et al. 2016). Building on these observations, I used spindle orientation to the long axis of cell as a reference point in trying to understand the role of spindle rotation.

5.2 Spindle rotation re-orients the spindle from NEB to anaphase

For this analysis, I focused on cells with aspect ratio (ratio of major length to minor length of fit ellipse) > 1.2 at metaphase with a clear long axis. As previously shown in Chapter 3, the long axis at metaphase correlates with the long axis at interphase, and this is especially clear in cells which are elongated at metaphase. The spindle angle was tracked as before in Chapter 4, and spindle orientation relative to the cell long axis ($\theta_{long\ axis}$) was calculated as the angle between the spindle and the long axis of the mitotic cell (defined by the major axis of the fit ellipse) in the plane of the spindle, at the timepoint before anaphase onset i.e. late metaphase (Fig 5.1a). I defined the long cell axis before anaphase onset (late metaphase) to avoid the cell shape remodelling that occurs during anaphase elongation.

5.2.1 Spindle orientation relative to the cell long axis changes from NEB to anaphase in WT *cell but not in MudIR cells*

I previously showed that spindle rotation is severely reduced in MudIR cells. Comparing MudIR cells to WT cells therefore is as a good way to directly test the role of dynamic spindle rotation in spindle orientation to the long axis.

To begin, I tracked the changes in spindle orientation relative to the cell long axis ($\theta_{long\ axis}$) from NEB to anaphase (Fig 5.1a) for WT and MudIR cells. In WT cells (Fig 5.1b), there appeared to be a dramatic change in spindle orientation relative to the cell long axis from NEB to anaphase. By contrast, there was little change in the distribution of $\theta_{long\ axis}$ from NEB to anaphase for MudIR spindles (Fig 5.1c).

Spindles might rotate a lot, but orientation to the long axis may not change if for example, the spindle rotated 180°. To account for this, I compared the distributions of the acute $\theta_{long\ axis}$ at NEB and at anaphase (Fig 5.2). For both WT and MudIR cells, spindle orientation relative to the long axis was random at NEB (Kolmogorov-Smirnov test p-value = 0.1821 [WT] and 0.8684 [MudIR] against a random generated uniform distribution) (Fig 5.2a, b). Thus, the spindle doesn't form along the long axis of the cell, and must rotate towards it before anaphase. In addition, Mud is required for spindle rotation after NEB, and doesn't influence the positioning of presumptive spindle poles at NEB.

Next, I looked at spindle orientations at anaphase to see if they were any different to that at NEB. For MudIR the distribution of $\theta_{long\ axis}$ is similar at anaphase, although a broad peak appears around $\theta_{long\ axis} \approx 30°$ (Fig 5.2b). However, the distributions of $\theta_{long\ axis}$ at NEB and anaphase were not significantly different (Kolmogorov-Smirnov test p-value = 0.488). This is consistent with a role for spindle rotation by pulling forces on the astral MTs in changing spindle orientation.

For WT cells at anaphase, $\theta_{long\ axis}$ appears to peak around $\theta_{long\ axis} \approx 20°$. Despite the apparent differences, the distributions of $\theta_{long\ axis}$ at NEB and at anaphase were not significantly different (Kolmogorov-Smirnov test p-value = 0.6885). Nevertheless, plotting the spindle orientation at anaphase by NEB showed that spindle rotations were indeed changing spindle orientations (Fig 5.3a). In WT cells, spindles further from the cell long axis at NEB ($\theta_{long\ axis}$ at NEB = 60-90° or $\theta_{long\ axis}$ at NEB = 30-60°) were close to the cell long axis at anaphase ($\theta_{long\ axis}$ at anaphase < 45°). Their distributions at anaphase onset were therefore significantly different from that at NEB (Kolmogorov-Smirnov test p-value = 1.885^{e-05} [WT, short axis at NEB] and 0.0006739 [WT, intermediate axis at NEB]) (Fig 5.3a). Meanwhile, spindles that formed close to the long axis at NEB ($\theta_{long\ axis}$ at NEB = 0-30°) also had significantly different orientations at anaphase, suggesting that they had moved away from the long axis (Fig 5.3a) (Kolmogorov-Smirnov test p-value = 0.001401 [WT, long axis at NEB]). It is worth noting that the changes were more significant for the spindles that form furthest from the long axis, suggesting a bias for spindle rotation from the short to the long axis. Consistent with this, spindle displacement ($\theta_{displacement}$) was significantly higher for spindles where $\theta_{long\ axis}$ at NEB = 60-90°, compared to spindles where $\theta_{long\ axis}$ at NEB = 0-30° (Mann-Whitney U test p-value = 0.0269, N: 14 cells [WT, $\theta_{long\ axis}$ at NEB = 60-90°] and 24 cells [WT, NEB = 0-30°]) (Fig 5.3c). The persistence of spindle rotations is consequently higher for spindles that form at the short axis compared to those forming at the long axis of the cell (Fig 5.3e), suggesting that spindles further from the long axis at NEB are more likely to move in a directed manner.

This contrasts with what was seen in MudIR cells, where spindle orientations at anaphase did not change significantly from their orientations at NEB (Fig 5.3b). Although spindles where $\theta_{long\ axis}$ at NEB = 60-90° appeared to move away from their

NEB position by anaphase onset (Kolmogorov-Smirnov test p-value = 0.01878 [MudIR, short axis at NEB]) (Fig 5.3b), this was not accompanied any significant spindle rotation from NEB to anaphase (Fig 5.3d) (Mann-Whitney U test p-value = 0.1906 N: 14 cells [MudIR, short axis] and 24 cells [MudIR, long axis]). Additionally, the spindle rotations from the short axis were not as directed as those in WT cells (Fig 5.3f).

This indicates that spindle rotations, mediated by cortical pulling forces, are resulting in a change in spindle orientations relative to the cell long axis.

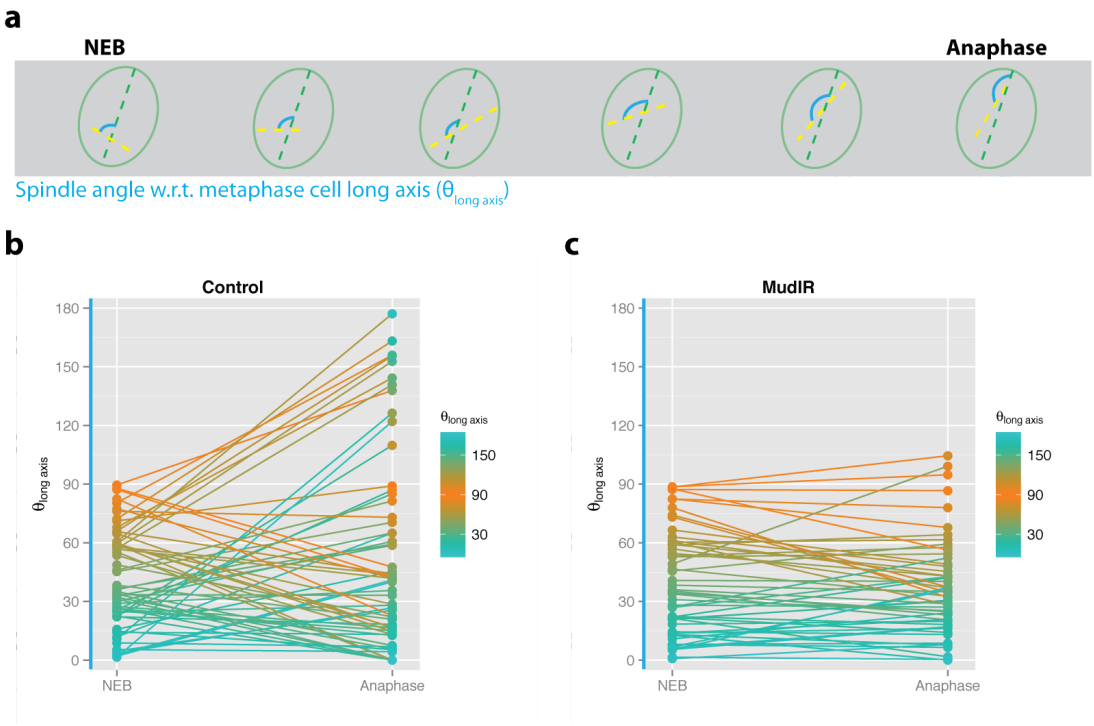

Figure 5.1: Spindle rotations result in a change in spindle orientations relative to the cell long axis from NEB to anaphase.

a. Schematic of analysis for spindle angle wrt metaphase cell long axis ($\theta_{long\ axis}$).

The angle between the spindle and the long axis of the cell at metaphase was tracked from NEB to anaphase. Cells with an aspect ratio of > 1.2, and hence a clear long axis, were used for analysis.

b. Line plots for individual WT cells showing $\theta_{long\ axis}$ at NEB and at anaphase. Colour map indicates spindles close to the metaphase cell long axis (cyan) and to the short axis (orange). Points indicate $\theta_{long\ axis}$, with line connecting corresponding points from NEB to anaphase. Line colours follow that of $\theta_{long\ axis}$ at NEB. The slope of the line reflects the degree of displacement from NEB to anaphase ($\theta_{displacement}$). It is evident that spindles rotate significantly from NEB to anaphase, and that these often result in changes in spindle orientation relative to the cell long axis. Spindle rotations from the short to the long axis seem prevalent.

c. Line plots as in **b** for MudIR cells. It is apparent that in MudIR cells, spindles do not rotate much from NEB to anaphase, and that spindle orientations relative to the long axis do not change significantly.

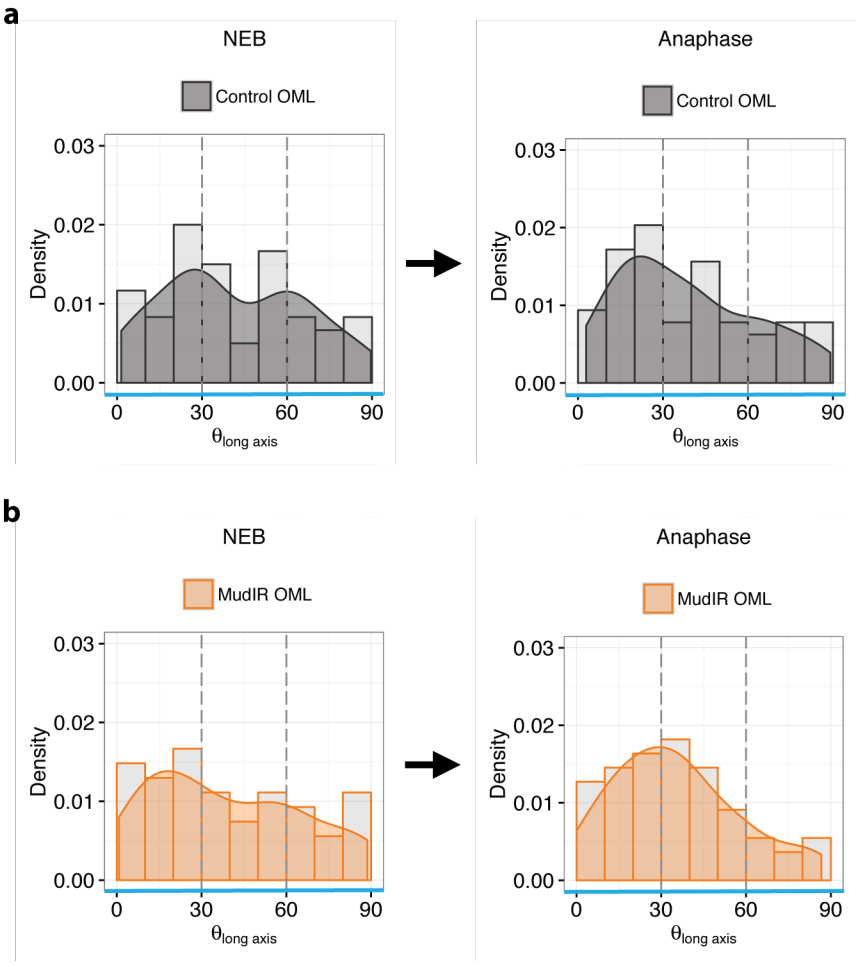

Figure 5.2: Acute spindle orientation relative to cell long axis at NEB and anaphase for WT and MudIR cells.

a. Density plot of acute $\theta_{long\ axis}$ at NEB and anaphase for spindles in WT cells. The distribution of $\theta_{long\ axis}$ is random at NEB (Kolmogorov-Smirnov test p-value = 0.1821; N: 75 cells, 6 experiments [WT] and N: 60 cells [random generated uniform distribution]). At anaphase, $\theta_{long\ axis}$ appears to peak at ≈ 20°. However, distributions of $\theta_{long\ axis}$ at NEB and at anaphase are not significantly different (Kolmogorov-Smirnov test p-value = 0.6885, N: 75 cells, 6 experiments).

b. Density plot of acute $\theta_{long\ axis}$ at NEB and anaphase for spindles in MudIR cells. The distribution of $\theta_{long\ axis}$ is random at NEB (Kolmogorov-Smirnov test p-value = 0.8684; N: 55 cells, 3 experiments [MudIR] and N: 60 cells [random generated uniform distribution]), and is similar at anaphase. Distributions of $\theta_{long\ axis}$ at NEB and at anaphase are not significantly different (Kolmogorov-Smirnov test p-value = 0.488, N: 55 cells, 3 experiments).

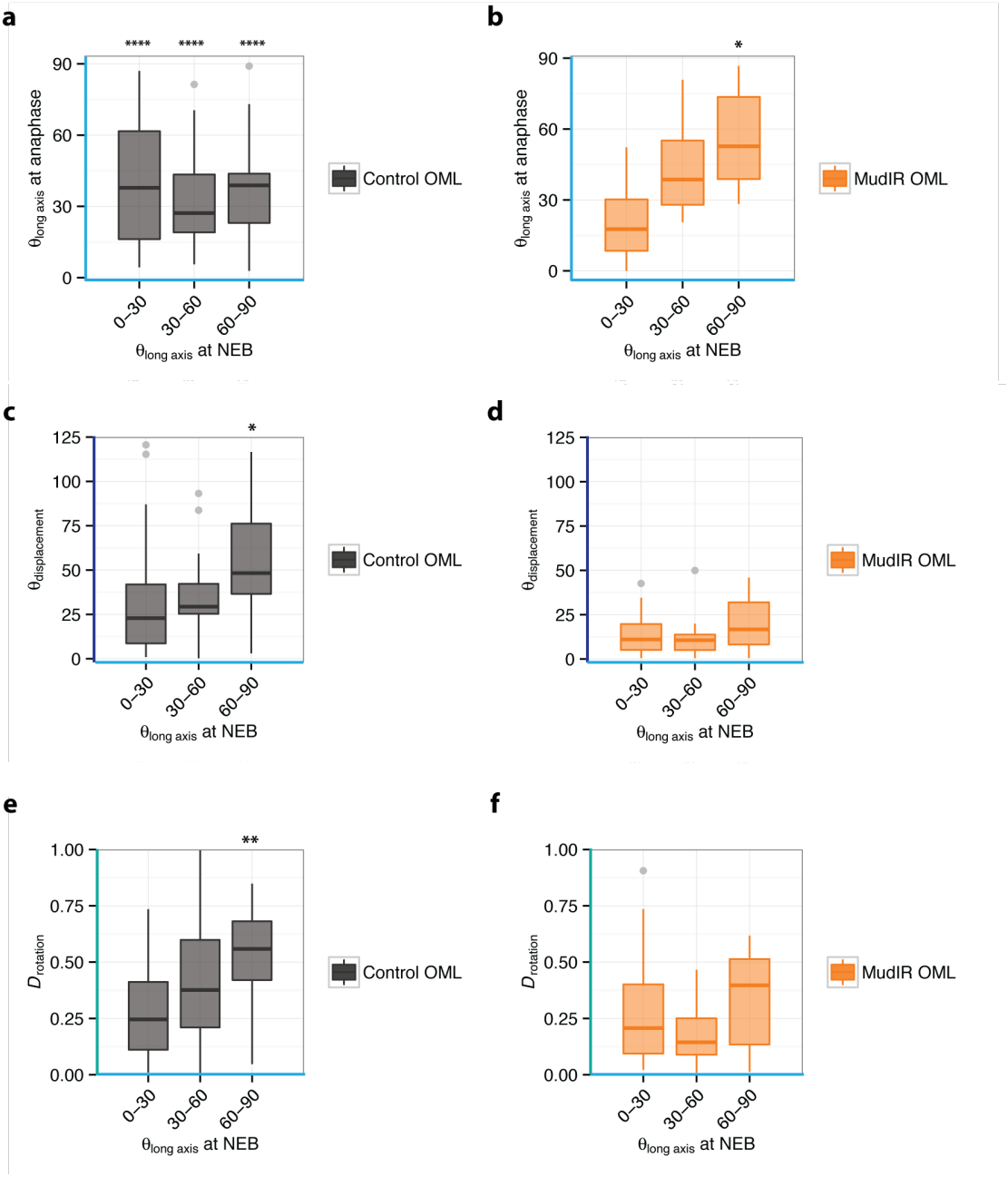

Figure 5.3: Spindles at the short and intermediate axes rotate in a directed way towards the long axis in WT cells but not in MudIR cells.

a. Spindle orientation relative to the long axis (acute $\theta_{long\ axis}$) at anaphase for WT spindles by spindle orientation at NEB. Spindle orientations of WT cells changed from the short ($\theta_{long\ axis}$ at NEB = 60-90°) or intermediate ($\theta_{long\ axis}$ at NEB = 30-60°) axes at NEB towards the cell long axis at anaphase, while spindles at the long axis at NEB ($\theta_{long\ axis}$ at NEB = 0-30°) moved towards the intermediate axis. (**** indicates $p < 0.001$. Distribution at anaphase was tested against corresponding distribution at NEB with the Kolmogorov-Smirnov test).

b. Spindle orientation relative to the long axis (acute $\theta_{long\ axis}$) at anaphase for MudIR spindles by spindle orientation at NEB. Spindle orientations of MudIR cells did not appear to change

from NEB, except when spindles formed at the short axis. There was a shift towards the intermediate axis at anaphase. (* indicates $p < 0.05$. Distribution at anaphase was tested against corresponding distribution at NEB with the Kolmogorov-Smirnov test).

c. Spindle rotation from NEB to anaphase ($\theta_{displacement}$) for WT spindles by spindle orientation at NEB. $\theta_{displacement}$ was significantly higher for WT spindles that formed at the short axis ($\theta_{long\ axis}$ = 60-90°), compared to spindles that form at the long axis ($\theta_{long\ axis}$ = 0-30°) (* indicates $p < 0.05$, Mann-Whitney U test. N: 14 cells [short axis] and 24 cells [long axis]). $\theta_{displacement}$ of spindles forming at the short axis was also significantly higher for WT than for MudIR cells.

d. Spindle rotation from NEB to anaphase ($\theta_{displacement}$) for MudIR spindles by spindle orientation at NEB. $\theta_{displacement}$ appears to be higher for MudIR spindles forming close to the short axis, although this was not significant (Mann-Whitney U test p-value = 0.1906, N: 14 cells [short axis] and 24 cells [long axis]).

e. Persistence of spindle rotation from NEB to anaphase ($\mathcal{D}_{rotation} = \frac{\theta_{displacement}}{\theta_{total}}$) for WT spindles by spindle orientation at NEB. $\mathcal{D}_{rotation}$ was significantly higher for WT spindles that form at the short axis ($\theta_{long\ axis}$ = 60-90°), compared to spindles that form at the long axis ($\theta_{long\ axis}$ = 0-30°) (** indicates $p < 0.01$, Mann-Whitney U test. N: 14 cells [short axis] and 24 cells [long axis]). $\mathcal{D}_{rotation}$ was also higher for WT spindles forming at the short axis compared equivalent MudIR spindles.

f. Persistence of spindle rotation from NEB to anaphase ($\mathcal{D}_{rotation} = \frac{\theta_{displacement}}{\theta_{total}}$) for MudIR spindles by spindle orientation at NEB. $\mathcal{D}_{rotation}$ was not significantly higher for MudIR spindles that form at the short axis ($\theta_{long\ axis}$ = 60-90°), compared to spindles that form at the long axis ($\theta_{long\ axis}$ = 0-30°) (Mann-Whitney U test p-value = 0.4101, N: 14 cells [short axis] and 24 cells [long axis]).

5.2.2 Mud-independent spindle displacement away from the short axis of the cell as spindles elongate.

MudIR spindles that are oriented along the short axis at NEB appear to have a higher displacement than those oriented along the long axis at NEB, although this was not significantly different (Fig 5.3b). Furthermore, there appears to be a decrease in spindles along the short axis at anaphase (Fig 5.2b, 5.3a). This suggested a possible role for pushing forces exerted by the spindle either at the poles by growing plus ends or by the spindle itself as it elongates (Grill & Hyman 2005; Laan et al. 2012; Minc & Piel 2012; Garzon-Coral et al. 2016). Looking at individual spindles that form at the short and long axis, it appears that this might be the case. In a cell where spindle formation occurs at the short axis (Fig 5.4a), $\theta_{\text{long axis}}$ decreases as spindle length increases (Fig 5.4b). In contrast, in a cell where spindle formation occurs in line with the long axis (Fig 5.4c), $\theta_{\text{long axis}}$ remains relatively constant as spindle length increases (Fig 5.4d).

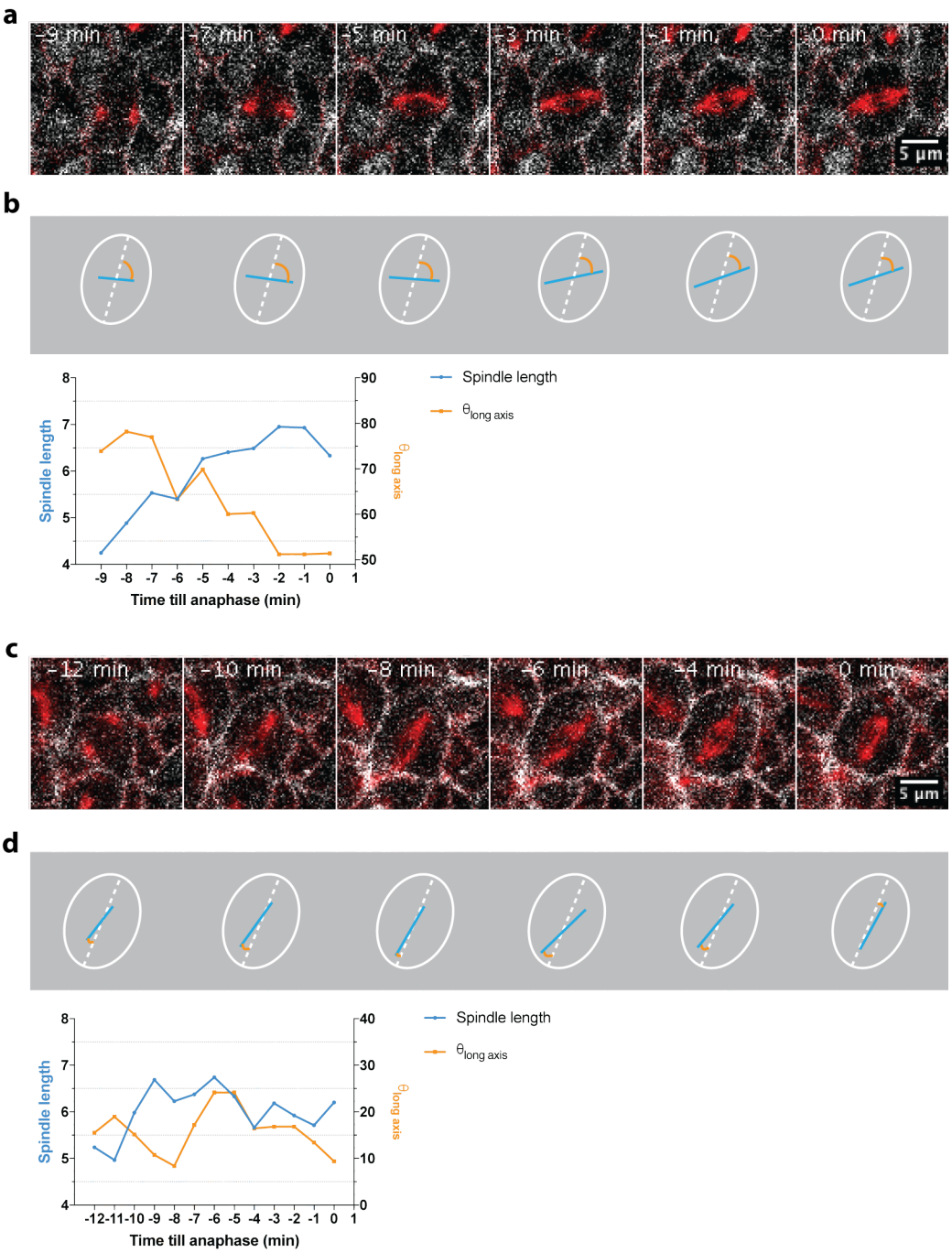

Figure 5.4: MudIR spindles forming at the short axis are likely to displace slightly away from NEB position during spindle elongation.

a. Montage of MudIR cell with spindle forming at short axis. Spindle is labelled with tubulin-mCherry (red) and cell membranes are labelled with Spider-GFP (white).

b. Graphical representation and line plot of spindle length and spindle orientation relative to the cell long axis ($\theta_{long\ axis}$) for cell in **a**. As spindle length increases, spindle orientation is displaced away from the short axis.

c. Montage of MudIR cell with spindle forming at long axis. Spindle is labelled with tubulin-

mCherry (red) and cell membranes are labelled with Spider-GFP (white).

d. Graphical representation and line plot of spindle length and spindle orientation relative to the cell long axis ($\theta_{long\ axis}$) for cell in **c**. As spindle length increases, spindle orientation remains close to long axis.

5.2.3 Mud-dependent spindle rotation re-orients spindles from the short axis of the cell at NEB towards the long axis of the cell at anaphase.

Spindle rotation from NEB to anaphase ($\theta_{displacement}$) was significantly higher for WT spindles that form close to the short axis of the cell. $\theta_{displacement}$ for spindles forming close to the short axis was also much higher than $\theta_{displacement}$ for MudIR spindles forming close to the short axis, indicating that Mud-mediated pulling forces on the spindle in WT cells are larger than that of pushing forces in MudIR cells. It also suggested that the displacement of spindles from the short axis in WT cells could not be explained with passive spindle elongation against the cell width.

To analyse the impact of spindle rotation on re-orienting the spindle, the distribution of spindle rotation from NEB to anaphase of MudIR cells was used to establish what would constitute as 'non-significant' displacement. The 90th percentile for MudIR cells ($\theta_{displacement}$= 34°) was used as the threshold, with 45% of WT cells categorised as having 'significant' displacement of $\theta_{displacement}$ > 34° (Fig 5.5a).

For spindles with $\theta_{displacement}$ > 34°, distributions of $\theta_{long\ axis}$ at NEB and at anaphase were significantly different (Fig5.6b, d) (Kolmogorov-Smirnov test p-value = 0.02167). Importantly, spindle orientation at NEB was largely random with an apparent peak close to the short axis ($\theta_{long\ axis}$ > 60°), but at anaphase there was an apparent shift in spindle orientation towards the long axis of the cell ($\theta_{long\ axis}$ < 30°) (Fig5.5b, 5.6b). This suggested that spindle rotation was biased towards the long axis. In line with this, when plotting the spindle orientations at anaphase by the orientations at NEB (Fig 5.6d), I find that spindles that form further from the long axis ($\theta_{long\ axis}$ at NEB = 30-60° or 60-90°), are close to the long axis by anaphase (70.37% of spindles with $\theta_{displacement}$ > 34°, 31.66% of all WT spindles) (Fig 5.6d). Surprisingly, I find some spindles that form at the long axis that move away and end up oriented along the short axis (29.62% of spindles with $\theta_{displacement}$ > 34°, 13.33% of all WT spindles). This implies that the mechanism for rotation towards the long axis may not be very well regulated.

In contrast, for spindles with $\theta_{displacement}$ < 34° spindle orientation at NEB appeared to cluster close to the cell long axis ($\theta_{long\ axis}$ < 30°) (Kolmogorov-Smirnov test p-value = 0.001763), however it appeared random at anaphase (Kolmogorov-

Smirnov test p-value = 0.18) (Fig 5.6a). This suggests that the bulk of spindles that do not rotate much are already close to the long axis at NEB, however they do not remain exactly at their NEB positions. When analysing the spindle orientations at anaphase by orientations at NEB for these spindles (Fig5.6c), I indeed observe that the majority of the spindles form close to the long or intermediate axis ($\theta_{long\ axis}$ = 0-60°) and remain far from the short axis at anaphase (90.90% of spindles with $\theta_{displacement} < 34°$, 45.45% of all WT spindles).

This data supports the model where spindle rotation movements are greatest for spindles that are far from the long axis, and serves to re-orient spindles to the long axis. Under these conditions, both pushing (Mud-independent) and pulling (Mud-dependent) forces act in synergy.

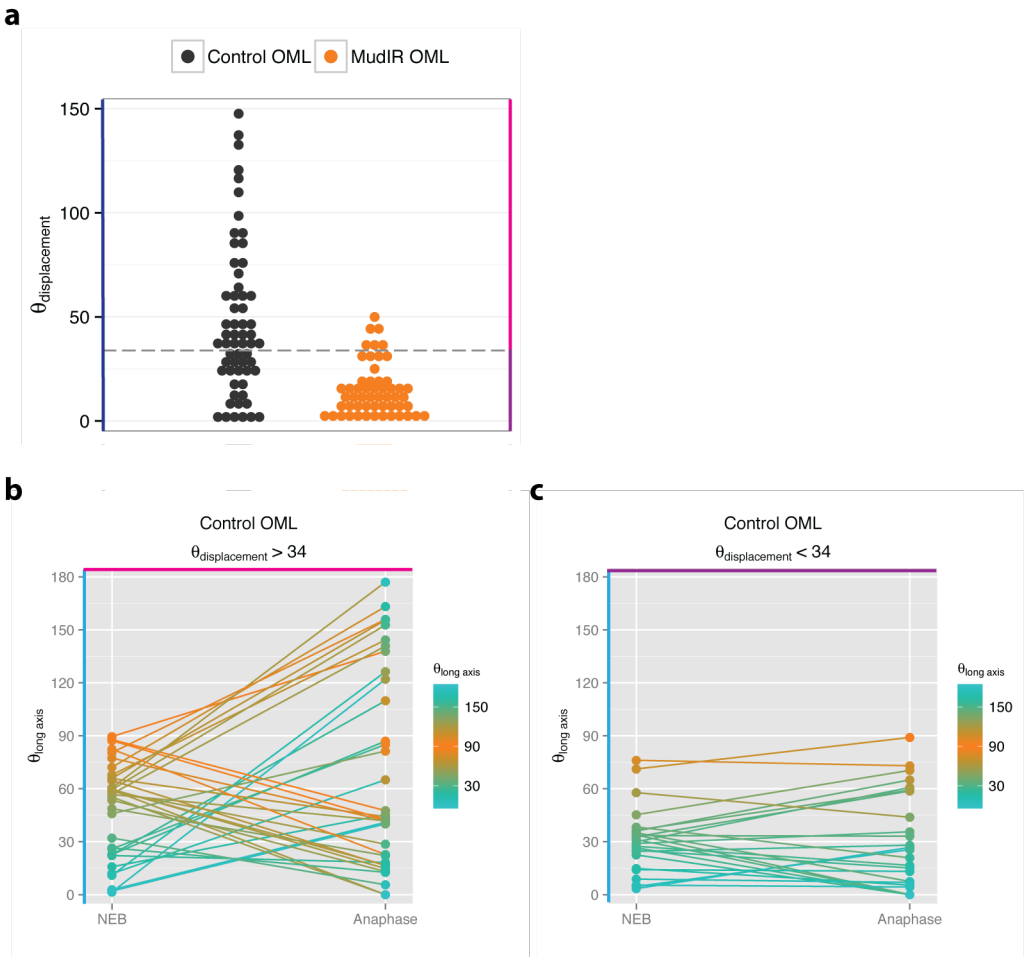

Figure 5.5: Spindle rotation changes the distribution of spindle orientations from NEB to anaphase.

a. Spindle rotation from NEB to anaphase ($\theta_{displacement}$) for WT and MudIR cells. The grey dashed line indicates the 90th percentile value of MudIR cells ($\theta_{displacement}$ = 34°), which was used as the threshold for classifying cells with significant or non-significant spindle displacement. In WT cells, 45% of cells have $\theta_{displacement}$ > 34°.

b. Line plots for individual WT cells with $\theta_{displacement}$ > 34°, showing $\theta_{long\ axis}$ at NEB and at anaphase. Colour map indicate spindles close to the metaphase cell long axis (cyan) and to the short axis (orange). Points indicate $\theta_{long\ axis}$, with line connecting corresponding points from NEB to anaphase. Line colours follow that of $\theta_{long\ axis}$ at NEB. Line plots suggest spindles close to short axis at NEB move towards long axis by anaphase.

c. Line plots as in **b** for individual WT cells with $\theta_{displacement}$ < 34°. Line plots suggest that spindles with low displacements are mostly at the long axis at NEB.

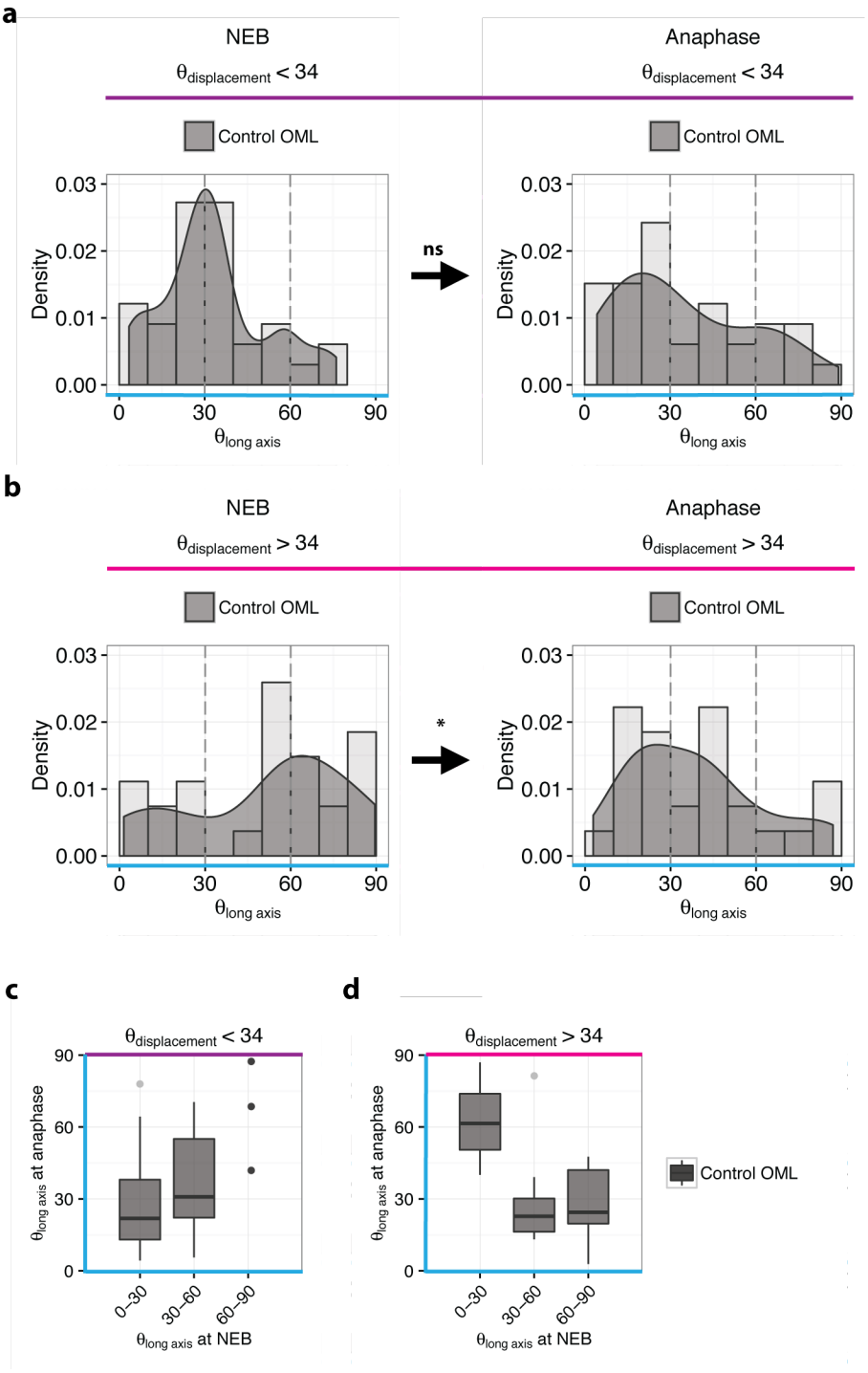

Figure 5.6: Spindle rotation re-orients spindles from the short to the long axis.

a. Density plot of acute $\theta_{long\ axis}$ at NEB and anaphase for spindles with $\theta_{displacement} < 34°$. Distributions of $\theta_{long\ axis}$ at NEB and at anaphase are not significantly different (Kolmogorov-Smirnov test p-value= 0.6543, n = 33 cells). Spindle orientations at NEB appears to cluster close to the cell long axis ($\theta_{long\ axis} < 30°$) (Kolmogorov-Smirnov test p-value = 0.001763; n: 33 cells [WT, $\theta_{displacement} < 34°$] and 60 cells [random generated uniform distribution]), however it is random at anaphase (Kolmogorov-Smirnov test p-value = 0.18; n: 33 cells [WT, $\theta_{displacement} < 34°$] and 60 cells [random generated uniform distribution]) – suggesting that

spindles which rotate little are initially at the long axis at NEB after centrosome separation, but do not tend to align to the cell long axis.

b. Density plot of acute $\theta_{\text{long axis}}$ at NEB and anaphase for spindles with $\theta_{\text{displacement}} > 34°$. Distributions of $\theta_{\text{long axis}}$ at NEB and at anaphase are significantly different (Kolmogorov-Smirnov test p-value = 0.02167, n = 27cells). Spindle orientation at NEB is largely random with an apparent peak close to the short axis ($\theta_{\text{long axis}} > 60°$) (Kolmogorov-Smirnov test p-value = 0.3551; n: 27 cells [WT, $\theta_{\text{displacement}} > 34°$] and 60 cells [random generated uniform distribution]), but at anaphase there is an apparent shift in spindle orientation towards the cell long axis ($\theta_{\text{long axis}} < 30$).

c. Spindle orientation at anaphase by spindle orientation at NEB for WT spindles with $\theta_{\text{displacement}} < 34°$. Spindles where $\theta_{\text{long axis}}$ at NEB = 0-60° remain within this range at anaphase (90.90% of spindles with $\theta_{\text{displacement}} < 34°$, 45.45% of all WT spindles).

d. Spindle orientation at anaphase by spindle orientation at NEB for WT spindles with $\theta_{\text{displacement}} > 34°$. Spindles where $\theta_{\text{long axis}}$ at NEB = 30-90° rotate towards the long axis by anaphase ($\theta_{\text{long axis}}$ at anaphase < 45°) (70.37% of spindles with $\theta_{\text{displacement}} > 34°$, 31.66% of all WT spindles).

5.3 Conclusions

Consistent with previous findings, I find that spindle orientations tend to be along the cell long axis by anaphase onset for elongated cells in the notum (Bosveld et al. 2016). Spindle orientation at NEB though is random, and is independent of Mud. Spindle orientation to the cell long axis at anaphase onset is the net result of spindles rotating from the short or intermediate axes towards the long axis. However, spindles that form at the long axis occasionally rotate away from this by anaphase onset. This suggests that the current model where Mud localization serves as landmarks for cell shape (Bosveld et al. 2016) may not have high fidelity, or that other mechanisms are at play.

Surprisingly, in cells depleted of Mud, and therefore cortical pulling forces, spindles could rotate slightly away from the short axis. Compared to WT, this was to a much smaller degree and towards the intermediate rather than the long axis. This movement is likely to occur by pushing of the spindle against the cortex. This hypothesis is supported by the observation that spindle elongation and displacement seem to be anti-correlated for spindles forming against the short axis but not for those forming along the long axis.

Chapter 6 The influence of tissue tension on spindle positioning

6.1 Introduction

In the previous chapters, I showed that spindle positioning is a dynamic process, regulated by pulling factors on astral microtubules. These pulling forces result in apparently noisy spindle movement and move the spindle off-centre, but also facilitate spindle rotation towards the cell long axis. This finding supports the observation of many before that the spindle tends to lie along the long axis of symmetrically dividing cells with anisotropic shapes (di Pietro et al. 2016; Minc & Piel 2012). Dividing with the long axis is proposed to relieve local tissue tension (Mao et al. 2011; Campinho et al. 2013; Wyatt et al. 2015) and improve cell packing in the tissue (Gibson et al. 2011).

I showed in particular that spindles that form far from the long axis rotate towards it in a directed fashion, which is reminiscent of the spindle re-orientation seen in experiments that affect cell shape (O'Connell & Wang 2000) or extracellular tension (Fink et al. 2011). In this chapter, I explore the influence of cell shape and tissue tension on this dynamic spindle positioning.

6.2 Spindle orientation to the cell long axis does not improve with cell shape anisotropy or length

As described in Chapter 3, cells in the notum undergo a dramatic change in cell shape as they enter and exit mitosis. However, not all cells lose their long axis during mitotic cell rounding. In particular, cells in the midline are more prone to retaining a well-defined long axis in mitosis than cells outside the midline (Fig 3.5, Fig 6.1a).

According to the model by Minc et al. where the tension along the astral MTs scales with the length of the astral MTs, the longer or more anisotropic a cell in mitosis, the more likely spindle alignment will be to the long axis. However, I failed to find a strong correlation between cell length at late metaphase and the accuracy of spindle alignment, even for ML cells which have a clear long axis (Fig 6.1b, c). Furthermore, spindle poles are often seen close to, if not on the cell cortex (Fig 6.2a), implying that in this tissue the model proposed by Minc et al. is not viable.

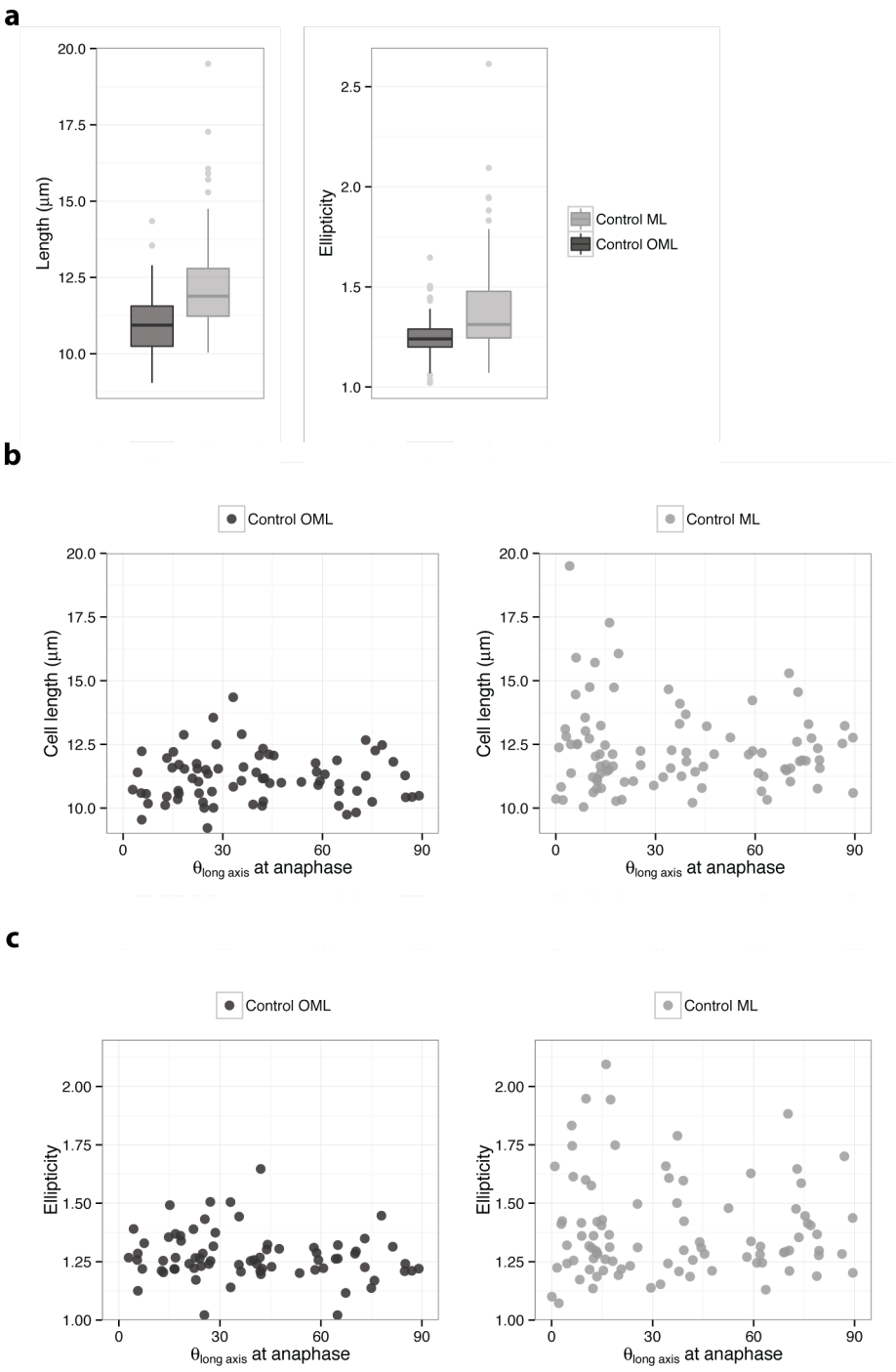

Figure 6.1: Spindle orientation to the cell long axis does not correlate with cell length or anisotropy in OML or ML cells.

a. Length of major axis of fit ellipse and ellipticity (ratio of major axis to minor axis of fit ellipse) for WT OML and ML cells. ML cells are longer and narrower than OML cells. (Mann-Whitney U test p-value = 1.862^{e-10} [length] and 1.483^{e-07} [ellipticity]; n = 100 cells [OML] and 98 cells [ML]).

b. Cell length against angle relative to the long axis ($\theta_{long\ axis}$) at anaphase onset for OML and

ML cells. Cell lengths do not show a negative correlation with $\theta_{long\ axis}$ at anaphase for OML or ML cells, except for at extreme lengths in ML cells. (R^2 = -0.01408 [OML]; R^2 = -0.00276 [ML]).

c. Cell ellipticity against angle relative to the long axis ($\theta_{long\ axis}$) at anaphase onset for OML and ML cells. Cell ellipticity does not show a negative correlation with $\theta_{long\ axis}$ at anaphase for OML or ML cells, except for at extreme values in ML cells. (R^2 = 0.007879 [OML]; R^2 = -0.0021 [ML]).

6.3 Spindle orientation to the cell long axis is impaired in cells in crowded regions of the tissue

The surprising lack of correlation between cell shape anisotropy and spindle orientation to the long axis, raised the possibility that other mechanisms besides cell geometry are at play. Tissue tension in stretched tissues in culture has been proposed to support cell divisions to the long axis, even when cell long axes are not aligned with the stretch axis (Wyatt et al., 2015). As described in Chapter 3, cell junctions in the midline (ML) of the notum are under almost negligible tension (Marinari et al., 2012). This, together with the fact that mitotic rounding is impaired in the ML, suggests that ML cells are subject to higher levels of cell crowding than cells outside the midline (OML), and therefore are likely to be within a relatively low tissue tension environment. The ML thus provides a unique opportunity to test the requirement for tissue tension in spindle orientation to the long axis.

6.3.1 Spindle rotation is similar in ML and OML cells

In the previous chapter, I showed that spindle rotation due to cortical pulling forces is important to re-orient the spindle towards the cell long axis. Before analysing any differences in spindle orientation between ML and OML cells, it was important to first establish if there were any differences in spindle rotation (Fig 6.2).

Spindle displacement ($\theta_{displacement}$) (Fig 6.2c), total spindle rotation (θ_{total}) (Fig 6.2d) and directionality ($\mathcal{D}_{rotation} = {}^{\theta_{displacement}}/_{\theta_{total}}$) (Fig 6.2e, f) were similar between WT ML and WT OML cells, indicating that cell crowding does not affect spindle rotation.

6.3.2 Spindle rotation does not result in a global shift in spindle orientation towards the long axis in ML cells

Spindle orientation to the cell long axis ($\theta_{long\ axis}$) at NEB was random in WT ML, similar to WT OML cells (Fig 6.3b, c). The orientation of spindles did not change significantly at anaphase onset, although there was a modest increase in

spindles close to the cell long axis, there was also a significant number of spindles that were at the short axis (Fig 6.3c).

Consistent with this, when comparing spindle orientations at NEB to their orientation at anaphase, WT ML spindles that form at the short and intermediate axes at NEB in particular, had a larger range at anaphase than WT OML cells (compare Fig 5.3a and Fig 6.3d). This indicated that in ML cells, spindles that form at the short or intermediate axes do not consistently rotate away from it and towards the long axis.

Although spindle rotations on average is similar in ML cells and OML cells, spindle rotation might be impaired specifically in spindles that are far from the cell long axis at NEB, which might explain why these spindles are less likely to move towards the long axis in ML cells. However, spindle displacement or the persistence of rotation was not impaired for spindles that are at the short or intermediate axes at NEB in ML cells is similar to that in OML cells (compare Fig 5.3 c, e and Fig 6.3 e, f). This suggested that spindle rotation is unperturbed in ML cells, rather it is the ability to recognise the long axis that might be affected.

To better see the effects of spindle re-orientation, spindles $\theta_{displacement} > 34°$ and $\theta_{displacement} < 34°$ were analysed separately. The proportions of ML and OML spindles with $\theta_{displacement} > 34°$ was similar, consistent with no defects in spindle rotation *per se* (Fig 6.4a).

For ML spindles with $\theta_{displacement} < 34°$, spindle orientation at NEB is non-random and towards the long axis (Fig 6.4a), which is similar to WT OML spindles. Interestingly, while spindles appear to move away from the long axis by anaphase in WT OML cells (Fig 5.5b, Fig 5.6a), in WT ML cells spindle orientation remains towards the long axis (Fig 6.4b, Fig 6.5a).

However, unlike in OML cells, for WT ML spindles with $\theta_{displacement} > 34°$, the orientations of spindles do not change significantly from NEB to anaphase (Fig 6.5b, Fig 6.4b). Specifically, while in OML cells there appears to be a global shift in spindle orientation from the short axis towards the long axis (Fig 5.6b), in ML cells

spindle orientations appeared random at NEB and at anaphase (Fig 6.5b). This suggests that in WT ML cells, spindle rotations shuffle spindle orientations rather than direct spindle orientations towards the long axis. In particular, ML spindles that form at the intermediate axis are more likely to have random orientation at anaphase, while in WT OML cells, these spindles would rotate towards the long axis (compare Fig 5.6d and Fig 6.5d). This is suggests that a tensile mechanical environment facilitates spindle rotation towards the long axis, and that reduction of isotropic tissue tension due to cell crowding might impair spindle rotation to the long axis.

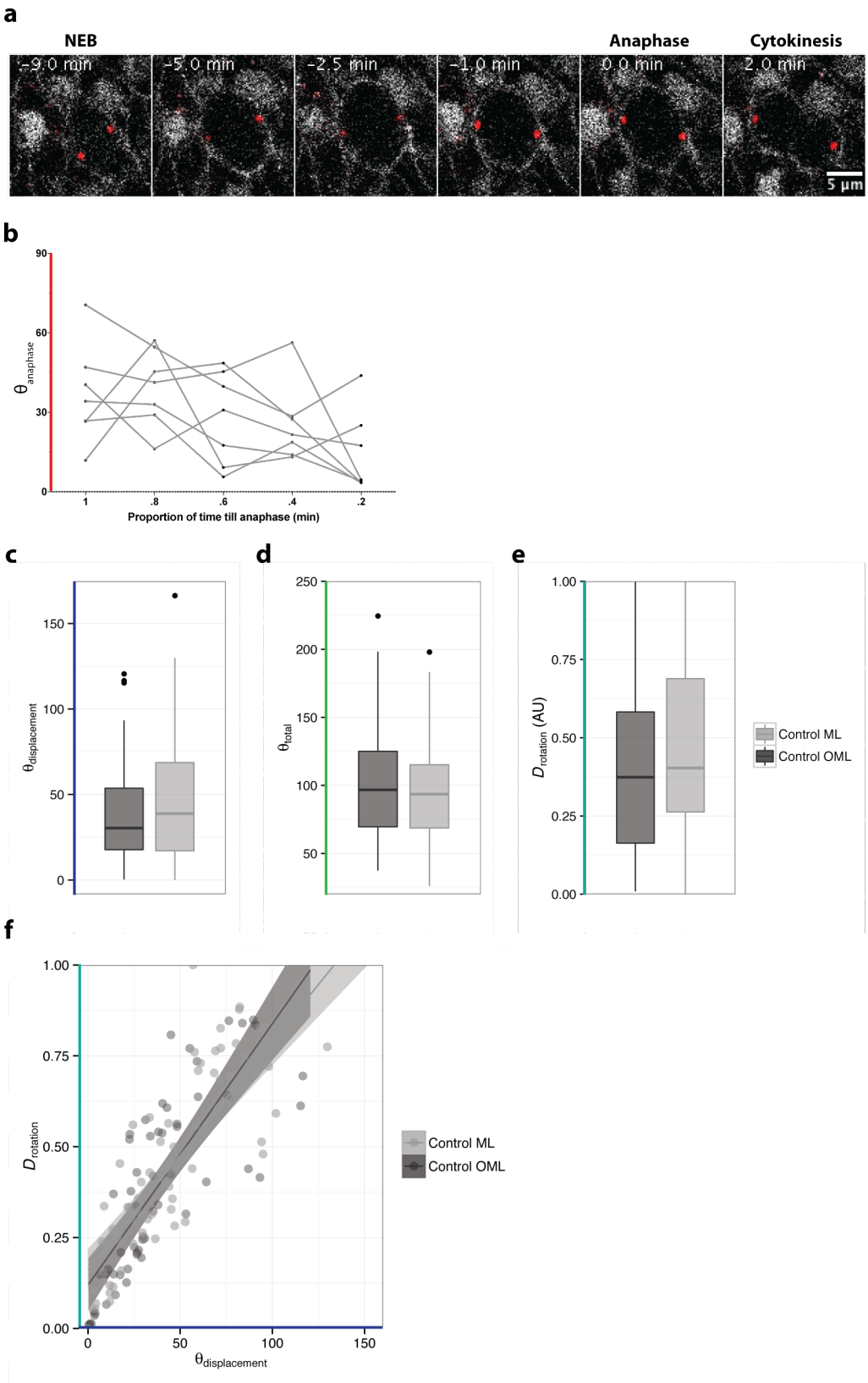

Figure 6.2: Spindle rotation in OML and ML cells is similar.

a. Representative WT ML cell dividing. Centrosomes are labelled with Centrosomin-RFP (red) and cell membranes are labelled with Spider-GFP (white). Anaphase onset was taken

as 2min before the onset of cytokinetic furrowing.

b. Representative line plots for WT ML cells. Spindle rotation is mostly towards the anaphase orientation (8 cells, 4 experiments).

c. Spindle rotation from NEB to anaphase ($\theta_{displacement}$) for WT OML and ML cells. $\theta_{displacement}$ was similar for OML and ML cells (Mean: 38.990 ± 3.943° [WT OML, n = 100 cells] and 44.75 ± 3.898° [WT ML, n = 98 cells], Mann-Whitney U test p-value = 0.5371).

d. Total accumulated rotation during mitosis (θ_{total}) for WT OML and ML cells. θ_{total} was similar for OML and ML cells (Mean: 102.00 ± 5.448° [WT OML, n = 100 cells] and 97.37 ± 4.668° [WT ML, n = 98 cells], Mann-Whitney U test p-value = 0.9559).

e. Persistence of rotation ($\mathcal{D}_{rotation}$) for WT OML and ML cells. $\mathcal{D}_{rotation}$ was similar for OML and ML cells (Mean: 0.3993 ± 0.03589 [WT OML, n = 100 cells] and 0.4456 ± 0.02971 [WT ML, n = 98 cells], Mann-Whitney U test p-value = 0.6792).

f. $\mathcal{D}_{rotation}$ as a function of $\theta_{displacement}$ for WT OML and ML cells. Lines indicate best-fit mean line and filled areas represent standard error of the mean. The relationship between $\mathcal{D}_{rotation}$ and $\theta_{displacement}$ is similar for WT OML and ML cells.

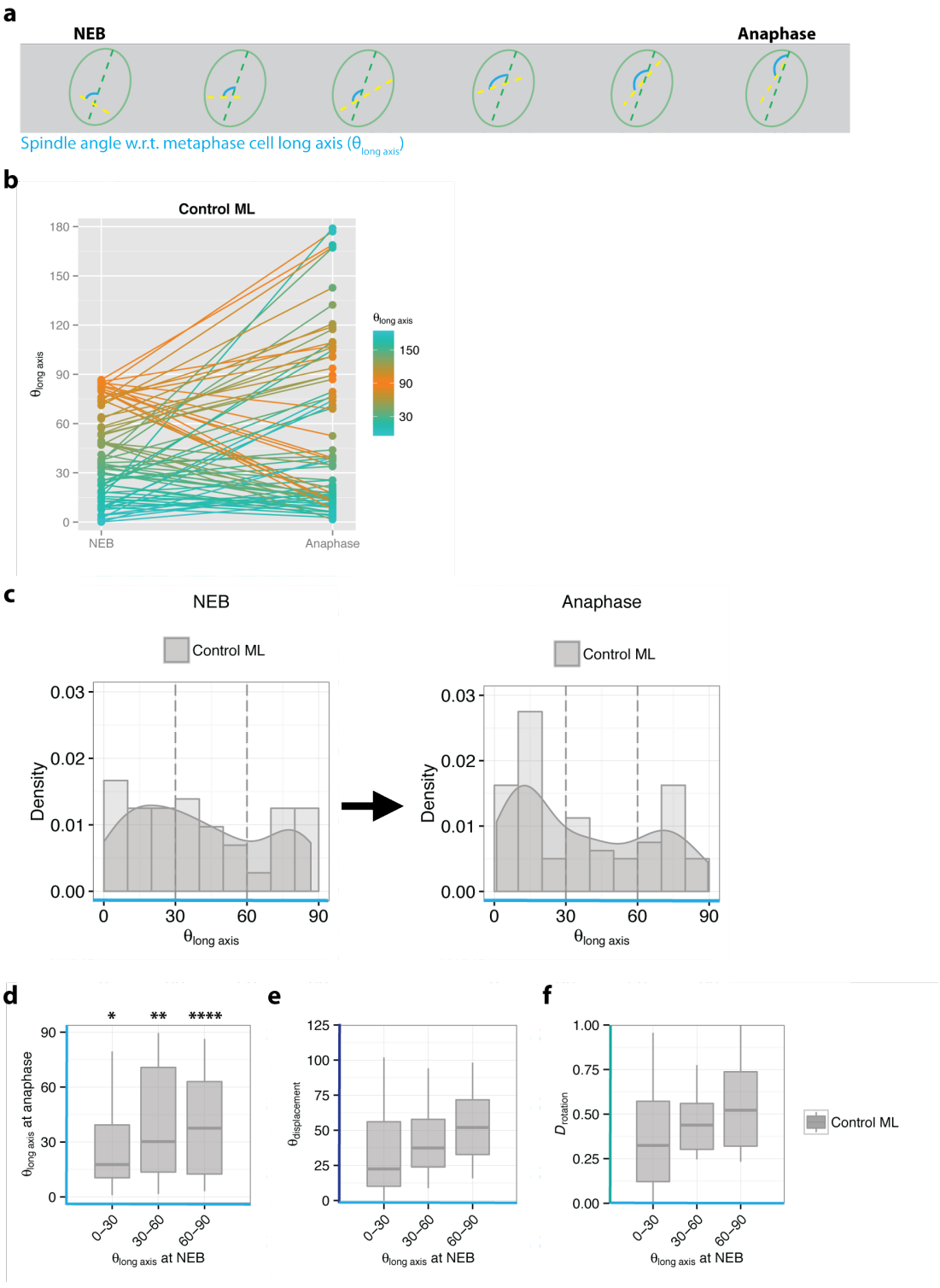

Figure 6.3: Spindle orientations from NEB to anaphase in WT **ML cells.**

a. Schematic of analysis for spindle angle w.r.t. metaphase cell long axis ($\theta_{long\ axis}$).

b. Line plots for individual WT ML cells showing $\theta_{long\ axis}$ at NEB and at anaphase. Colour map indicates spindles close to the metaphase cell long axis (cyan) and to the short axis (orange). Points indicate $\theta_{long\ axis}$, with line connecting corresponding points from NEB to

anaphase. Line colours follow that of $\theta_{long\ axis}$ at NEB. The slope of the line reflects the degree of displacement from NEB to anaphase ($\theta_{displacement}$).

c. Density plot of acute $\theta_{long\ axis}$ at NEB and anaphase onset for spindles in WT ML cells. The distribution of $\theta_{long\ axis}$ is random at NEB (Kolmogorov-Smirnov test p-value = 0.2024; N: 80 cells, 5 experiments [WT ML]). Distributions of $\theta_{long\ axis}$ at NEB and at anaphase are not significantly different (Kolmogorov-Smirnov test p-value = 0.2696, N: 80 cells, 5 experiments).

d. Acute spindle orientation relative to the long axis ($\theta_{long\ axis}$) at anaphase onset for WT ML spindles by acute $\theta_{long\ axis}$ at NEB. Spindle rotation from the short or intermediate axes ($\theta_{long\ axis}$ = 60-90°) at NEB towards the cell long axis ($\theta_{long\ axis}$ = 0-30°) at anaphase is impaired compared to WT OML cells; spindles at the long axis ($\theta_{long\ axis}$ = 0-30°) at NEB remain close to the long axis. (* indicates $p < 0.05$; ** indicates $p < 0.01$; **** indicates $p < 0.001$. Distribution at anaphase was tested against corresponding distribution at NEB with the Kolmogorov-Smirnov test).

e. Spindle rotation from NEB to anaphase onset ($\theta_{displacement}$) for WT ML spindles by spindle orientation ($\theta_{long\ axis}$) at NEB. $\theta_{displacement}$ of spindles by $\theta_{long\ axis}$ NEB of WT ML cells is similar to WT OML cells (Fig 5.3c).

f. Persistence of rotation ($\mathcal{D}_{rotation}$) for WT ML spindles by spindle orientation ($\theta_{long\ axis}$) at NEB. $\mathcal{D}_{rotation}$ of spindles by $\theta_{long\ axis}$ NEB of WT ML cells is similar to WT OML cells (Fig 5.3e).

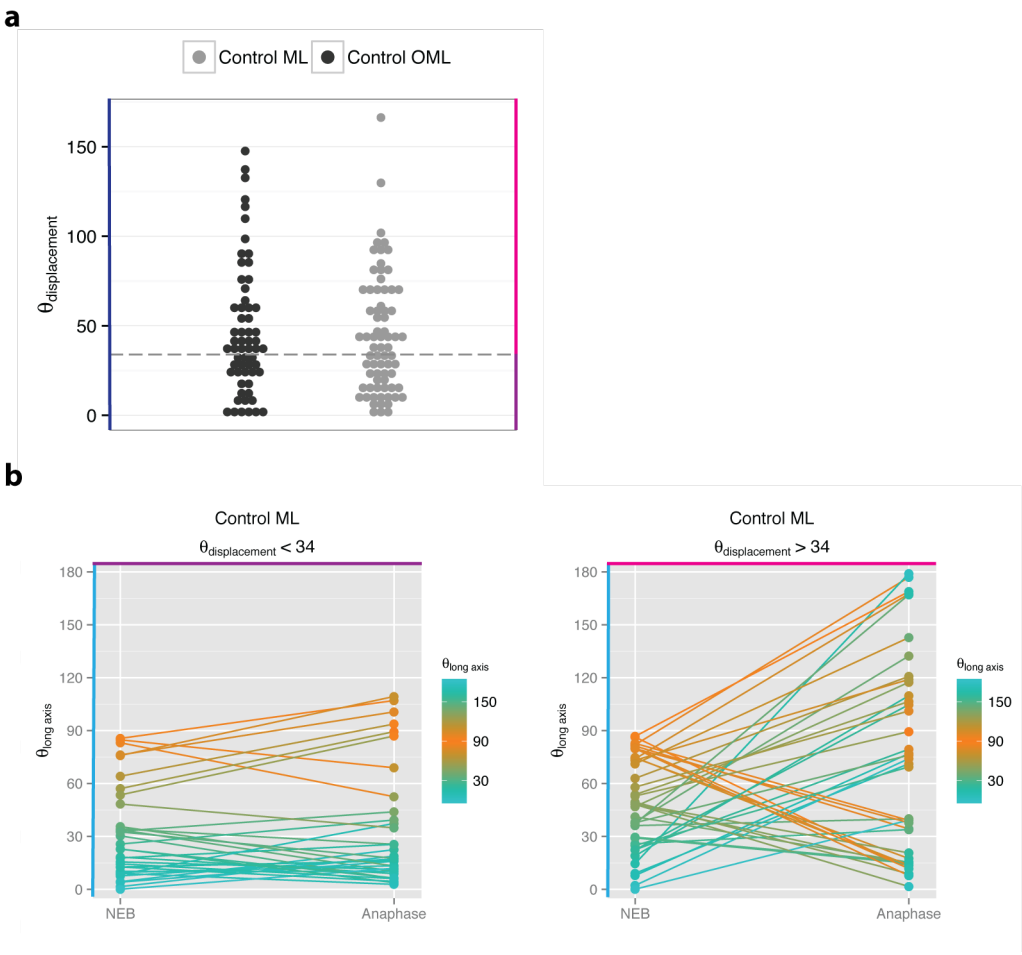

Figure 6.4: Spindle rotation in ML cells does not change the distribution of spindle orientations from NEB to anaphase.

a. Angular displacement of spindles from NEB to anaphase ($\theta_{displacement}$) for WT OML and ML cells. The grey dashed line indicates the 90th percentile value of Mud IR cells ($\theta_{displacement}$= 34°), which defines the threshold for classifying cells with significant or non-significant spindle rotation. The proportion of cells with $\theta_{displacement}$ > 34° is similar for WT OML and ML cells (54.16% [WT ML] and 45% [WT OML]).

b. Line plots for individual WT ML cells with $\theta_{displacement}$ < 34° or > 34°, showing $\theta_{long\ axis}$ at NEB and at anaphase. Colour map indicate spindles close to the metaphase cell long axis (cyan) and to the short axis (orange). Points indicate $\theta_{long\ axis}$, with line connecting corresponding points from NEB to anaphase onset. Line colours follow that of $\theta_{long\ axis}$ at NEB. Line plots suggest that spindle rotations from NEB to anaphase onset are not consistently towards the long axis.

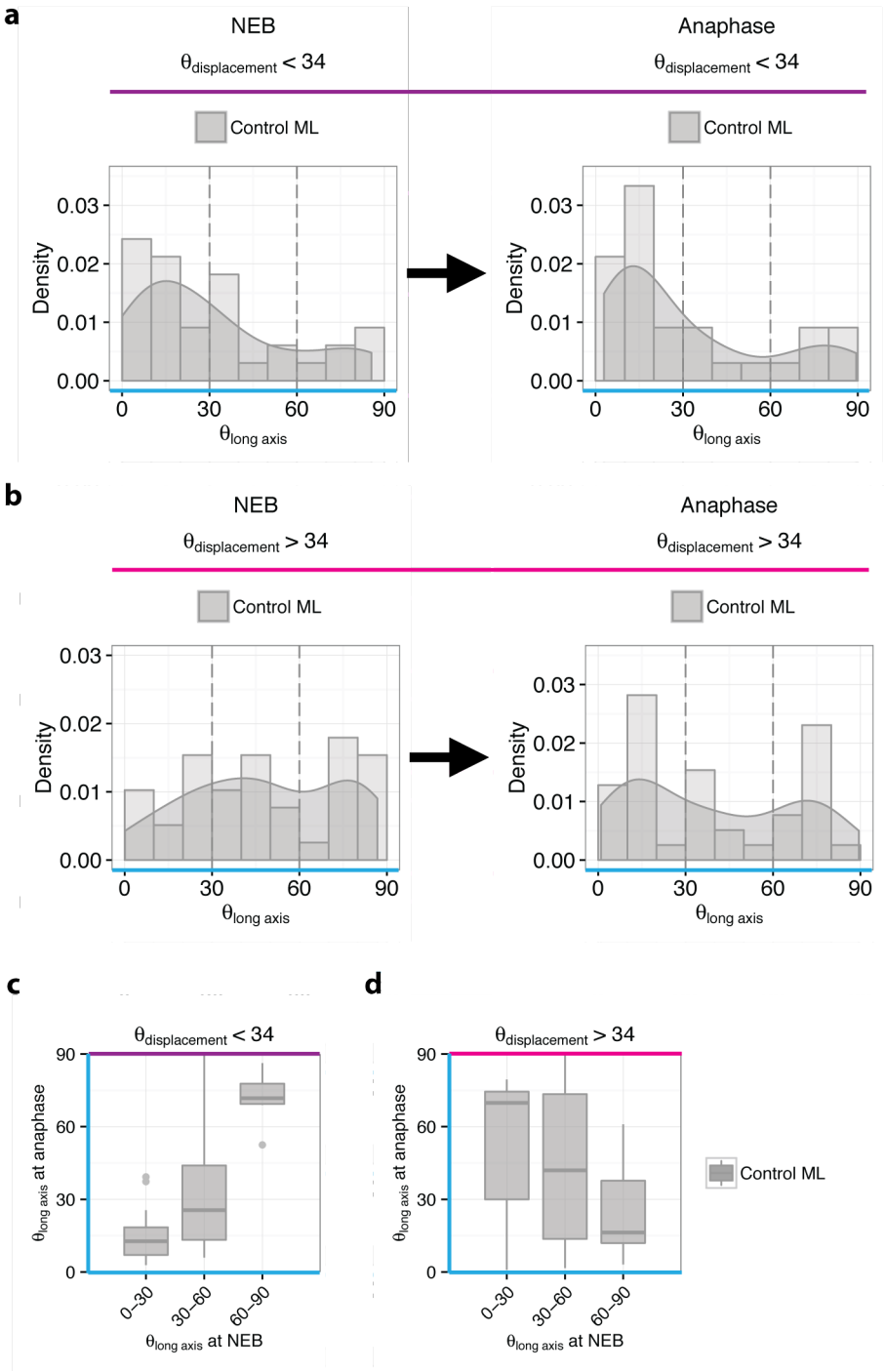

Figure 6.5: Spindle rotation in ML cells does not re-orient spindles from the short to the long axis.

a. Density plot of acute $\theta_{long\ axis}$ at NEB and anaphase onset for WT ML spindles with $\theta_{displacement} < 34°$. Distributions of $\theta_{long\ axis}$ at NEB and at anaphase onset are not significantly different (Kolmogorov-Smirnov test p-value= 0.6543, n = 33 cells). Spindle orientations at

NEB and anaphase appear to cluster close to the cell long axis ($\theta_{long\ axis} < 30°$) (Kolmogorov-Smirnov test p-value = 0.008152; n: 33 cells [WT ML, $\theta_{displacement} < 34°$]). This suggests that spindles that rotate little are initially at the long axis at NEB after centrosome separation and remain there.

b. Density plot of acute $\theta_{long\ axis}$ at NEB and anaphase onset for spindles with $\theta_{displacement} > 34°$. Distributions of $\theta_{long\ axis}$ at NEB and at anaphase onset are not significantly different (Kolmogorov-Smirnov test p-value = 0.08974, n = 39 cells). Spindle orientation at NEB is apparently random (Kolmogorov-Smirnov test p-value = 0.1785; n: 39 cells [WT, $\theta_{displacement} > 34°$]), and remains apparently random at anaphase. This implies that spindle rotations in ML cells are not serving to rotate spindles from the short or intermediate axes towards the long axis.

c. Spindle orientation ($\theta_{long\ axis}$) at anaphase onset by spindle orientation ($\theta_{long\ axis}$) at NEB for WT spindles with $\theta_{displacement} < 34°$. Spindles that form at the long or intermediate axis ($\theta_{long\ axis} = 0\text{-}50°$) remain or rotate towards the long axis at anaphase onset (69.23% of spindles with $\theta_{displacement} < 34°$, 37.5% of all WT ML spindles).

d. Spindle orientation ($\theta_{long\ axis}$) at anaphase onset by spindle orientation ($\theta_{long\ axis}$) at NEB for WT spindles with $\theta_{displacement} > 34°$. Spindles that form at the short axis ($\theta_{long\ axis} = 0\text{-}30°$) rotate to the long axis by anaphase (35.89% of spindles with $\theta_{displacement} > 34°$, 19.44% of all WT ML spindles). However, spindles that form at the intermediate axis ($\theta_{long\ axis} = 30\text{-}60°$) have a random distribution at anaphase onset (33.33% of spindles with $\theta_{displacement} > 34°$, 18.05% of all WT ML spindles).

6.4 Myosin activity regulates dynamic spindle rotation and spindle orientation relative to the cell long axis

The poor spindle rotation towards the long axis in ML cells, suggested a role for tissue tension. It has recently been shown that in stretched tissues, spindles orient toward the long axis even when the long axis of the cell is not aligned with the applied tension axis (Wyatt et al., 2015). In the developing zebrafish embryo, a similar phenomenon was observed, and was found to be mediated by myosin II (Campinho et al., 2013).

6.4.1 Spindle rotation and orientation to the long axis is perturbed in SqhAA cells

To test whether myosin activity and myosin-mediated tissue tension is involved in spindle movement and dynamic orientation towards the cell long axis, I turned to genetic perturbations targeting the actomyosin activity in the tissue. I expressed a phospho-dead version of the myosin light chain (SqhAA) (Winter et al., 2001) within the Pannier domain of the notum (Calleja et al., 2002), which acts like a dominant-negative to sequester endogenous activated myosin. The expression of this construct has also been previously shown in the lab to reduce junctional tension (Curran S., 2015). I then analysed SqhAA OML cells (Fig 6.6a), restricting my analysis to cells with an ellipticity of > 1.2 just like in WT OML cells, to see if spindle rotation to the long axis is now perturbed.

6.4.1.1 Spindle rotations are less directed in SqhAA cells

To begin with, I analysed if perturbing myosin activity had any effect on spindle rotation in general. Campinho et al.2013 observed that in cells treated with blebbistatin, a drug that inhibits myosin II activity, spindles appear to fluctuate more often. If spindle rotation itself is perturbed, it could explain why blebbistatin or ROK-inhibitors which also inhibit myosin activity, perturb spindle orientation to the long axis (Wyatt T., personal communication).

Spindle rotation in SqhAA cells appeared to be less directed, with spindles changing direction often (Fig 6.6b). However, spindle rotation from NEB to anaphase ($\theta_{displacement}$) was not affected by SqhAA expression (Fig 6.6c), although total accumulated spindle rotation (θ_{total}) increased (Fig 6.6d) **(**Mean: 102.00 ± 5.448° [WT OML] and 137.80 ± 7.199° [SqhAA OML], Mann-Whitney U test p-value = 0.0001864). This implies that spindles do indeed have noisier movement. Indeed, the calculated persistence of rotation ($\mathcal{D}_{rotation} = {\theta_{displacement}}/{\theta_{total}}$) is slightly lower in SqhAA cells (Fig 6.6e) (Mean: 0.3993 ± 0.0358 [WT OML] and 0.2942 ± 0.0309 [SqhAA OML], Mann-Whitney U test p-value = 0.0491), and is consistently lower than WT OML cells for equivalent values of $\theta_{displacement}$ (Fig 6.6f).

6.4.1.2 Spindle rotations are not consistently towards the long axis in SqhAA cells

The effects of SqhAA on directed spindle rotations could result in impaired spindle orientations different to those observed in endogenous regions of low tension (i.e. in ML cells).

Spindle orientation at NEB was random in SqhAA OML cells, similar to WT OML cells (Fig 6.7c). However, spindle orientation seemed even more uniform and random at anaphase in SqhAA OML cells (Fig 6.7c), while in WT OML cells there is an apparent peak close to the long axis (Fig 5.2a).

Spindle rotations also seem to be misregulated, in that spindles far from the long axis at NEB no longer consistently rotate towards the long axis, and spindles close to the long axis at NEB are seen to rotate away from the long axis (Fig 6.7b). In particular, spindles seemed to largely remain at their orientations at NEB to anaphase (Fig 6.7d), while in WT OML cells, spindles at the short or intermediate axes at NEB tend to rotate towards the long axis by anaphase.

This inability to rotate away from the short or intermediate axis might be due to poor spindle rotation. Spindle displacement and persistence of rotation was lower in SqhAA OML cells compared to WT OML cells, specifically for spindles that

formed at the short or intermediate axes (Fig 6.7e, f). This implies that spindle rotations are less effective in SqhAA cells, resulting in spindles not displacing from their NEB positions, and preventing a global shift in spindle orientations towards the cell long axis at anaphase onset.

To better observe the effects of re-orientation, the data was again split into spindles with significant ($\theta_{displacement} > 34°$) and non-significant displacements ($\theta_{displacement} < 34°$). Surprisingly, the proportion of spindles with $\theta_{displacement} < 34°$ was similar between SqhAA OML cells and WT OML cells (Fig 6.9a) (43.13% [SqhAA OML] and 45% [WT OML]). However, while in WT OML cells, spindles with $\theta_{displacement} < 34°$ tend to be those already oriented to the long axis at NEB (Fig 5.6a), in SqhAA OML cells spindles with $\theta_{displacement} < 34°$ have a random distribution at NEB (Fig 6.8b, Fig 6.9a). This suggests that spindles are able to recognise the long axis from NEB and either remain there till anaphase onset, and this is affected in SqhAA cells.

For spindles with $\theta_{displacement} > 34°$, spindle rotations tended to bring spindles to the intermediate axis, regardless of orientation at NEB (Fig 6.9b, d). This contrasts with WT OML cells, where spindles with $\theta_{displacement} > 34°$ that are at the short or intermediate axes at NEB are close to the long axis by anaphase (Fig 5.6b, d).

Overall, the data suggest that myosin activity is required for directed spindle rotation, such that in SqhAA OML cells, more spindles remain at the short or intermediate axis instead of rotating towards the long axis. But the data also suggest that myosin activity might be required for spindles to recognise where the cell long axis is when they do manage rotate away from their NEB positions. This is based on the observation that spindles with $\theta_{displacement} > 34°$ that form at the intermediate axis at NEB are equally likely to rotate towards the long or short axis at anaphase onset. This is a similar trend to what is observed in WT ML cells, where spindle rotations *per se* are unaffected. This provides some support for the theory that myosin-mediated tissue tension affects spindle rotations to the long axis, by modulating the information regarding cell geometry.

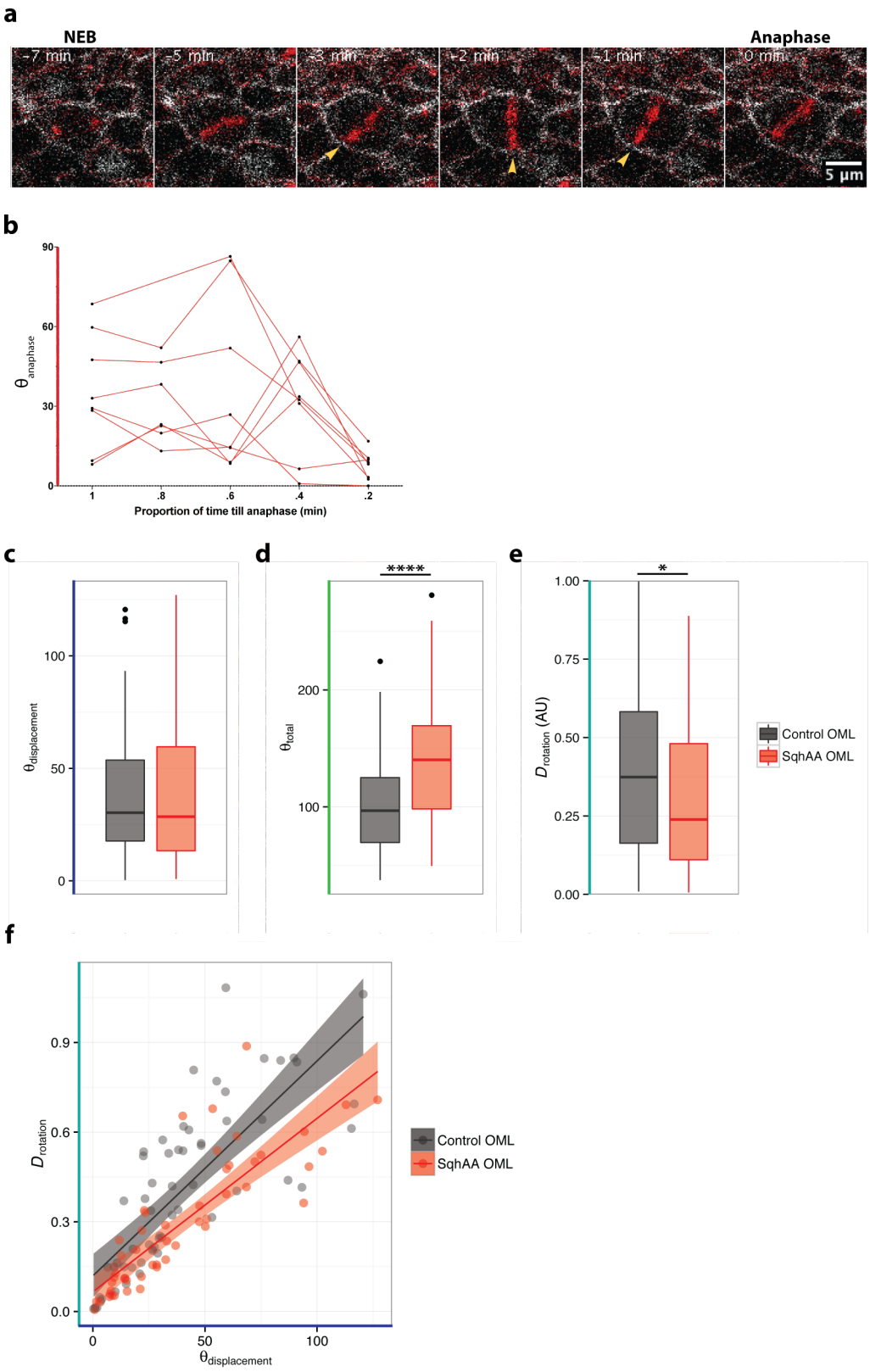

Figure 6.6: Spindle rotation is less directed in SqhAA OML cells.

a. Representative SqhAA OML cell dividing. Spindle is labelled with Tubulin-mCherry (red) and cell membranes are labelled with Spider-GFP (white). Spindles are seen frequently

changing directions during spindle rotations (yellow arrowheads).

b. Representative line plots for SqhAA OML cells. Spindle rotation is not consistently towards the anaphase orientation, indicating that spindles are changing directions (8 cells, 3 experiments).

c. Spindle rotation from NEB to anaphase ($\theta_{displacement}$) for WT OML and SqhAA OML cells. $\theta_{displacement}$ was similar for WT and SqhAA cells (Mean: 38.99 ± 3.943° [WT OML, n = 75 cells] and 39.37 ± 4.480° [SqhAA OML, n = 61 cells], Mann-Whitney U test p-value = 0.9269).

d. Total accumulated rotation during mitosis (θ_{total}) for WT OML and SqhAA OML cells. θ_{total} was higher for SqhAA OML compared to WT OML cells (Mean: 102.00 ± 5.448° [WT OML, n = 75 cells] and 137.80 ± 7.199° [SqhAA OML, n = 61 cells], Mann-Whitney U test p-value = 0.0001864).

e. Persistence of rotation ($\boldsymbol{\mathcal{D}}_{rotation}$) for WT OML and SqhAA OML cells. $\boldsymbol{\mathcal{D}}_{rotation}$ was slightly lower for SqhAA OML cells (Mean: 0.3993 ± 0.0358 [WT OML, n = 75 cells] and 0.2942 ± 0.0309 [SqhAA OML, n = 61 cells], Mann-Whitney U test p-value = 0.0491).

f. $\boldsymbol{\mathcal{D}}_{rotation}$ as a function of $\theta_{displacement}$ for WT OML and ML cells. Lines indicate best-fit mean line and filled areas represent standard error of the mean. $\boldsymbol{\mathcal{D}}_{rotation}$ for SqhAA OML spindles is consistently lower than WT OML spindles for equivalent values of $\theta_{displacement}$.

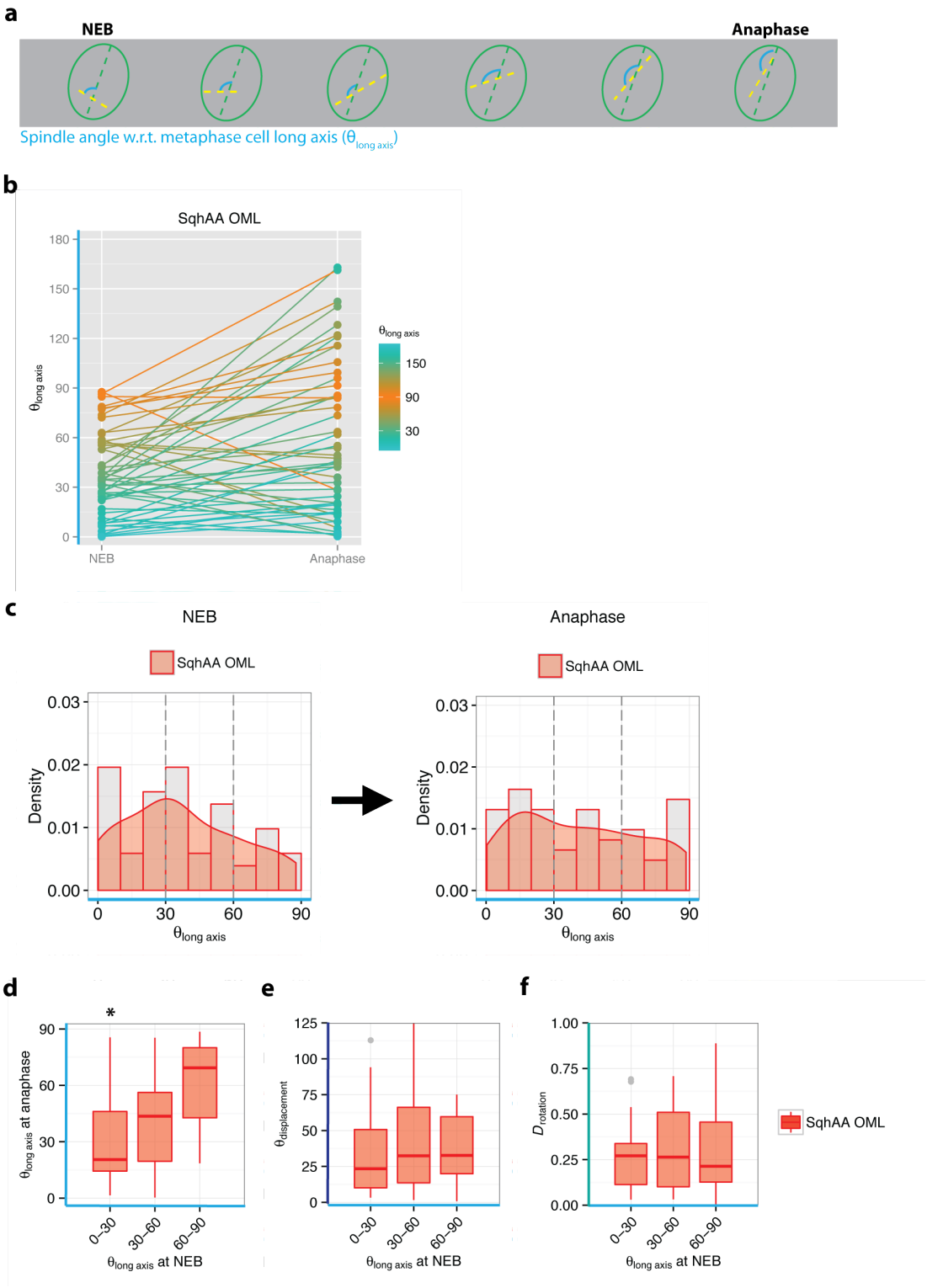

Figure 6.7: Spindle orientations do not change from NEB to anaphase in SqhAA OML cells.

a. Schematic of analysis for spindle angle wrt metaphase cell long axis ($\theta_{long\ axis}$).

b. Line plots for individual SqhAA OML cells showing $\theta_{long\ axis}$ at NEB and at anaphase onset. Colour map indicates spindles close to the metaphase cell long axis (cyan) and to the

short axis (orange). Points indicate $\theta_{long\ axis}$, with line connecting corresponding points from NEB to anaphase. Line colours follow that of $\theta_{long\ axis}$ at NEB. The slope of the line reflects the degree of displacement from NEB to anaphase onset ($\theta_{displacement}$). The line plots suggest that spindle rotations are not consistently towards the long axis, and spindles at the short axis at NEB do not rotate away from the short axis.

c. Density plot of acute $\theta_{long\ axis}$ at NEB and anaphase onset for spindles in SqhAA OML cells. The distribution of $\theta_{long\ axis}$ is random at NEB (Kolmogorov-Smirnov test p-value = 0.09344; N: 61 cells, 4 experiments [SqhAA OML]). At anaphase, the distribution of $\theta_{long\ axis}$ appears even more uniform and random with no apparent peak value. Distributions of $\theta_{long\ axis}$ at NEB and at anaphase are similar (Kolmogorov-Smirnov test p-value = 0.6324, N: 61 cells, 4 experiments).

d. Acute spindle orientation relative to the long axis ($\theta_{long\ axis}$) at anaphase onset for SqhAA OML spindles by acute $\theta_{long\ axis}$ at NEB. Spindle orientations tend to remain the same at NEB and anaphase (Compare to WT OML data in Fig 5.3a). (* indicates $p < 0.05$. Distribution at anaphase was tested against corresponding distribution at NEB with the Kolmogorov-Smirnov test).

e. Spindle rotation from NEB to anaphase ($\theta_{displacement}$) for SqhAA OML spindles by spindle orientation ($\theta_{long\ axis}$) at NEB. $\theta_{displacement}$ is equally low for SqhAA OML spindles regardless of orientation at NEB (Compare to WT OML data in Fig 5.3c).

d. Persistence of spindle rotation ($\mathcal{D}_{rotation}$) for SqhAA OML spindles by spindle orientation at NEB. $\mathcal{D}_{rotation}$ is equally low for spindles regardless of orientation at NEB (Compare to WT OML data in Fig 5.3e).

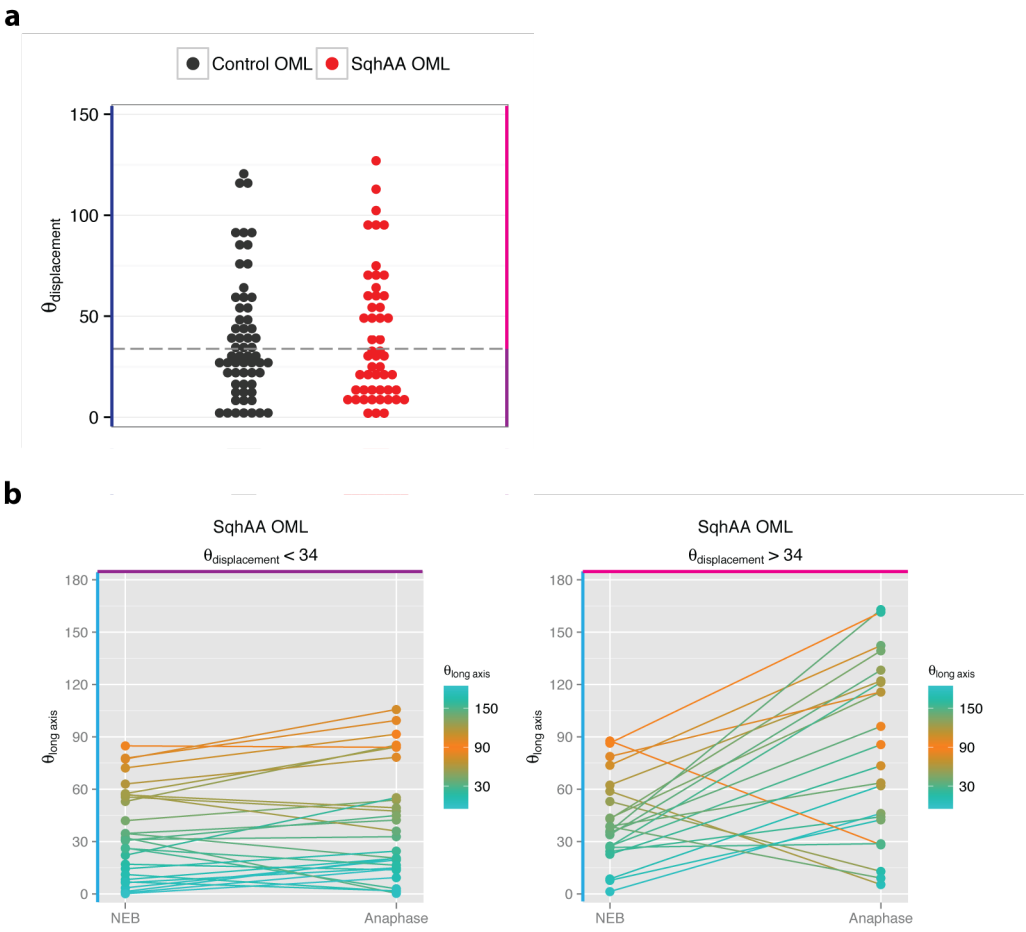

Figure 6.8: Spindle rotation in SqhAA OML cells does not change the distribution of spindle orientations from NEB to anaphase.

a. Angular displacement of spindles from NEB to anaphase ($\theta_{displacement}$) for WT OML and SqhAA OML cells. The grey dashed line indicates the 90th percentile value of Mud IR cells ($\theta_{displacement}$= 34°), which defines the threshold for classifying cells with significant or non-significant spindle rotation. The proportion of cells with $\theta_{displacement}$ > 34° is similar for SqhAA OML and WT OML cells (43.13% [SqhAA OML] and 45% [WT OML]).

b. Line plots for individual SqhAA OML cells with $\theta_{displacement}$ < 34° or > 34°, showing $\theta_{long\ axis}$ at NEB and at anaphase. Colour map indicate spindles close to the metaphase cell long axis (cyan) and to the short axis (orange). Points indicate $\theta_{long\ axis}$, with line connecting corresponding points from NEB to anaphase. Line colours follow that of $\theta_{long\ axis}$ at NEB. Line plots suggest that spindles remain at the short axis from NEB to anaphase onset, and spindle rotations are in fact from the long to the short axis.

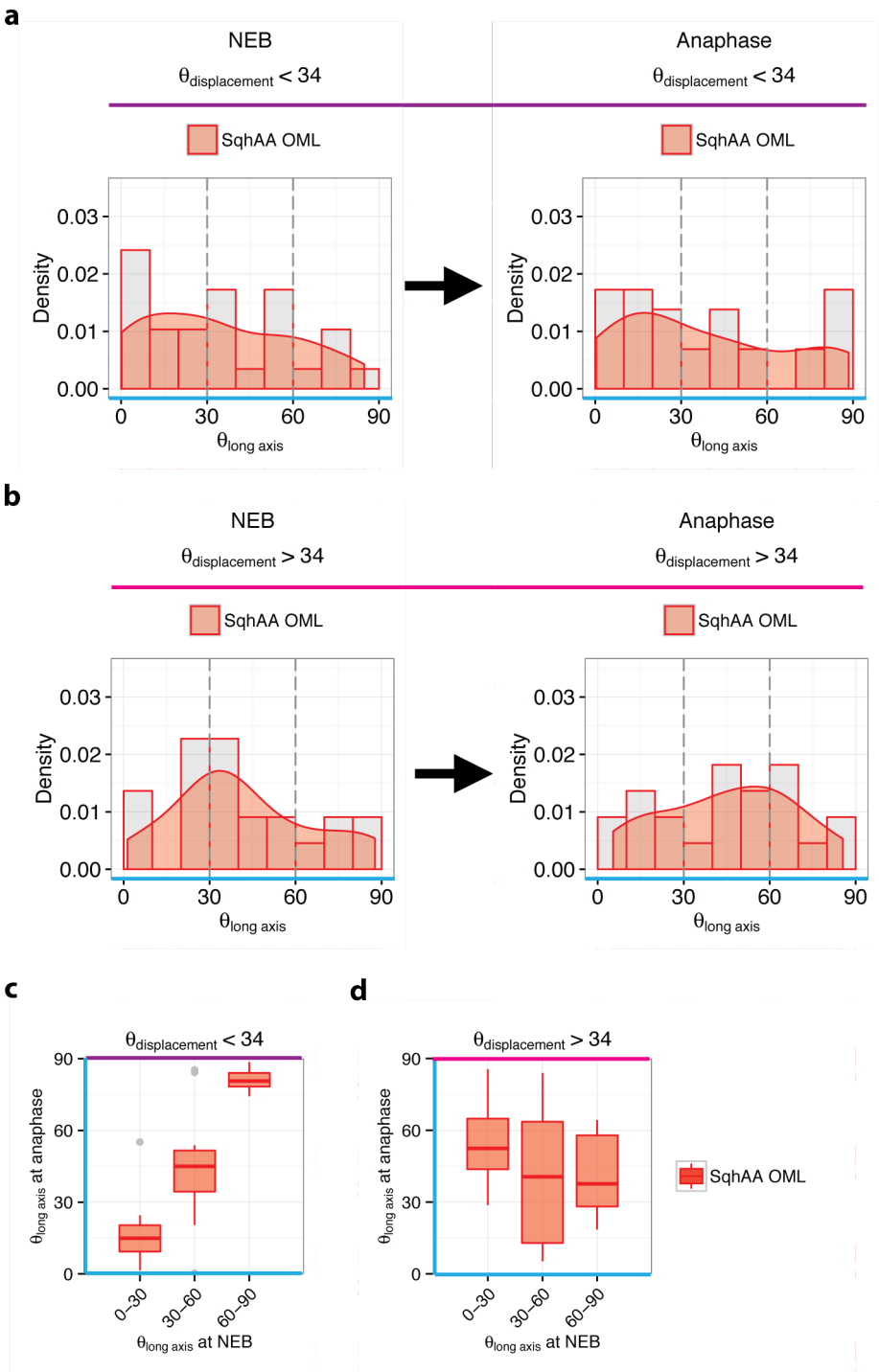

Figure 6.9: Spindle rotation from the short axis to long axis is disrupted in SqhAA OML cells.

a. Density plot of acute $\theta_{long\ axis}$ at NEB and anaphase onset for SqhAA OML spindles with $\theta_{displacement} < 34°$. Spindle orientations at NEB are random (Kolmogorov-Smirnov test p-value = 0.0828; n: 29 cells [SqhAA OML, $\theta_{displacement} < 34°$]). Distributions of $\theta_{long\ axis}$ at NEB and at anaphase are similar (Kolmogorov-Smirnov test p-value= 0.7912, n = 29 cells).

b. Density plot of acute $\theta_{long\ axis}$ at NEB and anaphase for spindles with $\theta_{displacement} > 34°$.

Spindle orientation at NEB is random (Kolmogorov-Smirnov test p-value = 0.4002; n: 22 cells [SqhAA OML, $\theta_{displacement} > 34°$]). Distributions of $\theta_{long\ axis}$ at NEB and at anaphase are similar (Kolmogorov-Smirnov test p-value = 0.6324, n = 22 cells). This implies that spindle rotations in SqhAA OML cells are shuffling the orientations from NEB to anaphase onset.

c. Spindle orientation ($\theta_{long\ axis}$) at anaphase by spindle orientation ($\theta_{long\ axis}$) at NEB for SqhAA OML spindles with $\theta_{displacement} < 34°$. $\theta_{long\ axis}$ does not change significantly from NEB to anaphase onset.

d. Spindle orientation ($\theta_{long\ axis}$) at anaphase by spindle orientation ($\theta_{long\ axis}$) at NEB for SqhAA OML spindles with $\theta_{displacement} > 34°$. Spindle rotation from the short or intermediate axes to the long axis is impaired in SqhAA OML cells compared to WT OML cells (Fig 5.6d).

6.4.2 *Spindle rotation and orientation to the cell long axis is improved in cells with SqhEE*

Myosin activity appears to be required for the persistence of spindle rotations, but also the spindle's ability to recognise the long axis. To test if myosin activity is sufficient to improve both spindle rotation and orientation, I expressed phospho-mimetic myosin light chain (SqhEE) (Winter et al., 2001), and looked to see if this could rescue spindle orientation to the long axis in ML and improve it in OML cells.

6.4.2.1 Spindle rotation is more directed in SqhEE OML cells

I first analysed if increased myosin activity was sufficient to improve directed spindle rotation in OML cells. Spindle rotations seemed more directed in SqhEE OML cells (Fig 6.10a, b). Although there was no significant change in spindle angular displacement from NEB to anaphase ($\theta_{displacement}$) (Fig 6.10c) (Mean: 38.99 ± 3.943° [WT OML] and 38.50 ± 3.434° [SqhEE OML], Mann-Whitney U test p-value = 0.6722), total accumulated rotation during mitosis (θ_{total}) was decreased in SqhEE compared to WT (Fig 6.10d) (Mean: 102.00 ± 5.448° [WT OML] and 81.80 ± 7.108° [SqhEE OML], Mann-Whitney U test p-value = 0.002473). This suggested an increase in the persistence of spindle rotation. Indeed, the calculated directionality of spindle rotation ($\mathcal{D}_{rotation} = {\theta_{displacement}}/{\theta_{total}}$) is increased for SqhEE OML cells (Fig 6.10e) (Mean: 0.3993 ± 0.0358 [WT OML] and 0.521600± 0.0309 [SqhEE OML], Mann-Whitney U test p-value = 0.02361). And by plotting $\mathcal{D}_{rotation}$ against $\theta_{displacement}$ it is clear that for similar degrees of spindle rotation in SqhEE OML and WT OML, SqhEE OML spindles have more persistent rotation (Fig 6.10f).

6.4.2.2 SqhEE affects spindle orientation at NEB and rotation towards the long axis by anaphase in OML cells

Since spindle rotations were more directed in SqhEE OML cells, it is likely that this will have an effect on spindle orientation relative to the long axis. Spindle orientation at NEB for SqhEE OML cells was non-random, with a strong bias towards the short axis, unlike in WT OML cells where it is random (Kolmogorov-Smirnov test p-value = 0.0002335) (Fig 5.2a, Fig 6.11c). This suggests a role for

myosin in centrosome positioning just before NEB, as proposed by previous studies (Rosenblatt et al., 2004; de Simone et al., 2016). Specifically, it implies that high myosin activity results in spindles being close to the short axis, possibly by encouraging the close association of the centrosomes and the cell cortex before NEB.

Despite being skewed towards the short axis at NEB, spindle orientation changes significantly from NEB to anaphase onset towards the long axis (Kolmogorov-Smirnov test p-value = 3.927^{e-10}) (Fig 6.11b, c). Majority of the SqhEE OML spindles that form at the short or intermediate axes are close to the long axis at anaphase onset (Fig 6.11d). Correspondingly, the spindles that form furthest from the long axis have the highest rotation from their NEB positions (Fig 6.11e), and they also have the most directed rotations (Fig 6.11f). Spindle orientation at anaphase onset in SqhEE OML cells is not significantly different to WT (Kolmogorov-Smirnov test p-value = 0.2425) (Fig 5.2a), but is different from SqhAA OML cells (Kolmogorov-Smirnov test p-value = 0.03015) (Fig 6.7c). This supports the hypothesis that myosin activity and possibly tissue tension facilitates spindle rotations towards the long axis, and suggests that the endogenous tissue is either at an intermediate level of myosin activity or a heterogenous population of cells with higher and lower myosin activity.

Interestingly, SqhEE spindles that form at the long axis tend to remain close to the long axis, with very low displacements, while in WT these spindles tend to rotate slightly away from the long axis (Fig 6.11d). This suggests that spindles might be better at recognising the long axis with more myosin activity, and consequently not rotate away from it. If this is true, spindles that form at the long axis would have very low displacements and spindles that form far from the long axis would consistently have higher displacements. However, the proportion of SqhEE OML spindles with low displacements was similar to that in WT OML cells (46.10% [SqhEE OML] and 55% [WT OML]) (Fig 6.12a), despite more spindles being at the short axis at NEB in SqhEE OML cells. Furthermore, when spindles with non-significant displacements ($\theta_{displacement} < 34°$) were analysed separately, I found that these spindles were not preferentially at the long axis at NEB, but had a random distribution (Kolmogorov-Smirnov test p-value = 0.7321) (Fig 6.12b, 6.13a). This

argues against spindles having a low displacement simply because they are close to the long axis. It is more likely that myosin activity might cause a general preference for the long axis, as even spindles with low displacements that form at the short axis move slightly towards the long axis (6.13a, c).

Consistent with this, spindles that rotate significantly from their NEB positions have a non-random orientation at NEB, which is towards the short axis (Kolmogorov-Smirnov test p-value = 1.306^{e-08}) (Fig 6.14b, 6.13b). At anaphase onset, spindle orientations have changed significantly towards the long axis (Kolmogorov-Smirnov test p-value = 7.248^{e-12}) (Fig 6.14b, 6.13b). This implies that spindle rotations in SqhEE OML cells are specifically moving spindles from the short axis to the long axis. This can be more clearly visualised when plotting the spindle orientation at anaphase onset by the corresponding orientation at NEB (6.13d).

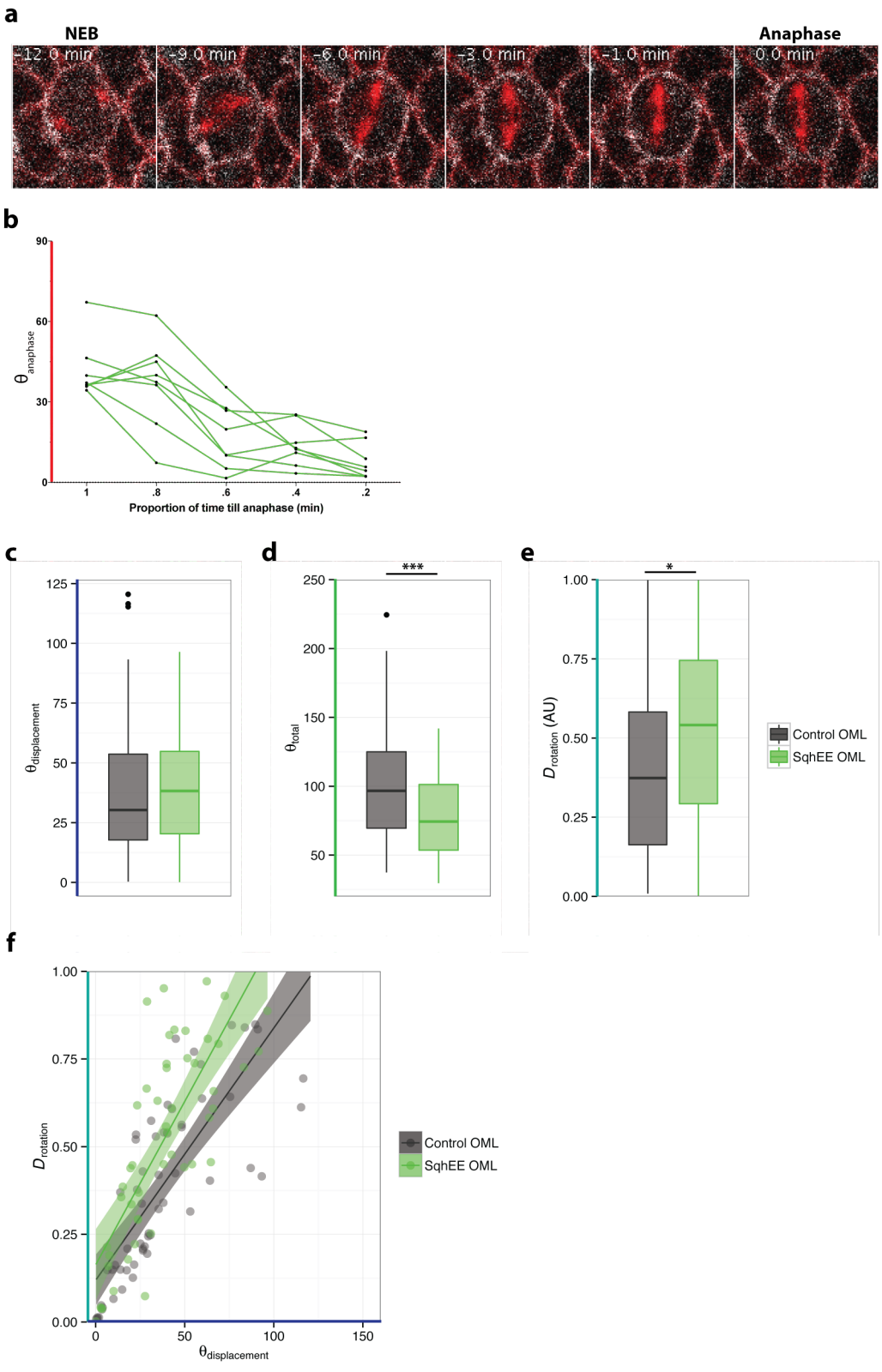

Figure 6.10: Spindle rotation is more directed in SqhEE OML cells.

a. Representative SqhEE OML cell dividing. Spindle is labelled with Tubulin-mCherry (red) and cell membranes are labelled with Spider-GFP (white). Spindles seem to move in a much

more directed manner in SqhEE cells. Note that increased myosin activity still cannot result in complete mitotic rounding within a tissue.

b. Representative line plots for SqhEE OML cells. Spindle rotation is consistently towards the anaphase orientation (8 cells, 2 experiments).

c. Angular displacement from NEB to anaphase ($\theta_{displacement}$) for WT OML and SqhEE OML cells. $\theta_{displacement}$ was similar for WT and SqhEE cells (Mean: 38.99 ± 3.943° [WT OML, n = 75 cells] and 38.50 ± 3.434° [SqhEE OML, n = 59 cells], Mann-Whitney U test p-value = 0.6722).

d. Total accumulated rotation during mitosis (θ_{total}) for WT OML and SqhEE OML cells. θ_{total} was lower for SqhEE OML compared to WT OML cells (Mean: 102.00 ± 5.448° [WT OML, n = 75 cells] and 81.80 ± 7.108° [SqhEE OML, n = 59 cells], Mann-Whitney U test p-value = 0.002473).

e. Persistence of rotation ($\mathcal{D}_{rotation}$) for WT OML and SqhEE OML cells. $\mathcal{D}_{rotation}$ was slightly higher for SqhEE OML cells (Mean: 0.3993 ± 0.0358 [WT OML, n = 75 cells] and 0.521600± 0.0309 [SqhEE OML, n = 59 cells], Mann-Whitney U test p-value = 0.02361).

f. $\mathcal{D}_{rotation}$ as a function of $\theta_{displacement}$ for WT OML and SqhEE OML cells. Lines indicate best-fit mean line and filled areas represent standard error of the mean. $\mathcal{D}_{rotation}$ for SqhEE OML spindles is consistently higher than WT OML spindles for equivalent values of $\theta_{displacement}$.

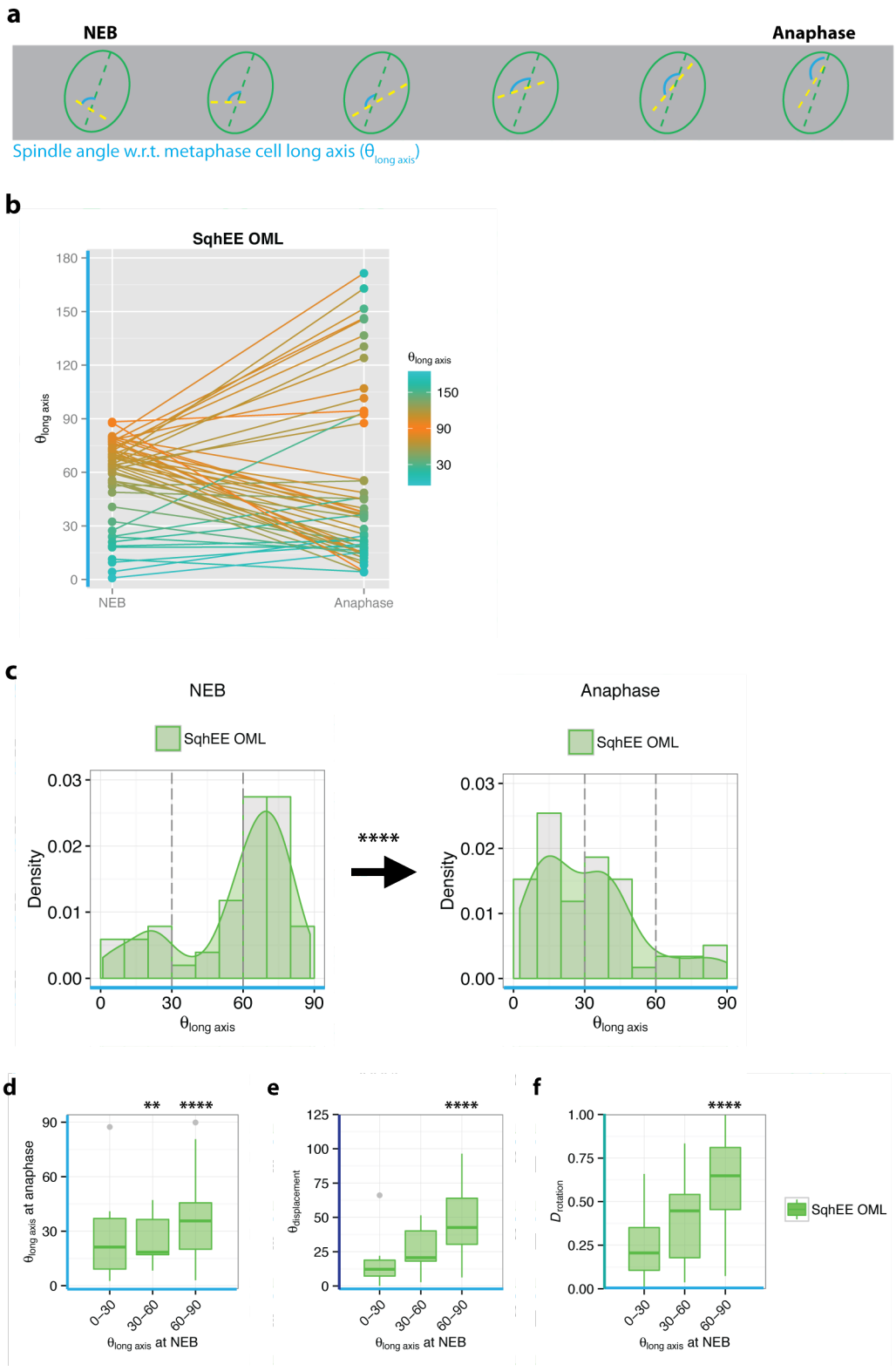

Figure 6.11: Spindle orientations change dramatically from NEB to anaphase onset in SqhEE OML cells.

a. Schematic of analysis for spindle angle wrt metaphase cell long axis ($\theta_{long\ axis}$).

b. Line plots for individual SqhEE OML cells showing $\theta_{long\ axis}$ at NEB and at anaphase.

Colour map indicates spindles close to the metaphase cell long axis (cyan) and to the short axis (orange). Points indicate $\theta_{long\ axis}$, with line connecting corresponding points from NEB to anaphase. Line colours follow that of $\theta_{long\ axis}$ at NEB. The slope of the line reflects the degree of displacement from NEB to anaphase ($\theta_{displacement}$). The line plots suggest that spindle rotations are consistently from the short axis at NEB to the long axis at anaphase.

c. Density plot of acute $\theta_{long\ axis}$ at NEB and anaphase onset for spindles in SqhEE OML cells. The distribution of $\theta_{long\ axis}$ is non-random and towards the short axis at NEB (Kolmogorov-Smirnov test p-value = 1.912^{e-05}; N: 59 cells, 3 experiments [SqhEE OML]). At anaphase, the distribution of $\theta_{long\ axis}$ are then towards the long axis. Consistent with this, distributions of $\theta_{long\ axis}$ at NEB and at anaphase are different (**** indicates $p < 0.001$, Kolmogorov-Smirnov test. N: 59 cells, 3 experiments). This suggests that positioning of the centrosomes before NEB, and consequent spindle rotation towards the long axis is regulated by myosin activity.

d. Acute spindle orientation relative to the long axis ($\theta_{long\ axis}$) at anaphase onset for SqhEE OML spindles by acute $\theta_{long\ axis}$ at NEB. $\theta_{long\ axis}$ at anaphase onset is close to the long axis regardless of $\theta_{long\ axis}$ at NEB in SqhEE OML cells. (** indicates $p < 0.01$; **** indicates $p < 0.001$. Distribution at anaphase was tested against corresponding distribution at NEB with the Kolmogorov-Smirnov test).

e. Spindle rotation from NEB to anaphase onset ($\theta_{displacement}$) for SqhEE OML spindles by spindle orientation ($\theta_{long\ axis}$) at NEB. $\theta_{displacement}$ is significantly higher for spindles that form at the short axis ($\theta_{long\ axis}$ = 60-90°) compared to those that form at the long axis ($\theta_{long\ axis}$ = 0-30°) (**** indicates $p < 0.001$, Mann-Whitney U test. N: 32 cells [short axis]; 10 cells [long axis]).

f. Directionality of spindle rotation ($\mathcal{D}_{rotation}$) for SqhEE OML spindles by spindle orientation at NEB. $\mathcal{D}_{rotation}$ is higher for SqhEE OML spindles that form further from the long axis, which corresponds to their higher $\theta_{displacement}$ (**** indicates $p < 0.001$, Mann-Whitney U test. N: 32 cells [short axis]; 10 cells [long axis]).

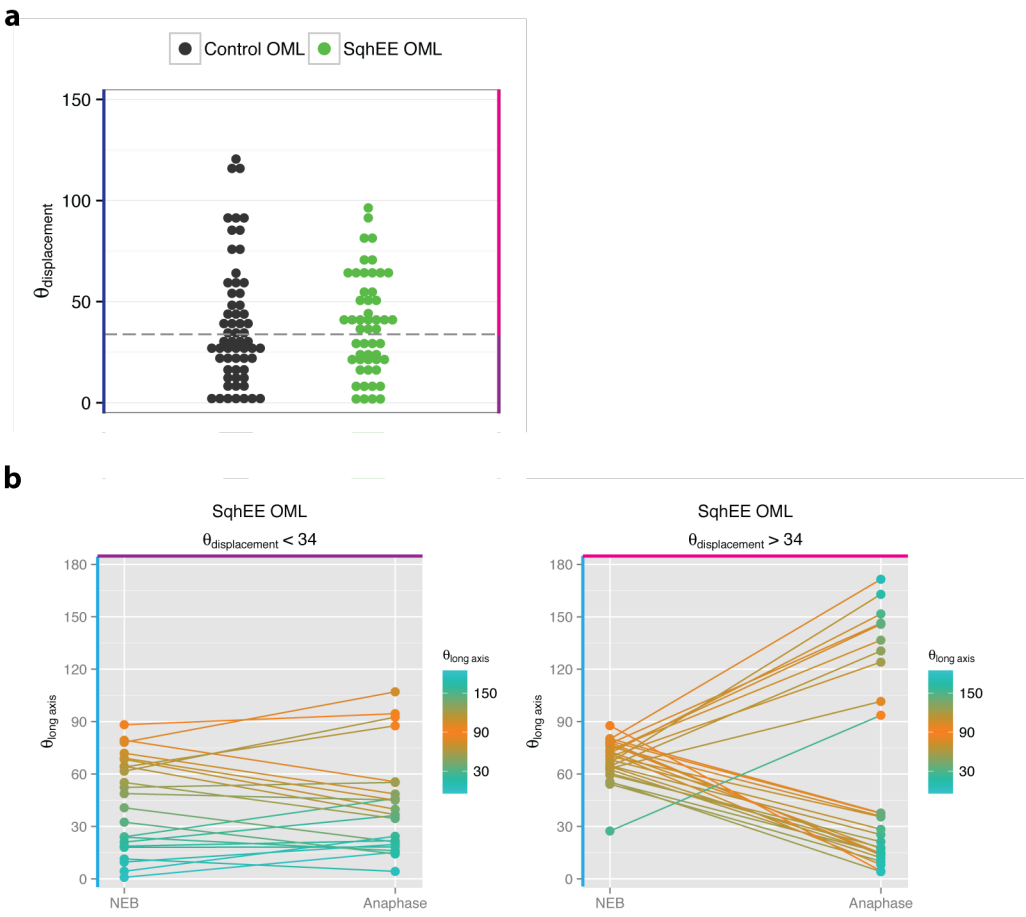

Figure 6.12: Spindle rotation in SqhEE OML cells changes the distribution of spindle orientations from NEB to anaphase onset.

a. Angular displacement of spindles from NEB to anaphase onset ($\theta_{displacement}$) for WT OML and SqhEE OML cells. The grey dashed line indicates the 90th percentile value of Mud IR cells ($\theta_{displacement}$= 34°), which defines the threshold for classifying cells with significant or non-significant spindle rotation. The proportion of cells with $\theta_{displacement}$ > 34° is slightly increased for SqhEE OML compared to WT OML cells (54.90% [SqhEE OML] and 45% [WT OML]).

b. Line plots for individual SqhEE OML cells with $\theta_{displacement}$ < 34° or > 34°, showing $\theta_{long\ axis}$ at NEB and at anaphase. Colour map indicate spindles close to the metaphase cell long axis (cyan) and to the short axis (orange). Points indicate $\theta_{long\ axis}$, with line connecting corresponding points from NEB to anaphase. Line colours follow that of $\theta_{long\ axis}$ at NEB. Line plots suggest that spindle rotations are almost exclusively from the short axis towards the long axis.

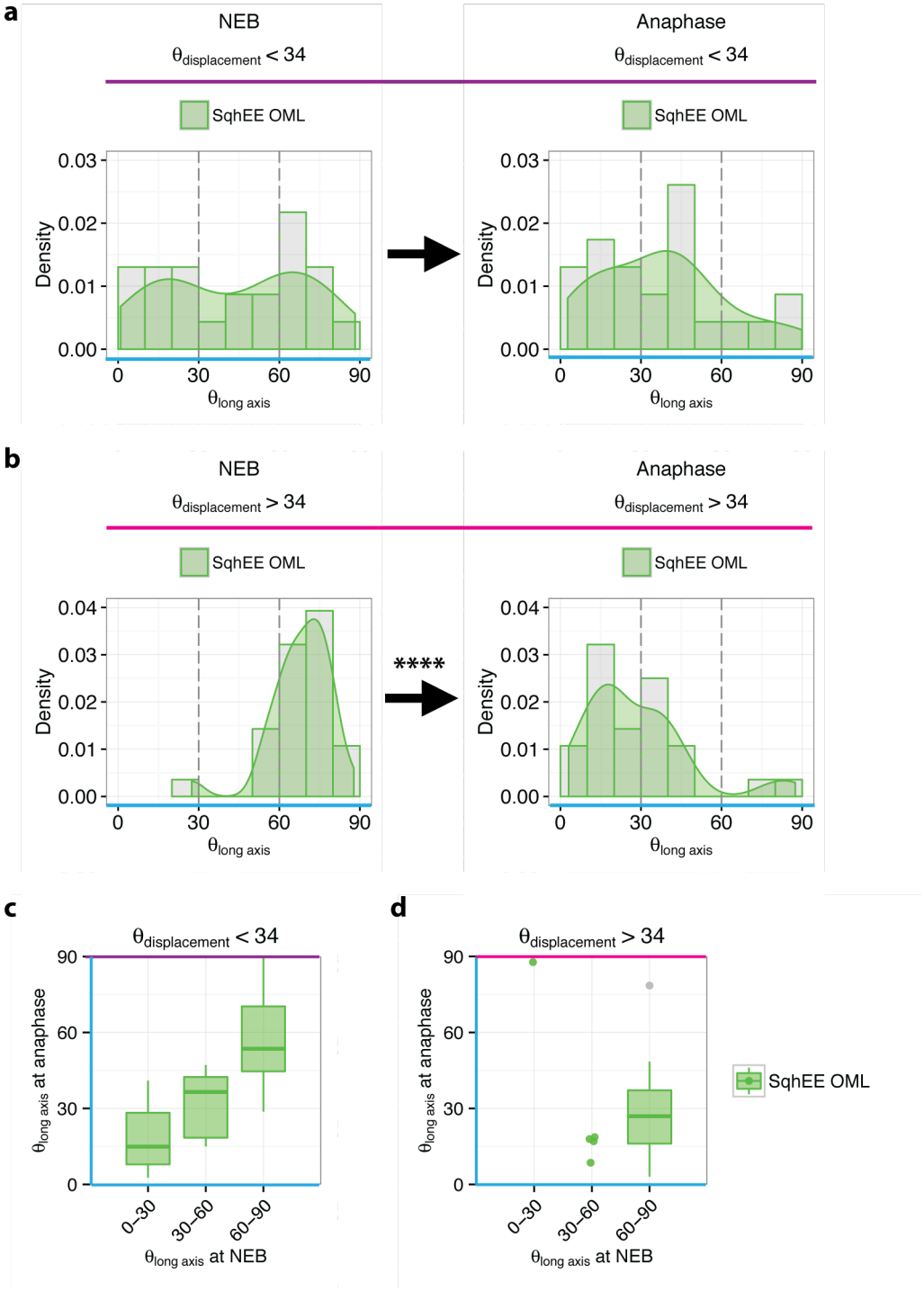

Figure 6.13: Spindles rotate towards the long axis at anaphase onset in SqhEE OML cells.

a. Density plot of acute $\theta_{long\ axis}$ at NEB and anaphase onset for SqhEE OML spindles with $\theta_{displacement} < 34°$. Spindle orientations at NEB are random (Kolmogorov-Smirnov test p-value = 0.878; n: 23 cells [SqhEE OML, $\theta_{displacement} < 34°$]). Distributions of $\theta_{long\ axis}$ at NEB and at anaphase onset are similar (Kolmogorov-Smirnov test p-value= 0.4218, n = 23 cells), although there appears to be a shift in spindle orientations away from the short axis.

b. Density plot of acute $\theta_{long\ axis}$ at NEB and anaphase for SqhEE OML spindles with $\theta_{displacement} > 34°$. Spindle orientation at NEB is non-random and clustered around the short axis (Kolmogorov-Smirnov test p-value = 2.161^{e-08}; n: 28 cells [SqhEE OML, $\theta_{displacement} > 34°$]). Spindle orientation at anaphase onset is significantly different, and towards the long axis (**** indicates $p < 0.001$, Kolmogorov-Smirnov test, n = 28 cells). This implies that spindle rotations in SqhEE OML cells are specifically moving spindles from the short axis to the long axis.

c. Spindle orientation at anaphase by spindle orientation at NEB for SqhEE OML spindles with $\theta_{displacement} < 34°$. SqhEE spindles shift slightly towards the long axis by anaphase.

d. Spindle orientation at anaphase by spindle orientation at NEB for SqhEE OML spindles with $\theta_{displacement} > 34°$. SqhEE spindles at the short or intermediate axes at NEB are close to the long axis by anaphase.

6.4.2.3 Spindle rotations are also more directed in SqhEE ML cells

The decrease in spindles rotating to the cell long axis in WT ML cells might be caused by the decrease in tissue tension due to local cell crowding. To check if myosin activity is sufficient to overcome these effects of cell crowding, I analysed spindle rotation and orientation to the cell long axis in SqhEE ML cells (Fig 6.14).

The average rotation from NEB to anaphase ($\theta_{displacement}$) was similar between SqhEE and WT ML cells (Fig 6.14c), however total accumulated rotation during mitosis (θ_{total}) was significantly lower for SqhEE ML cells compared to WT ML cells (Mann-Whitney U test p-value = 2.073^{e-05}) (Fig 6.14d). Although the calculated persistence of rotation ($\mathcal{D}_{rotation} = {\theta_{displacement}}/{\theta_{total}}$) was similar between SqhEE and WT ML cells (Fig 6.14e), when $\mathcal{D}_{rotation}$ was plotted against $\theta_{displacement}$, it was apparent that $\mathcal{D}_{rotation}$ for SqhEE ML cells is higher than WT ML cells for values of $\theta_{displacement} > 25°$ (Fig 6.14f). This indicates that spindles are indeed more directed than WT cells, for significant displacements in SqhEE ML cells.

6.4.2.4 Spindle orientation at NEB is dependent on cell size at NEB for SqhEE cells

Spindle orientation at NEB was random for SqhEE ML cells (Kolmogorov-Smirnov test p-value = 0.3376) (Fig 6.15b, c), similar to WT ML cells. This is in contrast to OML cells, where SqhEE expression resulted in a non-random distribution of spindle orientations at NEB at the short axis (Fig 6.11b, c). This might be due to the small sample size of SqhEE ML cells, or due to ML cells being larger than OML cells, even with increased myosin activity. Astral MT reach might be limited in these cells, especially in prophase in the early stages of MT nucleation by the centrosomes. Centrosomes that end up along the long axis after separation in long cells would be least likely to interact with cortical cues to move centrosomes close to the cortex and along the short axis. By plotting the cell area at NEB and the cell length at NEB against spindle orientation at NEB, this appears to be the case – SqhEE ML cells are larger than SqhEE OML cells in terms of cell area and cell

length, and the largest cells in both in SqhEE OML and ML cells are least likely to place their spindles close to the short axis at NEB (Fig 6.16).

6.4.2.5 SqhEE promotes spindle rotation towards the long axis in ML cells

Spindle orientations in SqhEE ML cells shifted from randomly oriented during NEB to towards the long axis at anaphase (Kolmogorov-Smirnov test p-value = 0.0001886) (Fig 6.15b, c). Additionally, when spindle orientation at anaphase was plotted by orientation at NEB, it was clear that spindles that are at the short or intermediate axes at NEB are close to the long axis at anaphase (Fig 6.15d). This could account for the observed shift in orientations towards the long axis by anaphase. This contrasts with what is observed in WT ML cells, where although spindles at the short axis appear to move away from the short axis, spindle orientation is not decidedly close to the long axis at anaphase (Fig 6.4d). Furthermore, WT ML spindles that form at the intermediate axis have an almost random distribution at anaphase (Fig 6.4d). Of note, SqhEE ML spindles that form at the short axis rotate the most (Fig 6.15e) and have the most persistent spindle rotation (Fig 6.15f). This supports the model where myosin activity, and myosin-mediated tissue tension promotes directed spindle rotation towards the cell long axis.

Analysing spindles with significant ($\theta_{displacement} > 34°$) and non-significant ($\theta_{displacement} < 34°$) displacements yielded similar trends to that of SqhEE OML cells (Fig 6.17b, Fig 6.12b). Similar to SqhEE OML cells, SqhEE ML spindles with $\theta_{displacement} > 34°$ are at the short axis at NEB (Kolmogorov-Smirnov test p-value = 0.0090, against a generated random uniform distribution) (Fig 6.18b, Fig 6.13b) and by anaphase, spindle orientations are significantly different (Kolmogorov-Smirnov test p-value = 2.514^{e-07}) and towards the long axis (Fig 6.18b, Fig 6.13b). Plotting the spindle orientation at NEB against their corresponding orientation at anaphase, it is clear that almost all the spindles at the short or intermediate axis at NEB in SqhEE ML cells rotate towards the long axis by anaphase, just like in SqhEE OML cells (Fig 6.18d, Fig 6.13d). This is in contrast to WT ML cells where spindles with $\theta_{displacement} > 34°$ that form at the intermediate axis end up with a random distribution

by anaphase (Fig 6.6d). This suggests that myosin-mediated tissue tension is involved in spindle re-orientation to the long axis.

SqhEE ML spindles with $\theta_{displacement} < 34°$ have an apparently random distribution of spindle orientations at NEB (Fig 6.18a), which is consistent with that seen in SqhEE OML cells (Fig 6.13a). Furthermore, just like SqhEE OML cells, SqhEE ML spindles with low displacements seem to drift towards the long axis, although the numbers are small (Fig 6.18c, Fig 6.13c).

The data from the experiments with SqhEE expression suggest that myosin activity promotes directed spindle rotation, and spindle rotation towards the cell long axis. However, it does not support the hypothesis that myosin activity promotes the recognition of cell long axis. This is because while majority of spindles that form farther from the long axis rotate towards it, spindles with low rotations are not more likely to be those that form at the long axis. Furthermore, the proportions of spindles with significant displacements are unaffected by myosin activity. It is therefore more likely that about half of spindles have a tendency to rotate away from their NEB positions, and myosin activity, perhaps through cortical flow, brings these spindles towards the long axis of the cell.

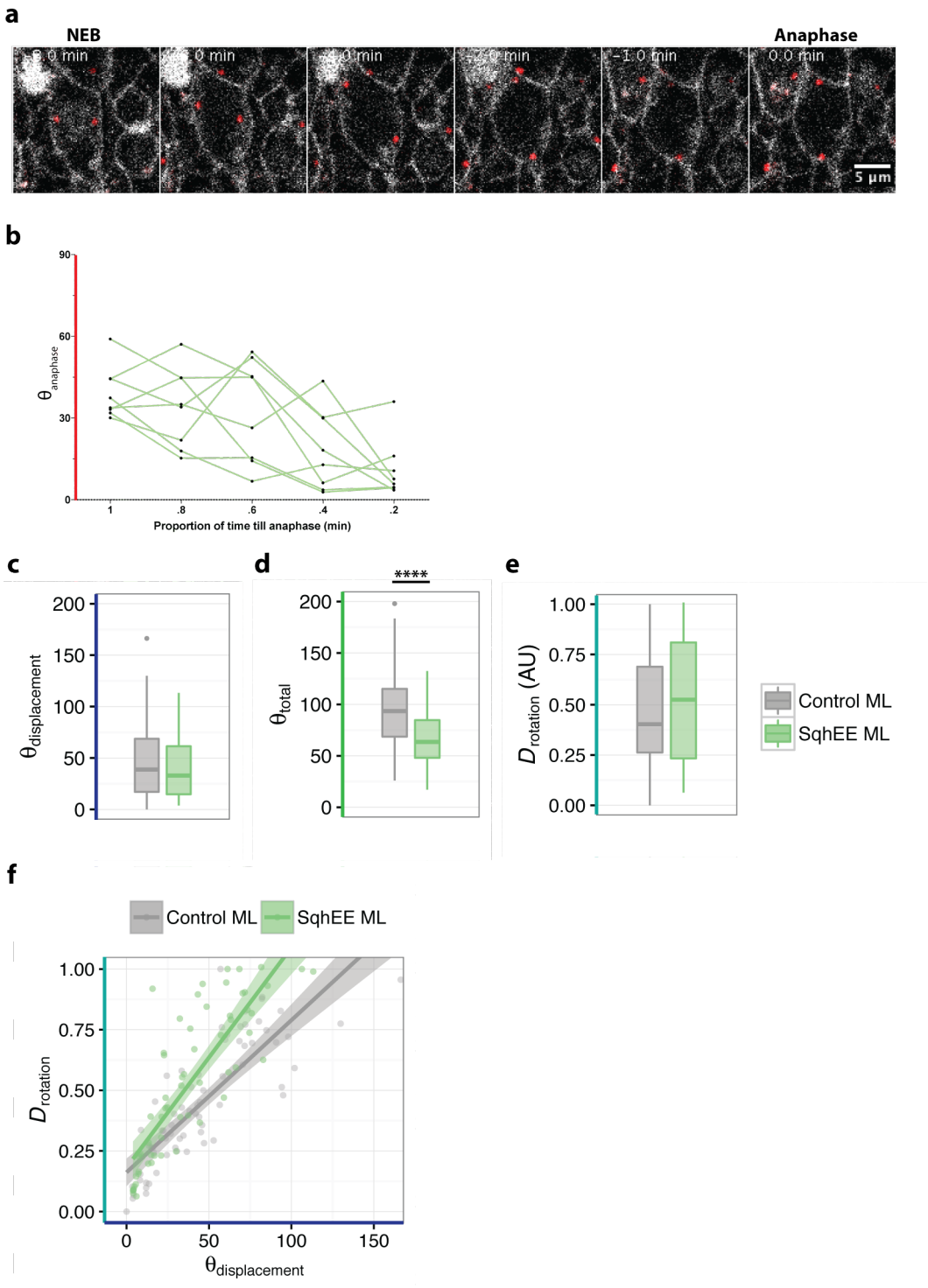

Figure 6.14: Spindle rotation is more directed in SqhEE ML cells.

a. Representative SqhEE ML cell dividing. Spindle poles are labelled with Centrosomin-RFP (red) and cell membranes are labelled with Spider-GFP (white). Spindles seem to move in a much more directed manner in SqhEE ML cells. Note that increased myosin activity cannot rescue mitotic rounding within the midline.

b. Representative line plots for SqhEE ML cells. Spindle rotation is mostly towards the

anaphase orientation (8 cells, 3 experiments).

c. Angular displacement from NEB to anaphase onset ($\theta_{displacement}$) for WT ML and SqhEE ML cells. $\theta_{displacement}$ was similar for WT and SqhEE cells (Mean: 44.75 ± 3.898° [WT ML, n = 80 cells] and 35.010 ± 3.399° [SqhEE ML, n = 67 cells], Mann-Whitney U test p-value = 0.09485).

d. Total accumulated rotation during mitosis (θ_{total}) for WT ML and SqhEE ML cells. θ_{total} was lower for SqhEE ML cells compared to WT ML (Mean: 97.37 ± 4.668° [WT ML, n = 80 cells] and 69.13 ± 3.432° [SqhEE ML, n = 67 cells], Mann-Whitney U test p-value = 2.073^{e-05}).

e. Persistence of rotation ($\mathcal{D}_{rotation}$) for WT ML and SqhEE ML cells. $\mathcal{D}_{rotation}$ was similar for SqhEE ML and WT ML cells (Mean: 0.4456 ± 0.0297 [WT ML, n = 80 cells] and 0.5281 ± 0.0398 [SqhEE ML, n = 67 cells], Mann-Whitney U test p-value = 0.1602).

f. $\mathcal{D}_{rotation}$ as a function of $\theta_{displacement}$ for WT ML and SqhEE ML cells. Lines indicate best-fit mean line and filled areas represent standard error of the mean. $\mathcal{D}_{rotation}$ for SqhEE ML spindles is higher than WT ML spindles for significant values of $\theta_{displacement}$ ($\theta_{displacement} \approx 34°$).

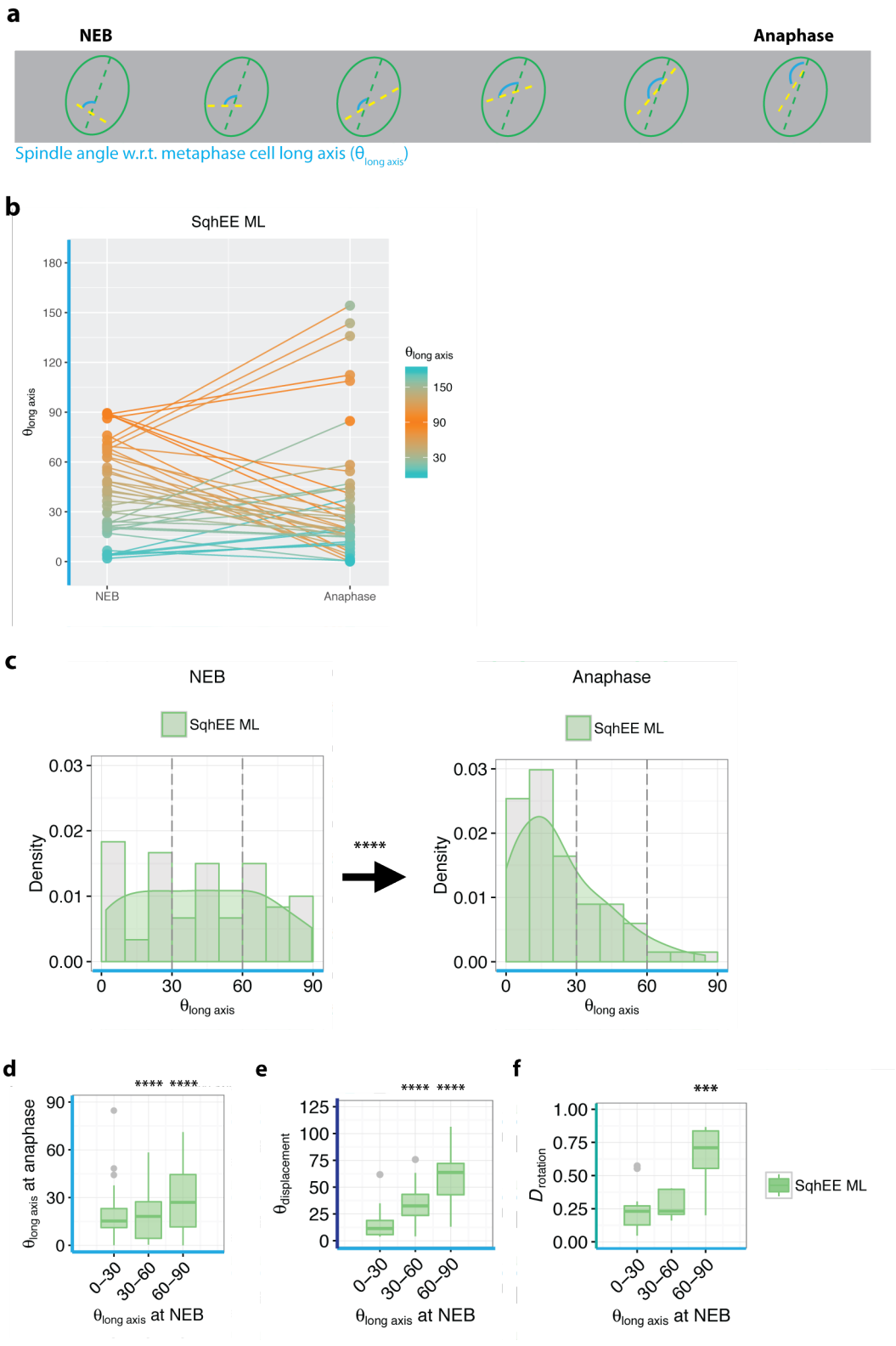

Figure 6.15: Spindles rotate from the short axis at NEB to the long axis at anaphase onset in SqhEE ML cells.

a. Schematic of analysis for spindle angle wrt metaphase cell long axis ($\theta_{long\ axis}$).

b. Line plots for individual SqhEE ML cells showing $\theta_{long\ axis}$ at NEB and at anaphase onset.

Colour map indicates spindles close to the metaphase cell long axis (cyan) and to the short axis (orange). Points indicate $\theta_{\text{long axis}}$, with line connecting corresponding points from NEB to anaphase onset. Line colours follow that of $\theta_{\text{long axis}}$ at NEB. The slope of the line reflects the degree of displacement from NEB to anaphase ($\theta_{\text{displacement}}$). The line plots suggest that spindle rotations are consistently from the short axis at NEB to the long axis at anaphase onset.

c. Density plot of acute $\theta_{\text{long axis}}$ at NEB and anaphase onset for spindles in SqhEE ML cells. The distribution of $\theta_{\text{long axis}}$ is random at NEB (Kolmogorov-Smirnov test p-value = 0.3376; N: 67 cells, 5 experiments [SqhEE ML]). At anaphase, the distribution of $\theta_{\text{long axis}}$ shifts towards the long axis. Distributions of $\theta_{\text{long axis}}$ at NEB and at anaphase are significantly different (**** indicates $p < 0.001$, Kolmogorov-Smirnov test, N: 67 cells, 5 experiments).

d. Acute spindle orientation relative to the long axis ($\theta_{\text{long axis}}$) at anaphase onset for SqhEE ML spindles by acute $\theta_{\text{long axis}}$ at NEB. Spindles rotate from the short or intermediate axis ($\theta_{\text{long axis}}$ = 60-90°) to the long axis ($\theta_{\text{long axis}}$ = 0-30°) in SqhEE ML cells, in contrast to WT ML cells (Fig 6.3d). (** indicates $p < 0.01$; **** indicates $p < 0.001$. Distribution at anaphase was tested against corresponding distribution at NEB with the Kolmogorov-Smirnov test)

e. Spindle rotation from NEB to anaphase onset ($\theta_{\text{displacement}}$) for SqhEE ML spindles by spindle orientation ($\theta_{\text{long axis}}$) at NEB. Dotted boxplot in grey indicates the median and interquartile range for WT ML cells (Fig 6.3e). $\theta_{\text{displacement}}$ is significantly higher for spindles that form at the short axis compared to those that form at the long axis (*** indicates $p < 0.005$, Mann-Whitney U test. N: 8 cells [short axis]; 11 cells [long axis]).

f. Directionality of spindle rotation ($\mathcal{D}_{\text{rotation}}$) for SqhEE ML spindles by spindle orientation at NEB. Dotted boxplot in grey indicates the median and interquartile range for WT ML cells (Fig 6.3f). $\mathcal{D}_{\text{rotation}}$ is highest for spindles that form furthest from the long axis, which corresponds to their higher $\theta_{\text{displacement}}$ (**** indicates $p < 0.001$, Mann-Whitney U test. N: 8 cells [short axis]; 11 cells [long axis]).

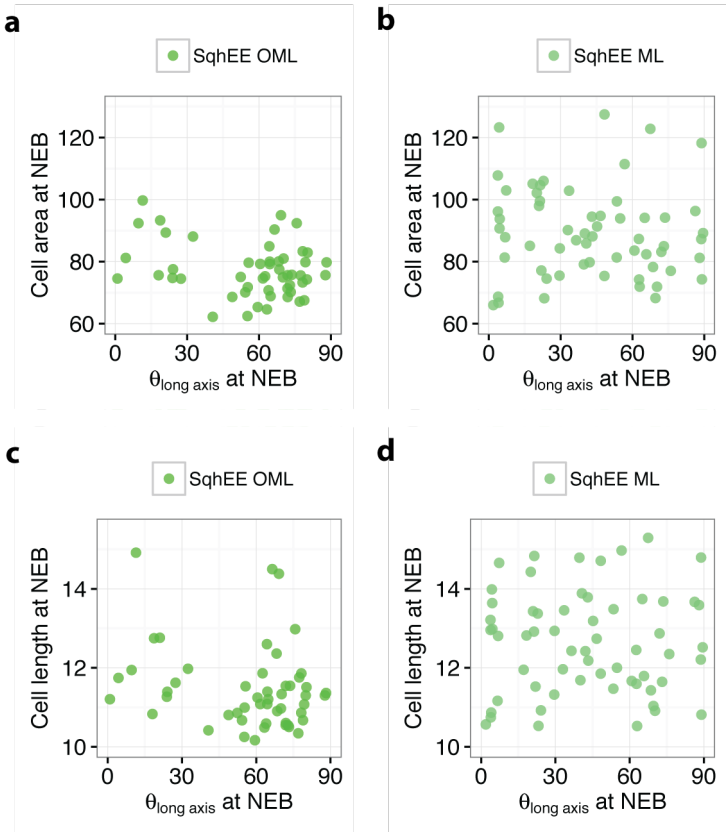

Figure 6.16: Relationship between cell area and cell length at NEB and spindle orientation at NEB in SqhEE OML and SqhEE ML cells.

a. Cell area at NEB against spindle orientation relative to the cell long axis ($\theta_{long\ axis}$) at NEB for SqhEE OML cells. Cell area has weak negative correlation with $\theta_{long\ axis}$ at NEB (R^2 = 0.0541, p-value= 0.0550, n = 51 cells). Cells where spindles are oriented to the short axis tend to have a small cell area at NEB, while cells where spindles are oriented to the long axis tend to have a large cell area at NEB.

b. Cell area at NEB against spindle orientation relative to the cell long axis ($\theta_{long\ axis}$) at NEB for SqhEE ML cells. Cell area at NEB is larger in SqhEE ML cells than in SqhEE OML cells. Cell area has no correlation with $\theta_{long\ axis}$ at NEB (R^2 = -0.0132, p-value = 0.6349, n = 60 cells).

c. Cell length at NEB against spindle orientation relative to the cell long axis ($\theta_{long\ axis}$) at NEB for SqhEE OML cells. Cell length has very weak negative correlation with $\theta_{long\ axis}$ at NEB (R^2 = 0.0293, p-value= 0.1196, n = 51 cells).

d. Cell length at NEB against spindle orientation relative to the cell long axis ($\theta_{long\ axis}$) at NEB for SqhEE OML cells. Cell length has no correlation with $\theta_{long\ axis}$ at NEB (R^2 = -0.01707, p-value = 0.921, n = 60 cells). SqhEE ML cells are longer than SqhEE OML cells at NEB.

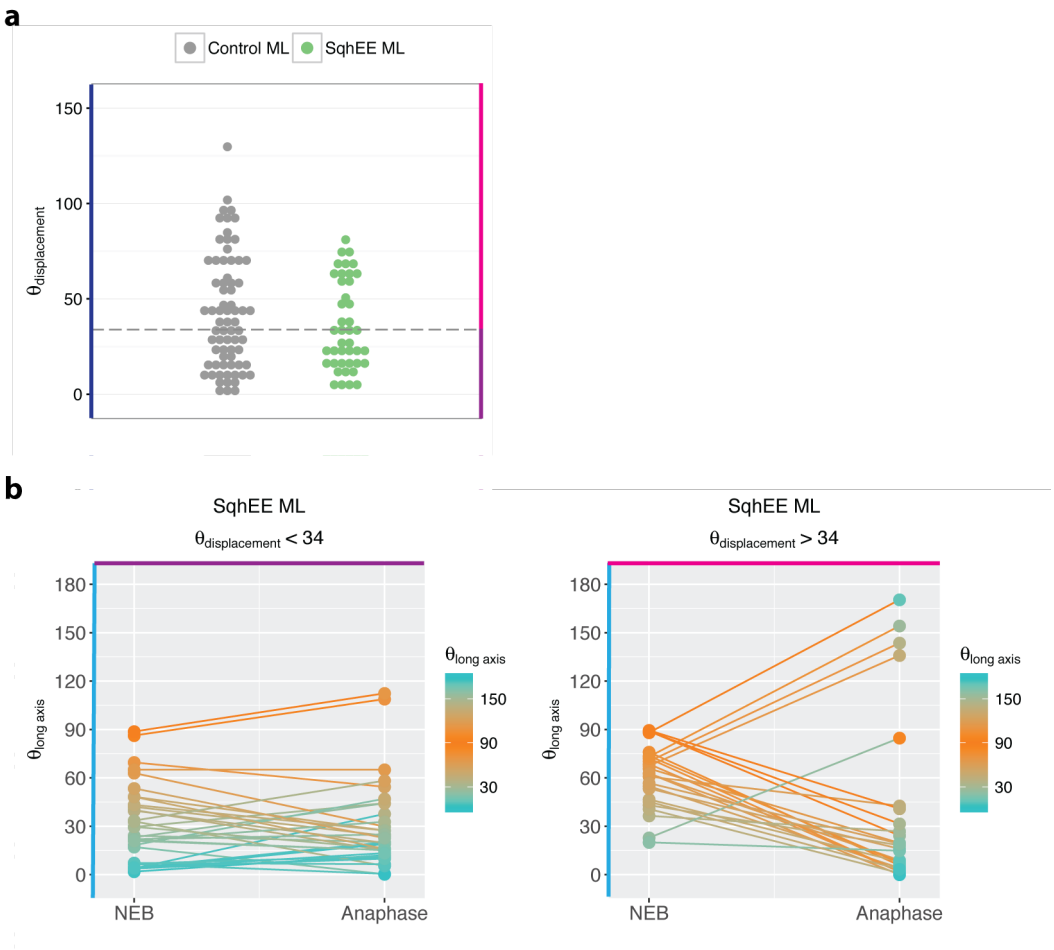

Figure 6.17: Spindles rotate from the short to the long axis in SqhEE ML cells.

a. Spindle rotation from NEB to anaphase onset ($\theta_{displacement}$) for WT ML and SqhEE ML cells. The grey dashed line indicates the 90th percentile value of Mud IR cells ($\theta_{displacement}$= 34°), which defines the threshold for classifying cells with significant or non-significant spindle rotation. The proportion of cells with $\theta_{displacement}$ > 34° is decreased for SqhEE ML and compared to WT ML cells (41.6% [SqhEE ML] and 54.16% [WT ML]).

b. Line plots for individual SqhEE ML cells with $\theta_{displacement}$ < 34° or > 34°, showing $\theta_{long\ axis}$ at NEB and at anaphase. Colour map indicate spindles close to the metaphase cell long axis (cyan) and to the short axis (orange). Points indicate $\theta_{long\ axis}$, with line connecting corresponding points from NEB to anaphase. Line colours follow that of $\theta_{long\ axis}$ at NEB. Line plots suggest that spindle rotations are almost exclusively from the short axis towards the long axis.

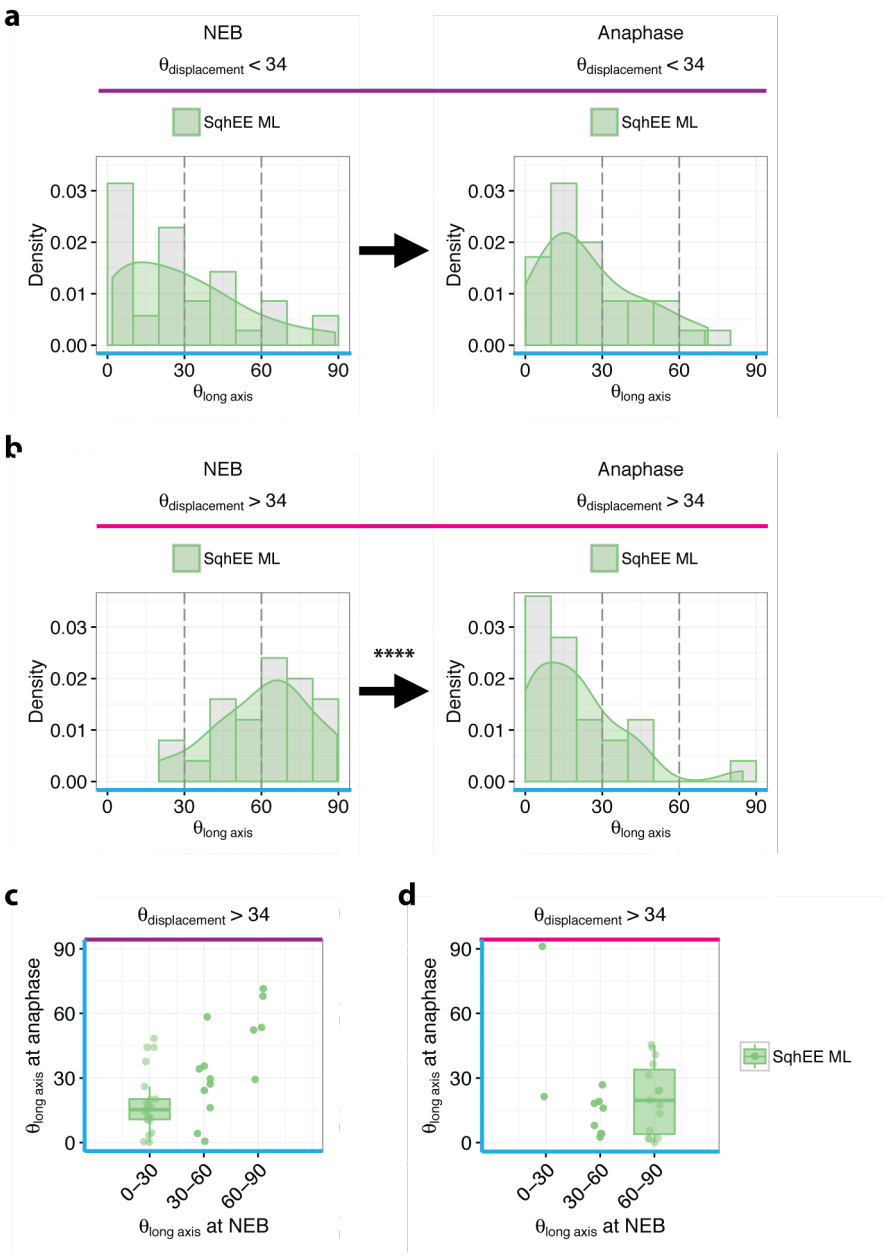

Figure 6.18: Spindles rotate from the short to the long axis in SqhEE ML cells.

a. Density plot of acute $\theta_{long\ axis}$ at NEB and anaphase for SqhEE ML spindles with $\theta_{displacement}$ < 34°. Spindle orientations at NEB is non-random, towards the long axis (Kolmogorov-Smirnov test p-value = 0.0032; n: 35 cells [SqhEE ML, $\theta_{displacement}$ < 34°]). Distributions of $\theta_{long\ axis}$ at NEB and at anaphase are similar (Kolmogorov-Smirnov test p-value= 0.6902, n = 35 cells).

b. Density plot of acute $\theta_{long\ axis}$ at NEB and anaphase for SqhEE ML spindles with $\theta_{displacement}$ > 34°. Spindle orientation at NEB is non-random and clustered around the short axis (Kolmogorov-Smirnov test p-value = 0.0090; n: 25 cells [SqhEE ML, $\theta_{displacement}$ > 34°]). Spindle orientation at anaphase is significantly different, and towards the long axis

(Kolmogorov-Smirnov test p-value = 2.514^{e-07}, n = 25 cells). This implies that spindle rotations in SqhEE ML cells are specifically moving spindles from the short axis to the long axis, similar to in SqhEE OML cells.

c. Spindle orientation at anaphase by spindle orientation at NEB for SqhEE ML spindles with $\theta_{displacement} < 34°$. SqhEE spindles shift slightly towards the long axis by anaphase.

d. Spindle orientation at anaphase by spindle orientation at NEB for SqhEE ML spindles with $\theta_{displacement} > 34°$. SqhEE spindles at the short or intermediate axes at NEB are close to the long axis by anaphase.

6.5 Conclusions

I show in this chapter that spindle rotation from the short or intermediate axes towards the long axis, which is characteristic in WT OML cells, is perturbed in cells in crowded conditions (ML cells) and cells with low myosin activity (SqhAA cells), and improved in cells with high myosin activity (SqhEE cells). Importantly, the impairment of this rotation towards the long axis in ML cells can be rescued by the exogenous increase in myosin activity (SqhEE ML cells). Previous studies investigating the role of tissue tension in orienting cell divisions have shown that a tension axis applied across the mitotic cell is able to orient divisions, most likely by polarising cell shape in the direction of tension (Wyatt et al. 2015; Campinho et al. 2013; Mao et al. 2013). I show here that even without a tension axis, isotropic tissue tension and myosin activity are able to promote spindle alignment to the cell long axis.

I also show that spindle orientation to long axis does not correlate with the increase in cell shape anisotropy. The model using astral MTs as mechanosensors to allow cells to read cell geometry (Minc et al. 2011) is therefore not likely to be true for cells in the *Drosophila* notum. This also suggests that the model for spindle orientation to the long axis via tricellular junctions in the notum proposed by Bosveld et al. 2016 is insufficient. Cells in crowded conditions, which are really elongated, do not divide more frequently with the long axis than cells which are in less crowded conditions, and are less elongated. In fact, spindle rotation from the short or intermediate axes towards the long axis is actually impaired in ML cells. Spindle rotation dynamics is similar between ML cells and OML cells, suggesting that impaired spindle rotation is not the reason for impaired rotation towards the long axis.

Myosin activity is proposed to be the main source of tissue tension through its interaction with actin filaments along cell junctions. However, myosin may also be involved in signalling pathways, independent of its motor activity along actin filaments. Spindles with perturbed myosin activity exhibited impaired persistent spindle rotation. Overall spindle displacement was not affected, indicating that on average, spindles are equally likely to re-orient from NEB to anaphase, and that

cortical pulling forces are active. However, the persistence of rotation is affected, as spindles often change directions during spindle rotation. This can be improved with increased myosin activity, showing that myosin activity alone can regulate these events. This suggests that the processivity of spindle pulling forces is affected by myosin activity. Actomyosin activity might affect the processivity of spindle rotation if astral MTs bind to the cortex and use actomyosin fibres as tracks for movement. When tracks are aligned, as in a highly contractile cortex, movement is more processive. To test this, experiments targeting the length of astral MTs could be done to attempt to recapitulate the effects of myosin perturbation as well as targeting the organisation of cortical actin directly. Alternatively, myosin activity might affect the dynamic localization of spindle orienting proteins such as Mud to the cortex, resulting in frequent switches in the directions of the pulling forces on the spindles. This can be verified by observing the dynamic localization of Mud in different conditions of myosin activity. Furthermore, because actin has recently been found at the centrosomes, and myosin is frequently colocalized with actin, experiments to identify which population of myosin in the mitotic cell is responsible for processive spindle rotation would be insightful. This might be done by targeting cortical actin specifically, or targeting the proposed nucleators of actin at the centrosome.

Besides affecting the persistence of spindle rotation, I found that myosin activity also had an effect on spindle orientation. Specifically, cells in tissues with high myosin activity or in less crowded conditions consistently move spindles from the short or intermediate axes to the long axis, while cells in tissue with low myosin activity or in crowded conditions such as ML cells are impaired in this ability. The data suggest that tissue tension promotes the integration of cell geometry in spindle orientation decisions. Interestingly, this behaviour can be improved in cells with high myosin activity, in that spindles that form at the long axis remain at the long axis, while all spindles forming further from the long axis rotate towards the long axis, even if just by a little. It is unclear how myosin activity and tissue tension might direct spindle movement towards the cell long axis. One hypothesis is that the localisation of actomyosin around the cell is heterogenous, or that actomyosin along the cortex moves towards the cell poles during rounding, and this movement might be more distinct for cells rounding in a more tensile environment. Cortical flows have been shown to be involved in centrosome separation at prophase, and correlate

with spindle pole movement before NEB (Rosenblatt et al. 2004; De Simone et al. 2016), and the actomyosin cortext is able to interact with astral MTs through interactors such as APC2, which also play a role in spindle orientation (McCartney et al. 2001; Cao et al. 2010; Hebert et al. 2012). High resolution imaging or FRAP of the mitotic actomyosin cortex might help to identify if the cortex does indeed move towards the cell poles, and bring spindle poles along with it.

In SqhEE OML cells, I find that spindle orientations at NEB are significantly towards the short axis. This might be due to the role of myosin in centrosome separation and positioning before NEB (Rosenblatt et al. 2004; De Simone et al. 2016), which positions centrosomes close to the cortex and therefore at the cell width before NEB. In SqhAA OML cells, there is a small increase in spindles oriented away from the short axis at NEB, which would be consistent with myosin activity promoting cortex-centrosome interaction at the cell width. In SqhEE ML cells however, spindles do not preferentially form along the short axis after NEB. This might be due to SqhEE ML cells being larger than SqhEE OML cells at NEB, which would make the interaction between the cortex and the centrosomes in prophase difficult if astral MTs at this stage have a limited reach. Consistent with this, I show that large cells both in terms of area and length are least likely to position their centrosomes along the short axis, both in SqhEE OML cells and SqhEE ML cells. This trend is not observed in WT OML and ML cells, probably because this phenomena only occurs with high levels of myosin activity promoting interaction between the cortex and prophase centrosomes. To better observe the effects of myosin activity on centrosome positioning before NEB, it would be better to track centrosomes from the moment of centrosome separation with a early marker, such as Centrin (Piel et al. 2000). Furthermore, SqhEE ML spindles that form close to the long axis are less good at remaining close to the long axis than spindles in SqhEE OML cells (Fig 6.18c, Fig 6.13c). Again suggesting that the limited reach of astral MTs in these larger cells, could result in poorer interaction between spindle poles and the cell cortex along the long axis.

Chapter 7 Discussion

Cell division requires the coordination of cell shape remodelling (Ramkumar & Baum 2016), spindle formation (Tanenbaum et al. 2010; Heald & Khodjakov 2015) and spindle positioning within the cell geometry. Cell division within an epithelium adds further levels of complication, as the cell has to regulate division not just with the internal geometry but also according to extracellular factors such as cell-cell adhesion and tissue tension (Le Bras & Le Borgne 2014; Panousopoulou & Green 2014; Bergstralh et al. 2015; di Pietro et al. 2016). In this thesis, I have investigated how cells within an epithelium change their shape during mitosis, and how the mechanical constraints of the tissue affect these changes in cell shape. I found that in the epithelium of the *Drosophila* notum, while cells round up significantly during mitosis tissue mechanics imposes limits on mitotic rounding.

Having established the typical changes in cell geometry, I then sought to understand how spindles position relative to cell geometry in an epithelium. As an important step towards this, I first studied spindle dynamics in mitotic cells in the notum. I found that spindles move in a dynamic and noisy manner continuously from NEB through till anaphase. This dynamic behaviour of the spindle was caused by the presence of canonical pulling forces on the spindle pole.

In cells where mitotic rounding is incomplete, cells retain a clear long axis during mitosis. I found that spindle orientation at NEB is random relative to the cell long axis, but spindle rotation during mitosis resulted in a global shift in spindle orientations toward the cell long axis. When exploring the influence of cell crowding on spindle orientation, I found that this behaviour was impaired. I next tested for a role in myosin activity in the tissue on spindle orientation, and found that it is involved in regulating rotations towards the cell long axis as well as the persistence of spindle rotation.

Below, I detail these findings and place them in the wider context of the known literature. I also present the model for spindle positioning in an epithelium and discuss future experiments to test the model.

7.1 Mitotic rounding in the epithelium is a combination of basal de-adhesion, cortical contractility and increase in cell volume

Mitotic rounding is the outcome of a variety of processes occurring in parallel, including basal de-adhesion, an increase in cortical contractility and rigidity, and an increase in volume (Ramkumar & Baum 2016). These processes change the mechanical forces at the cell's surface, causing cells to round as they reach a new mechanical equilibrium. As such, the process will likely be modulated by the mechanical microenvironment of a tissue, where cells experience additional forces due to cell-cell adhesion, and local crowding or stretching (Heisenberg & Bellaïche 2013; Guillot & Lecuit 2013b; Mao & Baum 2015; LeGoff & Lecuit 2015). In Chapter 3, I have studied mitotic cells in the epithelial monolayer of the *Drosophila* notum to understand the mechanisms and functions of mitotic rounding in the context of a tissue.

I find that although in single cells mitotic rounding is achieved by a retraction of cell spread (i.e. length and width) and an increase in cell height, in cells within a columnar epithelium, this is instead achieved by a retraction of cell height, and an expansion of cross-sectional area in the medial plane of the cell (Fig 7.1a). The expansion of cross-sectional area is accompanied by a decrease in anisotropy, i.e. cells become rounder, and is most prominent in the medial plane, while the apical plane remains relatively similar and does not undergo a large change in area (Fig 7.2a). This suggests that the apical plane is more rigid than the medial plane, and is therefore more resistant to intracellular forces. This may be due to the physical linkage of the apical surface with the overlying cuticle, through the large extracellular molecule Dumpy (Wilkin et al. 2000). In addition, cadherin-catenin complexes are localized to the apical plane along adherens junctions (AJs) where they recruit actomyosin. AJs are maintained throughout mitosis, ensuring epithelial stability (Le Bras & Le Borgne 2014). Consequently, the considerable actomyosin-based forces acting at AJs may render the apical surface resistant to shape changes driven by basal de-adhesion, actomyosin reorganisation and increases in hydrostatic pressure.

The medial plane is also the plane of spindle localisation. The spindle is the apparatus for segregating genetic material during mitosis, and *in vitro* studies have suggested that it requires a certain amount of space for normal bipolar formation that is simultaneously limited and isotropic enough for timely chromosome capture (Lancaster et al. 2013). It is therefore unsurprising to find that it is in the plane of the cell with the largest area and most isotropic shape. This led me to focus my analysis of mitotic rounding on the medial plane coincident with the spindle plane, as I reasoned that cell shape in this plane would be the most functionally relevant to spindle behaviour.

The forces generated during mitotic rounding in the medial plane were strong enough to deform neighbouring cells to provide sufficient space for normal spindle morphogenesis under crowded conditions, but not enough to overcome tissue-scale crowding. Thus, rounded mitotic cells have a residual shape anisotropy that is related to their interphase shape. Furthermore, the process of rounding was less effective in midline (ML) cells compared to cells outside the midline (OML) (Fig 7.2a, b), consistent with the shape at mitosis reflecting the tissue crowding from lateral to the ML.

Despite the apparent differences in the way cells round up in an epithelium compared to single cells, my analysis suggests that the key events that drive mitotic rounding are similar. These features include the basal de-adhesion via downregulation of Rap1, which may act either on basolateral contacts or on crosstalk between the basal surface and the underlying ECM. As a result, expression of a constitutively active Rap1 (Rap^{V12}) in mitotic cells in the notum resulted in a significant retention of the cell to basal planes, where normally the cell margin would retract towards the mediolateral planes (Fig 7.1c). To my knowledge, this is the first demonstration that mitotic de-adhesion within an epithelium is regulated by Rap1. In single cells, basal de-adhesion is important for normally spread and flat cells to become taller to prevent compression of the bipolar spindle (Dao et al. 2009; Lancaster et al. 2013). Such defects are not so profound in epithelial cells, probably because these cells are normally tall in interphase, and cell height is defined by lateral adhesions that remain intact during mitosis (Bergstralh et al. 2015; Rosa

2013). The prevention of basal de-adhesion however, was accompanied by a decrease in the area of the cell in the mediolateral plane (Fig 7.2d), consistent with a model where basal de-adhesion allows the bulk redistribution of cell mass. Mitotic rounding could not be completely abrogated by preventing cells from de-adhering – cells still expanded slightly and decrease in anisotropy was unchanged. This indicates the presence of other drivers of mitotic rounding.

Another driver of mitotic rounding is the formation of a contractile and rigid actomyosin cortex (Cramer & Mitchison 1997; Maddox & Burridge 2003; Matthews et al. 2012; Stewart et al. 2011a). *In vitro* studies suggest that this helps cells round up against mild confinement (Stewart et al. 2011a; Lancaster et al. 2013; Ramanathan et al. 2015). In MDCK cells confined between lateral micropillars, this allows cells to push out against confinement and successfully divide at the apical surface (Sorce et al. 2015). *In vivo,* in the *Drosophila* wing discs, the perturbation of myosin activity through depletion of its major kinase, ROK (Rho Kinase) led to a significant decrease in the ability of mitotic cells to expand against their neighbours (Nakajima et al. 2013). However, I find no evidence for this within the *Drosophila* notum, where cells with almost no mitotic cortex or perturbed myosin activity are still able to expand their medial plane (Fig 7.1b, 7.2c). This likely reflects the lower levels of tissue crowding in the *Drosophila* notum compared to the wing disc, and supports the notion that the mechanical environment of the cell plays a role in defining what is necessary for normal cell division. This also indicates that in this tissue, bulk redistribution of cell mass during basal de-adhesion together with an increase in cell volume is sufficient to expand the mitotic cell against endogenous levels of confinement, and the actomyosin cortex serves to restrict this expansion. It is also possible that some of the increase in cell area is due to a reduction in tissue tension in neighbouring cells. Clonal analysis where only the actomyosin in the mitotic cell is targeting will be important to verify this.

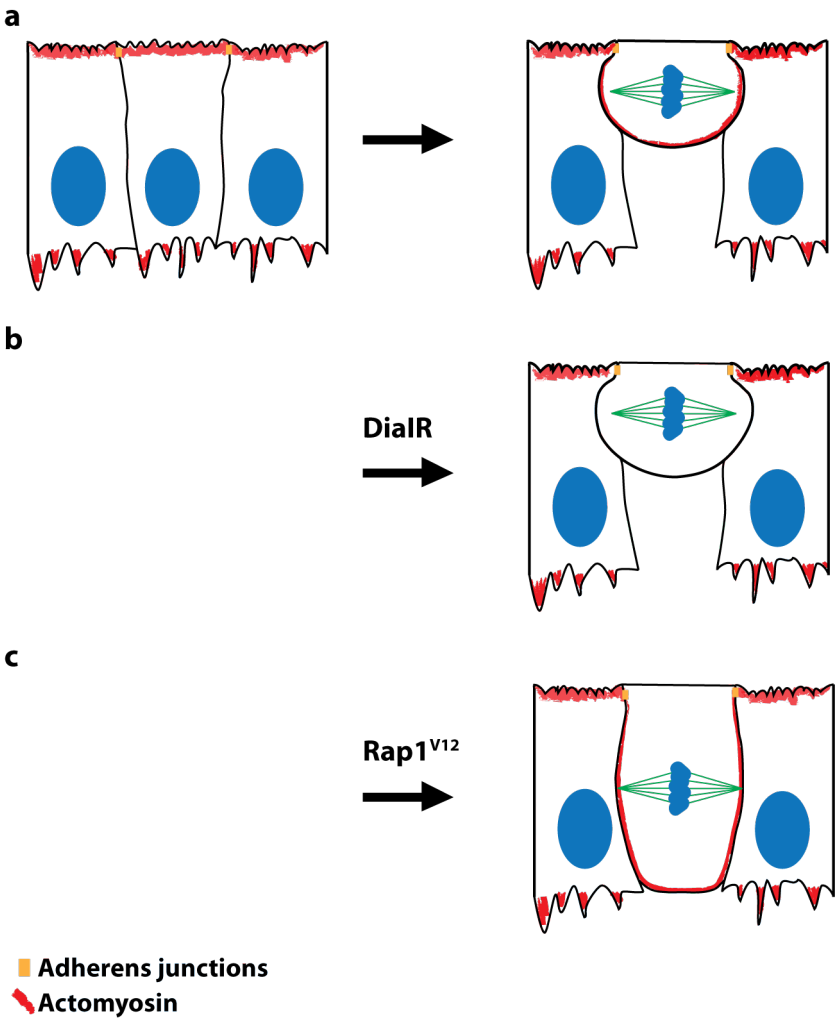

Figure 7.1: Graphical representation of mitotic rounding in a tissue.

a. Longitudinal view of a WT cell in the notum in interphase and mitosis. Cells retract the basal portion and remodel actin to form a basolateral cortex.

b. Longitudinal view of the effect of DiaIR on mitotic rounding in the notum. Cells still retract the basal portion and cells expand more in the medial plane.

c. Longitudinal view of the effect of Rap1V12 on mitotic rounding in the notum. Cells are unable to retract the basal portion effectively despite forming an actomyosin cortex, and area in the medial plane does not increase as much.

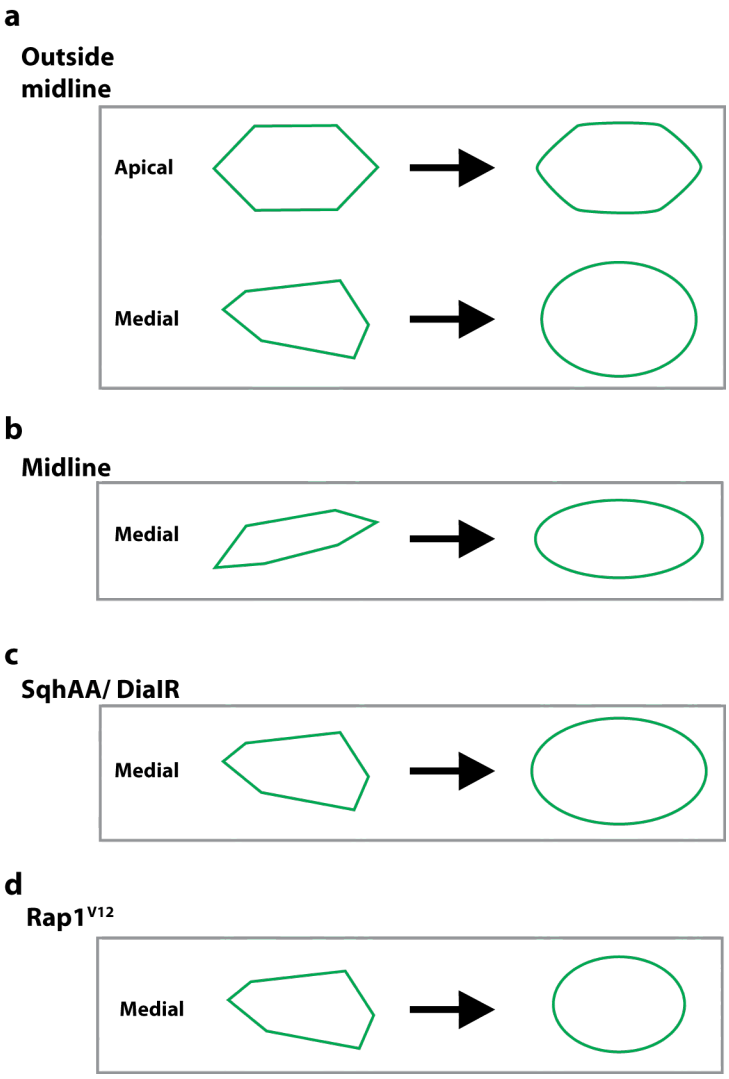

Figure 7.2: Graphical representation of mitotic rounding in the medial plane.

a. Cross-sectional view of a WT OML cell from NEB to late metaphase. Cell shape at the apical plane is similar, while in the medial plane cells become significantly rounder and larger.

b. Cross-sectional view of a WT ML cell from NEB to late metaphase. Cells are significantly elongated compared to WT OML cells, due to lateral crowding. Mitotic rounding is not able to overcome the crowding forces.

c. Cross-sectional view of SqhAA or DiaIR OML cells from NEB to late metaphase. Cells round up significantly during mitosis, but are larger and slightly less rounded than WT.

d. Cross-sectional view of Rap1V12 cells from NEB to late metaphase. Cells round up significantly during mitosis, but the increase in area is reduced.

The last component of mitotic rounding is an increase in cell volume (Son et al. 2015; Zlotek-Zlotkiewicz et al. 2015). Increase in cell volume has not been measured in mitotic cells *in vivo*. One experiment to visualise this would be a concurrent depletion of the actin cortex and the prevention of basal de-adhesion – changes in cell shape would then be likely due to an increase in cell volume. The upregulation of the Na+/H+ antiporter at mitosis (Putney & Barber 2003) is thought to increase cell volume and intracellular osmotic pressure (Stewart et al. 2011a; Son et al. 2015). However, the targetting of Nhe2 (*Drosophila* Na+/ H+ antiporter) by RNAi in this tissue had no effect on medial plane area (data not shown). This experiment needs to be replicated, and the efficacy of the RNAi has to be verified by immunostaining, or mutants for Nhe2 could be used. The use of mutants may not work, however, as the Na/H antiporter has been suggested to be a requirement for the G2/ M transition in human cells (Putney & Barber 2003; Stewart et al. 2011a).

There was an apparent conservation of elongation in mitosis, as indicated by the strong negative correlation between the change in ellipticity and ellipticity at NEB. This suggests that elongated cells have an intrinsic ability to round more than less elongated cells, such that the range of ellipticity at metaphase is much smaller. One explanation for this might be that cortical tension has a resultant force at regions of curvature that acts towards the inside of the cell (Stewart et al. 2011b; Salbreux et al. 2012). The more elongated cells are, the higher the curvature at cell poles along their lengths. At the same time, the increase in hydrostatic pressure due to the increase in cell volume and movement of cell mass towards the apical surface are likely to be unevenly distributed in narrow cells. An increase in hydrostatic pressure is more likely to be dissipated along the cell length, and higher across the cell width, driving the expansion of narrow cells.

There was a similar negative correlation between change in area and area at NEB for cells, such that area at mitosis appeared to converge on a narrower range of values. Mathematically, a decrease in ellipticity described above would lead to a similar passive increase in area, if cell perimeter remains constant. Alternatively, it has been suggested that cell volume at mitosis might be similar for cells of the same tissue (Conlon & Raff 2003; Mitchison 2003; Lloyd 2013; Sung et al. 2013). During

mitosis, when cells adopt a similar hemispherical morphology, cell areas would appear similar if cell height is constant. It would be important to therefore measure cell height during mitosis, to see if there is any conservation of mitotic volume in these cells.

In conclusion, mitotic rounding is a redundant process that gives mitotic cells their characteristic spherical shape, just like in single cells in culture, despite differences in the cell dimensions that are remodelled. Importantly, the reorganisation of actomyosin and basal de-adhesion affect mitotic rounding in the *Drosophila* notum and in single cells, but their effects on cell geometry are modulated by tissue mechanics. Surprisingly, basal de-adhesion and a contractile actomyosin cortex are dispensable for generating sufficient space for spindle morphogenesis in the *Drosophila* notum. This implies that the osmotic pressure of the mitotic cell alone is able to overcome the confinement forces due to crowding in this tissue. The round morphology in cells without actin also indicates that intracellular osmotic pressure is counteracted at the cell periphery. This suggests that in the absence of a contractile cortex, the surface tension due to the plasma membrane and lateral cell-cell adhesions might act against intracellular osmotic pressure. Understanding cell volume changes in the tissue would be an important next step towards explaining the changes in cell geometry during mitosis.

7.2 Pulling forces on astral microtubules are involved in positioning the spindle during mitosis

7.2.1 Dynamics of spindle positioning

The position of the spindle at the onset of anaphase has been the subject of many studies, as this has important consequences for daughter cell size, cell fate, and tissue organization. However, the dynamics of the spindle as it moves towards its anaphase positioning mitosis is not often not emphasised, despite it having a clear impact on the position of the spindle by anaphase (Corrigan et al. 2015).

In Chapter 4, I studied the dynamics of spindle positioning during mitosis and further breakdown the movements of spindles into their rotation and translation, using the movement of spindle poles as a proxy for both types of movement. This

revealed that spindles position dynamically during mitosis, and are not very persistent in their movement (Fig 7.3a, b). This is consistent with the hypothesis that spindles constantly survey their environment and react to changes at the cortex, as has been previously proposed (O'Connell & Wang 2000; Minc et al. 2011; Fernandez et al. 2011; Fink et al. 2011).

Spindle oscillations have been shown to be regulated by cortical pulling forces (Pecreaux et al. 2006; Kiyomitsu & Cheeseman 2012), and consistent with this, perturbation of cortical pulling forces by depletion of Mud or Dlg results in a decrease in the dynamicity of spindle movement (Fig 7.3c). Spindles oscillations have been explained as the result of a dynamic feedback system involving Plk1 at the spindle poles that negatively regulates the localization of cortical pulling forces at alternate spindle poles as they get pulled towards the cortex (Kiyomitsu & Cheeseman 2012). This mechanism is not likely to occur in the *Drosophila* notum, as spindle poles are frequently seen to have stable positions in very close proximity to the cortex and are not consequently repelled.

Another possibility is that cortical interactions with the astral MTs are weak and occasional (e.g. as the result of limited numbers of astral MTs), which prevents processive movement of the spindle poles towards cortical force generators. This is possible, as spindle poles are often very close to or on the cortex. This hints at a high depolymerisation rate or a low polymerization rate at the astral MT plus-ends, perhaps combined with poor cortical interactions. Measuring astral MT lengths and tracking their dynamics with +TIPs such as EB1 would be useful in understanding this behaviour. It would be interesting to test this hypothesis by stabilizing astral MTs to see if this improves the directionality of spindle movements.

7.2.2 Spindle centring

A surprising finding was that spindles are not often centred in endogenous conditions (1.008 ± 0.0709 μm distance from cell centre at late metaphase, or 9.320 ± 0.6519 % of cell length). Spindle centring is assumed in many models for symmetric divisions (Théry et al. 2007; Gibson et al. 2011; Minc et al. 2011; Bosveld et al. 2016), as positioning the spindle in the centre is thought to underlie the

formation of equal-sized daughter cells (Kiyomitsu 2015; Cadart et al. 2014). In fact, I find that many spindles pass through the cell centre, before eventually ending in their acentric position at metaphase. Spindle centring is often thought to be achieved by balancing the forces along astral MTs (Grill & Hyman 2005; Minc & Piel 2012), and in the *Drosophila* notum where spindle poles appear to be in close proximity to the cell cortex, it might be expected that spindles are off-centre in large cells due to a loss in interaction between astral MTs and the cortex. However, I found that spindles were as likely to be off-centre in smaller and larger cells, arguing against this model. Instead, my data suggest that poor centring is due to asymmetries in cortical force generators, as has been suggested in cells which intentionally undergo asymmetric cell division (Grill & Hyman 2005; Pecreaux et al. 2006).

According to Bosveld et al., Mud accumulates at TCJs, concentrating cortical pulling forces on the spindle towards the TCJs. In such a scenario, spindles could be moved off-centre, if astral MTs do not probe the entire cell geometry and both poles are attracted to the nearest TCJs on the same side of the cell. Consistent with this, when I depleted the cells of Mud or Dlg, to remove all cortical force generators, or used mutants with no astral MTs and are therefore 'blind' to cortical forces, I found that spindles were more centred within the cell (Fig 7.3c).

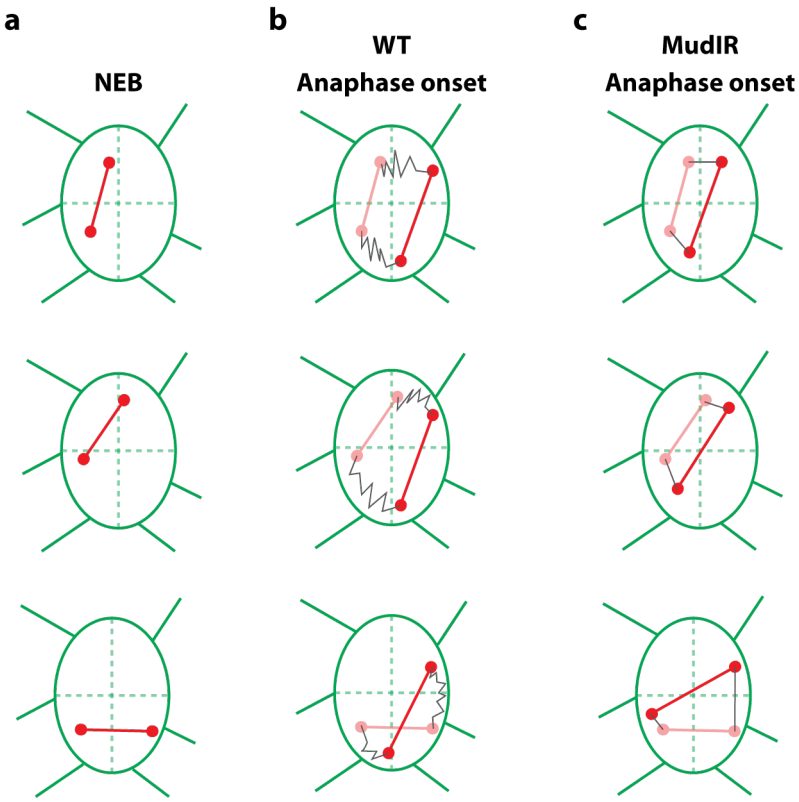

Figure 7.3: Graphical representation of spindle positioning by cortical force generators.
a. Spindle orientation at NEB close to long axis (first row), between the long and short axes (second row), or close to the short axis (third row).
b. Corresponding median spindle orientations for WT spindles at anaphase onset. On average, spindles remain or rotate close to the long axis, but do not centre relative to the cell geometry. Spindle movement is also noisy (grey lines represent spindle pole path).
c. Corresponding median spindle orientation for MudIR spindles at anaphase onset. Spindles remain close to NEB positions at anaphase onset. However, spindles are centred relative to cell geometry, and spindle movement is less noisy.

How does a spindle with no forces along its astral MTs centre so well? One possibility could be other Mud-independent pathways that allow cortex-spindle interaction. However, this theory is unlikely since spindles are centred even in mutant cells with no astral MTs, suggesting that the central positioning of the spindle might actually be linked to a pre-positioning of the centrosomes and/ or DNA. This is the case in the large cells of early amphibian and zebrafish embryonic divisions, where spindle positioning occurs during interphase and prophase at a time when MTs span the entire length of the cell, and are involved in nuclear positioning (Wühr et al. 2009; Manneville & Etienne-Manneville 2006). The nucleus is usually positioning close to the centre of cell mass by interphase MTs, which connect to the perinuclear MTOC. If this were the case, the apparent movement of the spindle towards the centre in cells without Mud or Dlg might in reality reflect the changes in cell geometry that shift the entire cell mass, including the space previously occupied by the nucleus towards the cell centre.

7.2.3 Spindle rotation to the cell long axis

Spindle rotation, despite the noise, often leads to a significant displacement in cells in the notum. Without Mud or Dlg, spindle rotation in terms of its displacement from NEB to anaphase onset, is significantly reduced. This is consistent with a recent finding that spindle poles in these cells are pulled towards the cortex, in a Mud- and Dlg-dependent manner (Bosveld et al. 2016). In this study, cells with high anisotropy were found to be more likely to divide according to the cell shape, which was dependent on these pulling forces from the cortex. I confirm this finding by analysing spindle orientation in cases of incomplete mitotic rounding, where cells retain a clear long axis during mitosis. Additionally, I find that spindle orientation at NEB is random, and that spindles at the short and intermediate cell axes at NEB rotate in a directed manner towards the long cell axis at anaphase onset. However, spindles that aligned along the long cell axis at NEB did not consistently remain there, suggesting that these spindles remain dynamic.

The fact that spindle orientations were also random at NEB in the presence and the absence of Mud indicates that spindle orientation at NEB is not regulated. This is unexpected because Mud was observed at the cortex in the notum from

prophase, which would make it a good candidate for pre-positioning the spindle. However, Mud has been shown to be regulated by mitotic kinases (Radulescu & Cleveland 2010; Kotak et al. 2013), which might render it inactive before NEB. Mud is required instead for spindle orientation after NEB. Without Mud, spindle rotation was severely impaired and spindles remained within 34° of their NEB position at anaphase onset. Despite this, spindles that were along the short axis at NEB had slightly higher displacements than spindles at the long or intermediate axes. Close inspection suggests that as spindles elongate along this axis, they deflect against the cell cortex and get displaced towards the intermediate axis. Current estimates for spindle rigidity are limited to studies in meiotic spindles in *X. laevis*, and place spindle rigidity at ~ 3 x 10^{-3} Pa (Itabashi et al. 2009), which is at least 3 orders of magnitude larger than the rigidity of a single short polymerizing astral MTs (Dumont & Mitchison 2009), but much lower than that of the cortex which is estimated to be from 0.1-1 x 10^{3} Pa (Salbreux et al. 2012). This means that the spindle body is stiffer than astral MTs, and suggests that the elongating spindle can in theory push off at an angle without buckling against the much stiffer cortex. Experimental studies into the rigidity of mitotic spindles, and modulating the spindle length through MT stabilization or destabilization would help to test this hypothesis.

7.3 Tissue mechanics influence spindle positioning relative to cell shape

According to the model proposed by Bosveld et al to explain spindle orientation to the cell long axis in the notum, spindle orientation to the long axis is more likely for elongated cells, as their TCJs that localise Mud are closer together along the cell poles (Bosveld et al. 2016). However, I find that ML cells, which are more elongated than OML cells on average, are no better at aligning to the long axis than OML cells.

Spindle rotation in ML cells was similar to OML cells in terms of average displacement and dynamicity, but rotation from the short and intermediate cell axes to the long cell axis in ML cells was specifically impaired (Fig 7.4a, b). Tissue tension has been suggested to regulate spindle orientation, either directly by polarizing the cell cortex (Fink et al. 2011), or indirectly by causing cell shapes to be elongated in the direction of stretch (Mao et al. 2011; Campinho et al. 2013) and

generally promoting spindle orientation to the long axis (Wyatt et al. 2015). In the *Drosophila* notum, laser ablations of adherens junctions of ML cells revealed that they are under less tension than OML cells due to cell crowding (Marinari et al. 2012). I find that ML cells are less likely to orient their spindles to the long axis than OML cells, despite being more elongated, supporting a role for tissue tension in general facilitating orientation to the long axis. Tissue tension might support long axis divisions by somehow reinforcing the cortical cues at the cell long axis (Fig 7.5a), possibly by polarising the cell cortex as has been suggested in single cells (Théry et al. 2007; Fink et al. 2011; Machicoane et al. 2014). Live-imaging of Mud along the cortex in the ML comparing this to OML cells would be required to check if tissue mechanics affects the localisation of cortical force generators.

The decrease in spindles orienting to the long axis has implications for homeostatic epithelial packing (Patel et al. 2009; Gibson et al. 2011; Farhadifar et al. 2007). However, in the notum at this stage of development cells also delaminate (Marinari et al. 2012) and junction exchanges (Curran 2015) are frequent. The combined efforts of these morphological processes might provide robust mechanisms for achieving homeostatic packing.

7.4 Myosin activity promotes directed spindle rotation to the cell long axis

Finding that lower tissue tension affects spindle orientation, prompted the testing of the requirement for myosin activity. Myosin activity in the tissue is commonly regarded as the driving force for the generation of tissue tension, through its ability to cause actin filaments to contract towards each other, generating tension along surfaces where actin filaments are bound.

Consistent with a role for myosin-mediated tissue tension in spindle orientation, perturbing myosin activity in the tissue by expressing SqhAA recapitulated the spindle orientation phenotype in ML cells, in OML cells (Fig 7.4c). However, this was also accompanied by a decrease in the persistence of spindle rotation, suggesting that myosin activity has intracellular effects on mitosis besides affecting extracellular tension. On the other hand, an increase in myosin activity by

expressing SqhEE was able to improve persistent spindle rotation and spindle orientation to the long axis in both OML and ML cells (Fig 7.4d). This suggests that myosin activity does indeed play a role in regulating spindle dynamics and rotation towards the cell long axis.

To further distinguish between the effects of cell-intrinsic and extrinsic myosin, I have generated flies to enable the clonal analysis of myosin activity in the notum, using the hsFLP/ FRT system in *Drosophila* (Golic & Lindquist 1989) to stochastically express Zip (*Drosophila* myosin heavy chain) RNAi. If myosin-mediated tissue tension is required for spindle orientation to the long axis, I will observe that spindles in WT cells surrounded by ZipIR clones will fail to orient to the long axis. Meanwhile if intracellular myosin activity is required for spindle orientation, I will observe that ZipIR clones surrounded by WT cells will have poor persistent spindle rotation as well as impaired spindle orientation to the long axis.

7.4.1.1 Potential sources of the effects of intracellular myosin on spindle rotation

A change in spindle dynamics might be an indication of a change in the localization of cortical pulling forces, or a change in the dynamics of astral MTs interacting with the cortex. Because the average displacement of spindles was unchanged from WT in SqhAA and SqhEE cells, it seems unlikely that there is a change in total levels of cortical pulling forces. However, the dynamic localization of these factors might be affected by myosin activity (Fig 7.5b). Live-imaging of Mud in these conditions would allow us to distinguish this.

Besides influencing the localisation of cortical force generators, actomyosin cortical flows might promote centrosome movement towards the cell poles (Fig 7.5b), which are disrupted or disorganised upon expression of SqhAA. Cortical flows have been found to be involved in centrosome separation at prophase and correlate with the movement of spindle poles after NEB (Rosenblatt et al. 2004; De Simone et al. 2016). Indeed, I find that in SqhEE cells, centrosomes are at the short axis at NEB, suggesting that the cortex is engaging the centrosome in these conditions.

The actomyosin cortex interacts with astral MTs through actin-MT interactors such as APC2 during centrosome separation and have been shown to play a role in spindle orientation (McCartney et al. 2001; Cao et al. 2010; Hebert et al. 2012). Cortex-spindle pole interaction could therefore promote the movement of spindles towards the cell poles by if cortical flows are towards the cell poles, working in parallel with Mud-dependent cortical cues. FRAP experiments to elucidate if there is a cortical flow of actomyosin towards the cell poles would help to support this hypothesis. Alternatively, perturbations of the cortical actin through the targeting of actin-membrane linkers such as Moesin might recapitulate the loss of persistent spindle rotation seen in SqhAA cells.

Alternatively, myosin activity might be required at the centrosome, to promote processive spindle rotation through centrosome-cortex interactions. ROK has been found on centrosomes, although it has only been shown to be required for centrosome positioning in cells outside of mitosis (Chevrier et al. 2002; Pitaval et al. 2010). One key downstream effect of ROK activity is the phosphorylation and activation of Myosin II (Somlyo & Somlyo 2000), which opens up the possibility that during mitosis, ROK activation by Ect2 might lead to a centrosome-specific role for myosin.

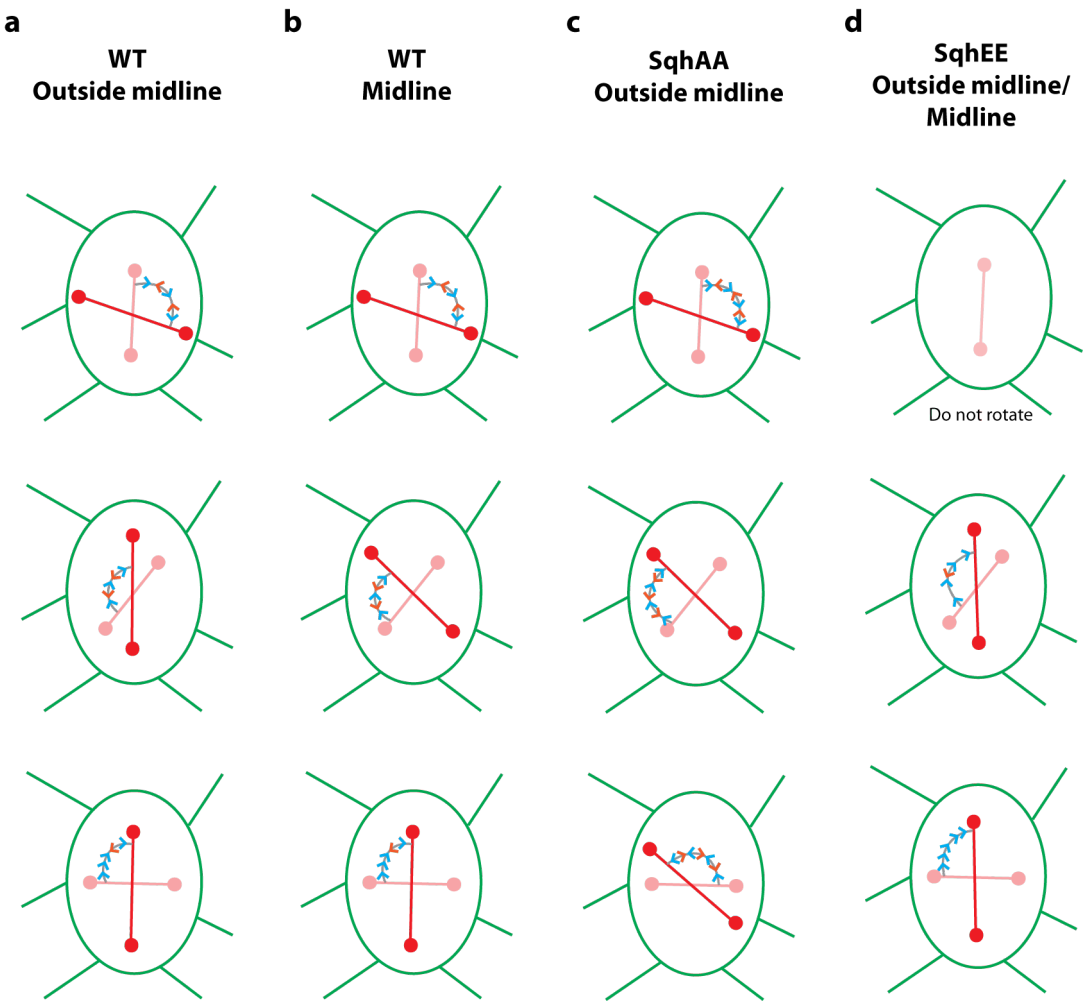

Figure 7.4: Graphical representation of the effects of spindle rotation.

Illustrated median angles at NEB and anaphase onset for spindles with a displacement of >34°. Pink baton represents spindle and orientation at NEB; red baton represents spindle and orientation at anaphase onset. Blue arrows and orange arrows indicate rotation towards and away from anaphase position, respectively. First row depicts spindles at NEB that are close to the cell long axis; second row depicts spindles between the long and short axis; third row depicts spindles close to the short axis.

a. Median spindle orientations for WT OML cells. Spindles forming at the long axis at NEB (first row) were likely to rotate to the short axis at anaphase onset; spindles forming at the intermediate (second row) or short axis (third row) were likely to rotate to the long axis at anaphase onset.

b. Median spindle orientations for WT ML cells. Spindles behaved similarly to WT OML cells but spindles forming at the intermediate axis (second row) were not good at finding the cell long axis.

c. Median spindle orientations for SqhAA OML cells. Spindle rotation was noisier that in WT cells, and spindle rotations were not towards the cell long axis.

d. Median spindle orientations for SqhEE OML and ML cells. Spindle rotation was more persistent than in WT cells, and spindle rotations were almost exclusively from the short or intermediate axes to the cell long axis.

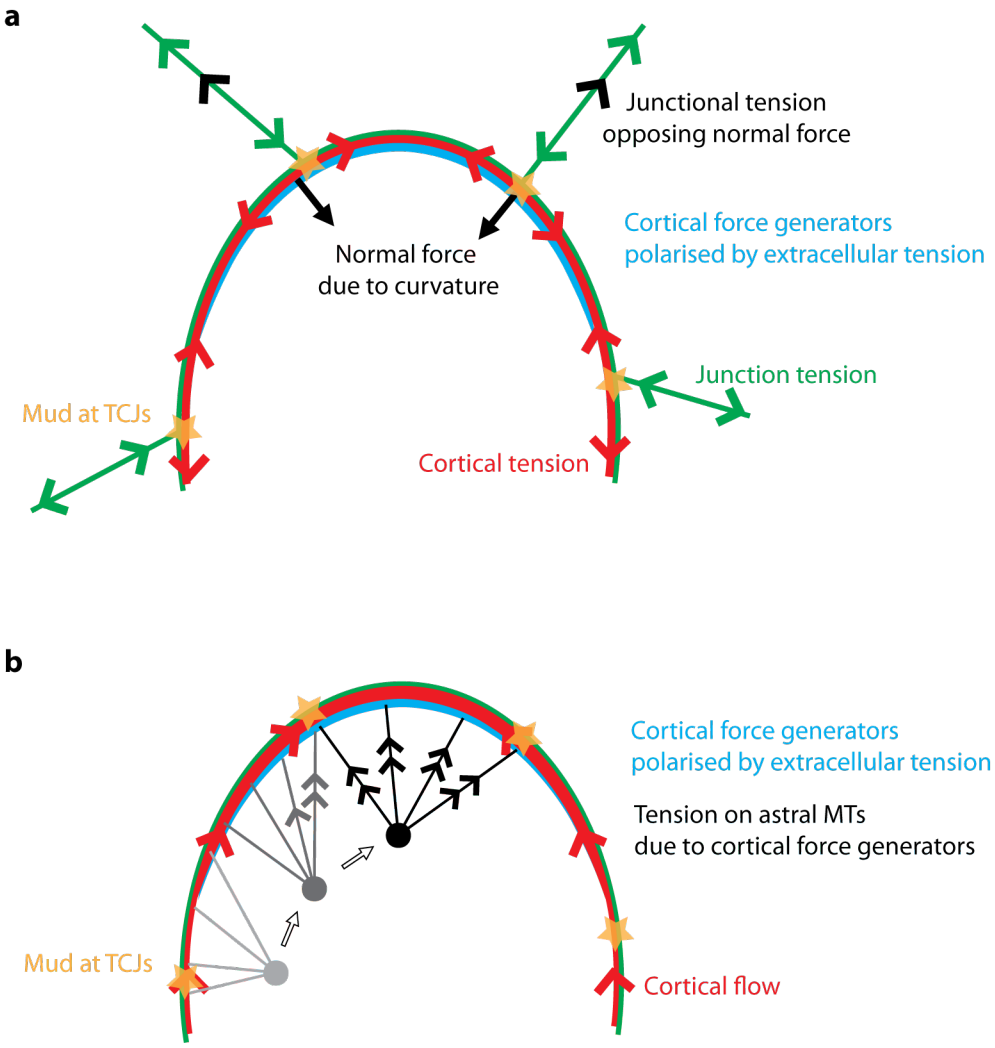

Figure 7.5: Model for spindle orientation in response to extracellular and intracellular tension.

a. Model for how mitotic rounding generates a tension anisotropy around the cortex to promote polarisation of the cortical force generators. As elongated cells build an actomyosin cortex, cortical tension increases. Cortical tension results in an inward force (normal force) at cell poles due to the curvature, and neighbouring junction tension increases in response to this normal force. The asymmetry in extracellular tension polarises the actomyosin cortex and/ or cortical force generators along the cell long axis.

b. Model for how intracellular myosin might facilitate processive spindle rotation towards the cell long axis. Spindle pole capture after NEB is facilitated by MT-cortex interactors, Mud at nearby TCJs, and possible actomyosin interactions between the centrosome and cortex. Cortical flows towards cell poles due to asymmetry in cell cortex due to extracellular tension bring astral MTs passively toward cell poles. Cortical force generators and/ or polarised actomyosin cortex stabilise and pull on astral MTs as they near cell poles.

7.5 Conclusion and future perspectives

In conclusion, I found that mitotic rounding occurs by similar mechanisms as in single cells, but that tissue-level mechanical constraints such as apical and lateral adhesions as well as cell crowding play a role in the degree of mitotic rounding in an epithelium. In cells where mitotic rounding is incomplete, spindle orientation at anaphase onset was towards the long axis, which has been previously reported (Bosveld et al. 2016). The model for spindle orientation to the long axis by Bosveld et al assumes spindle centring and rotation about the centre. However, I found that spindles are in fact pulled off-centre by canonical pulling forces on the spindle. Spindle off-centring has significant consequences for the model, since both poles would now be able to be within the same half of the cell, and potentially both experiencing cortical pulling forces from the same region of the cell cortex. The predictive model in Bosveld et al has a 30° error when compared to the experimental data, and it would be interesting to incorporate spindle off-centring into a theoretical model to see if this recapitulates the experimental data better.

Additionally, I found that spindle orientations at NEB are random, which means spindles far from the long axis must rotate towards it in time. Spindle rotations to the long axis were mediated by Mud, and were affected by cell crowding and myosin activity. Here, I propose a model for how extracellular tension and intracellular actomyosin forces together may lead to a polarization of cortical force generators, as well as promote the processive rotation of spindles towards the long axis. Importantly, the model proposed can act in parallel to the proposed TCJ model by Bosveld et al, to achieve even better spindle alignment along the long axis. Future experiments to test the model proposed in this thesis include differentiating between the role of intracellular and extracellular myosin, and the effect of cell crowding and myosin activity on Mud localisation.

Bibliography

Akhmanova, A. et al., 2010. Microtubule +TIPs at a glance. *Journal of cell science*, 123(Pt 20), pp.3415–9.

Andersen, S.S.., 2000. Spindle assembly and the art of regulating microtubule dynamics by MAPs and Stathmin/Op18. *Trends in Cell Biology*, 10(7), pp.261–267.

Andrianantoandro, E. & Pollard, T.D., 2006. Mechanism of actin filament turnover by severing and nucleation at different concentrations of ADF/cofilin. *Molecular cell*, 24(1), pp.13–23.

Baena-López, L.A., Baonza, A. & García-Bellido, A., 2005. The orientation of cell divisions determines the shape of Drosophila organs. *Current biology : CB*, 15(18), pp.1640–4.

Bartles, J.R., 2000. Parallel actin bundles and their multiple actin-bundling proteins. *Current opinion in cell biology*, 12(1), pp.72–8.

Basto, R. et al., 2006. Flies without Centrioles. *Cell*, 125(7), pp.1375–1386.

Baum, B. & Georgiou, M., 2011. Dynamics of adherens junctions in epithelial establishment, maintenance, and remodeling. *The Journal of cell biology*, 192(6), pp.907–17.

Bellaïche, Y. et al., 2001. The Partner of Inscuteable/Discs-Large Complex Is Required to Establish Planar Polarity during Asymmetric Cell Division in Drosophila. *Cell*, 106(3), pp.355–366.

Bergstralh, D.T. et al., 2016. Pins is not required for spindle orientation in the Drosophila wing disc. *Development (Cambridge, England)*, 143(14), pp.2573–81.

Bergstralh, D.T., Lovegrove, H.E. & St Johnston, D., 2013. Discs large links spindle orientation to apical-basal polarity in Drosophila epithelia. *Current biology : CB*, 23(17), pp.1707–12.

Bergstralh, D.T., Lovegrove, H.E. & St Johnston, D., 2015. Lateral adhesion drives reintegration of misplaced cells into epithelial monolayers. *Nature Cell Biology*, advance on.

Bertet, C., Sulak, L. & Lecuit, T., 2004. Myosin-dependent junction remodelling controls planar cell intercalation and axis elongation. *Nature*, 429(6992), pp.667–671.

Bhabha, G. et al., 2016. How Dynein Moves Along Microtubules. *Trends in Biochemical Sciences*, 41(1), pp.94–105.

Bilder, D. et al., 2000. Cooperative regulation of cell polarity and growth by Drosophila tumor suppressors. *Science (New York, N.Y.)*, 289(5476), pp.113–6.

Blachon, S. et al., 2008. Drosophila asterless and vertebrate Cep152 Are orthologs essential for centriole duplication. *Genetics*, 180(4), pp.2081–94.

Block, J. et al., 2012. *FMNL2 Drives Actin-Based Protrusion and Migration Downstream of Cdc42*,

Bonaccorsi, S., Giansanti, M.G. & Gatti, M., 1998. Spindle self-organization and cytokinesis during male meiosis in asterless mutants of Drosophila melanogaster. *The Journal of cell biology*, 142(3), pp.751–61.

Borghi, N. et al., 2012. E-cadherin is under constitutive actomyosin-generated tension that is increased at cell-cell contacts upon externally applied stretch. *Proceedings of the National Academy of Sciences*, 109(31), pp.12568–12573.

Borisy, G.G., Chausovsky, A. & Bershadsky, A.D., 2000. Cadherin-mediated regulation of microtubule dynamics. *Nature Cell Biology*, 2(11), pp.797–804.

Bornens, M., 2002. Centrosome composition and microtubule anchoring mechanisms. *Current Opinion in Cell Biology*, 14(1), pp.25–34.

Bos, J.L., de Rooij, J. & Reedquist, K.A., 2001. Rap1 signalling: adhering to new models. *Nature Reviews Molecular Cell Biology*, 2(5), pp.369–377.

Bosveld, F. et al., 2016. Epithelial tricellular junctions act as interphase cell shape sensors to orient mitosis. *Nature*.

Bourdages, K.G. & Maddox, A.S., 2013. Dividing in Epithelia: Cells Let Loose during Cytokinesis. *Developmental Cell*, 24(4), pp.336–338.

Bovellan, M. et al., 2014. Cellular control of cortical actin nucleation. *Current Biology*, 24(14), pp.1628–1635.

Bowman, S.K. et al., 2006. The Drosophila NuMA Homolog Mud Regulates Spindle Orientation in Asymmetric Cell Division. *Developmental Cell*, 10(6), pp.731–742.

Le Bras, S. & Le Borgne, R., 2014. Epithelial cell division - multiplying without losing touch. *Journal of cell science*, 127(Pt 24), pp.5127–37.

Brasch, J. et al., 2012. Thinking outside the cell: how cadherins drive adhesion. *Trends in Cell Biology*, 22(6), pp.299–310.

Bray, D. & White, J.G., 1988. Cortical flow in animal cells. *Science (New York, N.Y.)*, 239(4842), pp.883–8.

Buttrick, G.J. et al., 2008. Akt regulates centrosome migration and spindle orientation in the early

Drosophila melanogaster embryo. *The Journal of Cell Biology*, 180(3), pp.537–548.

Cabernard, C., Prehoda, K.E. & Doe, C.Q., 2010. A spindle-independent cleavage furrow positioning pathway. *Nature*, 467(7311), pp.91–4.

Cadart, C. et al., 2014. Exploring the Function of Cell Shape and Size during Mitosis. *Developmental cell*, 29(2), pp.159–169.

Campinho, P. et al., 2013. Tension-oriented cell divisions limit anisotropic tissue tension in epithelial spreading during zebrafish epiboly. *Nature Cell Biology*, advance on.

Cao, J. et al., 2010. *Cortical Actin Dynamics Facilitate Early-Stage Centrosome Separation*,

Carmena, A., Makarova, A. & Speicher, S., 2011. The Rap1-Rgl-Ral signaling network regulates neuroblast cortical polarity and spindle orientation. *The Journal of cell biology*, 195(4), pp.553–62.

Carminati, M. et al., 2016. Concomitant binding of Afadin to LGN and F-actin directs planar spindle orientation. *Nature structural & molecular biology*, advance on.

Carreno, S. et al., 2008. Moesin and its activating kinase Slik are required for cortical stability and microtubule organization in mitotic cells. *The Journal of cell biology*, 180(4), pp.739–46.

Cattin, C.J. et al., 2015. Mechanical control of mitotic progression in single animal cells. *Proceedings of the National Academy of Sciences*, p.201502029.

Chaigne, A. et al., 2013. A soft cortex is essential for asymmetric spindle positioning in mouse oocytes. *Nature cell biology*.

Chan, P.-C. et al., 2014. Adducin-1 is essential for mitotic spindle assembly through its interaction with myosin-X. *The Journal of Cell Biology*, 204(1), pp.19–28.

Chang, L. & Barford, D., 2014. Insights into the anaphase-promoting complex: a molecular machine that regulates mitosis. *Current Opinion in Structural Biology*, 29, pp.1–9.

Cheffings, T.H., Burroughs, N.J. & Balasubramanian, M.K., 2016. Actomyosin Ring Formation and Tension Generation in Eukaryotic Cytokinesis. *Current Biology*, 26(15), pp.R719–R737.

Chevrier, V. et al., 2002. The Rho-associated protein kinase p160ROCK is required for centrosome positioning. *The Journal of Cell Biology*, 157(5), pp.807–817.

Clark, I.E., Jan, L.Y. & Jan, Y.N., 1997. Reciprocal localization of Nod and kinesin fusion proteins indicates microtubule polarity in the Drosophila oocyte, epithelium, neuron and muscle. *Development (Cambridge, England)*, 124(2), pp.461–70.

Clarke, P.R. & Zhang, C., 2008. Spatial and temporal coordination of mitosis by Ran GTPase. *Nature Reviews Molecular Cell Biology*, 9(6), pp.464–477.

Cohen, D. et al., 2004. Mammalian PAR-1 determines epithelial lumen polarity by organizing the microtubule cytoskeleton. *The Journal of Cell Biology*, 164(5), pp.717–727.

Conlon, I. & Raff, M., 2003. Differences in the way a mammalian cell and yeast cells coordinate cell growth and cell-cycle progression. *Journal of Biology*, 2(1), p.7.

Corrigan, A.M. et al., 2015. Modeling of Noisy Spindle Dynamics Reveals Separable Contributions to Achieving Correct Orientation. *Biophysical Journal*, 109(7), pp.1398–1409.

Cramer, L.P. & Mitchison, T.J., 1997. Investigation of the mechanism of retraction of the cell margin and rearward flow of nodules during mitotic cell rounding. *Molecular biology of the cell*, 8(1), pp.109–19.

Curran, S., 2015. The changing role of junctional actomyosin in epithelial cell packing during Drosophila notum development.

Curtis, M., Nikolopoulos, S.N. & Turner, C.E., 2002. Actopaxin is phosphorylated during mitosis and is a substrate for cyclin B1/cdc2 kinase. *The Biochemical journal*, 363(Pt 2), pp.233–42.

Dao, V.T. et al., 2009. Dynamic changes in Rap1 activity are required for cell retraction and spreading during mitosis. *Journal of cell science*, 122(Pt 16), pp.2996–3004.

David, N.B. et al., 2005. Drosophila Ric-8 regulates Galphai cortical localization to promote Galphai-dependent planar orientation of the mitotic spindle during asymmetric cell division. *Nature cell biology*, 7(11), pp.1083–90.

De Simone, A., Nédélec, F. & Gönczy, P., 2016. Dynein Transmits Polarized Actomyosin Cortical Flows to Promote Centrosome Separation. *Cell Reports*.

Delgehyr, N., Sillibourne, J. & Bornens, M., 2005. Microtubule nucleation and anchoring at the centrosome are independent processes linked by ninein function. *Journal of cell science*, 118(Pt 8), pp.1565–75.

Desai, A. & Mitchison, T.J., 1997. Microtubule Polymerization Dynamics. *Annual Review of Cell and Developmental Biology*, 13(1), pp.83–117.

Desai, R. et al., 2013. Monomeric α-catenin links cadherin to the actin cytoskeleton. *Nature Cell Biology*, 15(3), pp.261–273.

Dimitracopoulos, A., 2016. The role of mitotic rounding in spindle assembly and positioning.

Dimitracopoulos, A., Lam, M. & Baum, B., 2016. Oriented Division: Using T-Junctions to Determine Direction. *Current Biology*, 26(9), pp.R371–R373.

Dimitrov, A. et al., 2008. Detection of GTP-tubulin conformation in vivo reveals a role for GTP remnants in microtubule rescues. *Science (New York, N.Y.)*, 322(5906), pp.1353–6.

Dogterom, M. et al., 2005. Force generation by dynamic microtubules. *Current Opinion in Cell Biology*, 17(1), pp.67–74.

Dujardin, D.L. & Vallee, R.B., 2002. Dynein at the cortex. *Current Opinion in Cell Biology*, 14(1), pp.44–49.

Dumont, S. & Mitchison, T.J., 2009. Force and length in the mitotic spindle. *Current biology : CB*, 19(17), pp.R749-61.

Farhadifar, R. et al., 2007. The influence of cell mechanics, cell-cell interactions, and proliferation on epithelial packing. *Current biology : CB*, 17(24), pp.2095–104.

Fehon, R.G., McClatchey, A.I. & Bretscher, A., 2010. Organizing the cell cortex: the role of ERM proteins. *Nature Reviews Molecular Cell Biology*, 11(4), pp.276–287.

Fernandez, P. et al., 2011. Mitotic spindle orients perpendicular to the forces imposed by dynamic shear. *PloS one*, 6(12), p.e28965.

Field, C.M. & Lénárt, P., 2011. Bulk Cytoplasmic Actin and Its Functions in Meiosis and Mitosis. *Current Biology*, 21(19), pp.R825–R830.

Fietz, S.A. et al., 2010. OSVZ progenitors of human and ferret neocortex are epithelial-like and expand by integrin signaling. *Nature Neuroscience*, 13(6), pp.690–699.

Fink, J. et al., 2011. External forces control mitotic spindle positioning. *Nature cell biology*, 13(7), pp.771–8.

Fischer-Friedrich, E. et al., 2014. Quantification of surface tension and internal pressure generated by single mitotic cells. *Scientific reports*, 4, p.6213.

Fischer-Friedrich, E. et al., 2016. Rheology of the Active Cell Cortex in Mitosis. *Biophysical Journal*, 111(3), pp.589–600.

Flemming, W., 1882. *Zellsubstanz, kern und zelltheilung*, Leipzig, F. C. W. Vogel.

Fletcher, D.A. & Mullins, R.D., 2010. Cell mechanics and the cytoskeleton. *Nature*, 463(7280), pp.485–492.

Foley, E.A. & Kapoor, T.M., 2013. Microtubule attachment and spindle assembly checkpoint signalling at the kinetochore. *Nature reviews. Molecular cell biology*, 14(1), pp.25–37.

Footer, M.J. et al., 2007. Direct measurement of force generation by actin filament polymerization using an optical trap. *Proceedings of the National Academy of Sciences*, 104(7), pp.2181–2186.

de Forges, H., Bouissou, A. & Perez, F., 2012. Interplay between microtubule dynamics and intracellular organization. *The International Journal of Biochemistry & Cell Biology*, 44(2), pp.266–274.

Fritzsche, M. et al., 2016. Actin kinetics shapes cortical network structure and mechanics. *Science Advances*, 2(4), pp.e1501337–e1501337.

Fyrberg, C. & Fyrberg, E., 1993. A Drosophila homologue of the Schizosaccharomyces pombe act2 gene. *Biochemical genetics*, 31(7–8), pp.329–41.

Garzon-Coral, C., Fantana, H.A. & Howard, J., 2016. A force-generating machinery maintains the spindle at the cell center during mitosis. *Science*, 352(6289), pp.1124–1127.

Giansanti, M.G., Gatti, M. & Bonaccorsi, S., 2001. The role of centrosomes and astral microtubules during asymmetric division of Drosophila neuroblasts. *Development (Cambridge, England)*, 128(7), pp.1137–45.

Gibson, W.T. et al., 2011. Control of the mitotic cleavage plane by local epithelial topology. *Cell*, 144(3), pp.427–38.

Gibson, W.T. & Gibson, M.C., 2009. Cell topology, geometry, and morphogenesis in proliferating epithelia. *Current topics in developmental biology*, 89(null), pp.87–114.

Golic, K.G. & Lindquist, S., 1989. The FLP recombinase of yeast catalyzes site-specific recombination in the drosophila genome. *Cell*, 59(3), pp.499–509.

Goshima, G. et al., 2007. Genes required for mitotic spindle assembly in Drosophila S2 cells. *Science (New York, N.Y.)*, 316(5823), pp.417–21.

Goshima, G. & Kimura, A., 2010. New look inside the spindle: microtubule-dependent microtubule generation within the spindle. *Current Opinion in Cell Biology*, 22(1), pp.44–49.

Goshima, G. & Vale, R.D., 2003. The roles of microtubule-based motor proteins in mitosis. *The Journal of Cell Biology*, 162(6), pp.1003–1016.

Green, R.A., Paluch, E. & Oegema, K., 2012. Cytokinesis in Animal Cells. *Annual Review of Cell and Developmental Biology*, 28(1), pp.29–58.

Grill, S.W. & Hyman, A.A., 2005. Spindle positioning by cortical pulling forces. *Developmental cell*, 8(4), pp.461–5.

Grissom, P.M. et al., 2009. Kinesin-8 from fission yeast: a heterodimeric, plus-end-directed motor that can couple microtubule depolymerization to cargo movement. *Molecular biology of the cell*, 20(3), pp.963–72.

Guillot, C. & Lecuit, T., 2013a. Adhesion Disengagement Uncouples Intrinsic and Extrinsic Forces to Drive Cytokinesis in Epithelial Tissues. *Developmental Cell*, 24(3), pp.227–241.

Guillot, C. & Lecuit, T., 2013b. Mechanics of epithelial tissue homeostasis and morphogenesis. *Science (New York, N.Y.)*, 340(6137), pp.1185–9.

Hall, A., 2012. Rho family GTPases. *Biochemical Society transactions*, 40(6), pp.1378–82.

Hall, A., 1998. Rho GTPases and the actin cytoskeleton. *Science (New York, N.Y.)*, 279(5350), pp.509–14.

Hampoelz, B. et al., 2005. Drosophila Ric-8 is essential for plasma-membrane localization of heterotrimeric G proteins. *Nature Cell Biology*, 7(11), pp.1099–1105.

Hanada, T. et al., 2000. GAKIN, a Novel Kinesin-like Protein Associates with the Human Homologue of the Drosophila Discs Large Tumor Suppressor in T Lymphocytes. *Journal of Biological Chemistry*, 275(37), pp.28774–28784.

Harris, T.J.C., 2012. Adherens junction assembly and function in the Drosophila embryo. *International review of cell and molecular biology*, 293, pp.45–83.

Heald, R. & Khodjakov, A., 2015. Thirty years of search and capture: The complex simplicity of mitotic spindle assembly. *The Journal of Cell Biology*, 211(6), pp.1103–1111.

Hebert, A.M. et al., 2012. Merlin/ERM proteins establish cortical asymmetry and centrosome position. *Genes & development*, 26(24), pp.2709–23.

Heisenberg, C.-P. & Bellaïche, Y., 2013. Forces in tissue morphogenesis and patterning. *Cell*, 153(5), pp.948–62.

Henty-Ridilla, J.L. et al., 2016. Accelerated actin filament polymerization from microtubule plus ends. *Science (New York, N.Y.)*, 352(6288), pp.1004–9.

Herszterg, S. et al., 2013. Interplay between the dividing cell and its neighbors regulates adherens junction formation during cytokinesis in epithelial tissue. *Developmental cell*, 24(3), pp.256–70.

Homma, K. et al., 2001. Motor function and regulation of myosin X. *The Journal of biological*

chemistry, 276(36), pp.34348–54.

Homma, K. & Ikebe, M., 2005. Myosin X is a high duty ratio motor. *The Journal of biological chemistry*, 280(32), pp.29381–91.

Howard, J. & Hyman, A.A., 2007. Microtubule polymerases and depolymerases. *Current Opinion in Cell Biology*, 19(1), pp.31–35.

Hudson, A.M. & Cooley, L., 2002. A subset of dynamic actin rearrangements in Drosophila requires the Arp2/3 complex. *The Journal of cell biology*, 156(4), pp.677–87.

Ingber, D.E., 1997. TENSEGRITY: THE ARCHITECTURAL BASIS OF CELLULAR MECHANOTRANSDUCTION. *Annual Review of Physiology*, 59(1), pp.575–599.

Itabashi, T. et al., 2009. Probing the mechanical architecture of the vertebrate meiotic spindle. *Nature Methods*, 6(2), pp.167–172.

Izumi, Y. et al., 2006. Drosophila Pins-binding protein Mud regulates spindle-polarity coupling and centrosome organization. , 8(6), pp.2–9.

Jayo, A. & Parsons, M., 2010. Fascin: A key regulator of cytoskeletal dynamics. *The International Journal of Biochemistry & Cell Biology*, 42(10), pp.1614–1617.

Jiang, K. & Akhmanova, A., 2011. Microtubule tip-interacting proteins: a view from both ends. *Current Opinion in Cell Biology*, 23(1), pp.94–101.

Jiang, T. et al., 2015. *A Par-1-Par-3-Centrosome Cell Polarity Pathway and Its Tuning for Isotropic Cell Adhesion*,

Johnston, C.A. et al., 2013. Formin-mediated actin polymerization cooperates with Mushroom body defect (Mud)-Dynein during Frizzled-Dishevelled spindle orientation. *Journal of cell science*, 126(Pt 19), pp.4436–44.

Johnston, C.A. et al., 2009. Identification of an Aurora-A/PinsLINKER/Dlg spindle orientation pathway using induced cell polarity in S2 cells. *Cell*, 138(6), pp.1150–63.

Jordan, P. & Karess, R., 1997. Myosin light chain-activating phosphorylation sites are required for oogenesis in Drosophila. *The Journal of cell biology*, 139(7), pp.1805–19.

Kardon, J.R. & Vale, R.D., 2009. Regulators of the cytoplasmic dynein motor. *Nature Reviews Molecular Cell Biology*, 10(12), pp.854–865.

Khodjakov, A. & Rieder, C.L., 1999. The sudden recruitment of gamma-tubulin to the centrosome at the onset of mitosis and its dynamic exchange throughout the cell cycle, do not require

microtubules. *The Journal of cell biology*, 146(3), pp.585–96.

Kim, J.H. et al., 2015. Mechanical Tension Drives Cell Membrane Fusion. *Developmental Cell*, 32(5), pp.561–573.

Kimura, K. & Kimura, A., 2011. A novel mechanism of microtubule length-dependent force to pull centrosomes toward the cell center. *BioArchitecture*, 1(2), pp.74–79.

Kiyomitsu, T., 2015. Mechanisms of daughter cell-size control during cell division. *Trends in cell biology*, 25(5), pp.286–95.

Kiyomitsu, T. & Cheeseman, I.M., 2012. Chromosome- and spindle-pole-derived signals generate an intrinsic code for spindle position and orientation. *Nature cell biology*, 14(3), pp.311–317.

Kiyomitsu, T. & Cheeseman, I.M., 2013. Cortical Dynein and asymmetric membrane elongation coordinately position the spindle in anaphase. *Cell*, 154(2), pp.391–402.

Kollman, J.M. et al., 2011. Microtubule nucleation by γ-tubulin complexes. *Nature Reviews Molecular Cell Biology*, 12(11), pp.709–721.

Kondo, T. & Hayashi, S., 2015. Mechanisms of cell height changes that mediate epithelial invagination. *Development, growth & differentiation*.

Kondo, T. & Hayashi, S., 2013. Mitotic cell rounding accelerates epithelial invagination. *Nature*.

Kosodo, Y. & Huttner, W.B., 2009. Basal process and cell divisions of neural progenitors in the developing brain. *Development, Growth & Differentiation*, 51(3), pp.251–261.

Kotak, S., Busso, C. & Gönczy, P., 2013. NuMA phosphorylation by CDK1 couples mitotic progression with cortical dynein function. *The EMBO journal*, 32(18), pp.2517–29.

Kotak, S. & Gönczy, P., 2013. Mechanisms of spindle positioning: cortical force generators in the limelight. *Current opinion in cell biology*, 16, pp.1–8.

Kovar, D.R. & Pollard, T.D., 2004. Insertional assembly of actin filament barbed ends in association with formins produces piconewton forces. *Proceedings of the National Academy of Sciences*, 101(41), pp.14725–14730.

Krendel, M., Zenke, F.T. & Bokoch, G.M., 2002. Nucleotide exchange factor GEF-H1 mediates cross-talk between microtubules and the actin cytoskeleton. *Nature Cell Biology*, 4(4), pp.294–301.

Kunda, P. et al., 2008. Moesin controls cortical rigidity, cell rounding, and spindle morphogenesis during mitosis. *Current biology : CB*, 18(2), pp.91–101.

Kwon, M. et al., 2015. Direct Microtubule-Binding by Myosin-10 Orients Centrosomes toward Retraction Fibers and Subcortical Actin Clouds. *Developmental Cell*.

Laan, L., Roth, S. & Dogterom, M., 2012. End-on microtubule-dynein interactions and pulling-based positioning of microtubule organizing centers. *Cell Cycle*, 11(20), pp.3750–3757.

Lancaster, O.M. et al., 2013. Mitotic Rounding Alters Cell Geometry to Ensure Efficient Bipolar Spindle Formation. *Developmental Cell*, pp.1–14.

Laprise, P. & Tepass, U., 2011. Novel insights into epithelial polarity proteins in Drosophila. *Trends in cell biology*, 21(7), pp.401–8.

Lazaro-Dieguez, F., Ispolatov, I. & Musch, A., 2015. Cell shape impacts on the positioning of the mitotic spindle with respect to the substratum. *Molecular Biology of the Cell*, 26(7), pp.1286–1295.

Lecuit, T. & Lenne, P.-F., 2007. Cell surface mechanics and the control of cell shape, tissue patterns and morphogenesis. *Nature Reviews Molecular Cell Biology*, 8(8), pp.633–644.

Lecuit, T., Lenne, P.-F. & Munro, E., 2011. Force Generation, Transmission, and Integration during Cell and Tissue Morphogenesis. *Annual Review of Cell and Developmental Biology*, 27(1), pp.157–184.

Lecuit, T. & Yap, A.S., 2015. E-cadherin junctions as active mechanical integrators in tissue dynamics. *Nature Cell Biology*, 17(5), pp.533–539.

LeGoff, L. & Lecuit, T., 2015. Mechanical Forces and Growth in Animal Tissues. *Cold Spring Harbor perspectives in biology*.

LeGoff, L., Rouault, H. & Lecuit, T., 2013. A global pattern of mechanical stress polarizes cell divisions and cell shape in the growing Drosophila wing disc. *Development*, 140(19), pp.4051–4059.

Liu, R. et al., 2010. Formins in development: orchestrating body plan origami. *Biochimica et biophysica acta*, 1803(2), pp.207–25.

Lloyd, A.C., 2013. The Regulation of Cell Size. *Cell*, 154(6), pp.1194–1205.

Logarinho, E. et al., 2004. Different spindle checkpoint proteins monitor microtubule attachment and tension at kinetochores in Drosophila cells. *Journal of cell science*, 117(Pt 9), pp.1757–71.

Lombillo, V.A., Stewart, R.J. & Richard McIntosh, J., 1995. Minus-end-directed motion of kinesin–coated microspheres driven by microtubule depolymerization. *Nature*, 373(6510), pp.161–164.

Lu, M.S. & Johnston, C.A., 2013. Molecular pathways regulating mitotic spindle orientation in animal cells. *Development (Cambridge, England)*, 140(9), pp.1843–56.

Lu, M.S. & Prehoda, K.E., 2013. A NudE/14-3-3 Pathway Coordinates Dynein and the Kinesin Khc73 to Position the Mitotic Spindle. *Developmental Cell*, 26(4), pp.369–380.

Lüders, J., Patel, U.K. & Stearns, T., 2006. GCP-WD is a γ-tubulin targeting factor required for centrosomal and chromatin-mediated microtubule nucleation. *Nature Cell Biology*, 8(2), pp.137–147.

Lüders, J. & Stearns, T., 2007. Microtubule-organizing centres: a re-evaluation. *Nature Reviews Molecular Cell Biology*, 8(2), pp.161–167.

Luxenburg, C. et al., 2011. Developmental roles for Srf, cortical cytoskeleton and cell shape in epidermal spindle orientation. *Nature cell biology*, 13(3), pp.203–14.

Machicoane, M. et al., 2014. SLK-dependent activation of ERMs controls LGN-NuMA localization and spindle orientation. *Journal of Cell Biology*.

Maddox, A.S. & Burridge, K., 2003. RhoA is required for cortical retraction and rigidity during mitotic cell rounding. *The Journal of cell biology*, 160(2), pp.255–65.

Mahoney, N.M. et al., 2006. *Making Microtubules and Mitotic Spindles in Cells without Functional Centrosomes*,

Mallik, R. et al., 2013. Teamwork in microtubule motors. *Trends in Cell Biology*, 23(11), pp.575–582.

Manneville, J.-B. & Etienne-Manneville, S., 2006. Positioning centrosomes and spindle poles: looking at the periphery to find the centre. *Biology of the Cell*, 98(9), pp.557–565.

Mao, Y. et al., 2013. Differential proliferation rates generate patterns of mechanical tension that orient tissue growth. *The EMBO Journal*, 32(21), pp.2790–2803.

Mao, Y. et al., 2011. Planar polarization of the atypical myosin Dachs orients cell divisions in Drosophila. *Genes & development*, 25(2), pp.131–6.

Mao, Y. & Baum, B., 2015. Tug of war - the influence of opposing physical forces on epithelial cell morphology. *Developmental biology*.

Maresca, T.J. et al., 2009. Spindle Assembly in the Absence of a RanGTP Gradient Requires Localized CPC Activity. *Current Biology*, 19(14), pp.1210–1215.

Marinari, E. et al., 2012. Live-cell delamination counterbalances epithelial growth to limit tissue overcrowding. *Nature*, 484(7395), pp.542–5.

Matsumura, F., 2005. Regulation of myosin II during cytokinesis in higher eukaryotes. *Trends in Cell Biology*, 15(7), pp.371–377.

Matthews, H.K. et al., 2012. Changes in Ect2 Localization Couple Actomyosin-Dependent Cell Shape Changes to Mitotic Progression. *Developmental Cell*, 23(2), pp.371–383.

Matthews, H.K. & Baum, B., 2012. The metastatic cancer cell cortex: an adaptation to enhance robust cell division in novel environments? *BioEssays : news and reviews in molecular, cellular and developmental biology*, 34(12), pp.1017–20.

McCartney, B.M. et al., 2001. Drosophila APC2 and Armadillo participate in tethering mitotic spindles to cortical actin. *Nature Cell Biology*, 3(10), pp.933–938.

McCartney, B.M. & Fehon, R.G., 1996. Distinct cellular and subcellular patterns of expression imply distinct functions for the Drosophila homologues of moesin and the neurofibromatosis 2 tumor suppressor, merlin. *The Journal of Cell Biology*, 133(4), pp.843–852.

McKenney, R.J. et al., 2014. Activation of cytoplasmic dynein motility by dynactin-cargo adapter complexes. *Science (New York, N.Y.)*, 345(6194), pp.337–41.

Meng, W. et al., 2008. Anchorage of Microtubule Minus Ends to Adherens Junctions Regulates Epithelial Cell-Cell Contacts. *Cell*, 135(5), pp.948–959.

Meyer, E.J., Ikmi, A. & Gibson, M.C., 2011. Interkinetic nuclear migration is a broadly conserved feature of cell division in pseudostratified epithelia. *Current biology : CB*, 21(6), pp.485–91.

Minc, N., Burgess, D. & Chang, F., 2011. Influence of cell geometry on division-plane positioning. *Cell*, 144(3), pp.414–26.

Minc, N. & Piel, M., 2012. Predicting division plane position and orientation. *Trends in cell biology*, 22(4), pp.193–200.

Mitchison, J.M., 2003. Growth During the Cell Cycle. *International Review of Cytology*, 226, pp.165–258.

Mitsushima, M. et al., 2010. Revolving movement of a dynamic cluster of actin filaments during mitosis. *The Journal of Cell Biology*, 191(3), pp.453–462.

Mogensen, M.M. et al., 2000. Microtubule minus-end anchorage at centrosomal and non-centrosomal sites: the role of ninein. *Journal of cell science*, (17), pp.3013–23.

Mogilner, A. & Oster, G., 2003. Force Generation by Actin Polymerization II: The Elastic Ratchet and Tethered Filaments. *Biophysical Journal*, 84(3), pp.1591–1605.

Moon, W. & Matsuzaki, F., 2013. *Aurora A kinase negatively regulates Rho-kinase by phosphorylation in vivo*,

Morais-de-Sá, E. & Sunkel, C., 2013. Adherens junctions determine the apical position of the midbody during follicular epithelial cell division. *EMBO reports*, 14(8), pp.696–703.

Morin, X. & Bellaïche, Y., 2011. Mitotic spindle orientation in asymmetric and symmetric cell divisions during animal development. *Developmental cell*, 21(1), pp.102–19.

Moss, D.K. et al., 2007. Ninein is released from the centrosome and moves bi-directionally along microtubules. *Journal of cell science*, 120(Pt 17), pp.3064–74.

Müsch, A., 2004. Microtubule Organization and Function in Epithelial Cells. *Traffic*, 5(1), pp.1–9.

Nakajima, Y. et al., 2013. Epithelial junctions maintain tissue architecture by directing planar spindle orientation. *Nature*, 500(7462), pp.359–62.

Nakajima, Y.-I. et al., 2011. Nonautonomous apoptosis is triggered by local cell cycle progression during epithelial replacement in Drosophila. *Molecular and cellular biology*, 31(12), pp.2499–512.

Niethammer, P. et al., 2007. Discrete States of a Protein Interaction Network Govern Interphase and Mitotic Microtubule Dynamics T. Misteli, ed. *PLoS Biology*, 5(2), p.e29.

Nipper, R.W. et al., 2007. Galphai generates multiple Pins activation states to link cortical polarity and spindle orientation in Drosophila neuroblasts. *Proceedings of the National Academy of Sciences of the United States of America*, 104(36), pp.14306–11.

Nogales, E. & Wang, H.-W., 2006. Structural mechanisms underlying nucleotide-dependent self-assembly of tubulin and its relatives. *Current Opinion in Structural Biology*, 16(2), pp.221–229.

O'Connell, C.B. & Wang, Y. -l., 2000. Mammalian Spindle Orientation and Position Respond to Changes in Cell Shape in a Dynein-dependent Fashion. *Molecular Biology of the Cell*, 11(5), pp.1765–1774.

O'Keefe, D.D. et al., 2012. Discontinuities in Rap1 activity determine epithelial cell morphology within the developing wing of Drosophila. *Developmental biology*, 369(2), pp.223–34.

Ohba, Y. et al., 2001. Requirement for C3G-dependent Rap1 activation for cell adhesion and embryogenesis. *The EMBO journal*, 20(13), pp.3333–41.

Ou, G. et al., 2010. Polarized Myosin Produces Unequal-Size Daughters During Asymmetric Cell Division. *Science*, 330(6004), pp.677–680.

Pacquelet, A. et al., 2015. PAR-4 and anillin regulate myosin to coordinate spindle and furrow position during asymmetric division. *The Journal of cell biology*, 210(7), pp.1085–99.

Padash-Barmchi, M. et al., 2013. Gliotactin and Discs large are co-regulated to maintain epithelial integrity. *Journal of cell science*, 126(Pt 5), pp.1134–43.

Panousopoulou, E. & Green, J.B.A., 2014. Spindle orientation processes in epithelial growth and organisation. *Seminars in Cell & Developmental Biology*, 34, pp.124–132.

Patel, A.B. et al., 2009. Modeling and inferring cleavage patterns in proliferating epithelia. *PLoS computational biology*, 5(6), p.e1000412.

Paul, A.S. & Pollard, T.D., 2008. The role of the FH1 domain and profilin in formin-mediated actin-filament elongation and nucleation. *Current biology : CB*, 18(1), pp.9–19.

Pawson, C., Eaton, B.A. & Davis, G.W., 2008. Formin-Dependent Synaptic Growth: Evidence That Dlar Signals via Diaphanous to Modulate Synaptic Actin and Dynamic Pioneer Microtubules. *Journal of Neuroscience*, 28(44), pp.11111–11123.

Pecreaux, J. et al., 2006. Spindle Oscillations during Asymmetric Cell Division Require a Threshold Number of Active Cortical Force Generators. *Current Biology*, 16(21), pp.2111–2122.

Piehl, M. & Cassimeris, L., 2003. Organization and Dynamics of Growing Microtubule Plus Ends during Early Mitosis. *Molecular Biology of the Cell*, 14(3), pp.916–925.

Piel, M. et al., 2000. The respective contributions of the mother and daughter centrioles to centrosome activity and behavior in vertebrate cells. *The Journal of cell biology*, 149(2), pp.317–30.

di Pietro, F., Echard, A. & Morin, X., 2016. Regulation of mitotic spindle orientation: an integrated view. *EMBO reports*, 17(8), pp.1106–1130.

Pitaval, A. et al., 2010. Cell shape and contractility regulate ciliogenesis in cell cycle–arrested cells. *The Journal of Cell Biology*, 191(2), pp.303–312.

Plak, K. et al., 2014. Rap1-dependent pathways coordinate cytokinesis in Dictyostelium. *Molecular Biology of the Cell*, 25(25), pp.4195–4204.

Pollard, T.D. et al., 2009. Actin, a central player in cell shape and movement. *Science (New York, N.Y.)*, 326(5957), pp.1208–12.

Pollard, T.D., 2007. Regulation of Actin Filament Assembly by Arp2/3 Complex and Formins. *Annual Review of Biophysics and Biomolecular Structure*, 36(1), pp.451–477.

Pollard, T.D. & Mooseker, M.S., 1981. Direct measurement of actin polymerization rate constants by

electron microscopy of actin filaments nucleated by isolated microvillus cores. *The Journal of Cell Biology*, 88(3), pp.654–659.

Poulton, J.S., Cuningham, J.C. & Peifer, M., 2014. Acentrosomal Drosophila Epithelial Cells Exhibit Abnormal Cell Division, Leading to Cell Death and Compensatory Proliferation. *Developmental Cell*, 30(6), pp.731–745.

Putney, L.K. & Barber, D.L., 2003. Na-H exchange-dependent increase in intracellular pH times G2/M entry and transition. *The Journal of biological chemistry*, 278(45), pp.44645–9.

Radulescu, A.E. & Cleveland, D.W., 2010. NuMA after 30 years: the matrix revisited. *Trends in Cell Biology*, 20(4), pp.214–222.

Ramanathan, S.P. et al., 2015. Cdk1-dependent mitotic enrichment of cortical myosin II promotes cell rounding against confinement. *Nature cell biology*, 17(2), pp.148–159.

Ramkumar, N. & Baum, B., 2016. Coupling changes in cell shape to chromosome segregation. *Nature Reviews Molecular Cell Biology*.

Rappaport, R., 1999. Absence of furrowing activity following regional cortical tension reduction in sand dollar blastomere and fertilized egg fragment surfaces. *Development, Growth and Differentiation*, 41(4), pp.441–447.

Rappaport, R., 1997. Cleavage furrow establishment by the moving mitotic apparatus. *Development, Growth and Differentiation*, 39(2), pp.221–226.

Rappaport, R., 1996. *Cytokinesis in Animal Cells*, Cambridge: Cambridge University Press.

Rebstein, P.J., Weeks, G. & Spiegelman, G.B., 1993. Altered morphology of vegetative amoebae induced by increased expression of theDictyostelium discoideum ras-related generap1. *Developmental Genetics*, 14(5), pp.347–355.

Redemann, S. et al., 2010. Membrane Invaginations Reveal Cortical Sites that Pull on Mitotic Spindles in One-Cell C. elegans Embryos D. Cimini, ed. *PLoS ONE*, 5(8), p.e12301.

Retta, S.F., Balzac, F. & Avolio, M., 2006. Rap1: A turnabout for the crosstalk between cadherins and integrins. *European Journal of Cell Biology*, 85(3), pp.283–293.

Reymann, A.-C. et al., 2012. Actin network architecture can determine myosin motor activity. *Science (New York, N.Y.)*, 336(6086), pp.1310–4.

Robinson, J.T. et al., 1999. Cytoplasmic Dynein Is Required for the Nuclear Attachment and Migration of Centrosomes during Mitosis in *Drosophila*. *The Journal of Cell Biology*, 146(3), pp.597–608.

Rodrigues, N.T.L. et al., 2015. Kinetochore-localized PP1–Sds22 couples chromosome segregation to polar relaxation. *Nature*, 524(7566), pp.489–492.

Rodriguez-Boulan, E. & Macara, I.G., 2014. Organization and execution of the epithelial polarity programme. *Nature Reviews Molecular Cell Biology*, 15(4), pp.225–242.

Rosa, A. et al., 2015. Ect2/Pbl Acts via Rho and Polarity Proteins to Direct the Assembly of an Isotropic Actomyosin Cortex upon Mitotic Entry. *Developmental Cell*, pp.604–616.

Rosa, A., 2013. The regulation and function of cortical actin remodelling upon entry into mitosis. , (October).

Rosenblatt, J. et al., 2004. Myosin II-Dependent Cortical Movement Is Required for Centrosome Separation and Positioning during Mitotic Spindle Assembly. *Cell*, 117(3), pp.361–372.

Saadaoui, M. et al., 2014. Dlg1 controls planar spindle orientation in the neuroepithelium through direct interaction with LGN. *The Journal of Cell Biology*, p.jcb.201405060-.

Salbreux, G. et al., 2012. Actin cortex mechanics and cellular morphogenesis. *Trends in Cell Biology*, 22(10), pp.536–545.

Schaedel, L. et al., 2015. Microtubules self-repair in response to mechanical stress. *Nature materials*, advance on.

Schliwa, M. & Woehlke, G., 2003. Molecular motors. *Nature*, 422(6933), pp.759–765.

Schmidt, A. & Hall, M.N., 1998. Signaling to the actin cytoskeleton. *Annual Review of Cell and Developmental Biology*, 14(1), pp.305–338.

Schuh, M. & Ellenberg, J., 2008. A New Model for Asymmetric Spindle Positioning in Mouse Oocytes. *Current Biology*, 18(24), pp.1986–1992.

Schwartz, M.A., 2010. Integrins and extracellular matrix in mechanotransduction. *Cold Spring Harbor perspectives in biology*, 2(12), p.a005066.

Sedzinski, J. et al., 2011. Polar actomyosin contractility destabilizes the position of the cytokinetic furrow. *Nature*, 476(7361), pp.462–6.

Ségalen, M. et al., 2010. The Fz-Dsh planar cell polarity pathway induces oriented cell division via Mud/NuMA in Drosophila and zebrafish. *Developmental cell*, 19(5), pp.740–52.

Sehring, I.M. et al., 2015. Assembly and positioning of actomyosin rings by contractility and planar cell polarity. *eLife*, 4, p.e09206.

Sellers, J.R., 2000. Myosins: a diverse superfamily. *Biochimica et Biophysica Acta (BBA) - Molecular Cell Research*, 1496(1), pp.3–22.

Sept, D. & Mccammon, J.A., 2001. Thermodynamics and Kinetics of Actin Filament Nucleation. *Biophysical Journal*, 81, pp.667–674.

Sharp, D.J., Yu, K.R., et al., 1999. Antagonistic microtubule-sliding motors position mitotic centrosomes in Drosophila early embryos. *Nature Cell Biology*, 1(1), pp.51–54.

Sharp, D.J. et al., 2000. Functional Coordination of Three Mitotic Motors in Drosophila Embryos. *Molecular Biology of the Cell*, 11(1), pp.241–253.

Sharp, D.J., McDonald, K.L., et al., 1999. The bipolar kinesin, KLP61F, cross-links microtubules within interpolar microtubule bundles of Drosophila embryonic mitotic spindles. *The Journal of cell biology*, 144(1), pp.125–38.

Sharp, L.W., 1921. *An Introduction to Cytology*, McGraw Hill Book Company Inc.

Siegrist, S.E. & Doe, C.Q., 2005. Microtubule-induced Pins/Galphai cortical polarity in Drosophila neuroblasts. *Cell*, 123(7), pp.1323–35.

Siller, K.H., Cabernard, C. & Doe, C.Q., 2006. The NuMA-related Mud protein binds Pins and regulates spindle orientation in Drosophila neuroblasts. *Nature Cell Biology*, 8(6), pp.594–600.

da Silva, S.M. & Vincent, J.-P., 2007. Oriented cell divisions in the extending germband of Drosophila. *Development (Cambridge, England)*, 134(17), pp.3049–54.

Simpson, P., 2007. The stars and stripes of animal bodies: evolution of regulatory elements mediating pigment and bristle patterns in Drosophila. *Trends in Genetics*, 23(7), pp.350–358.

Sit, S.-T. & Manser, E., 2011. Rho GTPases and their role in organizing the actin cytoskeleton. *Journal of cell science*, 124(Pt 5), pp.679–83.

Solinet, S. et al., 2013. The actin-binding ERM protein Moesin binds to and stabilizes microtubules at the cell cortex. *The Journal of cell biology*, 202(2), pp.251–60.

Somlyo, A.P. & Somlyo, A. V., 2000. Signal transduction by G-proteins, Rho-kinase and protein phosphatase to smooth muscle and non-muscle myosin II. *The Journal of Physiology*, 522(2), pp.177–185.

Son, S. et al., 2015. Resonant microchannel volume and mass measurements show that suspended cells swell during mitosis. *The Journal of cell biology*, 211(4), pp.757–63.

Sorce, B. et al., 2015. Mitotic cells contract actomyosin cortex and generate pressure to round against

or escape epithelial confinement. *Nature communications*, 6, p.8872.

Spiering, D. & Hodgson, L., 2011. Dynamics of the Rho-family small GTPases in actin regulation and motility. *Cell adhesion & migration*, 5(2), pp.170–80.

Stewart, M.P. et al., 2011a. Hydrostatic pressure and the actomyosin cortex drive mitotic cell rounding. *Nature*, 469(7329), pp.226–30.

Stewart, M.P. et al., 2011b. Hydrostatic pressure and the actomyosin cortex drive mitotic cell rounding. *Nature*, 469(7329), pp.226–30.

Stout, J.R. et al., 2006. Deciphering protein function during mitosis in PtK cells using RNAi. *BMC Cell Biology*, 7(1), p.26.

Sung, Y. et al., 2013. Size homeostasis in adherent cells studied by synthetic phase microscopy. *Proceedings of the National Academy of Sciences*, 110(41), pp.16687–16692.

Suzuki, K. & Takahashi, K., 2003. Reduced cell adhesion during mitosis by threonine phosphorylation of ?1 integrin. *Journal of Cellular Physiology*, 197(2), pp.297–305.

Taneja, N. et al., 2016. Focal adhesions control cleavage furrow shape and spindle tilt during mitosis. *Scientific reports*, 6, p.29846.

Tanenbaum, M.E. et al., 2010. Mechanisms of Centrosome Separation and Bipolar Spindle Assembly. *Developmental Cell*, 19(6), pp.797–806.

Tepass, U. et al., 1996. shotgun encodes Drosophila E-cadherin and is preferentially required during cell rearrangement in the neurectoderm and other morphogenetically active epithelia. *Genes & development*, 10(6), pp.672–85.

Terada, Y., Uetake, Y. & Kuriyama, R., 2003. Interaction of Aurora-A and centrosomin at the microtubule-nucleating site in *Drosophila* and mammalian cells. *The Journal of Cell Biology*, 162(5), pp.757–764.

Théry, M. et al., 2007. Experimental and theoretical study of mitotic spindle orientation. *Nature*, 447(7143), pp.493–6.

Théry, M. et al., 2005. The extracellular matrix guides the orientation of the cell division axis. *Nature cell biology*, 7(10), pp.947–53.

Théry, M. & Bornens, M., 2006. Cell shape and cell division. *Current Opinion in Cell Biology*, 18(6), pp.648–657.

Tolić-Nørrelykke, I.M. et al., 2004. Positioning and elongation of the fission yeast spindle by

microtubule-based pushing. *Current biology : CB*, 14(13), pp.1181–6.

Turlier, H. et al., 2014. Furrow Constriction in Animal Cell Cytokinesis. *Biophysical Journal*, 106(1), pp.114–123.

Vicente-Manzanares, M. et al., 2009. Non-muscle myosin II takes centre stage in cell adhesion and migration. *Nature Reviews Molecular Cell Biology*, 10(11), pp.778–790.

Vicente, J.J. & Wordeman, L., 2015. Mitosis, microtubule dynamics and the evolution of kinesins. *Experimental cell research*, 334(1), pp.61–9.

Vitiello, E. et al., 2014. The tumour suppressor DLC2 ensures mitotic fidelity by coordinating spindle positioning and cell-cell adhesion. *Nature Communications*, 5(Grenoble 1), pp.1–15.

Wang, C. et al., 2011. An Ana2/Ctp/Mud Complex Regulates Spindle Orientation in Drosophila Neuroblasts. *Developmental Cell*, 21(3), pp.520–533.

Wang, H. et al., 2005. Ric-8 controls Drosophila neural progenitor asymmetric division by regulating heterotrimeric G proteins. *Nature Cell Biology*, 7(11), pp.1091–1098.

Wang, Y. et al., 2015. Integrin Adhesions Suppress Syncytium Formation in the Drosophila Larval Epidermis. *Current biology : CB*, 25(17), pp.2215–27.

Wang, Y.-C., Khan, Z. & Wieschaus, E.F., 2013. Distinct Rap1 activity states control the extent of epithelial invagination via α-catenin. *Developmental cell*, 25(3), pp.299–309.

Weber, K.L. et al., 2004. A microtubule-binding myosin required for nuclear anchoring and spindle assembly. *Nature*, 431(7006), pp.325–9.

Wee, B. et al., 2011. Canoe binds RanGTP to promote Pins ^{TPR} /Mud-mediated spindle orientation. *The Journal of Cell Biology*, 195(3), pp.369–376.

Wegener, K.L. & Campbell, I.D., 2008. Transmembrane and cytoplasmic domains in integrin activation and protein-protein interactions (Review). *Molecular Membrane Biology*, 25(5), pp.376–387.

Wegner, A., 1976. Head to Tail Polymerization of Actin. *J. Mol. Biol*, 108, pp.139–150.

Wilkin, M.B. et al., 2000. Drosophila Dumpy is a gigantic extracellular protein required to maintain tension at epidermal–cuticle attachment sites. *Current Biology*, 10(10), pp.559–567.

Williams, S.E. et al., 2011. Asymmetric cell divisions promote Notch-dependent epidermal differentiation. *Nature*, 470(7334), pp.353–358.

Williams, S.E. & Fuchs, E., 2013. Oriented divisions, fate decisions. *Current opinion in cell biology*.

Wilson, E.B., 1925. *The cell in development and inheritance*, New York : London: Macmillan and Co.

Winter, C.G. et al., 2001. Drosophila Rho-Associated Kinase (Drok) Links Frizzled-Mediated Planar Cell Polarity Signaling to the Actin Cytoskeleton. *Cell*, 105(1), pp.81–91.

Woolner, S. et al., 2008. Myosin-10 and actin filaments are essential for mitotic spindle function. *The Journal of cell biology*, 182(1), pp.77–88.

Woolner, S. & Papalopulu, N., 2012. Spindle position in symmetric cell divisions during epiboly is controlled by opposing and dynamic apicobasal forces. *Developmental cell*, 22(4), pp.775–87.

Wu, X., Xiang, X. & Hammer, J.A., 2006. Motor proteins at the microtubule plus-end. *Trends in Cell Biology*, 16(3), pp.135–143.

Wühr, M. et al., 2010. A model for cleavage plane determination in early amphibian and fish embryos. *Current biology : CB*, 20(22), pp.2040–5.

Wühr, M. et al., 2009. How does a millimeter-sized cell find its center? *Cell Cycle*, 8(8), pp.1115–1121.

Wyatt, T.P.J. et al., 2015. Emergence of homeostatic epithelial packing and stress dissipation through divisions oriented along the long cell axis. *Proceedings of the National Academy of Sciences of the United States of America*, 112(18), pp.5726–31.

Yamakita, Y. et al., 1999. Dissociation of FAK/p130(CAS)/c-Src complex during mitosis: role of mitosis-specific serine phosphorylation of FAK. *The Journal of cell biology*, 144(2), pp.315–24.

Yildiz, A. et al., 2004. Kinesin walks hand-over-hand. *Science (New York, N.Y.)*, 303(5658), pp.676–8.

Yonemura, S., 2011. Cadherin–actin interactions at adherens junctions. *Current Opinion in Cell Biology*, 23(5), pp.515–522.

Zeitlinger, J. & Bohmann, D., 1999. Thorax closure in Drosophila: involvement of Fos and the JNK pathway. *Development (Cambridge, England)*, 126(17), pp.3947–56.

Zhai, Y. & Borisy, G.G., 1994. Quantitative determination of the proportion of microtubule polymer present during the mitosis-interphase transition. *Journal of cell science*, (4), pp.881–90.

Zhang, Y. et al., 2009. Resolving cadherin interactions and binding cooperativity at the single-molecule level. *Proceedings of the National Academy of Sciences*, 106(1), pp.109–114.

Zheng, Z. et al., 2013. Evidence for dynein and astral microtubule-mediated cortical release and transport of G i/LGN/NuMA complex in mitotic cells. *Molecular Biology of the Cell*, 24(7), pp.901–913.

Zlotek-Zlotkiewicz, E. et al., 2015. Optical volume and mass measurements show that mammalian cells swell during mitosis. *The Journal of Cell Biology*, 211(4), pp.765–774.